The *Drosophila* Nephrocyte -
Modeling Podocyte Function and Disease

DISSERTATION ZUR ERLANGUNG DES DOKTORGRADES
DER NATURWISSENSCHAFTEN (DR. RER. NAT.)
DER FAKULTÄT FÜR BIOLOGIE UND VORKLINISCHE
MEDIZIN DER UNIVERSITÄT REGENSBURG

vorgelegt von

Florian Hochapfel

aus Vilsbiburg

im Jahr 2018

Das Promotionsgesuch wurde eingereicht am:

_____

Die Arbeit wurde angeleitet von
Prof. Dr. Dr. Michael Krahn

Unterschrift:

To my mother.

Table of contents

Zusammenfassung

In den modernen Industrienationen haben sich chronische nicht-übertragbare Krankheiten zur Hauptursache menschlicher Sterblichkeit entwickelt. Während der letzten Jahre wuchs die globale Belastung der Gesundheitssysteme durch chronische Nierenleiden beträchtlich und in vielen dieser Fälle sind weder gezielte noch personalisierte Therapien verfügbar. Um mit den steigenden Herausforderungen schritthalten zu können, muss das Verständnis der Ursachen und Mechanismen, die chronischen Nierenkrankheiten zugrunde liegen, vertieft werden und neuartige Herangehensweisen müssen entwickelt und verfeinert werden, damit konventionelle Forschungsansätze gefördert und bereichert werden können. Diese Dissertation umfasst vier Manuskripte, die sich aus unterschiedlichen Blickwinkeln mit dem Potenzial von *Drosophila* Nephrozyten zur Modellierung von Nierenfunktion und -krankheit in Säugetieren beschäftigen und zeigen, wie diese auf schnelle und kosteneffiziente Weise wertvolle Erkenntnisse zu etablierten Nierenmodellen beitragen können.

Die morphologische Charakterisierung einer biologischen Probe mit Hilfe der Elektronenmikroskopie hängt stark vom Grad der Probenerhaltung ab. Im Rahmen des ersten Projektes konnte die ultrastrukturelle Erhaltung von präparierten Nephrozyten sowohl durch die Verwendung einer optimierten Präparationssaline wie auch durch die Umstellung von chemischer auf Kryofixierung während der Vorbereitung zur Transmissionselektronenmikroskopie (TEM) erheblich verbessert werden. Basierend auf Raster-TEM-Tomografie wurde zudem die dreidimensionale Ultrastruktur der komplexen subzellulären Strukturen in Nephrozyten durch die Erzeugung eines 3D-Modells des peripheren Netzwerks der Zellmembraneinstülpungen weiter charakterisiert. Außerdem wurde die epitheliale Polaritätsdeterminante Crumbs beispielhaft auf Epoxid-Ultradünnschnitten über einen indirekten Ansatz mittels GFP-Tag-Detektion nachgewiesen; eine Herangehensweise, die sich problemlos auch auf andere GFP-getaggte Transgene übertragen lässt.

Interagieren Fußfortsätze eines Säugetierpodozyten mit anderen Fußfortsätzen desselben Podozyten? Diese Frage blieb bisher unbeantwortet, da in der konventionellen zweidimensionalen Transmissionselektronenmikroskopie nur eine begrenzte Einschätzung der räumlichen Anordnungen von zellulären Strukturen möglich ist. Das zweite Manuskript kommt zu dem Schluss, dass eine Interaktion ausschließlich zwischen Fußfortsätzen unterschiedlicher Podozyten möglich ist. Diese Erkenntnis basiert auf der gründlichen Untersuchung des 3D-Modells eines vollständigen murinen Podozyten, von welchem mittels der FIB-SEM-Technologie schrittweise dünne Schichten abgetragen und aufgenommen wurden. Die Zell-Zell-Kontakte zwischen den Fußfortsätzen wurden mit Hilfe von Zweiachsentomografie in menschlichen und murinen Podozyten, wie auch in *Drosophila*-Nephrozyten, näher untersucht. Artenübergreifend wurde sowohl entlang des gesamten Schlitzdurchmessers ein quasiplanares Schlitzdiaphragma gefunden, wie auch zahlreiche zusätzliche punktuell-filamentöse Kontakte. Zusätzliche Untersuchungen sind notwendig,

um die Proteine zu identifizieren, aus denen diese zwei Arten der Zell-Zell-Kontakte aufgebaut sind.

Podozyzen sind hochkomplexe polarisierte Zellen. Für ein besseres Verständnis der molekularen Grundlagen von Entwicklung und Aufrechterhaltung der normalen podozytären Funktion wird im dritten Manuskript die Rolle von Pals1, eines Gerüstproteins und Schlüsselfaktors während der apikobasalen Polarisation in Epithelien, genauer beschrieben. Pals1 kann demnach die Funktion eines essenziellen, spezifischen und dosisabhängigen Regulators zugeschrieben werden, da gezeigt wurde, dass es in Mäusen die Hippo- und TGF-β-Signalwege negativ reguliert, was zusätzlich im *Drosophila*-Modell bestätigt werden konnte. Diese Erkenntnisse deuten auf eine Verbindung zwischen Nierenkrankheiten, insbesondere in Verbindung mit Zystendefekten, und apikalen Polaritätsproteinen hin. Indem die durch Pals1 regulierten Netzwerke in zukünftigen Studien weiter erforscht werden, kann die Pathogenese dieser Krankheiten besser verstanden werden.

Im Laufe des vierten Projektes wurde sodann die Rolle von *Drosophila* Crumbs (DmCrb) in Nephrozyten näher untersucht. DmCrb ist ein Interaktionspartner von Stardust, dem *Drosophila*-Homolog von Pals1, und ein maßgeblicher Faktor apikobasaler Polarität. Es wurde nachgewiesen, dass es an der Regulation der frühen Endozytose beteiligt ist, indem es über seine C-terminale FERM-Bindedomäne mit Moesin interagiert. Zudem trägt es über seine extrazelluläre Domäne zur Assemblierung und Aufrechterhaltung des Nephrozytendiaphragmas bei. Die Funktionen seiner verschiedenen Proteindomänen und evolutionäre Konservierung innerhalb der Crumbs-Proteinfamilie wurde untersucht, indem eine Reihe von Rettungsexperimenten mit verschiedenen Deletionskonstrukten von DmCrb, sowie auch seiner humanen Orthologe, durchgeführt wurde. Es ist davon auszugehen, dass die hier beschriebenen Mechanismen von Nephrozytenentwicklung und -funktion in Säugetierpodozyten konserviert sind.

Summary

In modern industrialized nations, chronic non-communicable diseases have become the main reason of mortality. During the last years, the global health burden of chronic kidney diseases (CKD) has grown considerably and in many of these cases, no targeted or personalized therapies are available. To keep up with the rising challenges, the understanding of the causes and mechanisms underlying CKD needs to be improved and novel approaches must be found and refined to support and enrich conventional research methods. This dissertation encompasses four manuscripts concerned with various aspects of utilizing *Drosophila* nephrocytes for modeling mammalian kidney function and disease and contributing valuable insights, in addition to established kidney models, in a quick and cost-effective way.

In general, the morphological characterization of a biological sample via electron microscopy strongly depends on the degree of sample preservation. In the first project, the ultrastructural preservation of nephrocytes after preparation for transmission electron microscopy could be greatly improved by using both an optimized dissection saline and cryofixation techniques. Also, the initially challenging immunogold detection of endogenous Crumbs protein could be realized by an indirect approach detecting GFP-tagged Crumbs using an antibody directed against the tag. The 3D ultrastructure of the complex subcellular structures in nephrocytes was further characterized by creating a 3D model of the outlying network of cell membrane invaginations based upon STEM tomography data.

In conventional two-dimensional TEM, only a limited assessment of the spatial arrangement of cellular structures in possible. The question whether foot processes of mammalian podocytes interact with other foot processes of the same cell therefore remained unanswered. The second manuscript arrives at the conclusion, that the interaction exclusively happens between foot processes of different podocytes, by thorough investigation of a 3D model, which was based on a whole podocyte, sectioned and imaged using FIB-SEM technology. The cell-cell contacts between foot processes were further characterized via dual-axis tomography in human and mouse podocytes, as well as *Drosophila* nephrocytes, leading to the realization that there is both one quasi-planar slit diaphragm spanning the whole slit diameter between two processes and additionally several filamentous contacts, which are locally limited. Additional studies are necessary to identify the proteins these two types of cell-cell contacts are composed of.

Podocytes are highly complex polarized epithelial cells. For a better understanding of the molecular fundamentals of development and maintenance of normal podocyte function, the role of Pals1, which acts as scaffolding protein and key factor necessary for apicobasal polarization, was more closely investigated in podocytes in the third manuscript. Therein, Pals1 was found to be an essential, specific and dose-dependent regulator of nephrogenesis, being a negative regulator of Hippo and TGF-β signaling in mouse,

which was then also confirmed in the *Drosophila* model. These findings indicate a connection between renal diseases, especially renal cyst diseases, and apical polarity proteins. The pathogenesis of these diseases needs to be better understood by studying the networks regulated by Pals1.

In the course of the last project, the role of *Drosophila* Crumbs (DmCrb) in nephrocytes was closer examined. DmCrb is an interaction partner of Stardust, the *Drosophila* homolog of Pals1, and a key determinant of apicobasal polarity. It was found to be involved in the regulation of early endocytosis via interaction with Moesin through its FERM-binding domain, located on its C-terminus. It further contributes to nephrocyte diaphragm assembly and maintenance via its extracellular domain. The functions of its different protein domains and the evolutionary conservation within the Crumbs family was examined by conducting a series of rescue experiments with various deletion constructs of DmCrb as well as its human orthologs. The herein describes mechanisms of nephrocyte development and function are likely also conserved in mammalian podocytes.

1 Introduction

1.1 Chronic kidney disease: a growing global health burden

In most parts of our modern society, the distribution of disease and death has transitioned from an "age of pestilence and famine" through a development of receding pandemics to a predominant state determined by degenerative and man-made diseases, shifting the major causes of death from acute and infectious diseases to chronic non-communicable and degenerative diseases, like cardiovascular disease and cancer (Omran, 2005). Reasons include the development of hygiene practices in the 19th century, the rising availability of medical technologies to combat or prevent parasitic or infectious diseases as well as the onset of antibiotics. Despite the re-emerging occurrence of infectious diseases and the residual persistence of pestilence and famine predominantly in developing countries, chronic non-communicable diseases (NCDs) have become the main reason of mortality in industrialized nations (Mascie-Taylor and Karim, 2003). According to the World Health Organization (2008), the four NCDs of greatest economic impact are cardiovascular disease, cancer, diabetes and chronic respiratory disease.

In recent years, the global burden of chronic kidney disease (CKD) has increased considerably, which in part depends on the widespread diabetes mellitus (DM) epidemic (Mathers and Loncar, 2006). Even though CKD is currently not considered a separate target of attention, it determines the poor health outcomes of cardiovascular disease and diabetes (Li and Ma, 2017). An individual is diagnosed with CKD, when their kidney structure or function is impaired for longer than three months, regarding markers like abnormal composition of the urine (e.g. albuminuria or unusual electrolyte levels) or a reduced glomerular filtration rate of $<$60 mL/min/1.73 m^2 (GFR; Levey et al., 2005). The severity of kidney disease is further subdivided into five stages depending on the degree of GFR reduction. One possible outcome of CKD is end-stage renal disease (ESRD), which is defined by a GFR of less than 15 ml/min/1.73 m^2. At this stage, possible treatments are dialysis and kidney transplantation, but already in earlier stages, patients are likely to suffer from secondary conditions like cardiovascular disease (CVD), strongly contributing to a high all-cause mortality in dialysis patients of roughly 22% per year in US patients around the last turn of the century (Eknoyan et al., 2004).

To further deepen the understanding of mechanisms and causes of CKD, novel methods of research are necessary to develop and refine targeted and personalized therapy for patients. In the last two decades, more than 45 genetic mutations have been found in patients suffering from hereditary steroid-resistant nephrotic syndrome (Machuca et al., 2009; McCarthy and Saleem, 2011; Bierzynska et al., 2014; Akchurin and Reidy, 2015; Chen and Liapis, 2015), strongly improving opportunities for personalized therapy for patients with hereditary nephrotic syndrome based on a multitude of factors like genetic constitution, age of onset and renal histology.

1.2 The vertebrate kidney

1.2.1 General structure

The kidneys are bean-shaped pairwise organs, located retroperitoneally on both sides of the spine. They play a central role in regulating various processes in the vertebrate body, including the homeostasis of water and electrolytes as well as keeping up the balance of the pH in the body fluids. They are essential for the excretion of metabolic wastes by producing urine.

Macroscopically, the kidneys of large mammals can be divided into several equal units, called the *lobi renales*, each made up of medulla and cortex. The medulla has a pyramid-like shape with a tapered tip (*papilla*), protruding into a calyx of the renal pelvis. The renal cortex makes up a layer covering the base of the medullar pyramids and separating them as *columnae renales* reaching the *sinus renalis* located near the center of the kidney.

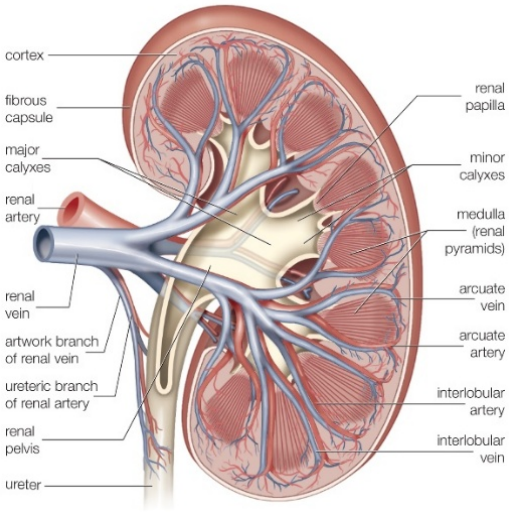

Figure 1.2-1 Kidney cross-section showing major blood vessels. Taken from Encyclopædia Britannica (2010).

1.2.2 Blood filtrations occurs in the glomerulus of the nephron

The essential functional unit of the kidney is the nephron. In rats, there are between 30,000 and 35,000 nephrons (Baines and Rouffignac, 1969), whereas each human kidney contains around one million (Smith, 1951). Each nephron is made up of the renal corpuscle connected to an unbranched tubule, which eventually ends into a collecting duct. Nephrons can be characterized as superficial, mid-cortical or juxtamedullary, depending on the position of their corpuscle. Beginning at the glomerular capsule, the tubule consists of a proximal stretch merging in a coiled convoluted part, followed by a straight part approaching the medulla becoming the loop of Henle. Following a U-turn, this loop ascends back towards the cortex forming a distal convoluted tubule, which finally joins a collecting duct. Each nephron filters blood, reabsorbs beneficial substances and excretes wastes in form of urine.

Each renal corpuscle consists of Bowman's capsule, the blind expanded end of a renal tubule, and a central glomerulus of vessels, which is deeply invaginating the capsule, held together by a delicate mesangial matrix and covered by the glomerular basement membrane (GBM). The glomerulus is supplied by an afferent arteriole, entering the capsule on the vascular pole and the efferent arteriole leaves the corpuscle at the same point.

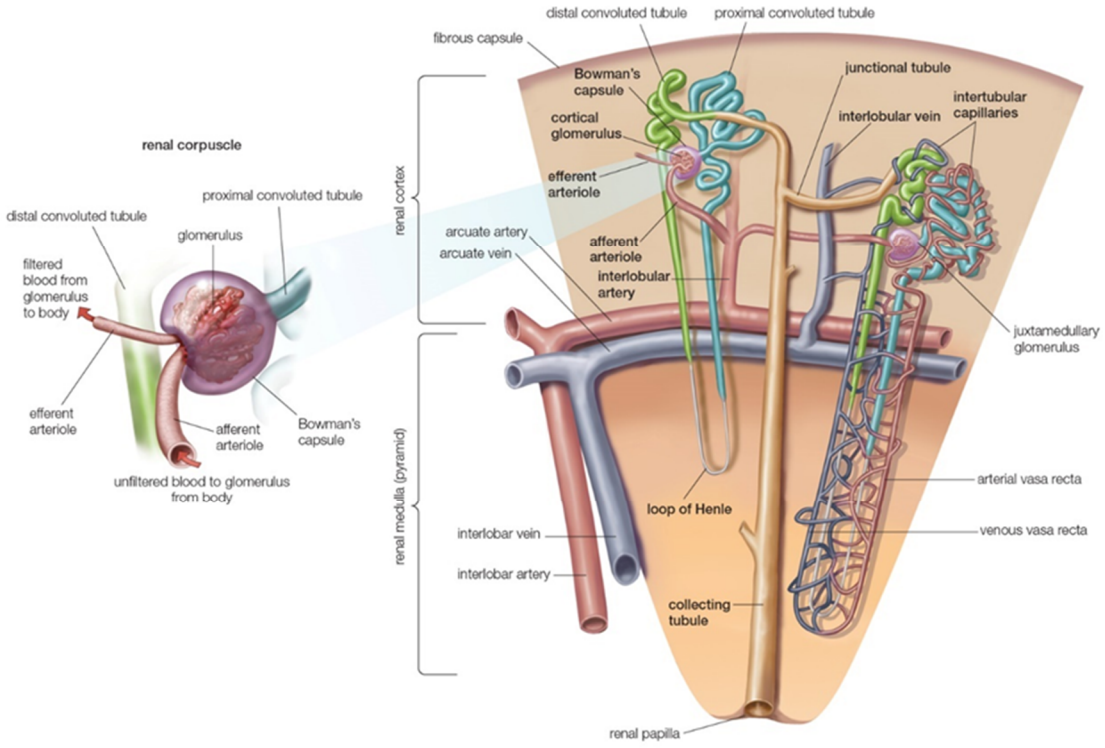

Figure 1.2-2 Depiction of a renal corpuscle located inside the renal cortex. Taken from Encyclopædia Britannica (2010).

On its outer (parietal) wall, Bowman's capsule is covered by a squamous epithelium, whereas it's juxtacapillary (visceral) wall is composed by specialized epithelial podocytes. The volume between these walls is described as Bowman's space. Podocytes are highly differentiated epithelial cells, which are characterized by a vastly branched three-dimensional architecture and the formation of actin-dependent projections called foot processes (FP; Quaggin and Kreidberg, 2008). Processes from adjacent podocytes interdigitate and get into contact with slit diaphragms. Passing the fenestrae of the glomerular arteries, blood is pushed through the glomerular filter, which can be defined as a perm-selective multi-layered and -cellular barrier comprising the fenestrated endothelium, the glomerular basement membrane and the slit-diaphragm (Patrakka and Tryggvason, 2009). Damage or dysfunction to any of these constituents leads to a functional loss of the charge- and size-selective filtration and subsequently proteinuria (Brinkkoetter et al., 2013).

1.2.3 Nephrogenesis and podocyte differentiation

In vertebrates, three organizational kidney variants of rising complexity can be found: pronephros, mesonephros and metanephros (Saxén and Sariola, 1987). During the embryonic development of mammals, the pronephros emerges only as a transient state of differentiation, eventually leading to a fully differentiated metanephric kidney, following a highly complex sequence of morphologic and molecular transformation (Costantini and

Kopan, 2010). During the process of glomerular maturation, one can observe four developmental stages: the renal vesicle stage, the S-shaped body stage, the capillary loop stage and the mature glomerulus (Saxén and Sariola, 1987). Regarding cell polarity and structure, immature podocyte precursor cells are like classical epithelial cells. During the S-shaped body stage, they exhibit a sub-apically localized junctional belt, are of cuboid shape and show high mitotic activity, apparent from strong expression of the proliferation marker PCNA (Nagata et al., 1993). Due to their high expression of Wilms' Tumor 1 protein (WT1; Kreidberg 1996), they are distinguishable from the other epithelial cells in the developing glomerulus.

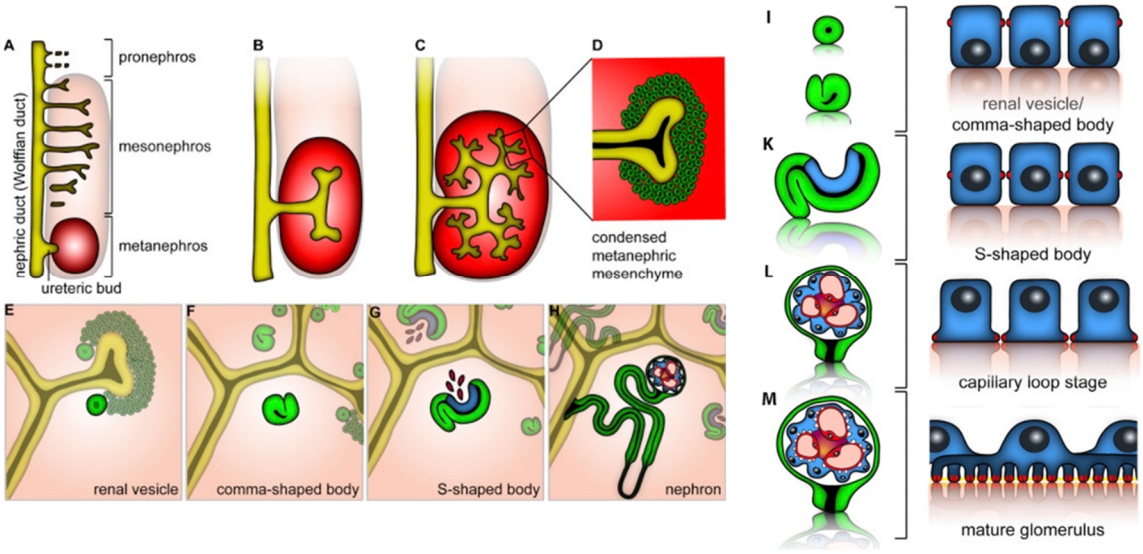

Figure 1.2-3 Nephrogenesis and podocyte development. (A) Kidney development in mammals starts with the invasion of the ureteric bud out of the nephric duct into the metanephric mesenchyme. (B and C) Branching of the ureteric bud commences inside the growing metanephric mesenchyme. (D) Near the ureteric bud, the mesenchyme condenses creating the Six2-positive cap mesenchyme. (E) Formation of renal vesicles from the condensed cap mesenchyme. (F) Development of a cleft in the comma-shaped bodies. (G) Attraction of angioblasts by podocyte progenitors in the s-shaped body. (H) Connection of the developing nephron with the collecting duct. Modified from Schell et al. (2014).

As differentiation progresses, the tight junctions of the podocyte progenitor descend to the basolateral aspect of the cell and form a specialized junction type, the slit diaphragm, which still exhibits markers characteristic for tight junctions (e.g. Par3 [partitioning defective 3] and ZO-1 [zonula occludens-1]), but also several slit diaphragm-specific proteins like Nephrin, Neph1 and Podocin (Grahammer et al., 2013). Parallel to this transition, podocytes start to expand their apical aspect and form primary and secondary foot processes, which make up their basolateral aspect (Hartleben et al., 2012). Foot processes alternatingly interdigitate with processes of an adjacent podocytes. Interestingly, slit diaphragms are only formed as bridges to adjacent podocytes and not between processes of the same cell, which will be described more elaborately in section 2.2.4.1.

The podocyte cytoskeleton is connected to the slit diaphragm proteins by adaptor proteins and acts as a signaling hub to transport information from the foot process surface

to the cytoplasm, thereby allowing for dynamic fine-tuning of podocyte structure (Simons et al., 2009). Mutations of proteins involved in the organization of the actin cytoskeleton, like Myosin 1e (Krendel et al., 2009; Mele et al., 2011), RhoGDIα (Gupta et al., 2013) and Cdc42 (Scott et al., 2012), as well as adaptors linking the slit diaphragm to the cytoskeleton, for example CD2-associated protein (Kim et al., 2003) and α-actinin-4 (Michaud et al., 2003) lead to GFR reduction, foot process effacement and proteinuria.

1.3 The podocyte: a polarized epithelial cell

The epithelium is defined as one of the four basic types of metazoan tissue, together with muscle tissue, nervous tissue and connective tissue. It covers the complete body surface and lines tubes, cavities and hollow organs (Campbell et al., 2003). In general, the organization of epithelial cells into tissues and the coordination of cell-cell communication heavily depends on cell polarity. Epithelial polarization is characterized by an asymmetric distribution of biomolecules enabling epithelia to form organized membrane subdomains for specialized functions. By polarizing, each cell contributes to a higher order of organization in its tissue, which mainly occurs along two axes, leading to planar cell polarity and apicobasal polarity.

Apicobasal polarity is established orthogonally to the plane of the epithelium and is characterized by the formation of cell-cell junctions, i.e. tight and adherens junctions, sealing off the organism from the exterior by creating a diffusion barrier, as well as the subdivision of the plasma membrane into an apical domain, directed to the extracellular lumen, and basolateral domain, facing the lateral side of neighboring cells and the extracellular matrix below (ECM). (Bryant and Mostov, 2008; Roignot et al., 2013; Pocha and Knust, 2013). To form and maintain a stable filtration barrier, podocytes strongly rely on apicobasal polarity, which is initiated by three major polarity complexes: The Crumbs and Par complexes defining the apical region of the lateral membrane, as well as the Scribble complex, essential for basolateral identity.

1.3.1 The Crumbs protein complex

In most polarized epithelia, the Crumbs (Crb) complex is crucial for the determination of the apical aspect of the plasma membrane (Rodriguez-Boulan and Macara, 2014). It consists of four core components: the single-span transmembrane protein Crb, which was first discovered in *Drosophila melanogaster* and the cytoplasmically localized proteins Pals1 (protein associated with Lin-7; Stardust[Sdt] in *Drosophila*), PATJ (Pals1 associated tight junction protein) and Lin-7. It has been demonstrated in the fly that the complex is established by physical interaction of the C-terminal ERLI motif of Crb with the PDZ (PSD-95, Dlg1, ZO-1) domain of Sdt (Hong et al., 2001; Bachmann et al., 2001). In addition, the two L27 domains of Sdt bind to the L27 domains of Lin-7 and PATJ (Roh et al., 2002; Bulgakova et al., 2008).

In *Drosophila* epithelia, the Crb and Par protein complexes work together to define the identity of the apical membrane domain and they are involved in counterbalancing

the activity of the basolateral determinants Lgl (Lethal giant larvae), Dlg (Disc-large homolog) and Scrib (Scribble) (Tepass, 2012), except of boundary cells in the hindgut (Kumichel and Knust, 2014).

The scaffolding protein Stardust (Sdt, Pals1 in mammals) is necessary to stabilize Crb at the tight junction (or the homologous region in *Drosophila*) (Bachmann et al., 2001; Hong et al., 2001; Makarova et al., 2003; Roh et al., 2003; Straight et al., 2004). *Drosophila* PATJ is characterized by four PDZ domains and an N-terminal L27 domain (Pielage et al., 2003) and is not required to stabilize Crb-Sdt in embryonic epidermis, but it is necessary in photoreceptor cells and mammalian cell culture (Michel et al., 2005; Shin et al., 2005; Pénalva and Mirouse, 2012; Zhou and Hong, 2012; Sen et al., 2012; Sen et al., 2015).

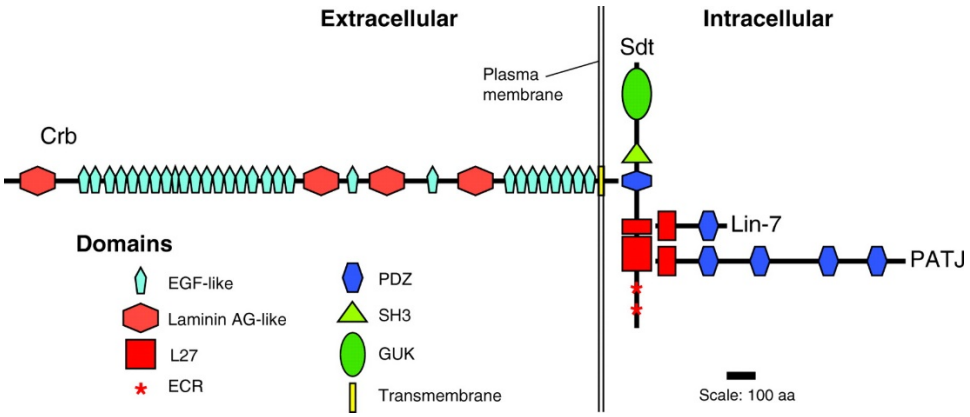

Figure 1.3-1 Scheme of the core components of the *Drosophila* Crumbs complex and its proposed structure. The complex is made up of four core components: Crb, Sdt, PATJ and Lin-7. AG, A-globulin. Taken from Bulgakova and Knust (2009).

1.3.2 Crumbs is an intermembrane protein with a long extracellular domain

Crb was first shown to regulate epithelial polarity in *Drosophila* (Tepass et al., 1990; Tepass and Knust, 1990), where it is expressed in most epithelia, in which it is not always essential for establishment of cell polarity (Tepass et al., 1990; Pellikka et al., 2002; Tanentzapf and Tepass, 2003; Campbell et al., 2009). The most prominent characteristics of Crb family proteins are two highly conserved regions at the C-terminus, the FERM (4.1 protein, Ezrin, Radixin, Moesin) and the PDZ binding domain, both located in its intracellular portion and necessary for protein-protein interactions.

In mammals, there are three homologs of the *Drosophila crumbs* gene, called *Crb1, Crb2* and *Crb3.* The Crb1 protein plays an important role in the retina and mutations in its gene have been linked to degenerative diseases related to photoreceptors, like retinitis pigmentosa (RP12) and Leber congenital amaurosis (LCA8) (den Hollander et al., 1999; den Hollander et al., 2001; Lotery et al., 2001). Crb2 is expressed in brain, retina and kidney (van den Hurk et al., 2005) and acts in tandem with Crb1 to ensure correct development and maintenance of the retina (Alves et al., 2013; Pellissier et al., 2013). In

zebrafish, loss of a Crb2 homolog causes strong defects in podocyte development. Furthermore, experiments in Crb2-KO mice indicate that Crb2 is involved in the coordination of gastrulation (Xiao et al., 2011) and mutations in the human *CRB2* gene cause congenital nephrotic syndrome (Ebarasi et al., 2015; Slavotinek et al., 2015). The third mammalian representative Crb3 shows strong expression in epithelia and constitutes the main Crumbs isoform in renal tissues (Makarova et al., 2003). The knockout of its encoding gene causes postnatal lethality in mice (Whiteman et al., 2014).

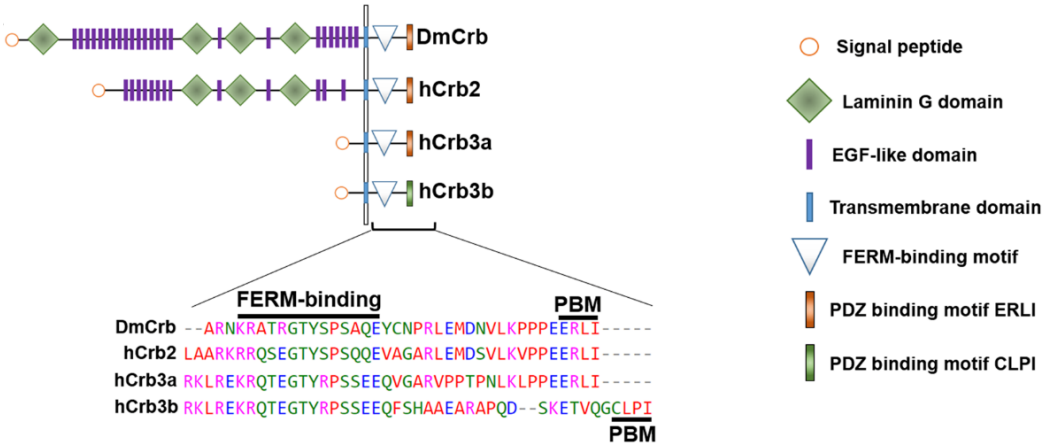

Figure 1.3-2 Scheme of *Drosophila* Crb and hCrb2 and hCrb3 proteins including a sequence alignment of the intracellular domain. PBM, PDZ-binding motif; FERM, 4.1-protein–Ezrin–Radixin–Moesin. Taken from section 2.4.2.

Like *Drosophila* Crb (DmCrb), two of its mammalian isoforms, Crb1 and Crb2, have long extracellular domains with many EGF-like domains, whereas the two different splicing variants of Crb3, a and b, only have very short extracellular domains lacking the EGF-like domains (Makarova et al., 2003; for expression patterns, cf section 2.4.2) and differ in the nature of their PDZ-domains. While Crb3a ends with an ERLI motif, Crb3b ends with CLPI at the C-terminus (cf. Figure 1.3-1), resulting in its inability to interact with Pals1 (Fan et al., 2007). Crb3a also binds Par6 with its PDZ-motif, entailing a direct interaction of the Crb complex with the Par complex (Hurd et al., 2003). In MDCK cell culture, Crb3a was shown to be a key factor in the establishment of apicobasal polarity and tight junction assembly (Roh et al., 2002; Fogg et al., 2005), whereas Crb3b seems to be involved in ciliogenesis (Fan et al., 2007). Evolutionary relation of the Crumbs orthologue and a functional characterization of its protein domains is closer described in section 2.4.

1.3.3 Pals1: a MAGUK family scaffolding protein

Pals1 belongs to the p55-like subfamily of the membrane-associated guanylate kinase (MAGUK) family and is encoded by the gene *Mpp5* (membrane protein, palmitoylated 5) in human (Kamberov, 2000). It shows high expression levels in all kidney tissues, as

well as in the placenta, and only weak presence in skeletal muscle, heart and brain. In polarized epithelia, it localizes to the tight junction and has been shown to interact with the transmembrane protein Crb via its PDZ domain. Also, it is the only member of the Crb complex interacting with all other of its members. (Kamberov, 2000; Roh et al., 2003; Straight et al., 2004; Weide et al., 2017).

Pals1 also contains a PDZ domain, and additionally a characteristic guanylate kinase (GUK) domain, which interestingly lacks kinase activity, but is assumed to be necessary for protein-protein interactions (McGee et al., 2001; Tavares et al., 2001; Bulgakova et al., 2008). Furthermore, it interacts with PATJ using its L27-domain and has orthologs in Zebrafish (Nok; Wei and Malicki, 2002) and *Drosophila* (Stardust[Sdt]; Knust et al., 1993). Knockdown of Pals 1 in epithelial cells causes a decrease of aPKC (atypical protein kinase C) and PATJ at the tight junctions, indicating a key role in the formation and maintenance of tight junctions (Straight et al., 2004). If Lin-7 and Crb3 are lost in mice, Pals1 gets destabilized and tight junctions show developmental defects (Whiteman et al., 2014). In *Drosophila,* mutations in either *Crb* or *Sdt* cause polarity defects in epithelia (Knust et al., 1993). Since proteins interacting with Pals1, namely Crb3 and Taz, have been connected to renal cyst formation in mice, the role of Pals1 in the polarization and differentiation of kidney development will be further investigated in section 2.2.

1.3.4 PATJ: a long PDZ domain containing protein

The third canonical member of the Crb complex, which was at first falsely annotated Discs lost, is a large scaffolding protein called PATJ. It contains ten PDZ domains (*Drosophila* PATJ: 4) and localizes to tight junctions in epithelia (Shin et al., 2005). Patj binds to Pals1 using its L27 domain (Figure 1.3-1, similar in mammals) and several of its PDZ domains have been shown to bind various other proteins (Roh et al., 2002; Wells et al., 2006; Ernkvist et al., 2009). Loss of Patj causes defects in directed cell migration of epithelial cells (Shin et al., 2005).

1.3.5 The Crb complex and its interaction with the Hippo pathway

In recent years, several indications have been found that the Crb complex acts upstream of the Hippo signaling pathway, a highly conserved kinase cascade responsible for regulation of organ size, tissue regeneration and cell proliferation (Chen et al., 2010; Grzeschik et al., 2010; Robinson et al., 2010; Varelas et al., 2010). In Mammals, the two core constituents of the Hippo pathway are Mst1/2 (mammalian STE20-like protein kinase 1 and 2 [*Drosophila* Hippo]) and Lats1/2 (large tumor suppressor homologs 1 and 2 [*Drosophila* Warts). Together with their regulatory protein Salvador (Sav1; Callus et al., 2006), Mst1/2 facilitate the phosphorylation and activation of Lats1/2 (Chan et al., 2005), with the support of the adaptor protein Mob1 (Mob kinase activator 1; Praskova et al., 2008).

The transcriptional coactivators Yap (Yes-associated protein) and Taz (transcriptional coactivator with PDZ-binding motif, encoded by *Wwtr1*) play a key role in the regulation of Hippo target genes. Upon activated signaling, Yap or Taz are phosphorylated by Lats1/2, thereby preventing their migration into the nucleus (Dong et al., 2007; Zhao et al., 2007; Hao et al., 2008; Oka et al., 2008; Lei et al., 2008). In their unphosphorylated state, Yap/Taz can freely enter the nucleus and activate the expression of target genes (Piccolo et al., 2014; Hansen et al., 2015), e.g. thereby also promoting TGF-β-SMAD signaling (Varelas et al., 2010). The Hippo pathway has been researched extensively in *Drosophila*, but the core constituents and downstream effectors are remarkably conserved in mammals. By expressing human Mst2, Lats1, Mob1 and Yap, the corresponding *Drosophila* mutants can be fully rescued *in vivo* (Tao et al., 1999; Wu et al., 2003; Huang et al., 2005; Lai et al., 2005).

Apart from its contribution to the formation of cell polarity via the PDZ binding motif (PBM) at its C-terminus (Hong et al., 2001), Crb also directly regulates the Hippo pathway by recruiting the upstream Hippo component Expanded to the apical membrane via interaction of its FERM binding motif (FBM; Chen et al., 2010; Robinson et al., 2010; Ling et al., 2010). Furthermore, the Crb complex directly interacts with Yap/Taz by promoting phosphorylation, which leads to cytoplasmic retention of Yap/Taz and suppression of Hippo target genes (Varelas et al., 2010). Knocking down Crb3 or Pals1 resulted in a shift of Yap/Taz localization towards the nucleus, leading to a deregulation of the pathway and increased expression of target genes. Impairments of Hippo pathway and consequently hyperactivation can also negatively influence cell polarity integrity. Data from Lats1/2 double knockout mice showed that loss of cytoplasmic retention of Yap/Taz leads to a loss of Crb3 and an impaired distribution of basolateral markers, indicating a tendency towards a loss of epithelial characteristics in differentiating epithelia that lack Lats function (McNeill and Reginensi, 2017).

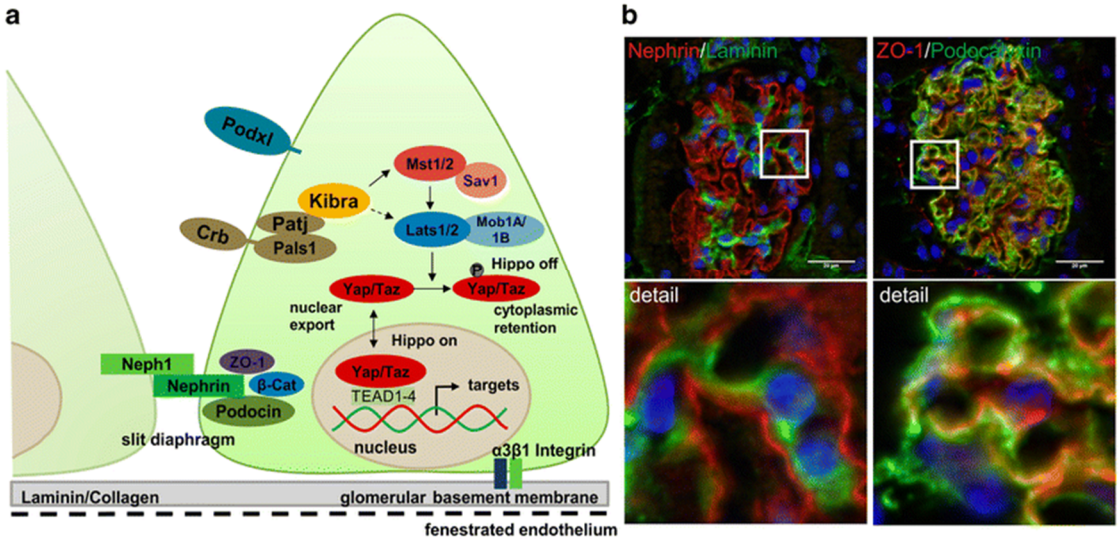

Figure 1.3-3 Schematic overview of a podocyte foot process and cross-section through a glomerulus. (A) The glomerular filtration barrier is build up by the podocyte slit diaphragm, the glomerular basement membrane (GBM) and the fenestrated endothelium. Podocytes are anchored to the GBM by α3-β1 integrins. The slit diaphragm (SD) can be characterized as a bridge between different

foot processes and shows both markers of tight junctions (ZO-1) and adherens junctions (β-catenin). Unique components like Nephrin, Neph1 and Podocin make up the slit diaphragm and are necessary for its integrity. Knockout of Podx1 leads to foot process effacement. Short description of the hippo pathway: cf. section 1.3.5. (B) Cross sections of mouse kidney. Nephrin (podocyte marker) and laminin α4 (GBM marker) are next to each other, but do not colocalize. ZO-1 (SD marker) and Podxl (Podocalyxin, marker for apical podocyte region) partially colocalize next to the SD. Scale bar and detail view 20µm. Taken from (Michgehl et al., 2017).

1.4 *Drosophila melanogaster* is suited as a cost- and time-efficient organism for modeling podocyte biology and pathophysiology

The mouse represents the most successful model organism used for glomerular development and disease. Due to its close phylogenetic similarity with human, it provides relevant insights into several ultrastructural and molecular topics of interest. Nevertheless, the long generation times of mice and their low number of progeny are making research time-consuming and expensive. Among vertebrates, zebrafish has been established as an additional model to research kidney development and function, partly alleviating the limitations. The *in vitro* approach was also problematic at first, since podocytes do not differentiate readily in cell culture, thereby lacking their characteristic 3D architecture. Notwithstanding the initial difficulties, Yaoita et al. (2017) induced podocyte differentiation *in vitro* using special culturing conditions, finding ultrastructural phenotypes reminiscent of *in vivo* conditions, thereby opening up another promising avenue of research.

In the past decade, several groups successfully utilized the fruit fly *Drosophila melanogaster* as a model for kidney disease, by harnessing the vast genetic potential of the most thoroughly studied organisms in biological research. *Drosophila* has been subject of biological studies for over a hundred years and offers convincing advantages compared to mammalian systems. They are easy to culture and offer short generation times of less than ten days at room temperature. Combined with their plentiful offspring, a female lays up to 100 eggs a day and over a thousand during a lifetime of more than 60 days (Reeve and Black, 2001), extensive data can be collected from the offspring produced by one single mating. Its genome is fully sequenced since 2000 (Adams, 2000) and according to a systematic blast analysis (Reiter et al., 2001), more than 75% of known human disease genes can be matched to genes in the fruit fly genome, demonstrating a high degree of homology to the human genome regardless of its superficial phylogenetic distance.

Having access to the genetic resources available for *Drosophila*, one can easily find homologs to human genes and knock them down using RNA-interference stocks available in extensive libraries (Dietzl et al., 2007) or edit the genome via CRISPR/Cas9 utilizing guide RNAs injected into the fly embryo (Bassett et al., 2013). Gene expression can be triggered ubiquitously, restricted to specific tissues/cells or time span dependent via the UAS/GAL4 system (Brand and Perrimon, 1993).

1.4.1 The *Drosophila* nephrocyte

At first glance, the excretory system of invertebrates is not organized in nephrons, yet several analogous elements, like cells conducting filtration and tubular structures modifying the organism's body liquid, can be found. The role of the proximal part of the mammalian nephron, comprising glomerulus and proximal tubule, responsible for filtration and reabsorption, is performed by the nephrocytes, acting as "fly podocytes" showing remarkable similarities regarding ultra-structural, molecular and functional characteristics (Weavers et al., 2009; Zhuang et al., 2009; Tutor et al., 2014; Na et al., 2015).

The renal tubular system of the fly, on the other hand, is physically separated from the nephrocytes. It presumably works independently of them and is, as in mammals, responsible for osmoregulation and the production of urine, which is then excreted into the intestinal lumen of the fly (Denholm and Skaer, 2009). These so-called Malpighian tubules have been successfully utilized to study conserved transport proteins, ion channels, as well as to model the development and morphogenesis of mammalian renal tubules (Dow and Romero, 2010). Notably, the filtrate of the nephrocytes is not relayed to the Malpighian tubules in any way but stored and metabolized instead (Figure 1.4-1C).

There are two populations of nephrocytes in *Drosophila,* which are immersed in hemolymph, the insect body fluid. These include the mono-nucleated pericardial nephrocytes, located alongside the dorsal heart, and the bi-nucleated garland nephrocytes, mesoderm-derived cells, which are attached to the anterior end of the proventriculus and undergo a fusion event mostly between the embryonic developmental stages 13 and 16 (Zhuang et al., 2009, Figure 1.4-1A and B). During nephrocyte differentiation, the transcription factor Klf15 is indispensable (Ivy et al., 2015), which is also the case in podocyte development (Mallipattu et al., 2012).

1.4.2 The nephrocyte filtration barrier

Nephrocytes are able to accumulate wastes and toxins from the hemolymph in a size- and charge-selective manner (Weavers et al., 2009) and exhibit a filtration barrier reminiscent to the one found in mammalian glomeruli (Figure 1.4-2A and B). Both nephrocyte populations are strategically located next to pulsating organs, effectively increasing hemolymph throughput, thereby improving filtration efficiency. During differentiation, nephrocytes form plasma membrane infoldings, flanked by protrusions resembling podocyte foot processes, which are connected to each other by nephrocyte diaphragms at their peripheral ends (Figure 1.4-2B, cf. Figure 2.4-2G). The thusly created compartment is then further differentiated to a strongly interconnected channel network spanning the cell periphery, maximizing membrane surface area and thereby filtrate endocytosis performance (Figure 1.4-1D, cf. section 2.1.3.4).

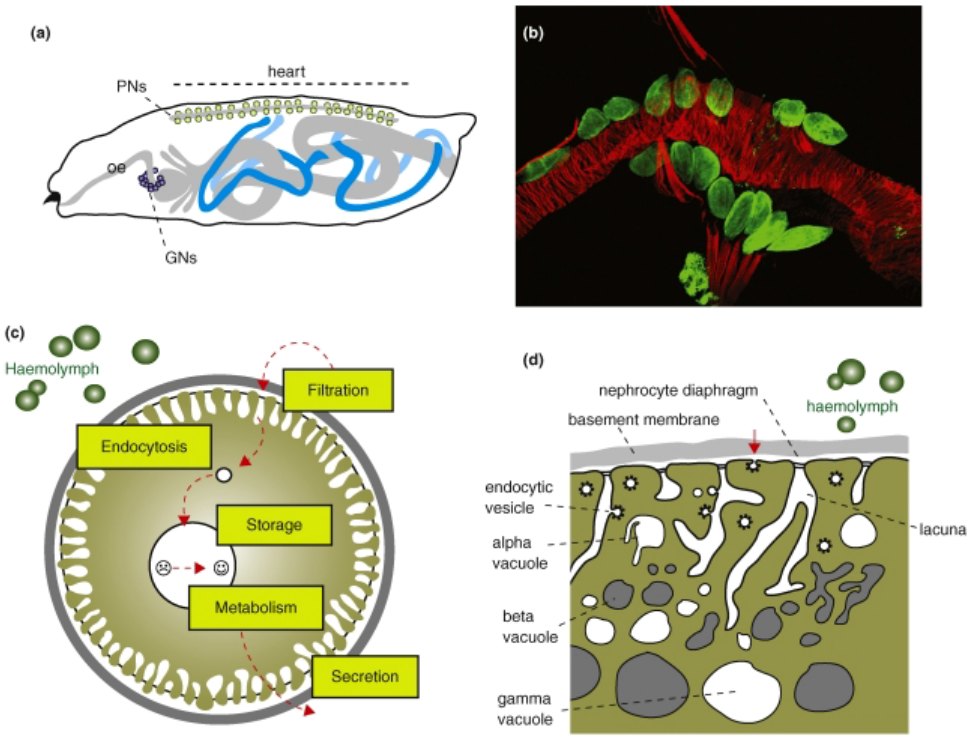

Figure 1.4-1 Location and ultra-structure of *Drosophila* nephrocytes. (A) Schematic drawing showing the position of pericardial nephrocytes (PN), garland nephrocytes (GN) and Malpighian tubules (blue) in the late embryo/larva. The digestive system is depicted in grey. (B) Pericardial nephrocytes from third instar larva (green; stained with anti-Sns antibody) lining the dorsal heart (red; phalloidin staining against actin cytoskeleton). (C) Scheme of nephrocyte describing filtration of hemolymph across filtration barrier. Particles (green spheres) pass the glomerular basement membrane (thick grey line) and the slit diaphragm (thin grey line) and enter the lacunar system. Subsequently, endocytosis takes place (small circle) and the material is metabolized and/or stored (large circle). (D) Detailed depiction of the nephrocyte periphery. Endocytosis takes place inside the lacunae as well as on foot process tips. Located inside the cytoplasm are vacuoles of different type (alpha, beta and gamma). Taken from (Denholm and Skaer, 2009).

On its way into the cell, the first barrier the hemolymph passes, is a basement membrane. It completely surrounds the nephrocyte, contains collagen IV and performs an initial charge- and size-specific selection of the filtered substances (Weavers et al., 2009). The next checkpoint is a nephrocyte diaphragm, which is made up of protein homologs known from the mammalian slit diaphragm (e.g. Nephrin and NEPH1; Figure 1.4-2C), which were shown to be associated with proteinuria and kidney failure in human patients (Kestila et al., 1998; D'Agati et al., 2011). It could further be demonstrated, that the filtration cutoff of the nephrocyte diaphragm is located between 60 and 88 kDa for hemolymph proteins, which is similar to the mammalian slit diaphragm (Hamano et al., 2002; Hermle et al., 2017).

Correct development of the nephrocyte diaphragm is impeded by loss or depletion of Sns and Kirre, the orthologs of the mammalian SD constituents Nephrin and Neph1 (Weavers et al., 2009), which interact in a heterophilic manner (Fischbach et al., 2009) and correct localization of one of them is lost upon reduction of the other (Hermle et al., 2017), leading to phenotypes resembling foot process effacement. Interestingly, agents

known to induce this phenotype, like puromycin aminonucleoside or protamine sulfate, produce similar results in both nephrocytes and podocytes (Tutor et al., 2014; Hermle et al., 2017).

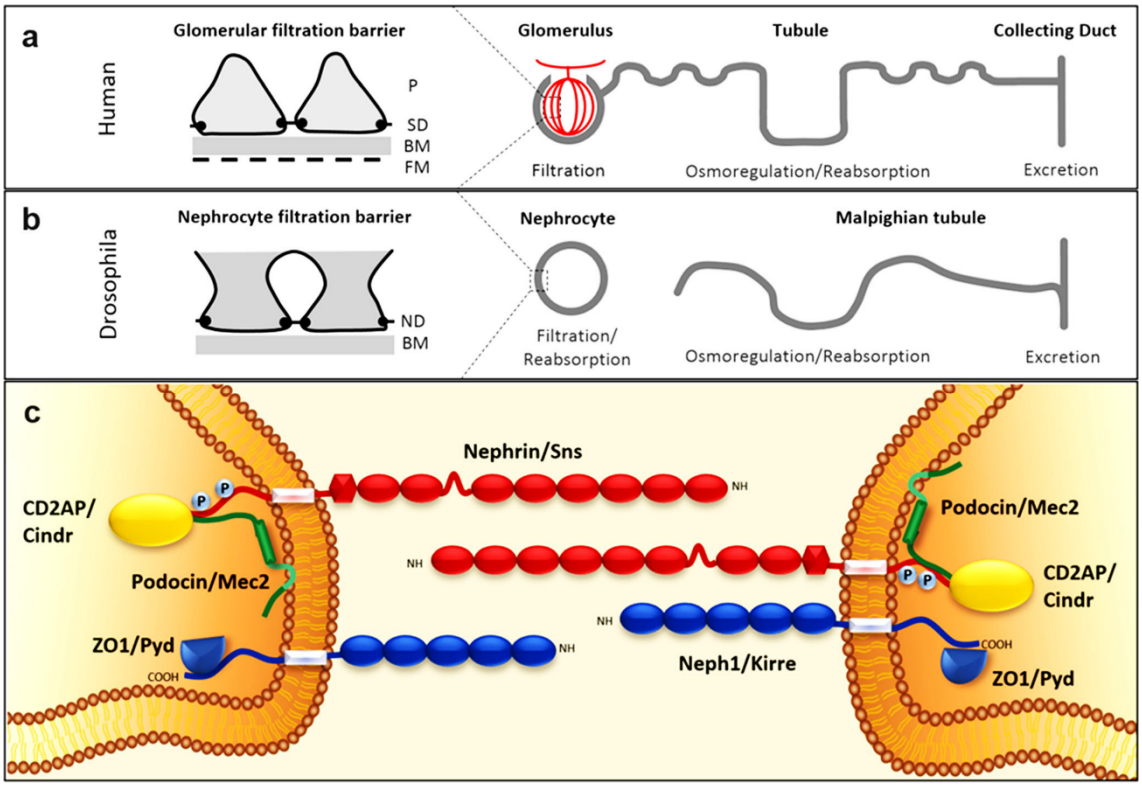

Figure 1.4-2 Schematic comparison of the filtration barrier in mammals and *Drosophila*. (a) Mammalian filtration barrier characterized by three layers: slit diaphragm (SD), glomerular basement membrane (BM) and fenestrated endothelial membrane (FM). On top are two foot processes of two different podocytes (P). After entering the tubule, the filtrate is modified and excreted. (b) Nephrocyte filtration barrier made up of the nephrocyte diaphragm (ND), between adjacent compartments of the cell membrane, and the basement membrane (BM). Filtration and reabsorption are conducted by the nephrocytes, which are spatially separated from the tubular system of the fly. (c) Schematic magnification of the human and the *Drosophila* slit diaphragm with conserved molecular components. Nephrin and Neph1 in the slit diaphragm are homologous to Sns and Kirre. The interacting proteins ZO-1, CD2AP and Podocin do have fly homologs designated Pyd, Cinrd and Mac2, respectively. Taken from Helmstädter and Simons (2017).

1.4.3 Large scale endocytosis as a special means of excretion

Nephrocytes act as storage kidneys by taking up wastes and harmful substances from the hemolymph, thereby modulating its composition and effectively maintaining proper functionality of certain tissues elsewhere in the body (Hartley et al., 2016). By passing the filtration barrier, the primary filtrate enters the labyrinthine channel system. Due to the complex interconnectedness of the lacunae, the surface of the plasma membrane and thus the possible endocytosis performance of the cell is vastly increased. The mechanisms of

uptake have been characterized as dynamin-independent for colloid particles via a Rudhira-dependent macropinocytotic pathway and dynamin-dependent for macromolecules (Das et al., 2008). Based on experiments with dextran tracers, Hermle et al. (2017) suggested a receptor mediated endocytosis rather than fluid-phase endocytosis, since they found both the uptake process to be dose-dependently saturable and exhibiting receptor competition. Depletion of the orthologs of Cubilin and Amnionless, which were previously shown to be necessary for the function of both nephrocyte populations (Zhang et al., 2013a; Gleixner et al., 2014), effectively abolished tracer uptake, indicating a mechanism dependent on a proximal tubule-like Cubilin/Amnionless receptor machinery. Large dextrans (500 kDa), which are not able to pass the filtration barrier, are taken up at a slower rate, presumably at the outer tips of foot processes, and are not affected by protamine sulfate treatment (Hermle et al., 2017).

Following a chronological order, particles taken up from the primary filtrate enter Rab5-positive early endosomes, which are located in a confined peripheral belt in the cytoplasm, and then progress to Rab7-positive late endosomes, before they are finally degraded in lysosomes located in the vicinity of the nucleus (Bechtel et al., 2013; Lőrincz et al., 2016; see also Figure 1.4-3).

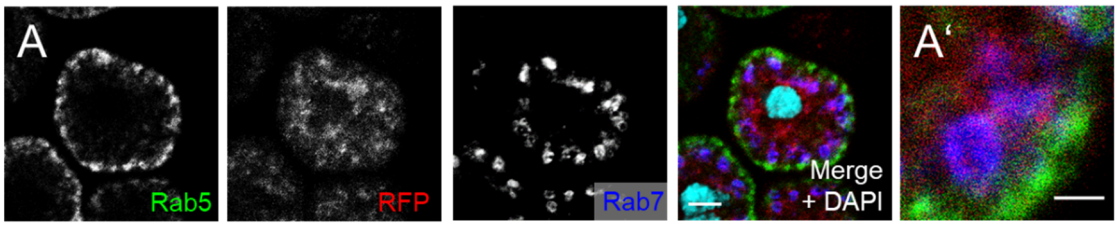

Figure 1.4-3 Immunostaining of garland nephrocytes with characteristic early (Rab5) and late (Rab7) endosomal markers. Secreted RFP-tracer accumulated by control garland nephrocytes both colocalizing with endosomal markers. Scale bars: (a) 5 µm; (a') 1.5 µm. Taken from section 2.4.4.6.

1.4.4 Established nephrocyte essays and read-outs

In recent years, nephrocyte research has made remarkable advances. Several manuscripts were published utilizing tracer-based functional approaches combined with localization studies as well as morphological insights gained from electron microscopy. To characterize nephrocytes of a certain genotype, functional tracer assays offer swift impressions on the overall performance of the cells, regarding filtration and/or endocytosis, hence allowing for screens of large numbers of candidate genes for abnormalities. However, it is necessary to substantiate the available data by more detailed examination of the ultra-structure, to assess diaphragm integrity or foot process effacement.

1.4.4.1 ANP-RFP endogenous tracer assay

In 2013, Zhang et al. published two manuscripts, in which they proposed an *in vivo* functional assay using endogenous tracer expression. Instead of feeding the tracer to the

larvae or injecting it into the body fluid, they induced the tracer synthesis in the myocardial and somatic muscle tissue, as well as its subsequent secretion into the hemolymph. This was facilitated via a transgenic fusion protein, which combines red fluorescent protein (RFP) and atrial natriuretic peptide (ANP) from rat, under the control of the myosin heavy chain (MHC) promoter. In a healthy larva, the secreted fusion protein is endocytosed by both nephrocyte populations, which are then imaged transcutaneously to assess the (Figure 1.4-4B-F'). Depletion of proteins necessary for proper filtration and endocytosis leads to a reduction of fluorophore accumulation in the nephrocytes (Figure 1.4-4G).

For the projects included in this thesis, a similar approach was employed. In contrast to their transcutaneous measurements, we micro-dissected nephrocytes in hemolymph-like medium, to avoid undesirable effects like signal weakening by the larval cuticle or measurement deviations due to undesirable movement, while keeping the cells in a quasi-native environment (cf. section 2.1.3.1).

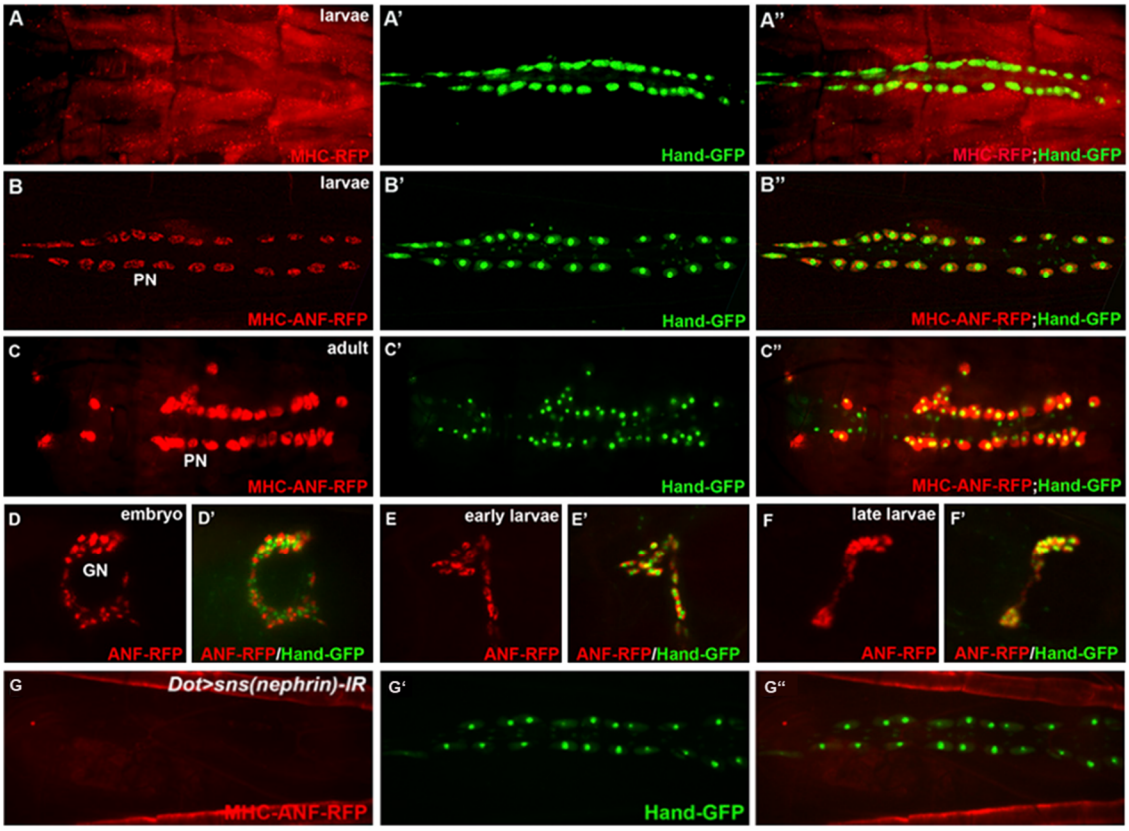

Figure 1.4-4 *Drosophila* nephrocytes take up endogenous fusion proteins after secretion by muscle tissue. (A-B"; G-G") Dorsal view on mid-section of a stage 3 larva. (A-A") MHC-RFP expression restricted to muscle tissue visible in red. Nephrocyte-specific GFP reporter displayed in green. No accumulation of RFP signal in nephrocytes visible. (B-B") Pericardial nephrocytes accumulate secreted MHC-ANP-RFP, co-localization with GFP reporter. (C-C") Same phenotype is visible in adult flies. (D-F') Garland nephrocytes accumulate secreted MHC-ANP-RFP. (G-G") Nephrocyte-specific knockdown of *sns* causing loss of tracer accumulation. ANF: atrial natriuretic factor; RFP: red fluorescent protein; GFP: green fluorescent protein; MHC: myosin heavy chain; Taken from (Zhang et al., 2013b)

1.4.4.2 Ultrastructural assessments of nephrocytes using transmission electron microscopy

The ultrastructure of a cell is inseparably connected to its function. In nephrocytes, morphological properties like an intact labyrinthine channel system or correctly developed diaphragms are paramount to the overall functional capability of the cell. Transmission electron microscopy (TEM) has contributed a great deal of high resolution ultrastructural data to the field, which originally made it possible to identify the similarity to vertebrate podocytes (Weavers et al., 2009). Conventional sample preparation for TEM is a complex process, which involves either chemical or cryo-fixation, dehydration in ethanol or acetone, and finally embedding in a plastic resin. To reduce the formation of artifacts, these profound changes need to be applied to the sample with care (Kellenberger et al., 1992). The published TEM data on nephrocytes are based on chemically fixed samples, which are chemically crosslinked by an aldehyde or a mixture of aldehydes. Depending on the fixation process employed, the fixative reaches some areas of the sample later than others, which may lead to a varying degree of fixation uniformity.

In the last decades, cryofixation emerged as a worthwhile alternative to chemical fixation, offering superior quality of fine structure preservation. With high-pressure freezing (HPF), a biological sample of limited thickness up to approx. 200 µm is frozen with a cryogen at high pressure of around 2048 bar (Studer et al., 2008), physically immobilizing all its contents in milliseconds, regardless of diffusion barriers like cell walls, while simultaneously suppressing a damaging volume increase caused by growing ice crystals (Dubochet, 2007). Depending on the research goal in question, HPF samples can be treated in different ways after cryofixation. During freeze-substitution, the water inside the sample is exchanged with an organic solvent like methanol or acetone at low temperatures between -90 and -78°C, with fixatives already present in the substitution mix. During a gradual warming, the chemical agents in the mixture can evenly distribute throughout the sample and become increasingly chemically active at rising temperatures (McDonald, 1999). Thus, shrinkage known from conventionally fixed specimens is prevented. Possible applications of these techniques on nephrocytes are further discussed in chapter 2.1.

1.5 Research objectives

In this thesis, the suitability of *Drosophila* nephrocytes as a worthwhile approach to research nephropathies is investigated from different perspectives. The fly model offers unique advantages to the vertebrate system and has contributed numerous insights to the big picture of kidney research within the last decade.

For a reliable understanding of the morphology of a certain sample, a fine preservation close to its living state is a mandatory prerequisite. This topic is examined in the first manuscript (chapter 2.1), in which both the importance of a hemolymph-like medium during micro-dissection of nephrocytes and the potential of optimized sample preparation techniques, involving cryofixation and -embedding, are illustrated, leading to a clear increase in ultra-structural preservation. Furthermore, a custom protein localization technique is discussed, involving immunogold detection of a GFP-tag on ultrathin epoxy resin

sections, combining preservation of intricate morphological details with detectable antigenicity. Also, the nephrocyte periphery with its complexly branched lacunae was subjected to STEM-tomography to study its three-dimensional ultrastructure.

In the second manuscript (chapter 2.2), focused ion beam-scanning electron microscopy (FIB-SEM) was used to examine, whether vertebrate podocyte slit diaphragms are assembled between the foot processes of the same or different podocytes. Moreover, high-resolution data was acquired via comparative dual-axis electron tomography of human, mouse podocytes as well as fly nephrocytes, to better understand the fine structure of the diaphragm and its evolutionary similarity across the species.

The third manuscript (chapter 2.3) deals with the role of Pals1 in the nephron, which is of interest, because Pals1-interacting proteins were linked to renal abnormalities in mice before. In this work, it was found that the loss of one Pals1 allele lead to a severe phenotype including cyst formation, an impairment of the filtration barrier and premature death in mice. Here, the fruit-fly model was used to substantiate the evidence: selective knock-down of the Pals1 orthologue (Stardust) lead to similar developmental defects in nephrocytes. Further investigation concentrated on the relation of Pals1 to target genes of Hippo- and TGF-β signaling pathways, suggesting a connection between apicobasal polarity and renal diseases.

Within the last manuscript included into this thesis (chapter 2.4), the role of *Drosophila* Crumbs, a key apicobasal polarity determinant, and its orthologues in cellular morphogenesis, nephrocyte diaphragm development and endocytosis was investigated. Rescue experiments were performed to assess cross-species conservation of the orthologues and specific functions of the different Crumbs protein domains. Interactions with the Hippo pathway could be found, since Crumbs depletion can be partly rescued by simultaneous Moesin overexpression. The extracellular domain of Crumbs, on the other hand, seems to be necessary for the assembly and maintenance of nephrocyte diaphragms.

2 Results

2.1 Electron microscopy of *Drosophila* garland cell nephrocytes: optimal preparation, immunostaining and STEM tomography

Authors
Florian Hochapfel[1,2], Lucia Denk[1], Christine Maaßen[1], Yulia Zaytseva[1], Reinhard Rachel[1], Ralph Witzgall[1] and Michael P. Krahn[1,2*]

Journal
Journal of Cellular Biochemistry

Author Affiliations
[1]Institute for Molecular and Cellular Anatomy, University of Regensburg, Regensburg, Germany;
[2] Medizinische Klinik und Poliklinik D, Universitätsklinikum Münster, Münster, Germany

Accepted for Publication
January 29, 2018.

Contribution
The author of this thesis wrote the manuscript and contributed everything for the project except parts of the TEM data on Drosophila nephrocytes.

2.1.1 Abstract

Due to its structural and molecular similarities to mammalian podocytes, the *Drosophila* nephrocyte emerged as a model system to study podocyte development and associated diseases. Similar to podocytes, nephrocytes establish a slit diaphragm between "foot process-like" structures in order to filtrate the hemolymph. One major obstacle is the distinct visualization of this subcellular structure to assess its integrity.

Therefore, we developed a specialized dissection protocol, including high-pressure freezing and freeze-substitution techniques, to improve the preservation of the intricate ultrastructural details necessary for electron microscopic assessment. By means of scanning transmission electron microscopy (STEM) tomography, a three-dimensional dataset was generated to further understand the complex architecture of the nephrocyte channel system. Moreover, a staining protocol for immunolabeling of ultrathin sections of Epon-embedded nephrocytes is discussed, which allows a reliable detection of GFP-tagged fusion proteins combined with superior sample preservation. Due to the growing number of available GFP-trap fly lines, this approach is widely applicable for high resolution localization studies.

2.1.2 Introduction

In the vertebrate kidney, podocytes play a key role in the formation and the maintenance of the renal filtration barrier. They make up the visceral layer of Bowman's capsule and develop a complex structure of emanating foot processes, which wrap around the glomerular capillaries and interdigitate with foot processes of neighboring cells. These foot processes are connected to each other by slit diaphragms (SD), which form pores of approx. 40 nm diameter (D'Agati et al., 2011; Burghardt et al., 2015). Damage or breakdown of this barrier leads to proteinuria and eventually kidney failure (Patrakka et al., 2000). Nowadays, most *in vivo* studies of podocyte related diseases rely on mammalian models. The preferred model organism to study nephropathies is the mouse. Unfortunately, effective research is currently limited, due to the long generation time of the mice and their comparatively expensive husbandry.

In recent years, the *Drosophila* nephrocyte arose as a model system to study podocyte-related diseases. Even though the excretory system of insects is not organized in functional units like vertebrate nephrons, remarkable similarities in cell morphology and protein expression suggest an evolutionary relation (Weavers et al., 2009; Zhuang et al., 2009). Being physically separated from the Malpighian tubules, which emerge from the insect midgut and play a role in osmoregulation and removal of nitrogenous wastes from the hemolymph (Campbell et al., 2003), two populations of nephrocytes exist. The garland cell nephrocytes (GCN) are located near the esophagus, whereas the pericardial nephrocytes line up alongside the heart. Nephrocytes seem to be important to adjust the contents of the hemolymph by filtration of potentially toxic substances, which are subsequently endocytosed and lifelong stored (Denholm and Skaer, 2009).

During embryogenesis and early larval instar stages, the plasma membrane of nephrocytes invaginates, forming lacunae that are flanked by foot process-like structures, eventually creating a complex channel system. This channel system is separated from the

outside with ~30-nm slit pores equipped with the so called nephrocyte diaphragm, reminiscent of the vertebrate slit diaphragm (SD; Aggarwal and King, 1967). In combination with the basement membrane, which completely surrounds the nephrocyte, the nephrocyte diaphragm constitutes a charge- and size-selective barrier for the filtration of the *Drosophila* hemolymph. After entering the channel system, wastes, proteins and other particles are endocytosed for modification, degradation and/or storage (Denholm and Skaer, 2009).

Recent studies are substantiating the suitability of *Drosophila* nephrocytes as a model for various renal diseases. For steroid-resistant nephrotic syndrome (SRNS), a frequent cause of kidney failure, more than 50 different genes were identified as a monogenetic cause (Lovric et al., 2016; Bierzynska et al., 2017). In extensive studies, *Drosophila* orthologs for these genes were subjected to protein and heavy metal uptake assays, leading to more than 60% of aforementioned genes showing significant functional impairments (Hermle et al., 2017; Fu et al., 2017b). Several studies involved in identification of the corresponding genes employed nephrocyte assays to substantiate their genetic results (Gee et al., 2013; Ashraf et al., 2013; Gee et al., 2015; Lovric et al., 2017). In addition, nephrocytes are suited as a model for diabetic nephropathy. In animals fed high dietary sucrose, nephrocyte function was disrupted and levels of the nephrin ortholog Sns were downregulated (Na et al., 2015). This was shown to be caused by transcriptional downregulation of *sns* caused by a pathway including *Knot*, which is the ortholog of mammalian *EBF2*, which could subsequently be confirmed in mouse models. In sub-Saharan ancestry population, two alleles of the *APOL1* gene increase the risk to develop chronic and end-stage kidney disease, while granting protection against special subsets of African sleeping sickness at the same time (Thomson et al., 2014). *APOL1* was transgenically expressed in *Drosophila* nephrocytes, which is necessary due to low conservation across the animal kingdom and hence lack in most model organisms. It caused abnormal accumulation of hemolymph proteins and cell death in later life, with even stronger phenotypes upon expression of the risk alleles (Kruzel-Davila et al., 2017). The effect increased with age and could be connected to conserved endosomal trafficking processes. The results were later confirmed in mice (Beckerman et al., 2017). Furthermore, the orthologs of Cubilin and Amnionless, whose mutations cause Imerslund-Gräsbeck syndrome, were shown to be expressed in nephrocytes fulfilling similar functions (Zhang et al., 2013a). Lastly, loss of nephrocytes led to cardiomyopathy, which was caused due to increased levels of a secreted protein (SPARC), which is connected to cardiac aging in humans (Hartley et al., 2016).

Compared to mammalian blood, insect hemolymph differs regarding content and function in several aspects. It is not involved in oxygen transport and serves as a sink of considerable amounts of CO_2. The ionic composition of its plasma is highly variable throughout the class of insects (Nation, 2016) and in addition, it acts as a depot for the disaccharide trehalose, the major blood sugar for flight energy in insects (Wyatt, 1957), which is neither synthesized nor stored by vertebrates (Argüelles, 2014). To guarantee optimal sample preservation of *Drosophila* nephrocytes, micro-dissection must be conducted in an environment mimicking the insect hemolymph's osmotic and chemical characteristics. The choice of the initial sample fixation method therefore determines and limits the achievable ultrastructural preservation.

Initially confronted with poor sample preservation, we compared two different dissection salines regarding their capacity to preserve cell ultrastructure in general and the intricate channel network in the cell periphery. Both sample groups were chemically crosslinked using 2% glutardialdehyde prior to dehydration and subsequent embedding in epoxy resin. After optimizing dissection conditions, we investigated the potential of high-pressure freezing (HPF) and freeze-substitution (FS) to further improve our sample preservation. To gain more insight into the three-dimensional properties of the highly branched and complex channel system in the nephrocyte periphery, we employed STEM tomography and created a three-dimensional dataset.

In addition to ultrastructural insights, determination of the distinct localization of certain proteins in nephrocytes contribute valuable information to developmental and disease-related studies. Fluorophores are commonly used as protein markers, but confocal laser microscopy is limited at certain physically determined magnification barriers. For high-resolution applications, immunogold antibody detection in the electron microscope is the method of choice. Unfortunately, many antibodies do not give satisfying results in both, immunolabeling and preservation of ultrastructure. Recently, our group successfully employed an indirect immunodetection approach on sections of larval garland nephrocytes (Hochapfel et al., 2017), using a fly line with a GFP-tagged protein and a commercially available anti-GFP antibody, which has been shown to facilitate reliable detection on epoxy resin, therefore enabling detection of the fusion protein at endogenous expression levels. Considering the rising number of commercially available GFP-trap fly lines (Morin et al., 2001; Kelso et al., 2004; Buszczak et al., 2007; Nagarkar-Jaiswal et al., 2015a; Nagarkar-Jaiswal et al., 2015b; Sarov et al., 2016), a reliable protocol for the immunodetection of GFP-tagged proteins greatly improves our tool box in nephrocyte research.

2.1.3 Results

2.1.3.1 Micro-dissection in hemolymph-like saline increases sample preservation of *Drosophila* garland cell nephrocytes (CGNs) after chemical fixation and microwave assisted embedding

Nephrocytes are part of the insect renal system and regulate hemolymph composition by filtration and subsequent endocytosis. To fulfill their function, the fragile peripheral channel system as well as the abundant cellular compartments corresponding to their high endocytic activity need to be kept in careful balance. For a sensitive analysis of nephrocyte defects, ultrastructural details need to be preserved throughout preparation.

In the third instar larva of *Drosophila*, the GCNs are attached to the anterior end of the proventriculus. Since GCNs are too small for direct manipulation with forceps, the removal of the surrounding digestive tract is the method of choice for preparation. Due to their unique architecture, GCNs are particularly vulnerable to osmotic stress caused by inadequate preparation media, after removal from the larval hemolymph. We compared two different preparation salines and their influence on ultrastructural preservation, followed by glutardialdehyde (GAD) fixation, agarose embedding and automatic microwave tissue processing.

Initially, we conducted the dissection in phosphate buffered saline (PBS), which is widely used during sample preparation for electron microscopy. It is considered isotonic and non-toxic, since it matches the ion concentration and osmolarity of the human body. For preparation of GCNs, however, the use of PBS resulted in poor ultrastructural preservation (Figure 1A). Boundaries and structure of organelles are lost and the intricate channel system in the peripheral area is not clearly distinguishable, suggesting osmotic stress or pH disequilibrium. Borders of vesicles are of ragged quality and their content appears washed out (Figure 1A'). Higher magnification reveals a regular distribution of nephrocyte diaphragms on the outmost edge of the cell and to some extent visible invaginations between foot processes (Figure 1A''; arrows/white asterisks). However, ultrastructural preservation strongly declines further towards the center of the cell. Early endosomes, late endosomes (α-vacuoles) and electron-dense lysosomes (β-vacuoles) cannot be clearly located (Figure 1A' and A'').

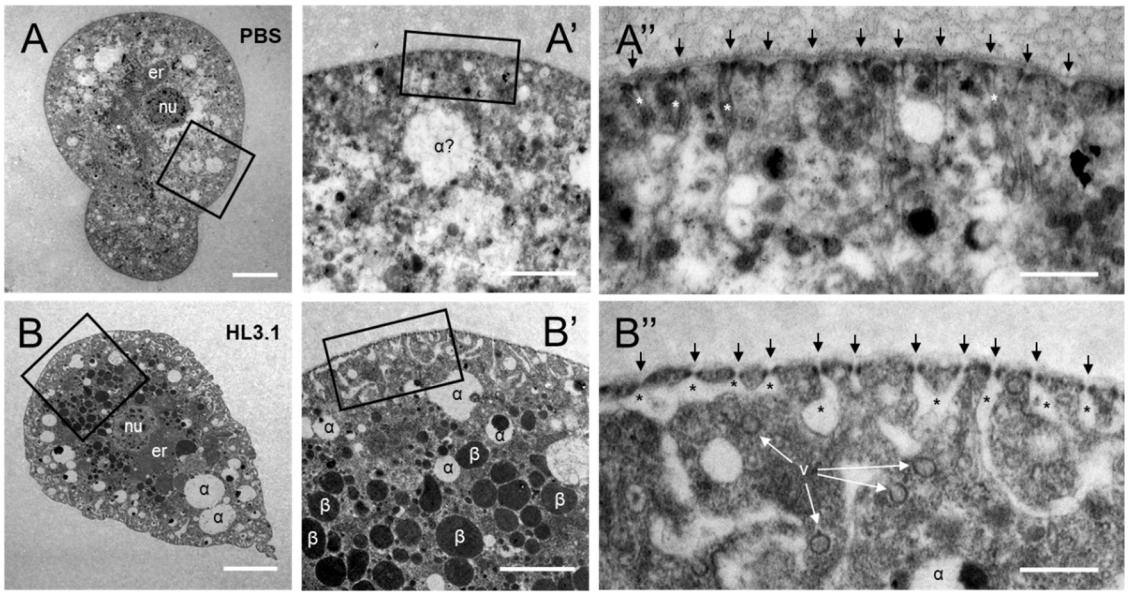

Figure 2.1-1. Micro-dissection in hemolymph like (HL) saline 3.1 improves sample preservation of *Drosophila* garland nephrocytes for electron microscopy preparation. Transmission electron micrographs of wild-type third instar garland nephrocytes dissected in phosphate buffered saline (PBS; A) or hemolymph-like (HL) saline 3.1 (Feng et al., 2004; B), chemically fixed in 2% glutaraldehyde with subsequent microwave-assisted embedding. (A, B) Overview containing nucleus (nu), endoplasmic reticulum (er), as well as bright α-vacuoles (late endosomes). (A', B') Magnification additionally showing electron-dense β-vacuoles (lysosomes). (A'', B'') Higher magnifications showing the periphery with nephrocyte diaphragms (arrows), lacunae/invaginations (*) and vesicles (v). Scale bars: (A, B) 5µm; (A', B') 2µm; (A'', B'') 500 nm.

By performing micro-dissection in HL3.1 saline, which mimics the hemolymph composition of the *Drosophila* larva (Feng et al., 2004), sample preservation could be strongly improved (Figure 2.1-1B). The cytoplasm appears more coherent and membrane compartments are sharper demarcated. In contrast to the PBS preparation, one can easily recognize endosomes and lysosomes (indicated as α- and β-vacuoles). At higher magnification, regularly distributed nephrocyte diaphragms can be observed (Figure 2.1-1B'';

arrows) and the frequent invaginations (black asterisks) between the foot processes can in most cases be easily distinguished from the cytoplasm of the foot processes, in which a high number of vesicles can be observed.

2.1.3.2 High-pressure freezing (HPF) and subsequent freeze-substitution (FS) offers superior sample preservation compared to chemical fixation and microwave assisted embedding

During classical chemical fixation, tissues are, depending on size and organization, immersed in or transfused with a chemical crosslinking agent to immobilize and retain cellular and subcellular structure. Depending on the fixative nature and concentration, as well as the delay until the reactions are completed, the sample may show varying degrees of fixation uniformity. Likewise, for immunodetection the antigenicity of distinct proteins is reduced due to obstructed antibody binding with rising fixation times and increasing amounts of fixative.

Despite the improvements due to the optimized saline, the cytoplasm of the chemically fixed sample appears grainy and details are lost at higher magnifications. Moreover, the membranes are often blurry (Figure 2.1-2B''; white arrowheads) and the content of vesicles do not strongly contrast from the cytoplasm.

To minimize introduction of structural artifacts during preparation and to keep the sample as close to its living state as possible, we employed a combination of HPF/FS. By freezing the sample in only 20 milliseconds at high pressure to -196°C, the containing water turns to amorphous ice without destroying intracellular structures by an increase of volume, or allowing considerable change of the cell contents after the point of dissection.

With this strategy, sample preservation could be strikingly increased. The cryofixed sample appears clear, demonstrating that the nephrocyte cytoplasm harbors many different vesicles with well distinguishable details regarding content density as well as form. Membrane borders are finely demarcated, which can be seen in particular at the edges of the foot processes (Figure 2.1-2B'').

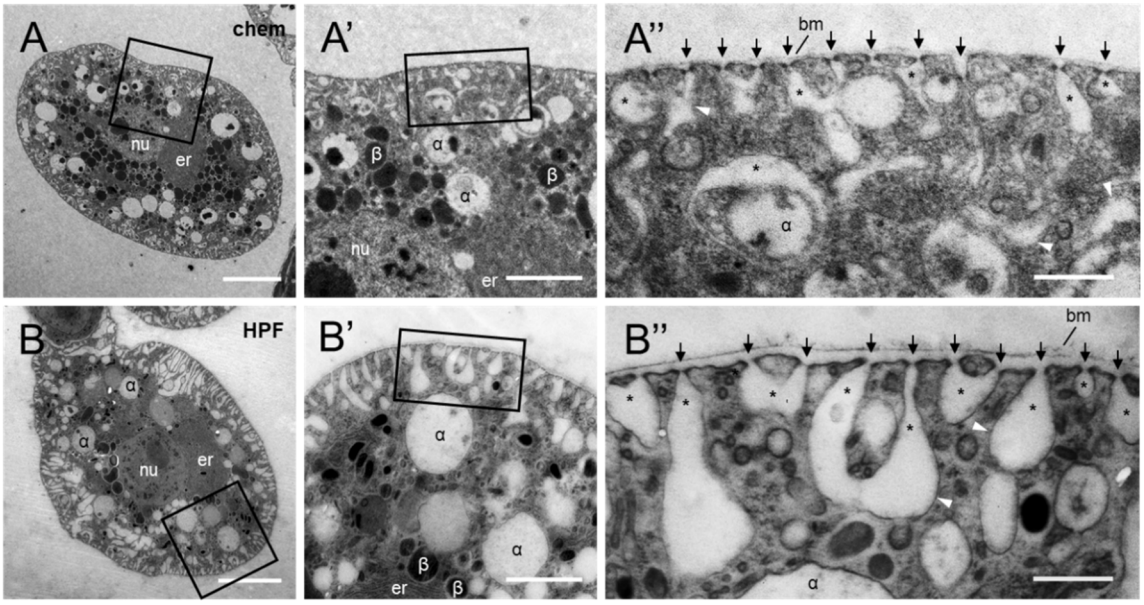

Figure 2.1-2. High-pressure freezing and freeze-substitution further improves sample preservation of *Drosophila* garland nephrocytes compared to chemical fixation and microwave assisted embedding for electron microscopy preparation. Transmission electron micrographs of wild-type third instar garland nephrocytes dissected in hemolymph-like (HL) saline 3.1, chemically fixed in 2% glutaraldehyde with subsequent microwave-assisted embedding (A) compared to high-pressure freezing and freeze-substitution (B). Overview containing nucleus (nu), endoplasmic reticulum (er), as well as bright α-vacuoles (late endosomes). (A', B') Magnification additionally showing electron-dense β-vacuoles (lysosomes). (A'', B'') Higher magnifications showing the periphery with nephrocyte diaphragms (arrows), lacunae/invaginations (*) and the basement membrane (bm). In the cytoplasm, white arrowheads indicate sharply demarcated boundaries around lacunae. Scale bars: (A, B) 5µm; (A', B') 2µm; (A'', B'') 500 nm.

2.1.3.3 STEM tomography of HPF garland nephrocytes offers valuable insights into the 3D structure of the peripheral channel system

Assessing the characteristics of a biological sample by traditional transmission electron microscopy of an ultra-thin section offers high resolution of a flat area, but is associated with a severe loss of information when it comes to objects with complex three-dimensional structures, e.g. the ultrastructural architecture of the nephrocyte channel system. Only examining a thin section makes the resulting shapes and characteristics difficult to interpret.

Taking our previous insights of sample preparation conditions into account, we subjected an 800 nm nephrocyte section to a STEM tomography, and reconstructed the obtained information into a three-dimensional dataset.

With the additional information of multiple layers, one can interpret the progression of shapes along the Z-axis. In Figure 2.1-3C, lacuna 1 and 2 do not seem to be connected. 17 nm further in Z-direction (Figure 2.1-3B), the separation grows faint and additional 25 nm further (Figure 2.1-3A), corridor 1 is fully established, which generates a direct connection between lacuna 1 and 2. Similarly, lacuna 5 is only in Figure 2.1-3A clearly connected to lacuna 4, but disappears in 3B and is no longer detectable in 3C and D. In

the upper half of the area, a quasi-spherical form seems to bud off from lacuna 4 (asterisk). Following the Z-axis by 65 nm, it is clear, that the resulting form is not tube-shaped, but its circumference is reduced to a spot, indicative of a vesicle. Within the range of Fig.3, lacunae 3 and 4 are not connected. Were the observed volume of greater size, a connection could presumably be observed. One round structure (T) can be found in all four Z-layers, which apparently has a tubular structure in the third dimension. Throughout the distance, virtually parallel to the Z-axis, five nephrocyte diaphragms are visible without interruption, indicating an elongated slit, rather than a round filtration "pore".

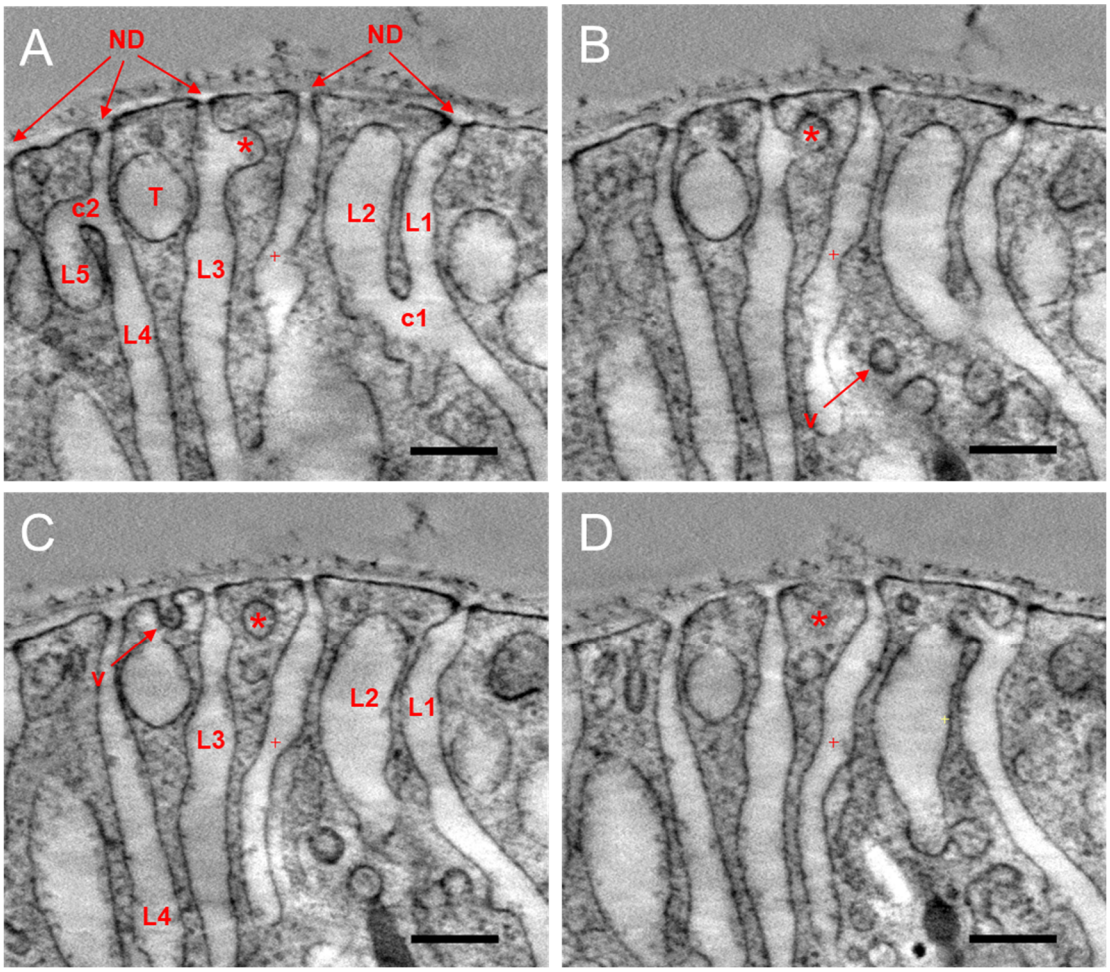

Figure 2.1-3. Multiple sections of a 3D reconstruction provide additional insights into nephrocyte channel system. Successive Z-layers taken from a 3D reconstruction of wild-type third instar garland nephrocytes dissected in HL3.1 saline, high pressure frozen and freeze substituted. Net specimen thickness:700 nm. Reconstructed from STEM tomography recorded in tilt angles from 60° to -60° degrees at 23k magnification. Snapshots taken 81 nm (A), 56 nm (B), 39 nm (C), 16 nm (D) along the Z-axis. Annotated are vesicle pinching off from lacunar space into foot process (*), connections between different lacunae (c1/c2), which are either separate or connected in different Z-layers, different lacunae (L1-5), tube-shaped lacuna (T); vesicle with dark cargo (v) and nephrocyte diaphragms (ND). Scale bars: 300 nm.

The limitations of two-dimensional sections become obvious, when additional 3D data is available. A structure that appears round in a two-dimensional section may belong to

a sphere, a straight tube or the tip of a curve. Subcellular organization in nephrocytes is determined by its high endocytic activity as well as the highly branched lacunar network and is thus very complex and produces a lot of different shapes. Taking a closer look at a large vesicle with electron-dense cargo next to a mitochondrion (Figure 2.1-4A) reveals a round shape in the XY-plane, as well in the XZ-plane, the YZ-section, however, has an elongated shape, demonstrating how incomplete the true shape of a 3D object is portrayed with a two-dimensional section.

Additionally, double secluded vesicles could be observed (Figure 2.1-4B), carrying electron-dense cargo, which is evenly covered by roughly 50nm thick layer of less dense material. The structure begins to appear around 310nm, has its maximum extent around 260nm and begins to exhibit a protrusion around 229nm and 21 nm later, it gets lost except for the narrow tube emerging from the protrusion reaching beyond the dataset. In the range of the dataset, we could also examine several Golgi cisternae and pinching off transport vesicle (Figure 2.1-4C). The trans face of the Golgi apparatus is fused to election dense transport vesicles, which extend towards the lacunae and presumably unload their cargo into the channel system.

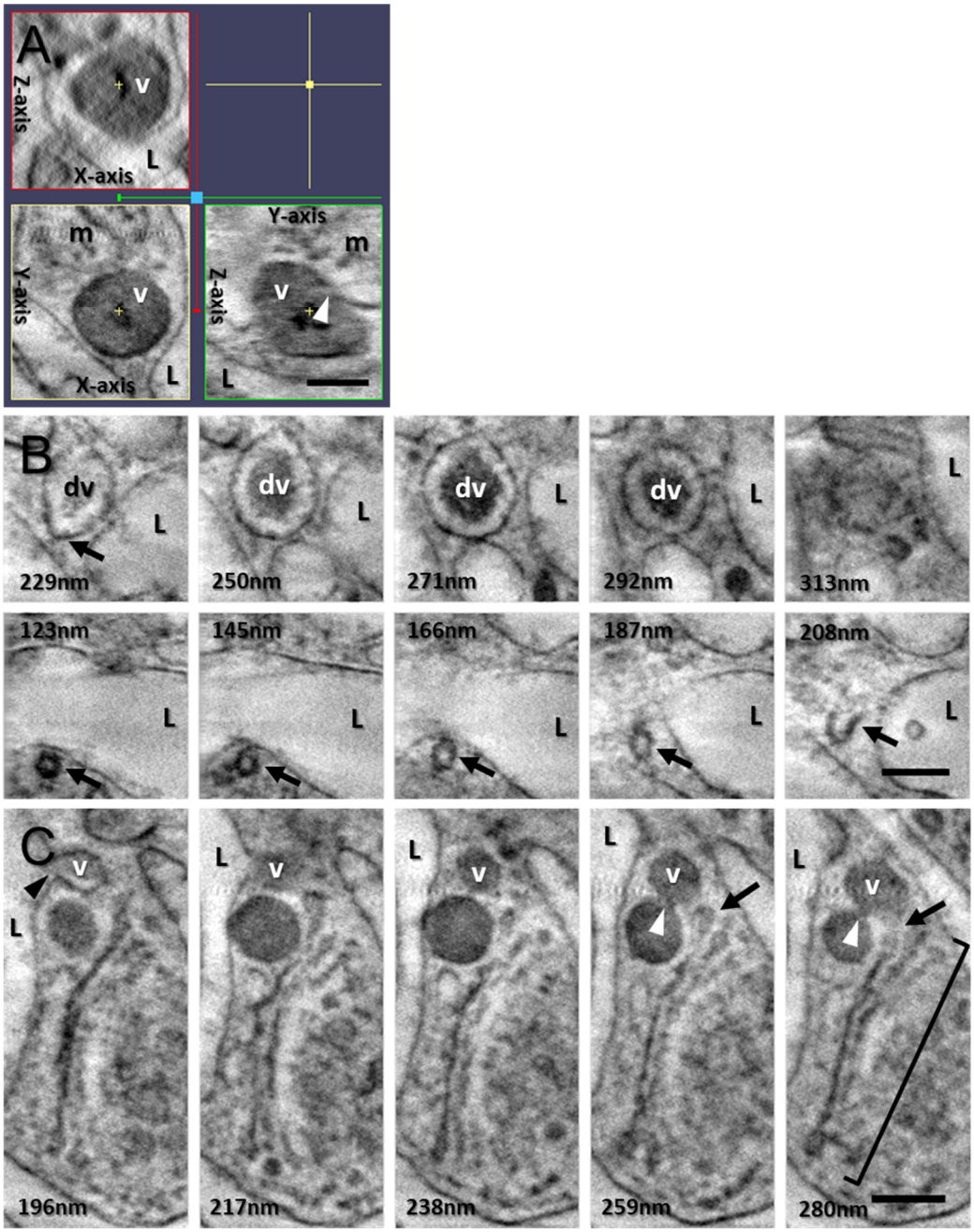

Figure 2.1-4. 3D reconstruction offers unique insights into sub-cellular dynamics of nephrocytes. Successive Z-sections taken from a 3D reconstruction of wild-type third instar garland nephrocytes. (A) Demarcated spheroid vesicle with electron-dense cargo bordering mitochondrion (m), lacunae nearby (L). Actual form depicted in XY-, ZY- and XZ plane aligned to the center of the structure (yellow cross). (B) Double-secluded vesicle (dv) transitioning between 229nm and 208nm into a narrow tube (black arrow) beyond position 123nm until the end of the dataset. (C) Golgi apparatus (black bracket) fused with electron dense transport vesicle (dv) at 280nm, vesicle separated from Golgi cistern at 259nm, connection to other vesicle still intact (white arrowhead), vesicle section appears round along Z-axis until presumptive secretion of content into nearby lacuna (black arrowhead). (B, C) Snapshot Z-distance described in panels. Scale bars: 200 nm.

2.1.3.4 A sectioned 3D model indicates that most lacunae in the periphery of garland nephrocytes are interconnected

To find out, to what extent the different lacunae are interconnected and to get a better overview of the channel system, we manually segmented the reconstructed dataset of the nephrocyte periphery, which resulted in a three-dimensional representation of lacunar space, limited by the cell membrane delineating the cytoplasm of the cell, and the nephrocyte diaphragms on the outer edge facing the extracellular space. Notably, most components of the channel system are interconnected, and lacunar identity is depicted in differently colored materials (Figure 2.1-5). Many lacunae either belong to the blue or the yellow material, whereas in other areas, the interconnection cannot be assessed due to the limited size of the analyzed section (orange, pink and cyan materials). In addition, we marked a mitochondrion (red material) and a cistern of the cell's Golgi apparatus (green material) in the reconstruction. Pockets filled with electron dense material, are signified as black material. Since the cell volume analyzed in the previous paragraph can also be found in Figure 2.1-5, nomenclature is adopted from Figure 2.1-4.

Generally, lacunae are often not tubular, but resemble flat caverns (Figure 2.1-5C), which stretch along the Z-axis and often form a projection of the corresponding nephrocyte diaphragm. The size of the sectioned dataset is sufficient to show that lacunae 3 and 4 are in fact connected to each other (Figure 2.1-5A). Also, the quasi-spherical form budding off from lacuna 4 interestingly spreads out into both directions along the Z-axis (Figure 2.1-5C; asterisk), an insight that could not have been taken from a single ultrathin section. For greater understanding of the sectioned model, see Supplemental Videos 1-3.

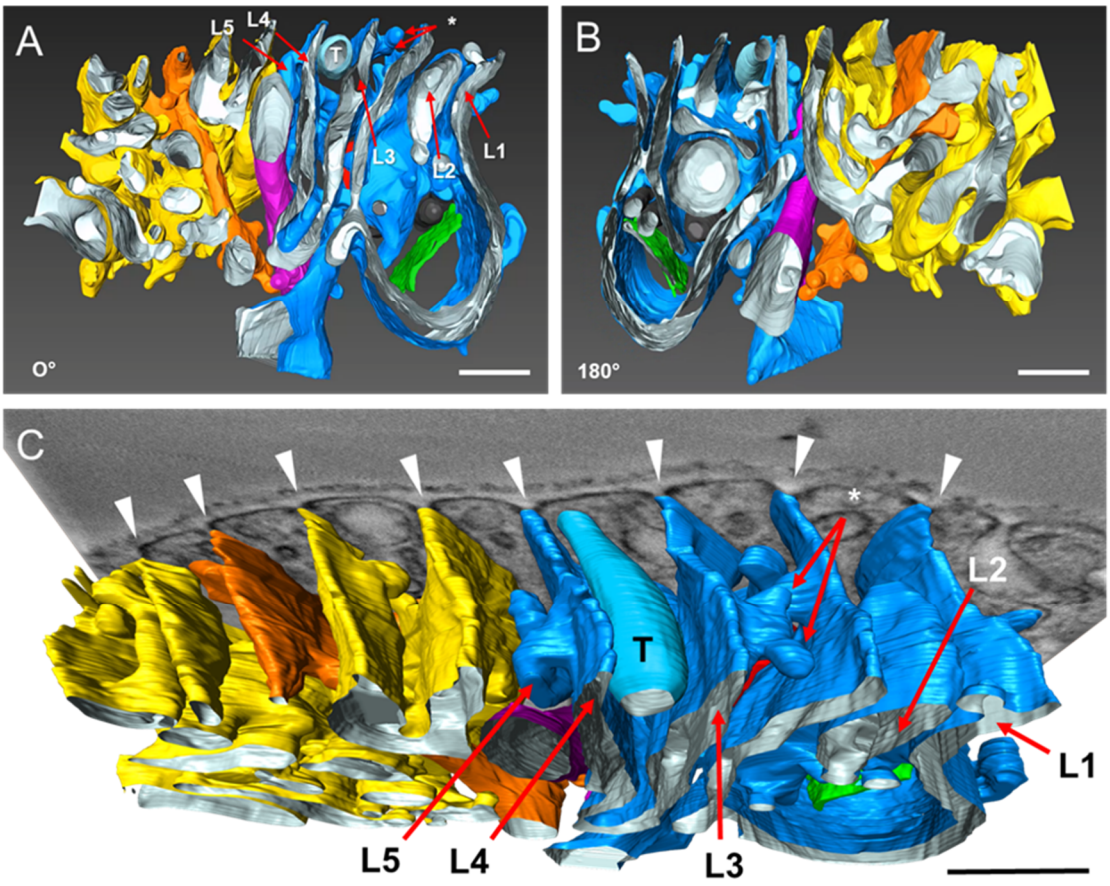

Figure 2.1-5. Sectioned lacunar system from 3D reconstruction of wild-type third instar garland nephrocyte. Three-dimensional model of the lacunar space in the periphery of wild-type third instar garland nephrocytes dissected in HL3.1 saline, high pressure frozen and freeze substituted. Net specimen thickness: 700 nm. Reconstructed from STEM tomography recorded in tilt angles from 60° to -60° degrees at 23k magnification. Color code resembles lacunar identity depending on direct connection or separation. (A, B) Frontal and rear view, with same nomenclature as in Fig.3. Annotated are vesicle pinching off from lacunar space into foot process (*), connections between different lacunae (c1/c2), which are either separate or connected in different Z-layers, different lacunae (L1-5), tube-shaped lacuna (T); vesicle (v) and nephrocyte diaphragms (white arrowheads). Scale bars: 500 nm.

2.1.3.5 Immunostaining of endogenous GFP-tagged Crumbs in epoxy resin

Depending on the nature of the biological sample and the protein of interest, finding a good compromise between ultrastructural preservation and antigenicity for immunodetection can be difficult.

Illustrated with *Drosophila* Crumbs, a transmembrane protein required for epithelial polarity and morphogenesis, we achieved specific protein detection in third instar garland nephrocytes using an indirect approach via a fly line with an EGFP tagged version of Crumbs (Klose et al., 2013) in immuno-electron-microscopy (Hochapfel et al., 2017). Samples were dissected in optimized saline and subsequently cryofixed with HPF/FS. Subsequently, 70nm thick sections were labeled using a goat-α-GFP antibody, which has previously been shown to detect over-expressed GFP on Epon sections (Peschke et al., 2013). Due to the comparably low abundance of the Crumbs fusion protein at endogenous

expression levels, we tested the dilutions 1:20 and 1:100 and 6nm gold rabbit-α- goat IgGs (diluted 1:20).

The results indicate that Crumbs is predominantly localized at the membranes of vesicles and lacunae, as well as near filtration slits (Figure 2.1-6A). Consistently, at a lower antibody concentration, less signal can be detected, which is also mainly located around membranes (Figure 2.1-6B). Unspecific binding of the secondary antibody can be excluded, since there is no signal visible in the negative control (Fig.5C).

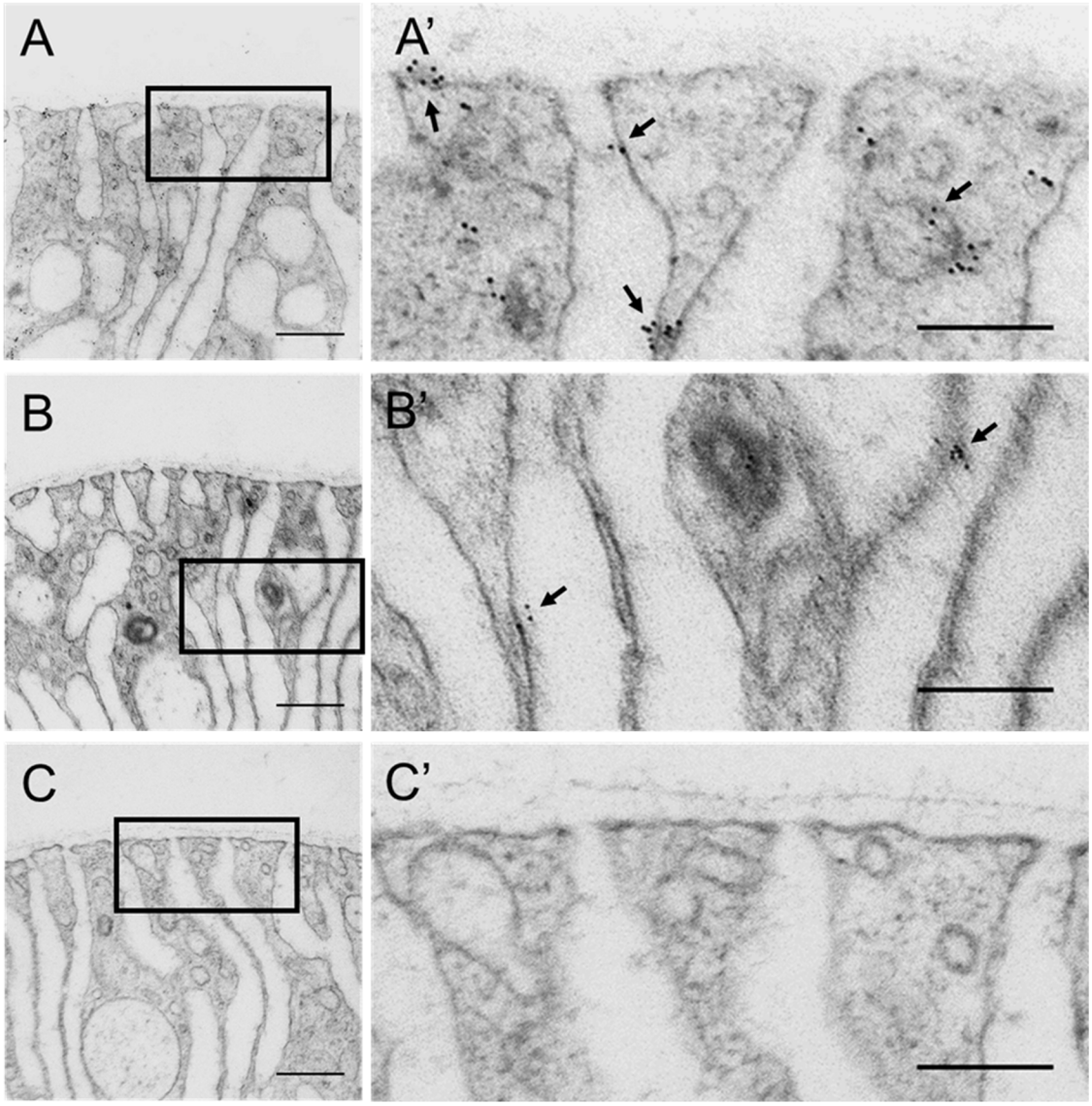

Figure 2.1-6. Immuno labeling of genomic Crumbs-GFP on ultrathin sections of Epon-embedded *Drosophila* nephrocytes. (A-C) Primary AB: goat-anti-GFP in different dilutions. Secondary AB IgG RAG diluted 1:20.; (A) Prim. AB diluted 1:20. (B) Prim. AB diluted 1:100. (C) Secondary AB only. Magnification 50,000x. Scalebar: (A-C) 400nm, (A'-C') 200 nm.

2.1.4 Discussion

In recent years, the *Drosophila* garland nephrocyte turned out to be a valuable model for kidney diseases, both exhibiting characteristics of podocytes and proximal tubular cells (Zhuang et al., 2009; Weavers et al., 2009; Helmstädter et al., 2012; Zhang et al., 2013b; Zhang et al., 2013a; Tutor et al., 2014; Ivy et al., 2015; Na et al., 2015; Kruzel-Davila et al., 2017; Hermle et al., 2017; Fu et al., 2017b; Fu et al., 2017a; Fu et al., 2017c) as well as for endocytosis and vesicle trafficking (Das et al., 2008; Bechtel et al., 2013; Lőrincz et al., 2016; Hochapfel et al., 2017; Fu et al., 2017c). Large parts of the published data are either based on the analysis of subcellular morphology via electron microscopy or localization of proteins, which are homologous to mammalian counterparts involved in important developmental processes or (potentially) connected to diseases. The natural environment of nephrocytes exhibits a composition optimized for the special needs of a small ectothermic flying insect with an open circulatory system. For effective analysis, salines and protocols that are specifically optimized for the organism's characteristics are indispensable to achieve results that closely reflect the *in vivo* situation.

We demonstrated, that the choice of the preparation saline greatly influences the quality of the resulting data. Once removed from the organism, nephrocytes are particularly vulnerable to damage by osmotic stress or altered pH conditions, because their peripheral channel system is openly accessible to the surrounding liquid.

Equally important for sample preparation is the choice of the fixation method. Here we found that cryofixation in combination with freeze-substitution offers superior preservation quality. Within milliseconds, all subcellular structures in the sample are simultaneously immobilized by quickly freezing the cytoplasmic water under conditions inhibiting the formation of disruptive ice crystals. Gentle dehydration and infusion with resin at low temperatures minimizes destabilization of sensitive structures and the introduction of artifacts. Due to the limited size of the specimen carrier, it was not feasible to freeze the whole fly. Thus, the best possible option is an isolated preparation in a *de facto* native environment. Compared to chemical fixation, we demonstrated that HPF/FS preparation is suited to keep *Drosophila* nephrocytes very close to their natural state, increases the level of detail at higher magnifications, permits improved characterization of cytoplasmic structures and membrane structures, allowing for sensitive screens and subsequent characterization of potential disease-associated genes (Burghardt et al., 2015; Hochapfel et al., 2017; Weide et al., 2017).

Cells are three-dimensional objects, so their internal organization can only be fully understood by taking its spatial distribution into account. To gain access to this information, electron tomography (ET) is a resourceful technique. By collecting multiple projections of a static sample from different angles, specialized software can be employed to reconstruct a three-dimensional dataset via mathematical models. To get representative results, the sample needs to be well-preserved and the accumulated electron dose needs to be limited to reduce damage to the sample during repeated exposure (Frank et al., 2002). It turned out that scanning transmission electron microscopy (STEM) is the method of choice for tomography of thick specimens at relatively low induction of unnecessary damage (Aoyama et al., 2008). Unlike conventional transmission electron microscopy (CTEM), in which the electron beam evenly passes through the entire observed

area of the specimen, effectively limiting the sample thickness to around 300 nm, STEM uses a focused electron beam, which scans the specimen line by line along a rectangular grid. This permits ET of 1µm thick samples, even though the electron beam must pass through almost twice this distance at high tilt angles.

Existing literature on nephrocytes or homologous cells mainly relies on two-dimensional CTEM imaging or SEM. Tomography has been conducted by the team of Kokkinopoulou et al. (2014), who created a segmented CTEM tomography of chemically fixed rhogocytes from the red-blooded freshwater snail *Biomphalaria glabrata,* and by Burghardt et al. (2015), who prepared *Drosophila* nephrocytes with cryofixation and freeze-substitution and performed a segmented CTEM tomography as well. The datasets of both groups were around 200-300 nm thick. To our knowledge, we created the first STEM tomography of a *Drosophila* nephrocyte, prepared with optimal techniques. Due to the high sample thickness, we could demonstrate, that most of the lacunae within reach of the dataset were interconnected, and provided an insight to the complex organization of the nephrocyte periphery.

In future studies, however, a 3D model of a complete nephrocyte should be generated, to fully understand nephrocyte organization. Even though the maximum sample thickness for a STEM tomography surpasses that of a CTEM setup, this is still not sufficient to cover a whole nephrocyte with a usual diameter of approximately 20 µm. In general, a 3D model of thicker samples can be created by reconstructed serial sections of resin-embedded samples. Here, the resolution in Z-direction is limited by the mean thickness of the single sections. By utilizing focused ion beam-scanning electron microscopy (FIB-SEM), this can be facilitated at higher resolutions.

Depending on the nature of the biological sample, finding a good compromise between ultrastructural preservation and antigenicity for immunodetection can be difficult. In comparison to acrylic resins like Lowicryl or LR-White, epoxy resins offer superior preservation of ultrastructural details but lower antigenicity. In the past, we were not able to directly detect the polarity protein Crumbs in Epon-embedded samples using an anti-Crumbs antibody (data not shown). Indirect detection using Crumbs-GFP expressed under the endogenous promoter, however, could be successfully achieved. In view of the abundance of GFP-fusion proteins (Morin et al., 2001; Kelso et al., 2004; Buszczak et al., 2007; Nagarkar-Jaiswal et al., 2015a; Nagarkar-Jaiswal et al., 2015b; Sarov et al., 2016), the described standardized detection method can be employed to detect a whole list of proteins of interest, e.g. to examine the specific nature of the different vesicle types observed in the nephrocyte cytoplasm. Immunostainings could be performed, regarding vesicle coatings, e.g. caveolin stainings, or concerning vesicle cargo, e.g. glycocalyx material transported to and secreted at the outer cell membrane. Moreover, crossing in GFP-labelled transgenes (e.g. slit diaphragm markers) into mutant alleles provides a valuable tool to investigate defects (e.g. of the slit diaphragms or foot-processes architecture) on an ultrastructural level.

2.1.5 Materials and Methods

2.1.5.1 *Drosophila* stocks and genetics

Fly stocks were cultured on standard cornmeal agar food and maintained at 25°C.

2.1.5.2 Sample preparation for electron microscopy

For ultrastructural studies in microwave processed tissue, garland cell nephrocytes from wandering third instar larvae were micro-dissected in PBS or HL3.1 saline (70mM NaCl, 5mM KCl, 10mM $NaHCO_3$, 1.5mM $CaCl_2$, 4mM $MgCl_2$, 115 mM Sucrose, 5mM Trahalose, 5mM HEPES, pH 7.1; Feng et al., 2004), chemically fixed for 1h in 2% glutardialdehyde in the respective buffer, and subsequently processed with acetone / 0.5% OsO_4, embedded and polymerized in Epon (EM AMW, Leica, Wetzlar, Germany). Alternatively, dissected nephrocytes were high pressure frozen (EM-PACT2, Leica, Wetzlar, Germany), freeze-substituted in acetone / 2% OsO_4 / 5% H_2O / 0.25% uranyl acetate (AFS2, Leica, Wetzlar, Germany) and embedded in Epon. After polymerization, 70nm thick sections were cut using a diamond knife (Diatome, Biel, Switzerland) with an ultramicrotome (Leica UC6 or UC7, Wetzlar, Germany). For tilt series, 800nm thick HPF/FS sections were used.

2.1.5.3 Transmission electron microscopy and tomography

Transmission electron microscopy (TEM) was performed with an 80 kV TEM-902 microscope (ZEISS, Jena, Germany) equipped with a cooled CCD digital camera (TRS Tröndle Restlichtverstärkersysteme). Tilt series were taken on a JEM-2100F transmission electron microscope (JEOL Ltd., Tokyo, Japan) operating at 200 kV with a nominal magnification of 23k. Digital images were acquired using a TVIPS F416 CMOS camera with an effective pixel size of 0.54nm. The series were recorded from -66° to +66° with an angular increment of 1°. The 3D reconstructions were performed using IMOD (Kremer et al., 1996). Images were pre-processed, binned and aligned using randomly distributed 10 nm gold particles as fiducial markers. The generation of tomograms was performed by the simultaneous iterative reconstruction technique (SIRT). Lacunae and cell organelles were outlined and color-coded for each Z-layer using AMIRA 5.6 (Visage Imaging, Berlin, Germany). The final 3D model was smoothened, to reduce the ridges between the individual sections and supplemental videos were created using the movie maker feature.

2.1.5.4 Immunostaining

The immunogold labeling technique was derived from Rachel et al. (2010). Micro-dissected nephrocytes were high pressure frozen (EM-PACT2, Leica, Wetzlar, Germany), freeze substituted in acetone / 0.2% OsO_4 / 5% H_2O / 0.25% uranyl acetate and embedded in Epon. Grids with fresh 70nm sections were incubated stepwise on drops of different solutions on the surface of parafilm. The antibody solutions were always prepared freshly. The GFP fusion protein was stained using the primary antibody goat-α-GFP (1:20, 600-101-215, Rockland) and a 6-nm gold-coupled secondary rabbit-α-goat IgG (1:20, AU25224, Aurion). Each was incubated for 30 min. As a negative control, additional ultrathin sections were treated with PBS-BSA 0.1 % as a substitute for the primary

antibody. Stained sections were imaged with a TEM-902 transmission electron microscope (ZEISS, Jena, Germany) operating at 80 kV.

2.1.6 Acknowledgements

This work was supported by grants of the DFG to M. P. K. (DFG3901/1-2, SFB699-A13).

2.2 Advanced electron microscopic techniques provide a deeper insight into the peculiar features of podocytes

Authors
Tillmann Burghardt[1], Florian Hochapfel[1], Benjamin Salecker[1], Christine Meese[1], Hermann-Josef Gröne[2], Reinhard Rachel[3], Gerhard Wanner[3], Michael P. Krahn[1], Ralph Witzgall[1]

Journal
American Journal of Physiology - Renal Physiology Published 15 December 2015 Vol. 309 no. 12, F1082-F1089 DOI: 10.1152/ajprenal.00338.2015

Author Affiliations
1. Institute for Molecular and Cellular Anatomy, University of Regensburg, Regensburg, Germany
2. Division of Cellular and Molecular Pathology, German Cancer Research Center, Heidelberg, Germany
3. Center of Electron Microscopy, Faculty of Biology and Preclinical Medicine, University of Regensburg, Regensburg, Germany
4. Department of Botany, Ludwig Maximilians-Universität, Munich, Germany

Accepted for Publication
September 17, 2015.

Contribution
The author of this thesis performed the experiments necessary to generate TEM data obtained from *Drosophila* nephrocytes, including fly husbandry, micro-dissection of nephrocytes and resin ultrathin sectioning. The author also contributed text passages concerning nephrocyte data in the methods section and edited the manuscript.

2.2.1 Abstract

Podocytes constitute the outer layer of the glomerular filtration barrier, where they form an intricate network of interdigitating foot processes which are connected by slit diaphragms. A hitherto unanswered puzzle concerns the question of whether slit diaphragms are established between foot processes of the same podocyte or between foot processes of different podocytes. By employing focused ion beam-scanning electron microscopy (FIB-SEM), we provide unequivocal evidence that slit diaphragms are formed between foot processes of different podocytes. We extended our investigations of the filtration slit by using dual-axis electron tomography of human and mouse podocytes as well as of *Drosophila melanogaster* nephrocytes. Using this technique, we not only find a single slit diaphragm which spans the filtration slit around the whole periphery of the foot processes but additional punctate filamentous contacts between adjacent foot processes. Future work will be necessary to determine the proteins constituting the two types of cell-cell contacts.

2.2.2 Introduction

Podocytes represent the outermost cell layer of the glomerular filtration barrier. Based on results obtained with conventional imaging techniques, the current model pictures the podocyte cell body as floating in Bowman's space while being anchored to the glomerular basement membrane via its arborizing cellular extensions. The finest branches, the foot processes, are arranged in an interdigitating pattern on the outer surface of the basement membrane (Rodewald and Karnovsky, 1974). Neighboring foot processes are connected by a slit diaphragm which supposedly contains the integral membrane proteins nephrin, Neph1, FAT-1, and P-cadherin. These proteins are linked to the actin cytoskeleton through the adapter proteins podocin, CD2AP, and zonula occludens (ZO)-1 (Tryggvason et al., 2006). It has been suggested that the urinary space between the podocyte and the glomerular basement membrane, the subpodocyte space, impedes the flow of the primary filtrate into Bowman's space and that therefore the subpodocyte space contributes to the filtration properties of the renal glomerulus (Neal et al., 2005; Neal et al., 2007; Salmon et al., 2007). Hereditary and acquired podocytopathies lead to the destruction of the intricate cytoarchitecture of podocytes and consequently to a failure of the renal filter. The hallmark of such podocytopathies is the disappearance of foot processes and ultimately a detachment of affected podocytes into the urine, thus causing albuminuria (Shankland, 2006; Kriz et al., 2013).

The current view on the structural basis of the renal filtration barrier was derived from classic transmission and scanning electron microscopy. While these techniques have provided valuable information, they also suffer from intrinsic limitations and therefore leave open fundamental questions: 1) What is the dimension of a single podocyte? 2) How are podocytes arranged on the glomerular basement membrane? and 3) Does a podocyte form slit diaphragms between its own foot processes? To answer these questions, we applied novel electron microscopic techniques, i.e., focused ion beam-scanning electron microscopy and dual-axis electron tomography, to podocytes from several species. This made it possible to obtain detailed information on the spatial arrangement of

an entire podocyte in its intact environment including visualization of the subpodocyte space.

2.2.3 Materials and methods

2.2.3.1 Scanning electron microscopy.

Preparation of the kidneys for scanning electron microscopy was done according to Tanaka et al. (1989) with modifications. Mice were perfusion-fixed with 4% paraformaldehyde/1× PBS through the distal abdominal aorta for 3 min. Kidneys were cut in half and incubated for 2 h in 2% glutaraldehyde/0.1 M Na cacodylate, pH 7.4, followed by overnight impregnation in 30% dimethylformamide at 4°C. Freeze fracturing was performed with a cold knife under liquid nitrogen followed by immersion in dimethylformamide at room temperature for 2 h. Finally, image data were acquired on a Zeiss LEO 1530 Gemini scanning electron microscope using the SE2 detector (Carl Zeiss Microscopy, Oberkochen, Germany).

2.2.3.2 Focused ion beam-scanning electron microscopy.

Perfusion-fixation of adult mice was done as described for scanning electron microscopy. Kidneys were stored at 4°C in 2% glutaraldehyde/0.1 M Na cacodylate, pH 7.4, overnight. Then, the tissues were incubated with 0.1 M cacodylate-buffered 1% OsO_4 for 4 h, followed by dehydration in an ethanol series at room temperature and Epon embedding.

Acquisition of tomographic data sets was performed on a Zeiss Auriga 60 dual-beam workstation (Carl Zeiss Microscopy). Slicing of the Epon block was set to a step size of 15 nm and a focused ion beam milling current of 1 nA with a Ga-emitter voltage at 30 kV. Scanning electron microscopic data were recorded in the high-current mode at 1.5 kV of the in-lens EsB detector with an aperture of 60 µm. The dimensions of the recorded images were 2,048 × 1,536 pixels, with a pixel size of 15 nm. The slice and view process was repeated 1,652 times to obtain the 3-dimensional dataset. Raw data were binned and aligned using the open source software package ImageJ (Schneider et al., 2012). Segmentation was performed manually using AMIRA (Visage Imaging, Berlin, Germany). The segmentation was smoothened by applying the "smooth labels" feature in the Label Field. One kidney was chosen for further analysis.

2.2.3.3 Tissue preparation.

Perfusion fixation of murine kidneys was performed as described above. Mouse kidney biopsies were high pressure frozen (EM-PACT2, Leica, Wetzlar, Germany) and freeze-substituted in acetone/2% OsO_4/5% H_2O/0.25% uranyl acetate (AFS2, Leica). Finally, samples were embedded in Epon. Fine needle biopsies of human kidneys were fixed with 4% buffered formaldehyde and embedded in Araldite R. Stocks of *Drosophila melanogaster* were cultured on standard cornmeal agar and maintained at 25°C. Garland nephrocytes from wandering third instar larvae were microdissected in HL3.1 saline, high-pressure frozen, freeze-substituted, and embedded in Epon. Treatment of mice was conducted in accordance with the German Animal Protection Law and was approved by the local

government. The use of human kidney biopsies was approved by the ethics committee of the University of Heidelberg.

2.2.3.4 Electron tomography.

For the tilt series, 200- to 300-nm thick sections were cut using a diamond knife (Diatome, Biel, Switzerland) with an ultramicrotome (UC6 or UC7, Leica). The thickness of the sections was determined on the reconstructed three-dimensional volume (see below). The tilt series was recorded on a JEM-2100F transmission electron microscope (JEOL, Tokyo, Japan) operating at 200 kV with a nominal magnification of 20,000. Digital images were collected by a TVIPS F416 CMOS camera with an effective pixel size of 0.54 nm. The tilt series was recorded from $-65°$ to $+65°$ with an angular increment of $1°$. The three-dimensional reconstructions were calculated using IMOD (Kremer et al., 1996). Images were preprocessed, binned, and aligned using randomly distributed 10-nm gold particles as fiducial markers. The generation of tomograms was performed by the simultaneous iterative reconstruction technique (SIRT).

2.2.4 Results

2.2.4.1 Foot processes of the same podocyte do not interdigitate with each other.

A regular scanning electron micrograph of a murine glomerulus shows the fine interdigitating foot processes of podocytes (Figure 2.3-1). From these pictures, however, it is impossible to determine whether foot processes of the same podocyte interact with each other. To answer this long-standing question, we decided to reconstruct a complete murine podocyte based on focused ion beam-scanning electron microscopy (FIB-SEM). In FIB-SEM, a gallium beam mills off 10- to 20-nm-thick layers of a plastic-embedded tissue sample, which is followed by scanning electron microscopy of the surface after each round of milling.

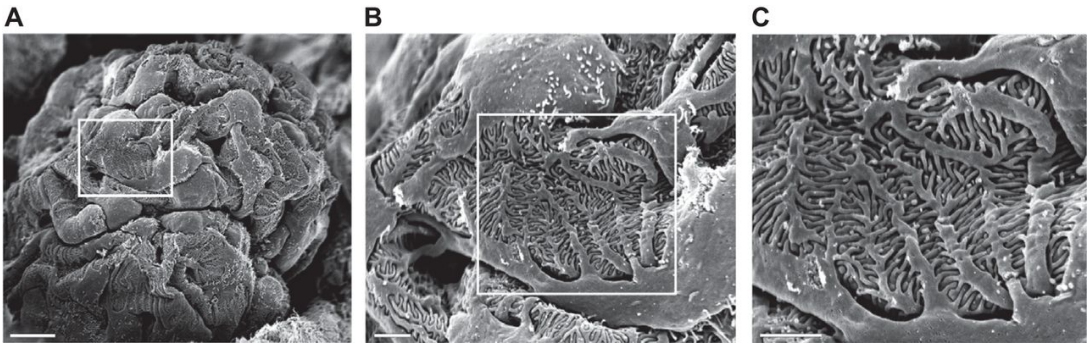

Figure 2.2-1 Scanning electron micrograph of a normal glomerulus. The micrograph was taken from the glomerulus of a 3-mo-old C57BL/6 mouse. It shows the intricate pattern of podocyte

processes and illustrates that it is impossible by this technique to determine whether foot processes of the same podocyte do or do not interact with each other. Bars = 10 µm (*A*) and 2 µm (*B* and *C*).

This way, large *z*-stacks of the desired objects can be created. In our analysis of a murine podocyte, we have created a 29.6 × 22.3 × 24.0-µm three-dimensional stack at 15-nm intervals. In portraying our results, we define primary processes as branches originating directly from the podocyte cell body without interdigitating with other processes, secondary processes as branches originating from primary processes without interdigitating with other processes, tertiary processes as branches originating from secondary processes without interdigitating with other processes, and foot processes as protrusions interdigitating with other foot processes (Figure 2.2-1). Foot processes may originate from all kinds of other processes and even from the cell body (Figure 2.2-2). The podocyte at the center of our 3-dimensional analysis elaborates 12 primary processes and 44 secondary processes; it spreads out over several capillaries (Figure 2.2-2 and Figure 2.2-3).

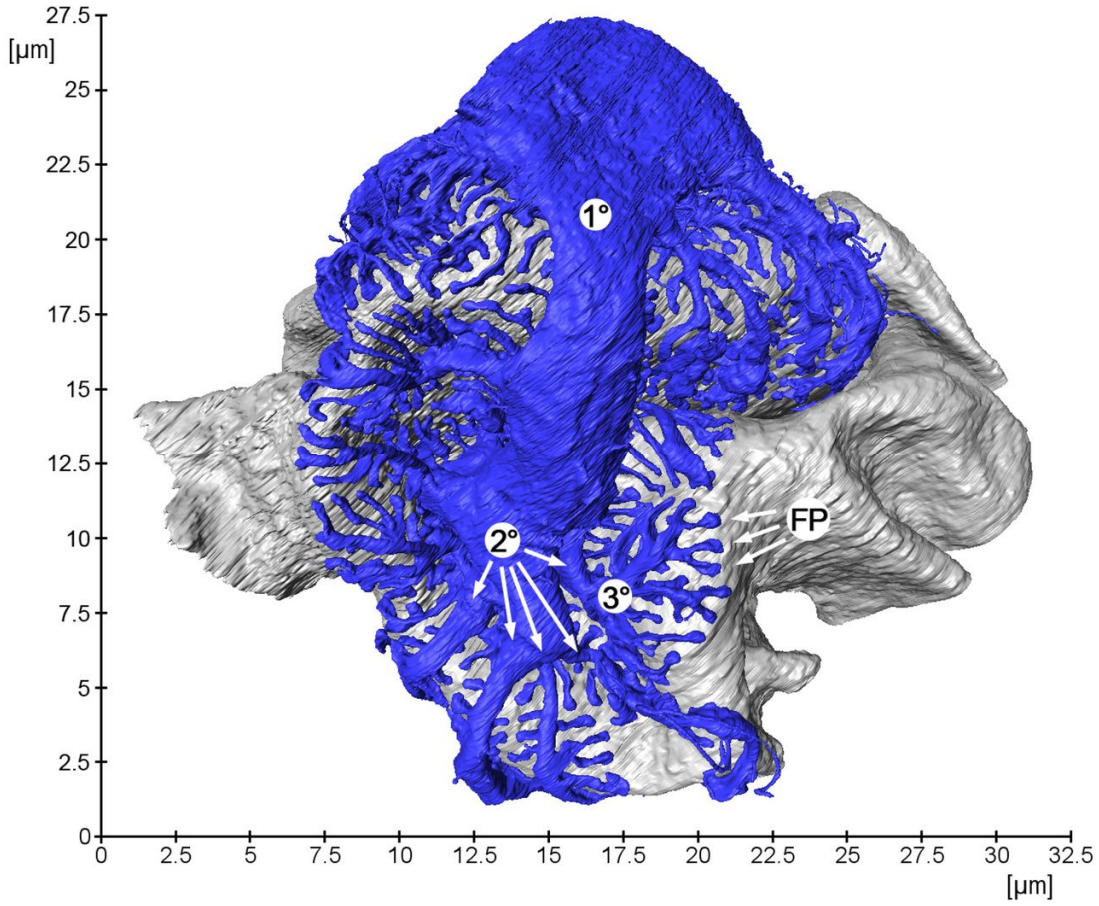

Figure 2.2-2 Three-dimensional reconstruction of a murine podocyte. On this side of the reconstructed cell, the primary (1°), secondary (2°), tertiary (3°), and foot processes (FP) can be seen. The capillaries are shown in grey.

The space between podocytes and the underlying glomerular basement membrane, i.e., the subpodocyte space, has gained recent attention because it may represent an

additional mechanism regulating the flow of the primary filtrate (Neal et al., 2007; Salmon et al., 2007). Our three-dimensional reconstruction shows an elaborate labyrinth below the podocyte cell body (Figure 2.2-4*A*) with narrow exit sites flanked by the cell body and the adjacent processes (Figure 2.2-4, *B–D*). As has been suggested before by conventional transmission electron microscopy, the cell body of the podocyte does not sit broadly on the glomerular basement membrane.

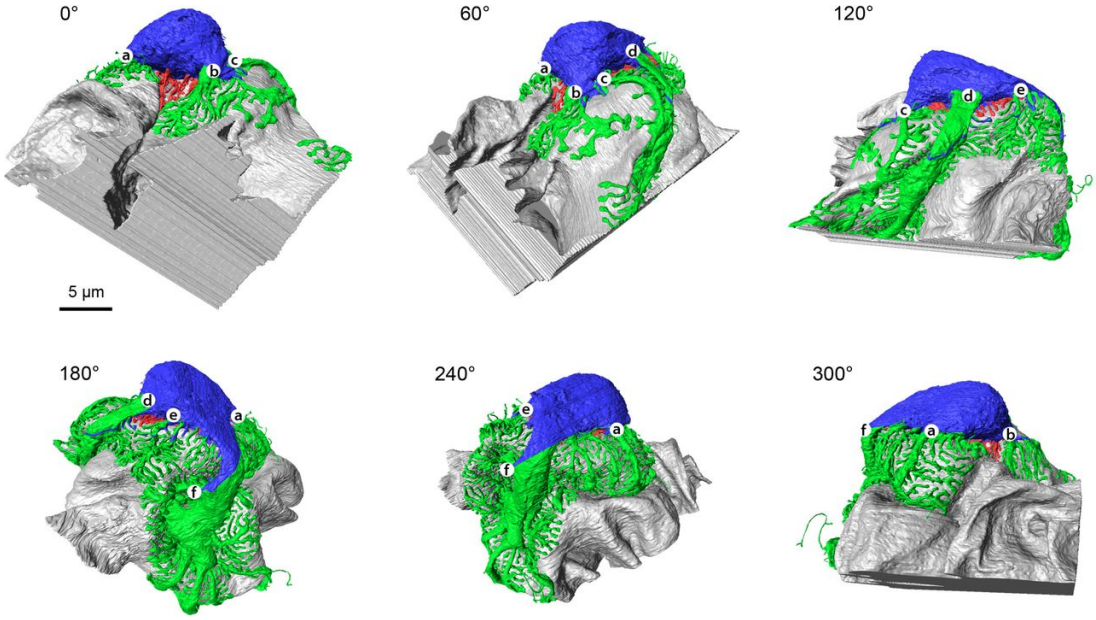

Figure 2.2-3 Three-dimensional reconstruction of a murine podocyte. The same podocyte as in Fig. 2 is shown. It was rotated in 60° intervals to better demonstrate its extensive processes. The cell body is shown in blue, processes extending sideways in green, and processes extending from the basal surface of the cell body in red; the capillaries are shown in grey. The letters *a–f* were inserted for better orientation and do not reflect the processes.

However, contrary to what has been called the freely floating cell body of the podocyte, we detected a number of processes extending directly from the basal surface, thus anchoring the podocyte cell body to the glomerular basement membrane (Figure 2.2-4*A*). Furthermore, the major processes are also anchored to the basement membrane. When viewed from the glomerular basement membrane, we were able to see the ridge-like prominences which have recently been described in rat podocytes (Ichimura et al., 2015). These ridges lie in an intimate spatial relationship with the glomerular basement membrane and may help to anchor the major processes to the extracellular matrix (Figure 2.2-4, *E–H*).

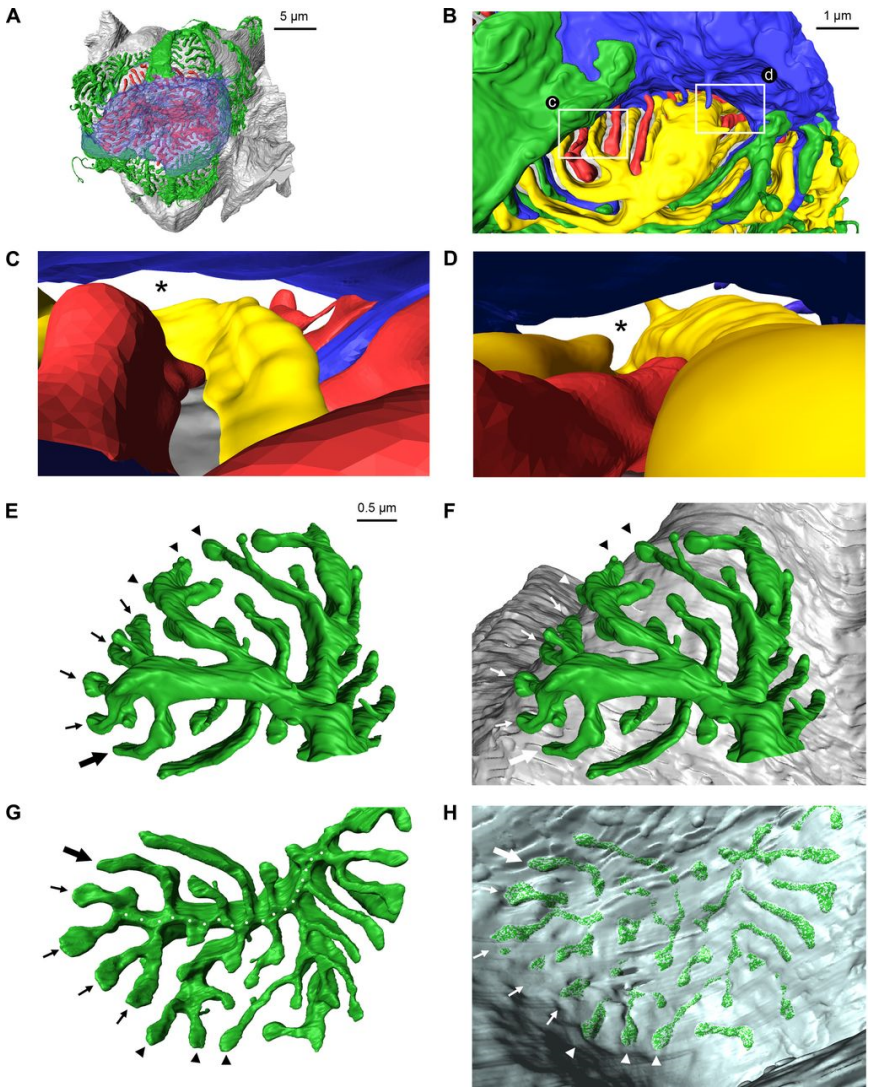

Figure 2.2-4 Illustration of the subpodocyte space and of the ridge-like prominences. The same podocyte as in Figure 2.2-2 is shown. Its cell body is shown in blue, processes extending sideways in green, and processes extending from the basal surface of the cell body in red; the capillaries are shown in grey. *A*: *top* view of the podocyte with the cell body made semitransparent demonstrates the many processes extending from the basal side of the cell body to the glomerular basement membrane. *B*: a second podocyte shown in yellow is added (view from Bowman's space). White rectangles indicate the exit sites from the subpodocyte space, which are shown as *c* and *d*. *C* and *D*: view from the subpodocyte space into Bowman's space demonstrates the narrow exit sites (asterisks) from the subpodocyte space into Bowman's space. *E*–*H*: *top* view of one podocyte branch shown without (*E*) and with (*F*) the glomerular basement membrane illustrated in grey. A *bottom* view of the same branch demonstrates the ridge-like prominence (dotted line in *G*) which leaves an imprint in the glomerular basement membrane (*H*), thus demonstrating the close spatial relationship between the 2 structures. Arrowheads and small and large arrows have been inserted for better orientation.

One crucial issue in podocyte biology concerns the question of whether slit diaphragms form between foot processes of the same podocyte or between foot processes of different podocytes. Our analysis clearly demonstrates that foot processes of the same podocyte do not interdigitate which each other and therefore slit diaphragms only connect foot processes of different podocytes (Figure 2.2-5).

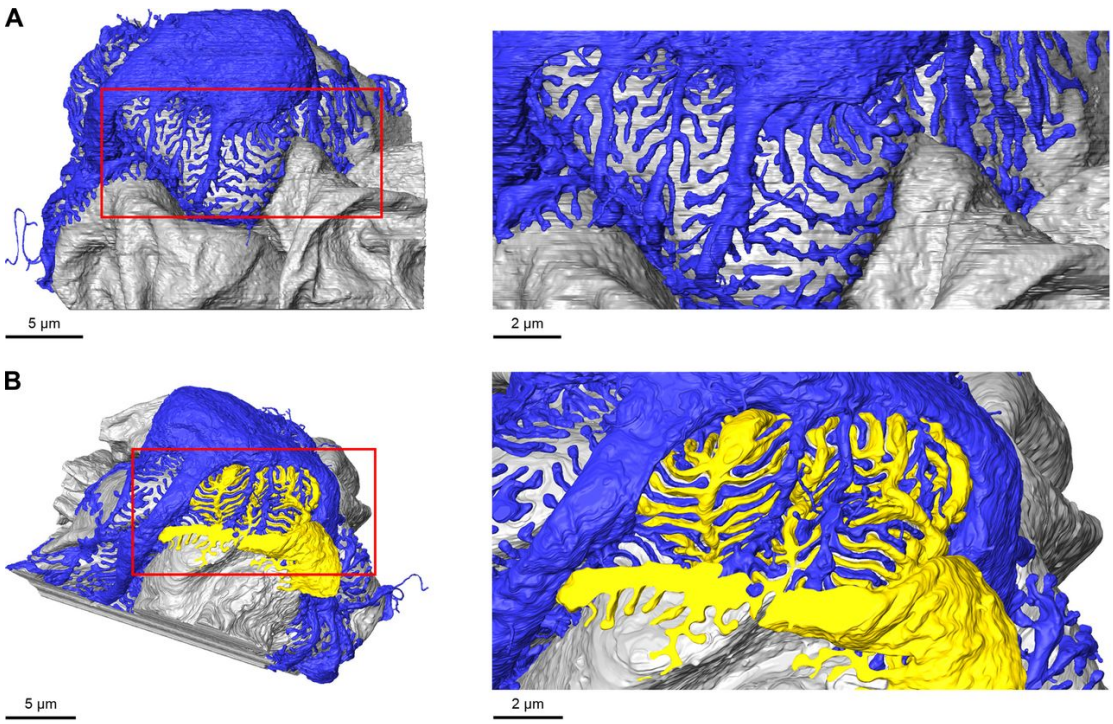

Figure 2.2-5 Pattern of interdigitating foot processes. Shown in blue is the same podocyte as in Fig. 2 (for reasons of clarity both the cell body and the processes are shown in blue; the capillaries are shown in grey). In *A*, only the "blue" podocyte is illustrated, whereas in *B* a second "yellow" podocyte is inserted. The spaces between the blue foot processes are filled by the foot processes of the yellow podocyte, thus demonstrating the heterophilic interaction of podocyte foot processes. Red rectangles indicate the regions which are shown at more detail in the panels on the *right*.

2.2.4.2 Electron tomographic characterization of connections between neighboring foot processes.

In previous publications, more than one cell-cell contact has been described between adjacent foot processes (Wartiovaara et al., 2004; Kramer-Zucker et al., 2005); these contacts have been interpreted as multiple layers of the slit diaphragm. Indeed, we were able to recapitulate by conventional electron microscopy that multiple cell-cell contacts existed between foot processes of murine and human podocytes, and this was true as well for nephrocytes of the fly *D. melanogaster*. As a matter of fact, only in a minority of filtration slits a single cell-cell contact was seen (~20% of filtration slits in the mouse, ~10% of filtration slits in human and the fly) (Figure 2.2-6*A*). Since some of the filtration slits were not represented in their entirety in our sections, it is likely that the frequency of filtration slits with only a single cell-cell contact is even lower. We would like to emphasize that the three specimens were generated by very different protocols. The mouse kidneys were perfusion-fixed, high-pressure frozen, and freeze-substituted. In the case of the human kidneys, needle biopsies were taken, and the biopsies were immersion-fixed and further processed at room temperature. Last, the fly nephrocytes were micro-dissected, high-pressure frozen, and freeze-substituted. Therefore, we consider it unlikely that the protocols for processing the tissues and cells, or that species differences account for the observed phenomenon.

However, due to the fact that conventional electron microscopic pictures originate from ultrathin sections of only 40-to 80-nm thickness it is impossible to be sure of the three-dimensional nature of the underlying cell-cell contacts. We therefore took a closer look at podocytes and nephrocytes by dual-axis electron tomography. Employing this technique, we were surprised to find two different categories of cell-cell contacts between neighboring foot processes. One layer (we never observed more than one) of the conventional slit diaphragm surrounded the whole periphery of foot processes, which is consistent with conventional thinking (Figure 2.2-6, *B*–*E*). In addition, we detected multiple punctate filamentous cell-cell contacts both below and above the slit diaphragm of podocytes (Figure 2.2-6, *B*–*D*), and above the slit diaphragm of nephrocytes (Figure 2.2-6*E*).

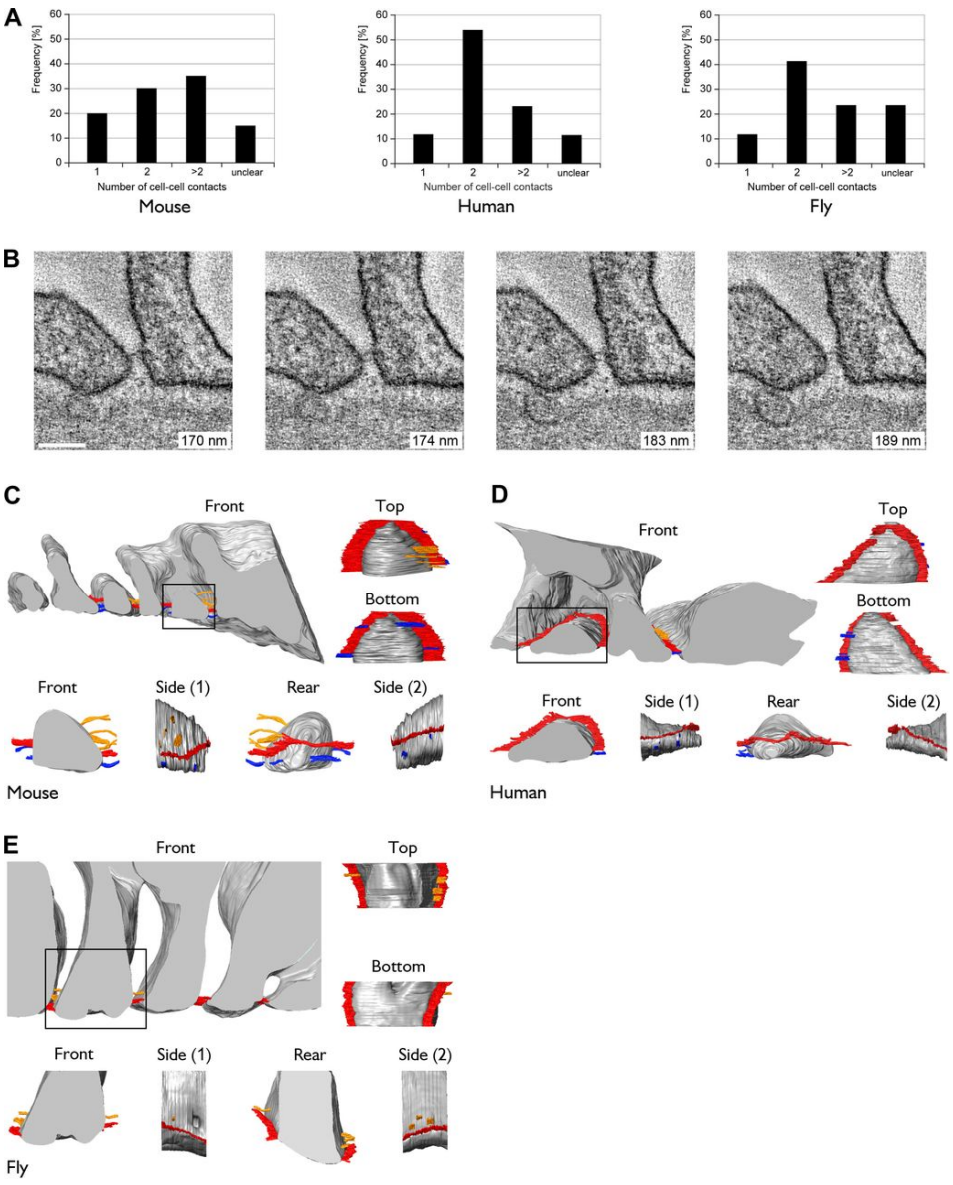

Figure 2.2-6 Neighboring foot processes are connected by 2 types of cell-cell contacts. A: bar graph demonstrates the occurrence of filtration slits with single or multiple cell-cell contacts of murine and human podocytes and *Drosophila melanogaster* nephrocytes. B: example of a 2-layered cell-cell contact in a human specimen. The panels on the far left and far right show only a single contact, whereas the 2 panels in the middle show two cell-cell contacts. The numbers listed in the individual panels correspond to the level in the section, meaning that for example the first 2 pictures lie 4 nm apart. Bar = 100 nm. C–E: 3-dimensional view of the filtration slits from the 3 species. The slit diaphragms are shown in red, the filamentous cell-cell contacts above the slit diaphragm in yellow, and the filamentous cell-cell contacts below the slit diaphragm in blue. In D, it appears as if there is a break in the slit diaphragm when viewed from the top or the bottom. We cannot, however, rule out that this is a technical artifact.

2.2.5 Discussion

Our data provide novel insight into the peculiar ultrastructure of podocytes by extending the conventional two-dimensional electron microscopic analysis into a third dimension. One long-standing puzzle in the podocyte field concerns the question of whether foot processes of the same podocyte can interact with each other. Very recent light microscopic investigations have suggested that this is not the case (Hackl et al., 2013; Höhne et al., 2013), but it has to be kept in mind that neighboring foot processes are separated by a slit with a width of only 40 nm, well below the resolution of conventional light microscopes. While this manuscript was prepared for submission, an article was published in which FIB-SEM tomography was used for the partial reconstruction of rat podocytes (Ichimura et al., 2015). Regrettably, however, the authors did not pay special attention to the question and therefore did not present any unequivocal evidence whether slit diaphragms form between foot processes of the same podocyte or between foot processes of different podocytes. Our ultrastructural reconstruction of a complete podocyte from an adult mouse clearly demonstrates that foot processes of the same podocyte do not form slit diaphragms between each other. This is very surprising and obviously raises the question of why such an arrangement is necessary and how it is achieved. If the foot processes of an individual podocyte would interact with each other (homophilic interaction), then podocytes would only be able to gather information locally. Through the interaction of foot processes originating from different podocytes (heterophilic interaction), the podocyte layer in essence would form a network covering the capillaries whereby podocytes could collect information such as capillary pressure over large distances.

How can it be achieved that slit diaphragms form exclusively between foot processes of different podocytes? One possibility is that podocytes are not a homogeneous population of cells but that podocytes exist in distinct "flavors." These populations would differ from each other by expressing different cell adhesion proteins which would not be able to establish homophilic interactions, i.e., foot processes of type "A" podocytes could not establish slit diaphragms between each other, and neither could foot processes of type "B" podocytes; instead, slit diaphragms would only form between type A and type B podocytes. Such a scenario is not completely unlikely because nephrin and Neph1, two integral membrane proteins of the slit diaphragm, preferentially interact in a heterophilic fashion (Dworak et al., 2001). Regrettably, our attempts to stain kidney sections for nephrin and Neph1 to subject them to high-resolution stimulated emission depletion (STED) light microscopy failed, and we therefore were not able to determine whether nephrin and Neph1 are located in a mutually exclusive pattern on foot processes. Furthermore, it has been pointed out that a given podocyte not only interacts with one, but at least two other podocytes, which in such a model would require at least three different types of podocytes (see for example Fig. 1 in [Ichimura et al., 2015]).

A more straightforward explanation comes from the pioneering work of Farquhar and colleagues (Reeves et al., 1978). In their characterization of the morphological events underlying podocyte differentiation, they have described the transition of podocytes from simple columnar cells to extensively arborized cells. Already the columnar epithelial cells are connected to each other by tight junctions; due to their shape, these cells can only

form tight junctions with neighboring cells and not with themselves. Upon differentiation, the prospective podocytes first elaborate rather coarse extensions which finally develop into the fine branches of the mature podocytes. During this process, cell-cell contacts apparently are maintained: the tight junctions move down from an apical to a basal location and are transformed into slit diaphragms. Since during this differentiation process a single podocyte never loses the cell-cell contacts with its neighbors, it follows automatically that slit diaphragms only form between neighboring cells. In principle, there is no reason why slit diaphragms cannot be established between foot processes of the same podocyte, and indeed this is true for *Drosophila*, where each nephrocyte is surrounded by its own basement membrane and nephrocytes do not interact with each other.

One other surprising result was the identification of two different types of cell-cell contacts between foot processes. Previous publications have described the occasional appearance of a supposedly two-layered slit diaphragm in human, rat, murine (Wartiovaara et al., 2004), and zebrafish glomeruli (Kramer-Zucker et al., 2005). In contrast, our data reveal the presence of only one layer of planar cell-cell contacts, i.e., the slit diaphragm, and of several additional punctate filamentous cell-cell contacts. Obviously, the misinterpretation in the previous publications was caused by looking only at conventional two-dimensional electron microscopic pictures. At present, we can only speculate on the nature and function of this novel type of contact. One rather trivial explanation would be that the filamentous cell-cell contacts represent transition states of the slit diaphragm, be it newly forming slit diaphragms or remnants of old slit diaphragms. Speaking against this hypothesis is the observation that despite the complete absence of slit diaphragms in patients suffering from mutations in the *NPHS1* gene, both regularly spaced filtration slits and altered filtrations slits were seen in the glomeruli of those patients (Ruotsalainen et al., 2000). In a model in which the slit diaphragm is required to establish the regular spacing of foot processes, one has to wonder how normal appearing filtrations slits are generated when a slit diaphragm is not present at any time during kidney development. The authors of that publication (Ruotsalainen et al., 2000) only mention “fuzzy cell surface material” between foot processes. It is quite feasible that the filamentous structures we describe in our current study have been missed in the patients' kidney sections because conventional electron microscopy was performed, and the kidney samples were not optimally preserved (kidney samples were obtained from aborted fetuses). We suggest that the filamentous cell-cell contacts we describe here are required to elaborate regularly spaced foot processes whereas the slit diaphragm would serve a sieving function and may possibly also be responsible for the formation of heterophilic cell-cell contacts.

The integral membrane proteins nephrin, Neph1, FAT-1, and P-cadherin are believed to be components of the slit diaphragm. These molecules belong to different families of cell-cell adhesion molecules: nephrin and Neph1 contain immunoglobulin-like domains, whereas FAT-1 and P-cadherin are members of the cadherin superfamily. Typically, only adhesion molecules of the same family are present in one type of cell-cell contacts, such as cadherins in adherens junctions. If all those different molecules contribute to the formation of slit diaphragms, they would have to interact in one form or another to maintain a tight slit diaphragm. So far, this has not been demonstrated. We also would like to point out that all of them have been located by immunogold electron microscopy to the

filtration slit, a technique which interferes quite drastically with the preservation of the specimens and does not yield the necessary spatial resolution to precisely determine the location of the respective proteins. We speculate that the protein composition of the two types of cell-cell contacts described in our present study only partially overlaps or may even be distinct from each other, so that there are different sets of proteins which belong to one type of cell-cell contact or another.

2.3 Pals1 haplo-insufficiency results in proteinuria and cyst formation

Authors
Thomas Weide*, Beate Vollenbröker*, Ulf Schulze*, Ivona Djuric*, Maria Edeling*, Jakob Bonse*, Florian Hochapfel†, Olga Panichkina†, Dirk-Oliver Wennmann*, Britta George*, Seonhee Kim‡, Christoph Daniel§, Jochen Seggewiß‖, Kerstin Amann§, Wilhelm Kriz¶, Michael P. Krahn† and Hermann Pavenstädt*

Journal
The Journal of the American Society of Nephrology, July 2017 vol. 28 no. 7 2093-2107

Author Affiliations
*Internal Medicine D, University Hospital of Münster, Münster, Germany;
†Institute for Molecular and Cellular Anatomy, University of Regensburg, Regensburg, Germany;
‡Shriners Hospitals Pediatric Research Center, Department of Anatomy and Cell Biology, Lewis Katz School of Medicine, Temple University, Philadelphia, Pennsylvania;
§Nephropathology Department, Institute of Pathology, Erlangen-Nürnberg University, Erlangen, Germany;
‖Interdisciplinary Center for Clinical Research, University of Münster, Munster, Germany; and
¶Department of Neuroanatomy, Medical Faculty Mannheim, University of Heidelberg, Mannheim, Germany

Accepted for Publication
January 3, 2017.

Contribution
The author of this thesis performed the experiments necessary to generate TEM and RFP accumulation data obtained from *Drosophila* nephrocytes, including fly husbandry, micro-dissection of nephrocytes, resin ultrathin sectioning, microscopy, data analysis and figure design. The author also contributed text passages concerning nephrocyte data in the methods and results sections.

2.3.1 Abstract

The nephron is the basic physiologic subunit of the mammalian kidney and is made up of several apicobasally polarized epithelial cell types. The process of apicobasal polarization in animal cells is controlled by the evolutionarily conserved Crumbs (CRB), Partitioning-defective, and Scribble protein complexes. Here, we investigated the role of protein associated with LIN-7 1 (Pals1, also known as Mpp5), a core component of the apical membrane–determining CRB complex in the nephron. Pals1 interacting proteins, including Crb3 and Wwtr1/Taz, have been linked to renal cyst formation in mice before.

Immunohistologic analysis revealed Pals1 expression in renal tubular cells and podocytes of human kidneys. Mice lacking one Pals1 allele (functionally haploid for Pals1) in nephrons developed a fully penetrant phenotype, characterized by cyst formation and severe defects in renal barrier function, which led to death within 6–8 weeks. In *Drosophila* nephrocytes, deficiency of the Pals1 ortholog caused alterations in slit-diaphragm–like structures.

Additional studies in epithelial cell culture models revealed that Pals1 functions as a dose-dependent upstream regulator of the crosstalk between Hippo- and TGF-β–mediated signaling. Furthermore, Pals1 haploinsufficiency in mouse kidneys associated with the upregulation of Hippo pathway target genes and marker genes of TGF-β signaling, including biomarkers of renal diseases. These findings support a link between apical polarity proteins and renal diseases, especially renal cyst diseases. Further investigation of the Pals1-linked networks is required to decipher the mechanisms underlying the pathogenesis of these diseases.

2.3.2 Introduction

During nephrogenesis, renal epithelial tissues undergo constant growth and differentiation, including functional diversification of the various segments of the tubule (tubulogenesis) and formation of the glomerular filtration barrier. The complex balance between proliferation and apoptosis that controls nephron maturation and kidney size is organized by several signal transduction systems, including those activated by Hippo and TGF-β (Kobayashi et al., 2008; Costantini and Kopan, 2010; Bernascone and Martin-Belmonte, 2013; Krause et al., 2015).

Apicobasal epithelial cell polarization begins early during the renal vesicle stage and continues during tubulo- and glomerulogenesis until mature nephrons are formed (Kobayashi et al., 2008; Costantini and Kopan, 2010; Krause et al., 2015). Cell polarity is organized by evolutionarily conserved complexes assembled around the proteins CRB (Crumbs), PAR (Partitioning-defective), and SCRIB (Scribble), respectively. The CRB complex, which consists of Crumbs 3, Lin7c (lin-7 homolog C), Pals1 (protein associated with Lin7), and Patj (Pals1-associated tight junction protein), plays a central role in the determination of apical membranes in epithelial cells (Pieczynski and Margolis, 2011; Rodriguez-Boulan and Macara, 2014).

Pals1 is a member of the evolutionarily conserved membrane-associated guanylate kinase (MAGUK) family (Kamberov, 2000). It is encoded by the gene Mpp5 (membrane protein, palmitoylated 5) and its orthologs in *Drosophila* and zebrafish are referred to as

Stardust (Sdt) in *Drosophila* and Nagie Oko (Nok) (Knust et al., 1993; Wei and Malicki, 2002). Pals1 is the only apical polarity protein that interacts with all other components of the CRB complex (Kamberov, 2000; Roh et al., 2002; Roh et al., 2003). Moreover, Pals1 is also able to mediate binding between CRB and PAR complexes, because it interacts directly with the PAR component Par6 (Hurd et al., 2003). Knockdown studies in cell culture also revealed an essential role of Pals1 in the formation of tight and adherens junctions, indicating that cell junction assembly is closely linked to cell polarization in epithelial cells (Straight et al., 2004; Wang et al., 2007).

More recent studies suggest that the CRB complex acts upstream of the Hippo signaling pathway, which controls tissue growth and organ size (Chen et al., 2010; Varelas et al., 2010; Grzeschik et al., 2010; Robinson et al., 2010). Key proteins involved in the response to Hippo signaling are the transcriptional coactivators Yap (Yes-associated protein) and Taz (transcriptional coactivator with PDZ-binding motif, gene: Wwtr1). Active Hippo signaling results in the phosphorylation of Yap or Taz by the large tumor suppressor kinase (Lats kinase), which prevents their nuclear localization. By contrast, nonphosphorylated Yap/Taz can enter the nucleus to activate the expression of Hippo target genes (Piccolo et al., 2014; Hansen et al., 2015).

Because polarization and differentiation are highly coordinated during kidney development, we have investigated the role of Pals1 in these processes.

2.3.3 Results

2.3.3.1 Pals1 Haploinsufficiency in Nephrons Induces Early Cell Death, Proteinuria, and Renal Cyst Formation

IHC staining of a human kidney specimen revealed a high level of expression of Pals1 in all renal epithelia, including tubulus cells and podocytes (Figure 2.3-1A). In order to address the role of Pals1 in the kidney, we examined the *in vivo* function of Pals1 in the entire nephron. Because Six2-positive cap-mesenchymal cells are precursors of all nephron epithelia, including podocytes as well as cells of the proximal and distal tubuli, we took advantage of a Cre-driver mouse line which expresses an EGFP-Cre fusion protein under the control of the Six2 promoter (Kobayashi et al., 2008). Crosses between the Six2-Cre driver strain and homozygous conditional Pals1 knockout mice ($Pals1^{fl/fl}$) (Kim et al., 2010) resulted in heterozygous progeny ($Pals1^{wt/fl}$), of which 50% were Cre-positive (Six2-Cre+) and 50% Cre-negative (Six2-Cre−) (Figure 2.3-1B). When we compared 4-week-old Six2-Cre+ mice with their Cre-negative littermate controls, we discovered that the Six2-Cre+ mice, lacking only one of the two Pals1 alleles in the nephron, were significantly smaller in size and weight (Figure 2.3-1, C and D) and died within the first 45 days (Figure 2.3-1E).

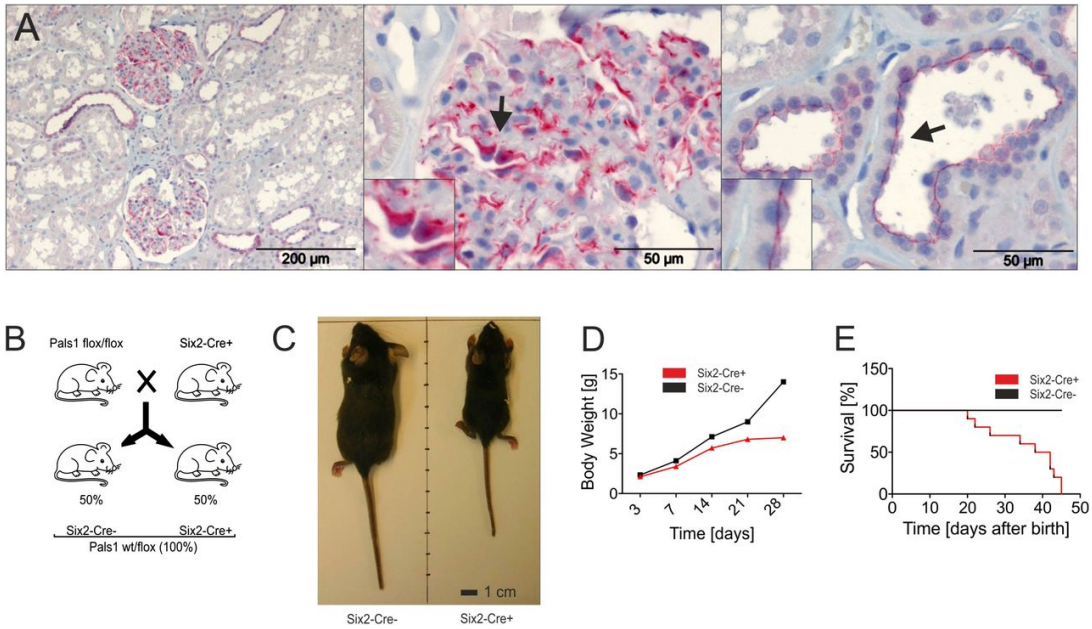

Figure 2.3-1 Pals1 expression is important for the mammalian kidney. (A) Immunohistochemical analysis of human kidney sections revealed high levels of expression of Pals1 (red) in both tubular and glomerular regions of the organ. Left: Overview of Pals1 staining in a control biopsy specimen from a tumor-free human kidney. Scale bar, 200 µm. Middle: In glomeruli, Pals1 is predominantly expressed in podocytes. Right: Pals1 could also be localized in the apical membrane of renal tubular cells. Scale bar, 50 µm. (B) Scheme: Crosses between Six2-Cre strain and mice homozygous for a conditional Pals1 knockout allele (Pals1fl/fl) resulted in heterozygous F1 progeny (Pals1wt/fl), half of which are expected to carry the Cre recombinase gene (Six2-Cre+; Pals1wt/fl), whereas half are not (Six2-Cre−; Pals1wt/fl). These genotypes are hereafter referred to as Six2-Cre+ and Six2-Cre−, respectively. (C) A Six2-Cre+ mouse and a Six2-Cre− control photographed 4 weeks after birth. Note that Six2-Cre+ mice were smaller than their littermate controls. (D) Bodyweight analysis of Six2-Cre− and Six2-Cre+ mice. (E) Kaplan–Meyer analysis of Six2-Cre+ and Six2-Cre− mice.

2.3.3.2 Pals1 Haploinsufficiency Is Accompanied by the Formation of Glomerular and Tubular Cysts

Kidneys derived from these mice were poorly perfused with blood (Figure 2.3-2A) and formed multiple cysts of varying size and morphology (Figure 2.3-2, B–E), which were completely absent in the littermate control (Figure 2.3-2, B and C). Moreover, Six2-Cre+ mice of both sexes developed proteinuria, starting 2 weeks after birth and increasing in severity over the following weeks (Figure 2.3-2F). This suggests that Pals1 expression is crucial for the formation and function of the renal filtration barrier (Figure 2.3-9).

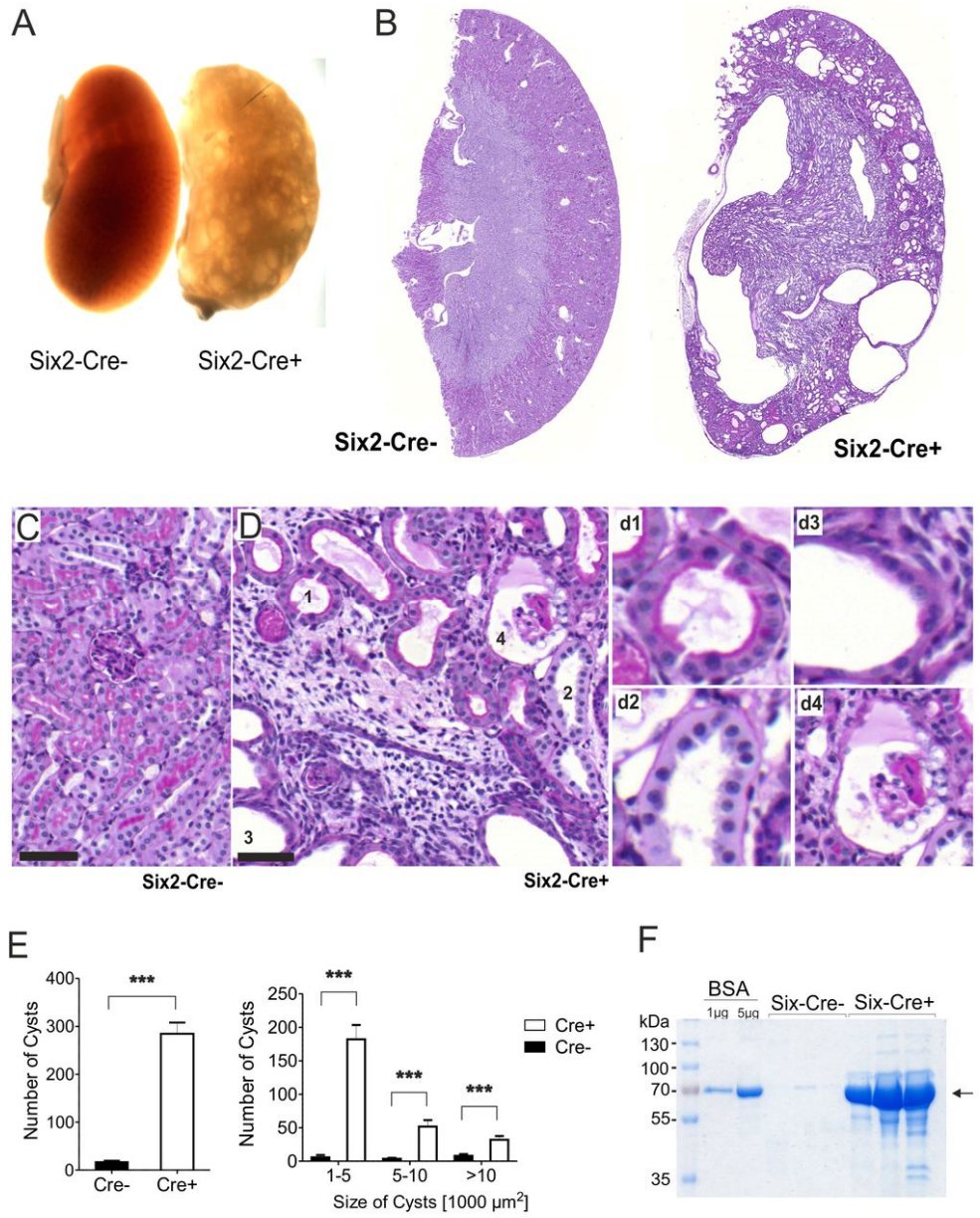

Figure 2.3-2 Pals1 is essential for the nephron function. (A) Bright-field microscopy of kidney sections from Pals wt/flox-Six2Cre+ (Six2-Cre+) and control mice (Six2-Cre−) shows that Six2-Cre+ kidneys are characterized by cyst-filled and bloodless tissues. (B–D) Periodic acid–Schiff staining of Six2-Cre+ and Six2-Cre− kidney sections shows the formation of multiple cysts in Six2-Cre+ kidneys. (C) Littermate control, higher magnification. (D) Pals1-depleted Six2-Cre+ kidney sections, higher magnification. Numbers mark different cysts, details on the right (d1–4). Scale bar, 50 μm. (E) Distribution of cyst numbers (left) and sizes (right) in Six2-Cre− and Six2-Cre+ kidneys. (F) SDS-PAGE analysis of urine from Six2 Cre− and Six2 Cre+ mice reveals proteinuria in Pals1-depleted mice.

Pals1 is expressed along the entire nephron (Figure 2.3-3, Figure 2.3-10). In tubular cysts, the overall apicobasal polarization of cyst-lining cells was preserved, as Pals1 was predominantly localized at the luminal side in the cysts, indicating that cyst formation was not necessarily linked to an unpolarized distribution of Pals1. Interestingly, staining for Pals1 of specimens obtained from patients with autosomal dominant polycystic kidney disease (ADPKD) confirmed that cyst-lining cells, even in strongly proliferating epithelia, maintained a predominantly apical Pals1 distribution (Figure 2.3-11).

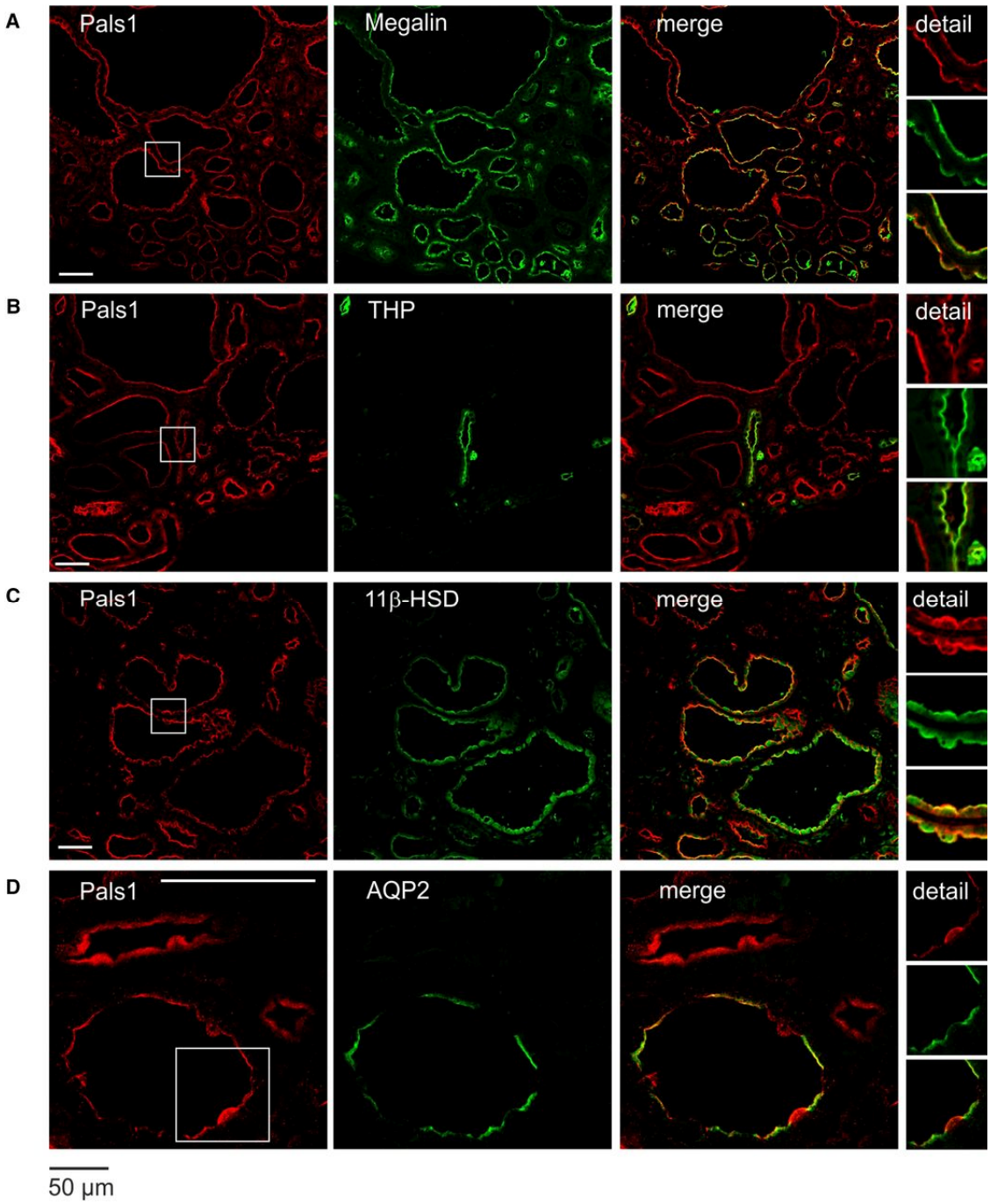

Figure 2.3-3 Reduced Pals1 expression during nephrogenesis results in the formation of cysts. Immunofluorescence staining of Pals1 and costaining with diverse tubulus markers in Six2-Cre+ kidneys shows that remaining Pals1 is located to the apical membrane of all tubular cysts. Costaining of Pals1 with Megalin (proximal tubule marker, [A]), Tamm–Horsfall protein (thick ascending limb of the loop of Henle, [B]), 11β-HSD (distal tubules, [C]), and AQP2 (collecting duct, [D]). Scale bar, 50 μm.

Cysts are formed in various segments of the nephron (Figure 2.3-3, Figure 2.3-10, Figure 2.3-12), namely in the glomeruli (glomerulocysts), in the proximal tubules (Megalin- and PNA-positive), in distal tubules (11β-HSD and PHA positive), and in the collecting duct (AQP2-positive). No cysts were observed in the thick ascending limb of the loop of Henle (Tamm-Horsfall–positive structures), although Pals1 is also expressed in this nephron segment. The presence of cysts even in regions that still contain both Pals1 alleles indicated the formation of secondary cysts, *e.g.,* in the collecting duct (Figure 2.3-3D, Figure 2.3-12B–D).

2.3.3.3 Pals1 Reduction Leads to an Elevated Expression of Hippo Signaling Target Genes and Nuclear Accumulation of Taz and Yap in Cyst-Lining Cells

Mice lacking Taz develop a cystic-kidney–like phenotype (Hossain et al., 2007; Tian et al., 2007; Makita et al., 2008), whereas Yap knockout mice die as embryos (Morin-Kensicki et al., 2006). In Pals1-deficient kidneys, levels of Yap and Taz were strongly reduced (Figure 2.3-4A). Real-time PCR analyses showed a significant increase in the expression of Hippo signaling target genes (*Ctgf, Birc2*, and *Cyr61*; Figure 2.3-4B) in Pals1-deficient kidneys, whereas basal expression of Hippo pathway genes (*Yap, Taz/Wwtr1,* members of the Amot and Lats families) and expression of apical polarity genes (with the exception of Pals1) remained unchanged (Figure 2.3-13). Cryo-immunofluorescence staining using antibodies with high preference against Yap or Taz (see also Figure 2.3-14) showed a predominant nuclear distribution of Yap and Taz in cyst-lining cells (Figure 2.3-4, C and D).

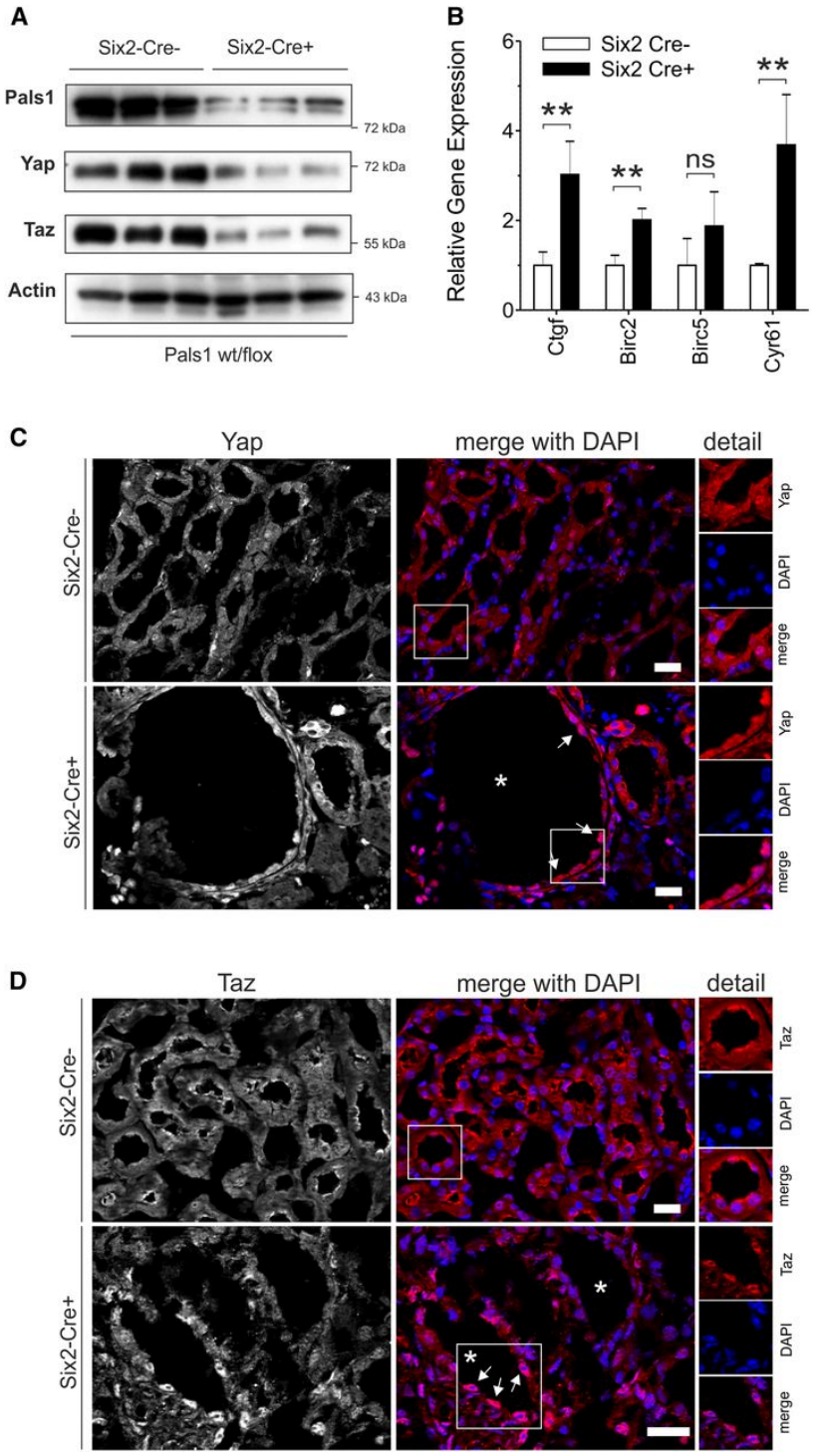

Figure 2.3-4 Reduced Pals1 expression results in altered Hippo signaling. (A) Western blot analysis revealed that Pals1, Taz, and Yap, but not actin (loading control), are downregulated in Pals1-depleted (Six2-Cre+) mice (n=3). (B) Real-time PCR analysis showed increased expression of the Hippo target genes *Ctgf, Birc2, Birc5*, and *Cyr61* in Six2-Cre+ mice (data are shown as mean±SD of at least three independent experiments). (C–D) Colocalization of Yap or Taz with the DNA-specific dye DAPI confirmed the nuclear accumulation of Yap and Taz in Six2-Cre+ cyst-lining cells. Asterisks mark cysts and arrows cyst-lining cells. All data shown in (A–D) were obtained from 4-week-old mice.

2.3.3.4 Stardust Knockdown Causes Dysfunctional Nephrocytes in *Drosophila*

Drosophila nephrocytes control the filtration of the hemolymph by means of a podocyte-like slit-diaphragm (Weavers et al., 2009; Zhuang et al., 2009) and show high reabsorption and endocytotic activity (Zhang et al., 2013b), thus exhibiting remarkable functional similarities with mammalian nephrons. Indeed, selective RNAi knockdown of Stardust/Sdt (by Sdt RNAi 111/+ or Sdt RNAi 69/+), the *Drosophila* ortholog of Pals1, reduced the uptake efficiency of nephrocytes (Figure 2.3-5A) and was accompanied by the appearance of malformed slit-diaphragm–like structures (Figure 2.3-5, B and C and details). These uptake defects were rescued by simultaneous downregulation of Yorkie (Yki RNAi), which is the *Drosophila* counterpart of both Yap and Taz (Figure 2.3-5D). This finding indicated that defects in Sdt-depleted nephrocytes were linked to increased activation of Yki-dependent gene expression. Taken together, our data indicate that an imbalance in the relative levels of Sdt and Yki cause defects in the architecture of slit-diaphragm–like structures and function in endocytosis of fly nephrocytes.

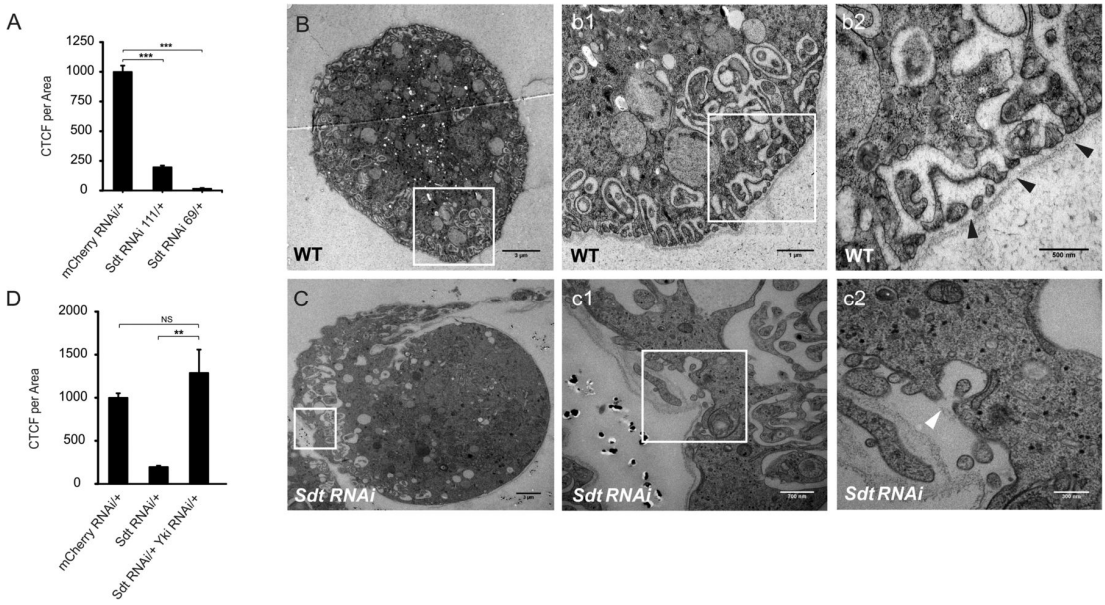

Figure 2.3-5 Stardust (Sdt) knockdown in *Drosophila* results in dysfunctional nephrocytes. (A) In comparison to the control strain (mCherry RNAi/+), depletion of Stardust (Sdt RNAi 111/+ and Sdt RNAi 69/+) led to strongly reduced filtration rates in RFP accumulation assays. CTCF, corrected total cell fluorescence. (B–C) Transmission electron microscopy analysis of wildtype (B) and Sdt-depleted nephrocytes (C) demonstrated that the defects in RFP endocytosis are accompanied by malformation of slit-diaphragm–like structures in Sdt RNAi nephrocytes ([C] and details in c1–c2; scale bars, 3 μm, 700 nm, and 300 nm, respectively) compared with the wildtype control ([B], details in b1–2; scale bars, 3 μm, 1 μm, and 500 nm, respectively). (D) Parallel downregulation of Yki in Sdt RNAi nephrocytes (Std RNAi/+ Yki RNAi/+) completely rescued the defect in RFP filtration shown in (A). For each genotype, >50 nephrocytes from at least six individuals were scored.

2.3.3.5 Reduced Pals1 Expression Results in an Inactivation of Hippo Signaling *In Vitro*

To explore the functional consequences of relative loss of Pals1 in more detail, we generated stable Pals1 MDCK and HEK293T knockdown cell lines. Introduction of the short hairpin RNAs sh1 and sh2 led to a 50%–70% reduction of endogenous Pals1 expression (Figure 2.3-6, Figure 2.3-16).

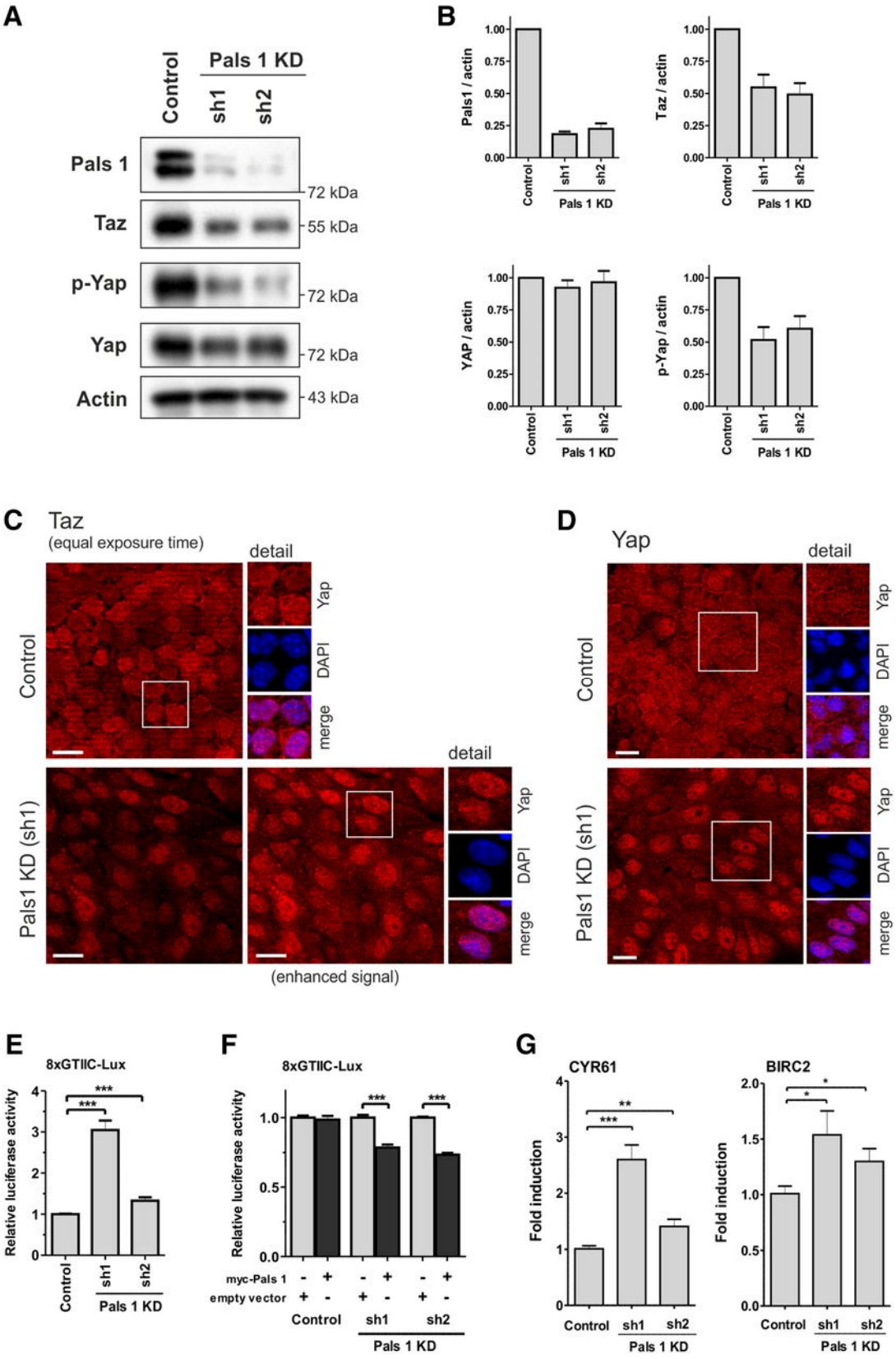

Figure 2.3-6 Pals1 controls Hippo signaling *in vitro.* (A) Knockdown of Pals1 in MDCK cells (sh1 and sh2) decreased expression of Taz and phosphorylation of Yap, relative to control cells. Expression level of Yap was not affected. Actin served as loading control. (B) Quantification of (A). (C) Analysis of confluent cells by immunofluorescence microscopy revealed a reduction in the expression and an increased nuclear localization of Taz (red) in Pals1 KD cells. (C–E) We used the 8xGTIIC

reporter gene system, which expresses luciferase only when Yap/Taz is present in the nucleus, to analyze inactivation of Hippo signaling. The results of the 8xGTIIC-Lux reporter gene assay showed that Pals1 knockdown significantly enhances Yap/Taz-dependent transcriptional activity (data are presented as mean±SD and normalized to lane 1). (F) Conversely, Pals1 overexpression suppressed the enhanced Yap/Taz-dependent transcriptional activity in Pals1 KD cells. MDCK cells were transfected with myc-Pals1 or the empty vector. The data were normalized to the respective lane without Pals1 overexpression. (G) Expression of the Hippo target genes *CYR61* and *BIRC2* is increased in Pals1 KD cells (RT-PCR data are shown as mean+SD of at least three independent experiments).

In MDCK Pals1 KD cell lines, Taz expression and Yap phosphorylation (p-Yap S127) was significantly reduced, whereas Yap levels remained nearly unchanged (Figure 2.3-6, A and B) indicating that Hippo signaling, which triggers phosphorylation and cytoplasmic retention of Yap/Taz, is at least partially inactivated in the knockdown lines. This is supported by immunofluorescence analysis with Taz and Yap showing a predominant nuclear distribution in Pals1 KD cells (Figure 2.3-6, C and D). Increasing confluence of MDCK cells resulted in a stepwise export of Yap into the cytoplasm and cell junctions. By contrast, in Pals1 KD cells Taz/Yap kept a predominant nuclear localization even in confluent cells (Figure 2.3-15).

We further tested whether the altered Yap/Taz localization in Pals1 KD cells was linked to enhanced expression of Yap/Taz target genes. We took advantage of the 8xGTIIC reporter gene system, which expresses luciferase only when Yap/Taz is present in the nucleus, to analyze inactivation of Hippo signaling (Dupont et al., 2011). We found that reduced Pals1 expression resulted in a significant increase of luciferase activity in MDCK and HEK293T Pals1 KD cell lines (Figure 2.3-6E, Supplemental Figure 8B). Ectopically expressed Pals1, which compensates the reduced endogenous Pals1 expression in MDCK Pals1 KD cell lines, was able to reduce the 8xGTIIC reporter gene activity (Figure 2.3-6F). Real-time PCR revealed significant upregulation of Hippo target genes *CYR61* and *BIRC2* in Pals1 KD cell lines, indicating again (see also Figure 2.3-4B) that decreased Pals1 expression levels correlate with an activation of Yap/Taz-dependent gene expression (Figure 2.3-6G, Figure 2.3-16C).

2.3.3.6 Cell Junction Dissociation Leads to Inactivation of Hippo Signaling *In Vitro*

Knockdown studies in cell culture revealed an essential role of Pals1 in the formation of tight and adherens junctions, indicating that junction assembly is closely linked to cell polarization in epithelial cells (Straight et al., 2004; Wang et al., 2007). In order to analyze if the dissociation of cell-cell contacts influences Hippo signaling, monolayers of MDCK wildtype cells were cultivated under low Ca^{2+} conditions. Ca^{2+} depletion leads to disassembly of E-Cadherin–positive adherens junctions and ZO-1–positive tight junctions (Figure 2.3-7A), which results in a change of Yap and Taz localization (Figure 2.3-7B) accompanied by an increased expression of Yap/Taz target genes (Figure 2.3-7C).

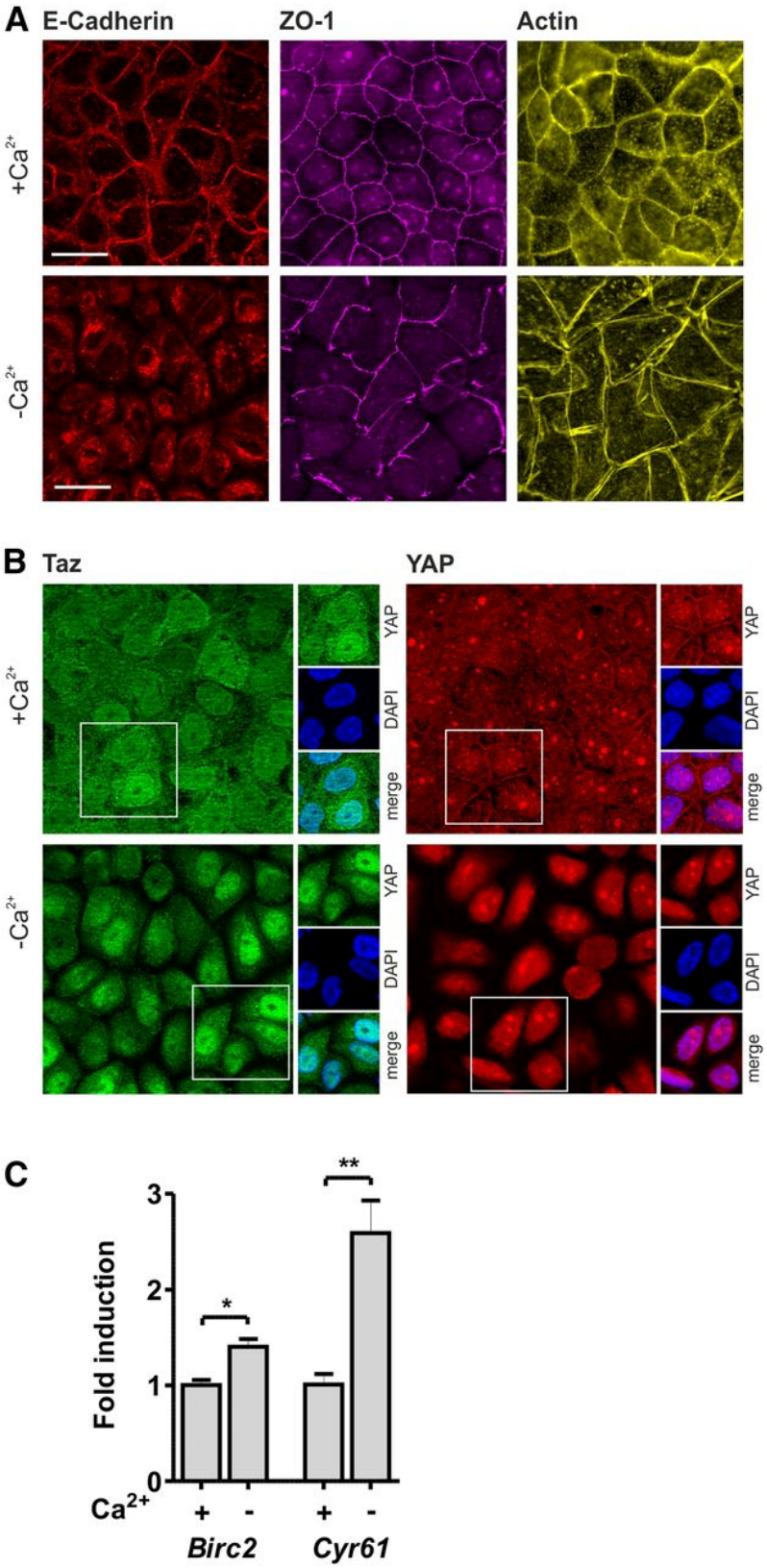

Figure 2.3-7 Disassembly of cell-cell contacts inactivates Hippo signaling. (A) Disassembly of cell-cell contacts in MDCK cells (wildtype) cultivated with Ca2+ (upper panel) and without Ca2+ (lower panel) stained for E-Cadherin (adherens junctions), ZO-1 (tight junctions), and actin cytoskeleton (Phalloidin). Scale bar, 20 µm. (B) Disassembly of cell-cell contacts by Ca2+ depletion in confluent wildtype MDCK cells increased nuclear localization of Taz (green) and Yap (red). Scale bars, 20 µm. (C) Ca2+ depletion resulted in an increased expression of Yap/Taz target genes CYR61 and BIRC2.

2.3.3.7 Pals1 Depletion Results in an Increase in Responsiveness to TGF-β

Similar to Ca^{2+}-depleted MDCK cells, Pals1 KD cells showed a reduced formation of cell-cell contacts (Figure 2.3-8, Figure 2.3-15). Previous studies have pointed to a link between Hippo- and TGF-β–mediated signaling where disruption of the CRB complex enhances signaling by TGF-β and promotes EMT (Varelas et al., 2010). In order to test whether Pals1 depletion in MDCK cells has an effect on TGF-β signaling, or TGF-β responsiveness, we used the 3TP-lux reporter gene system (Wrana et al., 1992). We treated Pals1 KD and control cell lines with SB431542, an inhibitor of the TGF-β receptor, to completely block the endogenous basal activity of the receptor.

Untreated Pals1 KD cells showed increased reporter gene activity relative to the untreated control cells. Administration of TGF-β (100 pM) led to a five-fold increase in the control, but to an 11- to 15-fold increase in reporter gene activity in Pals1 KD cells (Figure 2.3-8B), indicating that Pals1 serves as negative regulator of TGF-β–linked signaling. To confirm this, we analyzed expression levels of the TGF-β target gene *Pai-1* (Figure 2.3-8C). The basal level of *Pai-1* expression was found to be higher in Pals1 KD cell lines. After treatment with TGF-β, *Pai-1* expression increased much more strongly than in the Pals1 KD cell lines. Thus, Pals1 depletion results in elevated responsiveness to TGF-β.

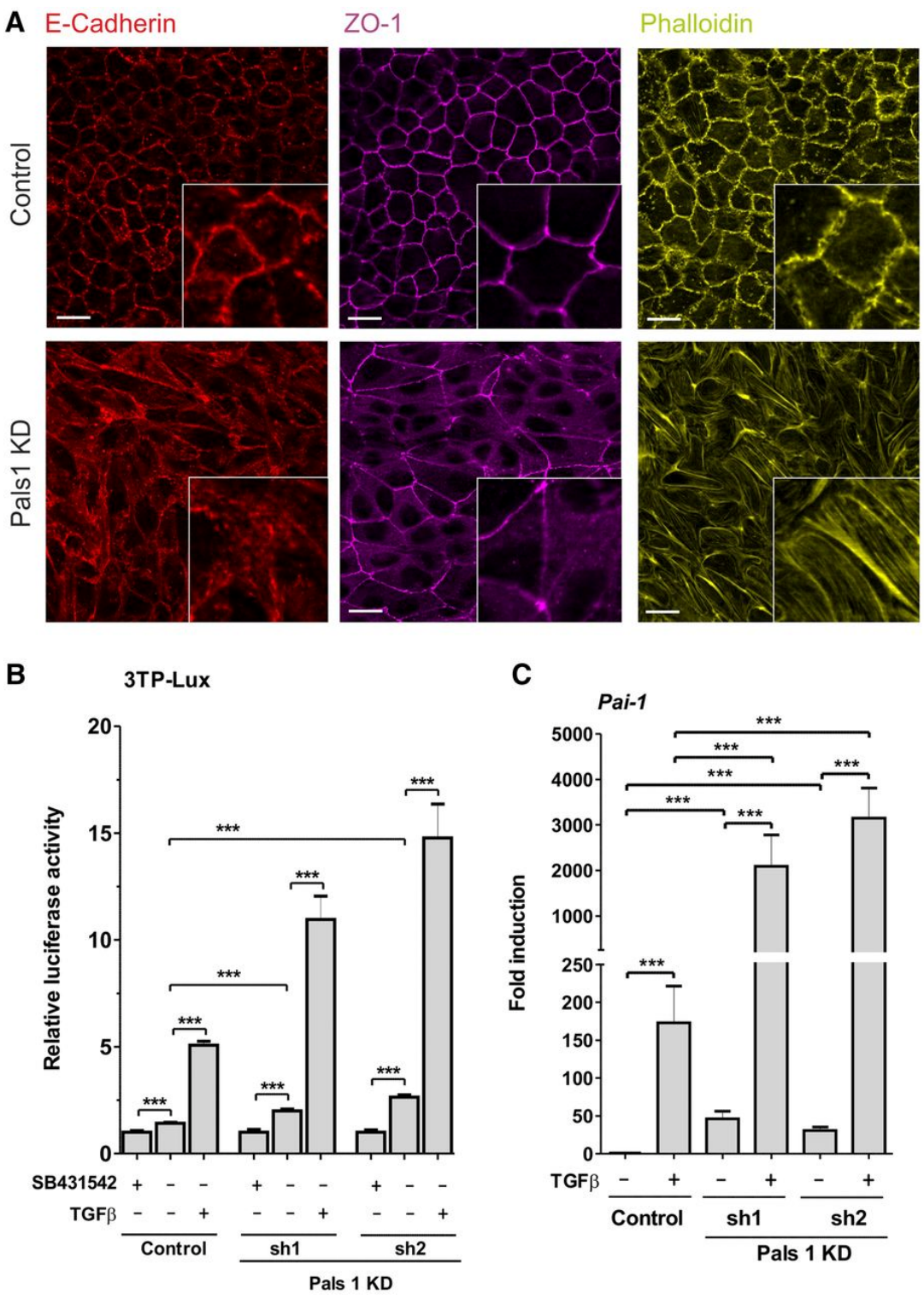

Figure 2.3-8 Pals1 depletion increases responsiveness to TGF-β. (A) In Pals1 KD cells, the junction proteins E-cadherin and ZO-1 are more diffusely distributed and larger fractions of both remain in the cytoplasm. Instead of showing the normal cortical localization of actin, the knockdown cells form many stress fibers. MDCK cells were grown to high density, and E-cadherin, ZO-1, and actin were detected by immunofluorescence microscopy. Scale bars, 20 μm. (B) Pals1 knockdown resulted in an increased luciferase activity in the TGF-β–responsive 3TP-Lux luciferase reporter gene assay. Twenty-six hours after transfection with p3TP-Lux, control and Pals1 KD cells were treated with the TGF-β receptor antagonist SB431542 (10 μM), TGF-β (100 pM), or the corresponding solvent controls for 20 hours. 3TP-Lux reporter activity is presented as mean±SD and normalized to

the value for the respective inhibitor-treated sample. (C) MDCK cells were grown to high density and treated with TGF-β (500 pM) or control solvent for 2 hours. Real-time PCR analysis revealed increased expression of the TGF-β target gene *Pai-1* even under basal conditions, and the gene was highly induced upon TGF-β treatment.

2.3.3.8 Target Genes of the Hippo Pathway and Marker Genes of TGF-β Signaling Are Upregulated in Pals1-Depleted Kidneys

Next, we performed microarray analysis and compared the gene expression profile of kidneys of 4-week-old Six2-Cre+ mice with their corresponding Six2-Cre− littermate controls. The analyses showed, as expected, a 50% reduction in Pals1 expression in Six2-Cre+ kidneys.

The data set for each group (each n=3, Figure 2.3-17A) was homogenous, therefore permitting the gene expression profiles of control (Six2-Cre−) and Pals1-depleted (Six2-Cre+) kidneys to be compared. By using the Pals1 regulation value (±1.5-fold) as threshold for further analysis, we found 1412 transcripts to be differentially expressed (Six2-Cre+ versus Six2-Cre− littermate controls, see Figure 2.3-17), of which 624 were up- and 788 were downregulated.

Similar to our *in vitro* results (Figure 2.3-6 and 8), target genes of the Hippo pathway, but also marker genes of TGF-β signaling, were significantly upregulated in Pals1-depleted kidneys (Figure 2.3-17, Table 1 Expression of Hippo pathway–associated genes in Pals1-deficient kidneys compared with the littermate controls. Target genes of the Hippo signaling pathway and of genes that are affected by crosstalk between the Hippo and Wnt or Hippo and TGF-β are differentially regulated in Six2-Cre+ kidneys. The table lists a selection of genes that are significantly (see P value) upregulated in Pals1-deficient kidneys (Six2-Cre+) and are given in fold-change compared with the littermate controls (Six2-Cre−). Details of the microarray analysis are summarized in the Supplemental Material.). Moreover, many of the most highly upregulated genes were biomarkers of renal diseases, including marker genes for tubular-intestinal (*e.g., Kim-1/Havcr1, Ngal/Lcn2, End1*) and glomerular injury (*Tagln1/2; Nphs1/2, Podxl*), as well as for fibrosis and inflammation (*Ccl2/Mcp-1, Gpnmb/Osteoactivin*; Supplementary Material, Table 2).

Table 1 Expression of Hippo pathway–associated genes in Pals1-deficient kidneys compared with the littermate controls. Target genes of the Hippo signaling pathway and of genes that are affected by crosstalk between the Hippo and Wnt or Hippo and TGF-β are differentially regulated in Six2-Cre+ kidneys. The table lists a selection of genes that are significantly (see *P* value) upregulated in Pals1-deficient kidneys (Six2-Cre+) and are given in fold-change compared with the littermate controls (Six2-Cre−). Details of the microarray analysis are summarized in the Supplemental Material.

Gene	Name	Signaling Pathway	Six Cre2- versus Six2-Cre+	
			Fold Change	P Value
Myc	myelocytomatosis oncogene	Hippo	3.94	1.31E-04
Ctgf	connective tissue growth factor	Hippo	2.52	4.01E-04
Cyr61	cysteine rich protein 61	Hippo	2.48	5.28E-03
Axl	AXL receptor tyrosine kinase	Hippo	2.04	6.85E-03
Birc2	baculoviral IAP repeat-containing 2	Hippo	1.87	3.86E-03
Runx2	Runt-related transcription factor 2	Hippo	1.54	9.33E-03
Sox4	SRY (sex-determining region Y)-box 4	Hippo	2.33	6.34E-05
Tead1	TEA domain family member 1	Hippo	1.59	9.94E-04
Serpine1	Serine/cysteine peptidase inhibitor, clade E, member 1 (Pai-1)	Hippo/TGF-β	8.60	3.56E-04
Runx1	Runt-related transcription factor 1	Hippo/TGF-β	4.72	1.95E-04
Cdkn1a	cyclin-dependent kinase inhibitor 1A	Hippo/TGF-β	2.98	6.59E-05
Col1a1	collagen, type I, alpha 1	Hippo/TGF-β	2.81	6.20E-03
Tgfbi	TGF, β induced	Hippo/TGF-β	2.61	3.55E-03
Col1a2	collagen, type I, α 2	Hippo/TGF-β	2.47	7.88E-03
Tgfb1	TGF, β 1	Hippo/TGF-β	2.20	3.59E-03
Fos	FBJ osteosarcoma oncogene	Hippo/TGF-β	2.04	1.25E-02

Gene	Name	Signaling Pathway	Six Cre2- versus Six2-Cre+	
			Fold Change	P Value
Junb	jun B proto-oncogene	Hippo/TGF-β	2.30	2.34E-05
Thbs1	thrombospondin 1	Hippo/TGF-β	2.06	1.17E-02
Tgfb3	TGF, β 3	Hippo/TGF-β	1.90	2.96E-02
Tsc22d1	TSC22 domain family, member 1	Hippo/TGF-β	1.78	2.60E-03
Dcn	decorin	Hippo/TGF-β	1.92	2.86E-02
Ifrd1	IFN-related developmental regulator 1	Hippo/TGF-β	1.63	3.29E-03

2.3.4 Discussion

In this study, we identified Pals1 as an essential regulator of renal epithelial morphogenesis. Intriguingly, heterozygous mice lacking one Pals1 *(Mpp5)* allele in the nephron developed a severe proteinuria, showed glomerular and tubular cysts, and died within 2 months of birth. The fact that even a partial reduction in Pals1 expression was sufficient to cause this complex renal phenotype is particularly interesting, given that other murine models lacking apical polarity proteins, such as Crb3 (Whiteman et al., 2014; Szymaniak et al., 2015; Charrier et al., 2015) or Lin7c knockout mice (Olsen et al., 2007), showed milder phenotype in the kidney, which moreover requires the loss of both alleles. These findings strongly support an essential, specific, and dose-dependent function for Pals1 in the nephron, especially during nephrogenesis.

Previous studies in the cerebral cortex and the retina have shown that partial removal of Pals1 causes severe cortical malformations in the brain and in retinal precursor cells, respectively (Kim et al., 2010; Cho et al., 2012). This is in line with our data, as it emphasizes that the level of Pals1 expression is crucial for the proper development of complex tissues. The defects seen at the renal filtration barrier in mice indicate that podocyte injury is a main factor for the severe proteinuria, suggesting that Pals1-deficiency affects podocytes during glomerulogenesis. The loss of the slit-diaphragm–like structures in Sdt-depleted nephrocytes, which are the fly model for glomerular podocytes, confirmed the important role of Pals1 at the renal filtration barrier. Moreover, our studies in nephrocytes confirmed the role of Pals1 as an upstream regulator of Hippo signaling, as the defects caused by knockdown of the Pals1 ortholog Sdt were rescued by a simultaneous knockdown of Yki. These data extend recent findings that have pointed to a tight link between polarity proteins and Hippo signaling (Chen et al., 2010; Varelas et al., 2010; Robinson et al., 2010; Grzeschik et al., 2010).

Despite the evolutionarily conserved role of Pals1 and Sdt in controlling Hippo signaling, the presence of two Yki orthologs in mammals, Yap and Taz, argues for tissue-specific roles of the two proteins in mammalian systems. Indeed, loss of Taz is linked to pronounced formation of glomerular (Hossain et al., 2007) and tubular cysts (Tian et al.,

2007; Makita et al., 2008) in several mice models, whereas Yap knockout mice die at early embryonic stages (Morin-Kensicki et al., 2006). Distinct roles for Yap and Taz in the kidney have also been shown by Reginensi *et al.* (2013). These authors generated mice lacking either Taz, Yap, or both in the nephron and found that only Taz depletion is linked to a cystic-kidney–like phenotype (Reginensi et al., 2013). Pals1 KD cells might therefore—at least in part—reflect the kidney phenotype seen in Taz knockout mice (Tian et al., 2007; Hossain et al., 2007; Makita et al., 2008; Reginensi et al., 2013).

Although the overall expression of the cotranscriptional factors Yap and Taz in the nephron was downregulated in Pals1-deficient kidneys, we observed an increase in the expression of Yap/Taz target genes. This change is associated with a shift of Yap/Taz from the cytoplasm into the nucleus in cyst-lining cells. This is also seen in our *in vitro* model, in which Taz and Yap show mainly nuclear localization. Consequently, partial loss of Pals1 leads to incomplete inactivation of the Hippo pathway. Our data are in agreement with findings of Happé *et al.* who investigated the localization of Yap in mice models of polycystic kidney disease, as well as in renal tissues from patients with ADPKD and autosomal recessive polycystic kidney disease (2011). They did not only observe an upregulation of Yap target genes in an ADPKD mouse model, but also found increased nuclear localization of Yap in cystic epithelia of renal tissues from patients with ADPKD and autosomal recessive polycystic kidney disease.

Margolis and colleagues have shown that a loss of Pals1 delays the formation of tight junctions, and is accompanied by a decrease in the transepithelial electrical resistance (Straight et al., 2004; Wang et al., 2007). These data in turn imply that defects in the formation of cell-cell contacts prevent the establishment of a tight lateral diffusion barrier in epithelial cells, which is essential for the separation of apical and basolateral transmembrane proteins within the plasma membranes. In this study, we observed that both Ca^{2+} as well as Pals1 depletion triggers Yap/Taz-dependent gene expression, suggesting that the tightness of junctions is a crucial factor in the control of Hippo signaling. Thus, our *in vitro* data probably supports the hypothesis that a reduced Pals1 level *in vivo* results in a reduced tightness of the various renal epithelia of the nephron, leading to a more inactivated Hippo signaling pathway in Pals1 knockout animals compared with control animals. However, these conclusions need further confirmation by further *in vivo* and *in vitro* studies.

Intriguingly, it was recently shown that failure to establish mature cell-cell contacts prevents correct basolateral distribution of TGF-β receptors, and leads to the accumulation of TGF-β receptors at the apical membrane accompanied by a concomitant increase in the expression of TGF-β target genes. This observation suggests that delays in the formation of cell-cell junctions make epithelial cells more susceptible to TGF-β–linked signaling processes (Varelas et al., 2010; Narimatsu et al., 2015). Indeed, gene expression analyses of Pals1-deficient kidneys and Pals1 KD cell lines revealed an upregulation of target genes of the TGF-β pathway. Thus, our data are compatible with a model in which Pals1, beyond its function as a crucial polarity protein, plays a key role as upstream regulator of Hippo- and TGF-β–mediated signaling in the nephron. Whether altered TGF-β signaling is linked to CRB complex–dependent cell-density sensing in a Hippo signaling–dependent (Varelas et al., 2010; Narimatsu et al., 2015) or –independent

manner (Nallet-Staub et al., 2015) is currently a matter of debate. In any case, imbalances between Hippo and TGF-β signaling may result in a "signaling catastrophe," triggering cyst formation due to incomplete inactivation of the Hippo pathway accompanied by highly increased susceptibility to pathogenic TGF-β signaling. Numerous studies showed the contribution of impaired TGF-β signaling on glomerular diseases (Tossidou and Schiffer, 2012; Herman-Edelstein et al., 2013; Edeling et al., 2016). Moreover, it has been reported that TGF-β signaling contributes to cyst progression and fibrogenesis (Norman, 2011; Małgorzewicz et al., 2013). Thus, both processes, inactivation of Hippo and activation of TGF-β signaling, contribute to the injury of glomerular and tubular nephron epithelia and cyst progression in the nephron.

So far, no mutations in Pals1 gene *(MPP5)* have been associated with renal, and in particular renal-cystic diseases in humans. The severity of the phenotypes observed in Pals1-deficient mice emphasizes the central role of this protein in the brain and the kidney. The fact that Pals1 haploinsufficiency causes lethal phenotypes in mice underlines the importance of Pals1, and makes it unlikely that *Pals1/MPP5* itself could be a target gene for rare inherited diseases. However, Pals1-interacting proteins have been linked to renal cyst formation in mice (Crb3, Lin7c, and Taz) (Hossain et al., 2007; Olsen et al., 2007; Tian et al., 2007; Makita et al., 2008; Reginensi et al., 2013; Whiteman et al., 2014; Szymaniak et al., 2015; Charrier et al., 2015) and to certain kinds of nephronophthisis (nephrocystin-1 and -4), a human inherited cystic disease of childhood (Delous et al., 2009). These findings support the hypothesis that apical polarity complexes (CRB and PAR) are directly or indirectly linked to renal diseases, especially renal cyst diseases.

In summary, our data provide initial insights that Pals1 is a negative regulator of the Hippo and TGF-β signaling pathways, and is thus directly involved in the process of nephrogenesis. Future studies should therefore target the Pals1-linked networks, as well as factors that might control the intracellular turnover and stability of these proteins, in order to decipher the mechanisms underlying pathogenesis.

2.3.5 Concise Methods

2.3.5.1 Mouse Strains and Genotyping

The *Pals1/Mpp5* cKO (conditional knockout, in a C56Bl/6 background) mouse was described earlier (Kim et al., 2010). Transgenic Six2-Cre mice were purchased from JAX (Kobayashi et al., 2008). To provide for EGFP-labeling of Cre-expressing cells and quantification of Cre penetrance in the Pals1 cKO mice, we included the double fluorescence mTomato/mGFP (mT/mG) reporter mouse in our studies (Muzumdar et al., 2007). For DNA isolation and genotyping, tissue was incubated in lysis buffer (50 mM KCl, 1.5 mM $MgCl_2$, 10 mM Tris/HCl pH8.3, 0.45% NP-40 0,45% Tween 20) containing 0.05 μg/μl proteinase K (Peqlab Biotechnology, Erlangen, Germany) at 55°C overnight. The proteinase K was then inactivated by incubation at 95°C for 10 minutes, the sample was centrifuged, and the DNA-containing supernatant was used for genotyping. Cre-positive mice were identified by PCR, using the primers *Cre for* (5′ GCATTACCGTCGATGCAACGAGTGATGAG 3′) and *Cre rev* (5′ GAGTGAACGAACCTGGTCGAAATCAGTGCG 3′), which results in a 450-bp PCR product. Pals1 mice were genotyped as previously described (Kim et al., 2010).

2.3.5.2 Tissue Preparation and Histologic Analyses

Blocks of cortical tissue were processed by standard procedures for paraffin sections (2 μm) and stained with periodic acid–Schiff.

2.3.5.3 Immunohistologic Analyses

Characterization of Pals1 protein expression was done in kidneys from Six-Cre2− (wildtype) and Six2-Cre+ mice (n=2–3 each) using immunofluorescence microscopy. Paraffin-embedded formalin-fixed sections (2 μm) were deparaffinized and rehydrated using standard protocols. Kidney sections were blocked for 45 minutes with 1% (wt/vol) skim milk (Bio-Rad Laboratories, Munich, Germany) followed by incubation with primary antibodies (see Table 1) overnight at room temperature and subsequent washing in Tris buffer (50 mM Tris pH 7.4 supplemented with 0.05% [vol/vol] Tween 20; three times 5 minutes).

Afterwards, the secondary fluorescence-labeled antibodies (see Table 3) were applied for 30 minutes followed by subsequent washing. For double staining of Pals1 with Aquaporin 2 the protocol was modified. Sections were stained for Pals1 followed by blocking first with 10% (vol/vol) rabbit serum diluted in Tris buffer and second with donkey anti-rabbit Fab fragments (1:50 in Tris buffer) for 30 minutes each and interrupted by intensive washing in Tris buffer. DAPI was used to stain nuclei (1:1000 in distilled water for 5 minutes) followed by rinsing in Tris buffer (three times 5 minutes). Finally, sections were covered with mowiol mounting medium (Calbiochem, La Jolla) and analyzed using laser scanning confocal microscopy (LSM Zeiss 710 and Zen software; Zeiss GmbH, Jena, Germany).

2.3.5.4 Cryo-Sections

After explantation, kidney tissue was directly embedded in Tissue-Tek (Sakura Finetek BV, Leiden, The Netherlands), and frozen sections (4–5 μm) were cut in a cryostat and mounted on slides. The slides were fixed with methanol/10% H_2O_2 at −20°C for 10 minutes, washed three times with PBS and incubated with 0.1% Triton-X-100 for 10 minutes at room temperature. For staining, the slides were first treated with blocking solution (5% BSA) for 20 minutes, then incubated with the first antibody solution (in 1% BSA) overnight at room temperature. After washing with PBS, the slides were incubated with the secondary antibody solution (in 1% BSA) for 45 minutes at room temperature. After further repeated washing the nuclei were stained for 5 minutes with DAPI and embedded in Fluoromount (Sigma-Aldrich) for microscopy.

We analyzed the number and size of glomeruli per kidney section as well as the distance between visceral and parietal epithelial cells in each glomerulus, and the size and number of cysts. Kidneys of six littermates (Six2-Cre+ versus Six2-Cre−) and one section of each kidney were used for quantification purposes. The number of glomeruli represents the total amount of glomeruli seen per kidney section (whole slides). The size of glomeruli and the distance between visceral and parietal cells were measured using panoramic viewer (3DHISTECH). We defined “cysts” as epithelium-lined fluid-filled cavities larger than approximately 35 μm in diameter and 1000 μm^2 in area. The total number of cysts

per kidney section was taken into account. To determine the mean area of cysts per section, the cysts were treated as circles ($A = \pi r^2$). The diameter was measured with panoramic viewer, and the area of the cyst ($A = \pi r^2$) was calculated.

2.3.5.5 Fly Stocks and RFP Accumulation Assay

Drosophila melanogaster stocks were cultured on standard cornmeal-agar food and maintained at 25°C. RFP filtration assays were performed at 29°C. Briefly, secreted RFP (ANP-RFP) is filtrated and taken up by garland nephrocytes, in which protein expression was downregulated using the nephrocyte-specific UAS/GAL4 driver line sns-GCN:GAL4 (Zhuang et al., 2009) and the following responder lines: UAS::mCherry-RNAi (negative control, #35778; Bloomington Stock Center, Bloomington, BL), UAS::Sdt-RNAi-111 (#37510; BL), and UAS::Sdt-RNAi-69 (#15342R-2; National Institute of Genetics, Shizuoka, Japan). For rescue experiments, sns-GCN::GAL4, ANP-RFP was recombined with UAS::Sdt-RNAi-111 and crossed to UAS::Yki-RNAi (#40497; Vienna *Drosophila* Resource Center, Austria) and UAS::Yki-S168A (Oh and Irvine, 2009). Garland nephrocytes were isolated from wandering third-instar larvae by microdissection in HL3.1 saline (Feng et al., 2004), fixed in 4% PFA in PBS for 1 hour, stained with DAPI for 20 minutes, washed with PBS, and mounted in Mowiol. Samples were imaged using an LSM-510 confocal microscope (ZEISS, Jena, Germany) and RFP accumulation in garland nephrocytes was subsequently analyzed using ImageJ. For each genotype, >50 nephrocytes from at least six individuals were scored.

Evaluation of nephrocyte ultrastructure was done by transmission electron microscopy. Briefly, garland nephrocytes were microdissected in HL3.1 saline, high-pressure frozen (EM-PACT2; Leica, Wetzlar, Germany), freeze-substituted in acetone/2% OsO_4/5% H_2O/0.25% uranyl acetate (AFS2; Leica, Wetzlar, Germany), and finally embedded in Epon. For transmission electron microscopy, 70-nm-thick sections were cut using a diamond knife (Diatome, Biel, Switzerland) with an ultramicrotome (Leica UC6 or UC7; Wetzlar, Germany). Samples were subsequently imaged with a TEM-902 transmission electron microscope (ZEISS, Jena, Germany).

2.3.5.6 Cell Culture and Generation of Stable Cell Lines

MDCK and HEK293T cells were grown in standard DMEM medium (Life Technologies) supplemented with glutamine and antibiotics (37°C and 5% CO_2) as described previously (Schulze et al., 2014; Wennmann et al., 2014). For Ca^{2+} depletion experiments, MDCK cells were cultivated in Ca^{2+}-free DMEM (Life Technologies) for 16 hours. Stable knockdowns of endogenous canine Pals1 in MDCK cells were generated using pSuperior-Puro (Oligoengine) according to the manufacturer's instructions. The short hairpin sequences used for silencing of endogenous canine Pals1 in MDCK cells were 5′-GCATGGTACGCTGACATTTGT-3′ (cPALS1-sh1) and 5′-AGAGGATAGTAGACAAGTTCT-3′ for (cPALS1-sh2), and for endogenous human Pals1 in HEK293T cells 5′-GCCAGTTCATCATAAGGAAGG-3′ (hPals1-sh1), and 5′-GCTACAGTTCGTAATGAAATG-3′ (hPals1-sh2), and 5′-CCTAAGGTTAAGTCGCCCTCG-3′ for the sh control. Selection of pSuperior-Puro–containing cells was done with 1 μg/ml puromycin.

2.3.5.7 Luciferase Assays

Luciferase assays were performed in MDCK cells to measure Yap/Taz-dependent (8xGTIIC-Lux system) or TGF-β signaling–dependent (3TP-Lux system) gene expression as described earlier (Varelas et al., 2010; Dupont et al., 2011). To normalize transfection, luciferase reporter genes were cotransfected with pCMV-β gal plasmids. All transfections were done with Lipofectamin 2000 (Life Technologies) according to the manufacturer's instructions.

2.3.5.8 Preparation of Cell and Tissue Lysates and Western Blot

Kidneys were homogenized using an ULTRA-TURRAX (IKA) high-performance disperser in 1× Laemmli buffer (4% SDS, 5% 2-mercaptoethanol, 10% glycerol, 0.002% bromophenol blue, 0.0625 M Tris-HCl; pH 6.8). Cells grown on dishes were lysed in 1× Laemmli. After boiling for 5 minutes, the sample was pushed through a 20-gauge needle and equal volumes of lysates were fractionated on 8%–15% SDS-PAGE gels (Biorad, Munich, Germany) and analyzed by western blot as described previously (Schulze et al., 2014; Wennmann et al., 2014). Nonspecific binding of antibodies to unoccupied areas of the PVDF membrane was prevented by preincubation in blocking solution (5% BSA in TBS-T) for 1 hour. Afterwards, the membranes were incubated with primary antibodies overnight at 4°C. After washing the membrane several times in TBS-T, the secondary antibody was applied for 30 minutes at room temperature and the membrane was washed three times before incubating with Lumi-Light (Roche) to visualize the specific antigens.

2.3.5.9 Antibodies

The antibodies used for western blot analyses or immunofluorescence studies are listed in Table 3.

2.3.5.10 Real-Time PCR Analysis and Evaluation

Total RNA was isolated from cells and from mouse tissues using the Mammalian Total RNA Miniprep Kit (Sigma-Aldrich). To verify the quality of RNA obtained from mouse tissue samples, the RNA integrity number (RIN) was determined using the RNA 6000 Nano LabChip technology (Agilent Technologies, Santa Clara). Only RNA with RIN≥6.7 was used for further analysis. RNA purity values (260/280 and 260/230) were above 1.99, and 1.8, respectively. The Agilent Bioanalyzer RIN values of the samples indicated no interfering degradation. Aliquots (1–3 μg) of total RNA were converted into cDNA using the SuperScript III Reverse Transcription Kit (Invitrogen, Darmstadt, Germany) according to the manufacturer's instructions.

Real-time PCR was performed using the SYBR Green PCR Master Mix (Life Technologies), the Biorad CFX384 Touch (Bio-Rad Laboratories GmbH, Munich), and Bio-Rad CFX Manager v3.0 software. Relative expression levels of genes of interest were calculated as ΔCt values normalized to the GAPDH control. Sequences of the primers used are listed in the Supplemental Material.

2.3.5.11 DNA Microarrays

RNA concentration and purity were measured using a Nanodrop spectrophotometer (Thermo Fisher Scientific Inc., Waltham, MA). RNA integrity was checked using an Agilent Bioanalyzer (software version B.02.07.SI532) on an RNA Nano Chip (both Agilent Technologies Inc., Santa Clara, CA). Probing of Affymetrix GeneChip Mouse Gene 2.0 ST microarrays (Affymetrix UK Ltd., High Wycombe, UK) was performed as described in the manufacturer's protocols. The probes were prepared from 100-ng aliquots of total RNA in accordance with the instructions supplied with the Affymetrix WT PLUS Reagent Kit. After hybridization, the arrays were washed and stained using the Affymetrix GeneChip Fluidics Station 450 and scanned using the Affymetrix GeneChip Scanner 3000 7G.

2.3.5.12 Microarray Data Analyses

Microarray data quality was checked as recommended by the manufacturer and quantified using the quality metrics in the Partek Genomics Suite software (Partek Inc., St. Louis, MO). Statistical analyses of microarray data were performed using the Partek Genomics Suite. CEL-files (containing raw expression measurements) were imported into Partek GS. The robust multiarray average algorithm was used for normalization. The array data were quantile-normalized and log-2–transformed. For each probe, a one-way ANOVA was performed: Yij = μ + Groupi + εij, where Yij represents the jth observation on the ith group and μ is the common effect for the whole experiment. εij represents the random error present in the jth observation on the ith group. The errors εij are assumed to be normally and independently distributed with mean 0 and SD δ for all measurements (Eisenhart, 1947). For each probe, the Fisher least significant difference was tested to statistically compare the difference between the means of the groups' expression measurements. An FDR value ≤0.05 was used as the threshold for significance (Klipper-Aurbach et al., 1995). Only genes with a fold-change of ±1.4 were regarded as significantly changed in expression. Microarray raw data will be available through Gene Expression Omnibus accession number GSE77628.

2.3.5.13 Statistical Analyses

The evaluation was done using GraphPad prism (Graph Pad software). All data show SD of at least three independent experiments and were analyzed using paired *t* test. * P<0.05; ** P<0.01; *** P<0.001.

2.3.6 Disclosures

None.

2.3.7 Acknowledgments

We thank Katja Brinkmann, Brunhilde Hähnel, Julia Schröer, Truc Van Le, and Karin Wacker for excellent technical assistance. In addition, we thank Prof. Xaralabos Varelas

(Boston, MA) and Prof. Stefano Piccolo (Padua, Italy) for providing constructs, Prof. Thomas Benzing and Prof. Berhard Schermer (Cologne, Germany) for $Taz^{-/-}$ tissue, and Prof. Christopher A. Walsh (Boston, MA) for the conditional Pals1 knockout mice.

The work was supported by grants from the German Research Foundation to T.W. (DFG, SCHL 1845/2-1) and M.P.K. (SFB699, KR3901/1-2) and by a grant from the Else Kröner-Fresenius-Stiftung (EKFS 2014_A271) to T.W. and H.P., respectively.

2.3.8 Footnotes

T.W. and B.V. contributed equally to this work.

2.3.9 Supplementary material

2.3.9.1 Pals1 expression during nephrogenesis is crucial for formation of a functional renal filtration barrier

Pals1 expression is crucial for the function of the renal filtration barrier. Numbers of glomeruli were reduced in 4-week-old Six2-Cre; Pals1wt/fl mice (Figure 2.3-9A). Furthermore, in these mice the average distance between the glomerulus and Bowman´s capsule was much larger than in control littermates (Figure 2.3-9B). In contrast to α-actinin 4 and GAPDH, expression of the slit-diaphragm proteins nephrin and podocin was strongly reduced in Pals1-deficient kidneys (Figure 2.3-9C). In addition, the nephrin-like distribution of Pals1 (Figure 2.3-9D, upper panel) was clearly altered in injured glomeruli (Figure 2.3-9D, lower panel).

Examination of Six2-Cre; Pals1wt/fl kidneys by light microscopy (Figure 2.3-9E) and transmission electron microscopy revealed advanced stages of glomerular injury (Figure 2.3-9F, G) and an expansion of the mesangio-capillary area, with podocyte detachment from the glomerular basement membrane leaving large areas of the GBM bare. In some areas detached podocytes assembled into clusters that formed crescent-like bridges between the tuft and Bowman‘s capsule. In early stages of glomerular degeneration podocytes exhibiting widespread foot-process loss and cytoplasm shedding were observed (Figure 2.3-9G).

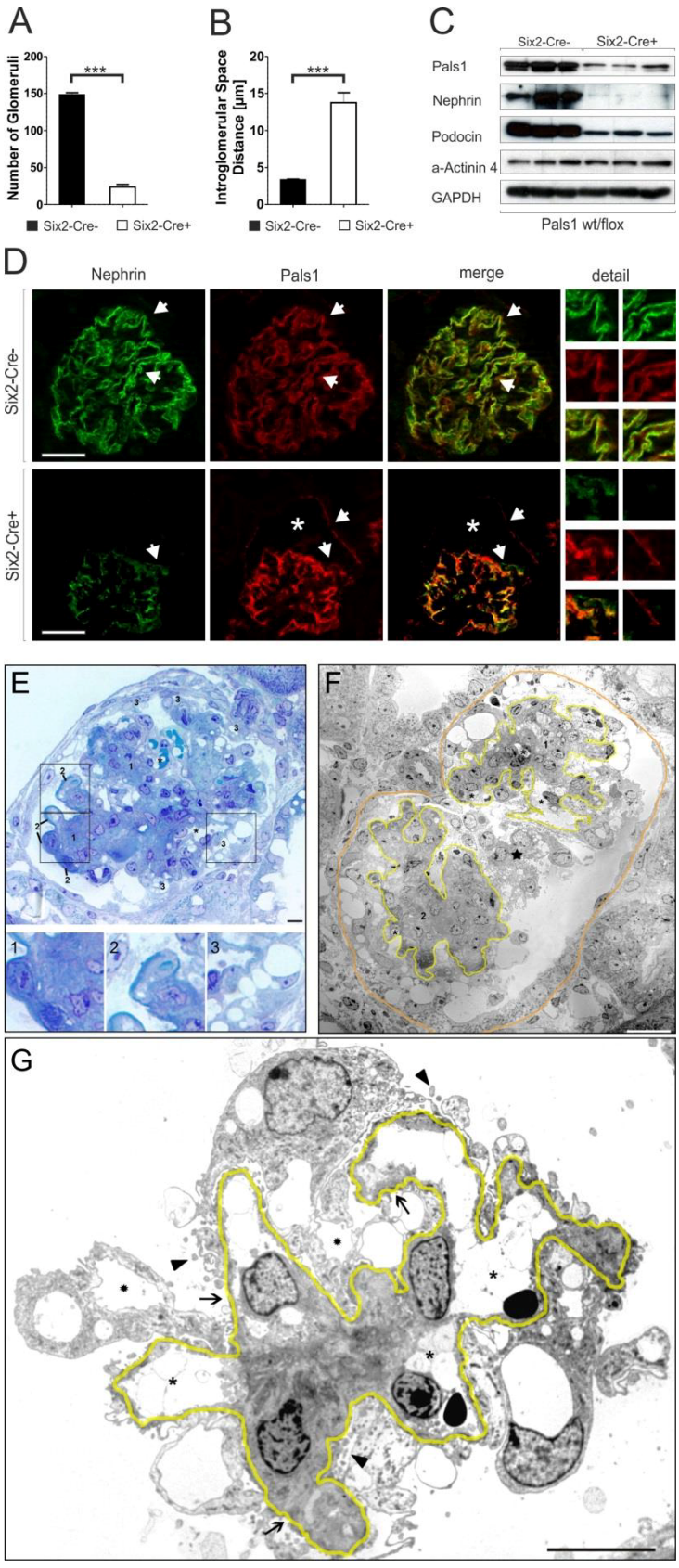

Figure 2.3-9 Pals1 expression during nephrogenesis is crucial for formation of a functional renal filtration barrier. Analysis of the glomerular phenotype of the Six2-Cre; Pals1wt/fl (Six2-Cre+) mutant at 4 weeks of age in comparison with the Pals1wt/fl (Six2-Cre-) control. A: Distribution of

glomerular numbers in Six2-Cre+ and Six2-Cre- mice. B: Distribution of intraglomerular distances (glomerulocyst formation) in Pals1-depleted (Six2-Cre+) and control versus (Six2-Cre-) kidneys. C: Western blot analysis of expression of Pals1, the slit-diaphragm-specific proteins nephrin and podocin, and α-actinin 4 and GAPDH (loading controls) in independent samples from three Six2-Cre+ and three Six2-Cre- mice. D: IF analysis of glomeruli derived from Six2-Cre+ and Six2-Cre- mice stained for Pals1 (red) and nephrin (green). Arrows mark areas shown in detail on the right, asterisks mark the glomerulocyst in the Six2-Cre+ glomerulus. Scale bar: 20 µm. E: Advanced stage of glomerular degeneration: Glomerular profile with massive expansion of the mesangio-capillary area (1), but with only a few clearly defined capillaries (asterisks). Podocytes have lost contact with the GBM over wide areas, leaving behind extensive bare tracts of GBM (2). At other sites (3), detaching podocytes with many pseudocysts have assembled into clusters that form bridges between the tuft and Bowman‘s capsule. LM, Scale bar: 5 µm. F: Advanced stage of glomerular degeneration: The glomerular basement membrane (GBM) is outlined in yellow, the parietal basement membrane (PBM) in orange. Glomerular profile containing two lobules (1 and 2) with podocytes that are in the process of detaching or have already detached from the GBM. The mesangio-capillary area (enclosed by the GBM) is massively expanded but contains only very few obvious capillaries (star). The detaching podocytes form a cell cluster floating within Bowman‘s space (star). The lower-left side of lobule 2 is covered by a huge crescent consisting of fully or partially detached podocytes that connect the tuft to Bowman‘s capsule. A similar but smaller crescent is seen at the upper side of lobule 1; TEM. Scale bar: 20 µm. G: Comparatively early stage of glomerular degeneration: Glomerular lobule with podocytes that are severely damaged, characterized by widespread loss of foot processes, pseudocysts (stars) and cytoplasm shedding (arrowheads). Bare areas of GBM are seen at a few sites (arrows). Major damage is also seen in the GBM (outlined in yellow). Empty spaces in the mesangium (asterisks) seem to coalesce with remnants of capillaries that contain a trapped erythrocyte at two sites. TEM. Scale bar: 10 µm.

For TEM analysis small cortical tissue blocks were fixed overnight in Sörensen's buffer containing 2.5% glutaraldehyde. Blocks were then treated with 4% OsO_4 and embedded in Epon. Thin sections (1 µm) were stained with methylene blue and studied by light microscopy. Ultrathin sections were stained with uranyl acetate and studied by transmission electron microscopy (Kriz et al., 2014).

2.3.9.2 Pals1 is expressed in the nephron

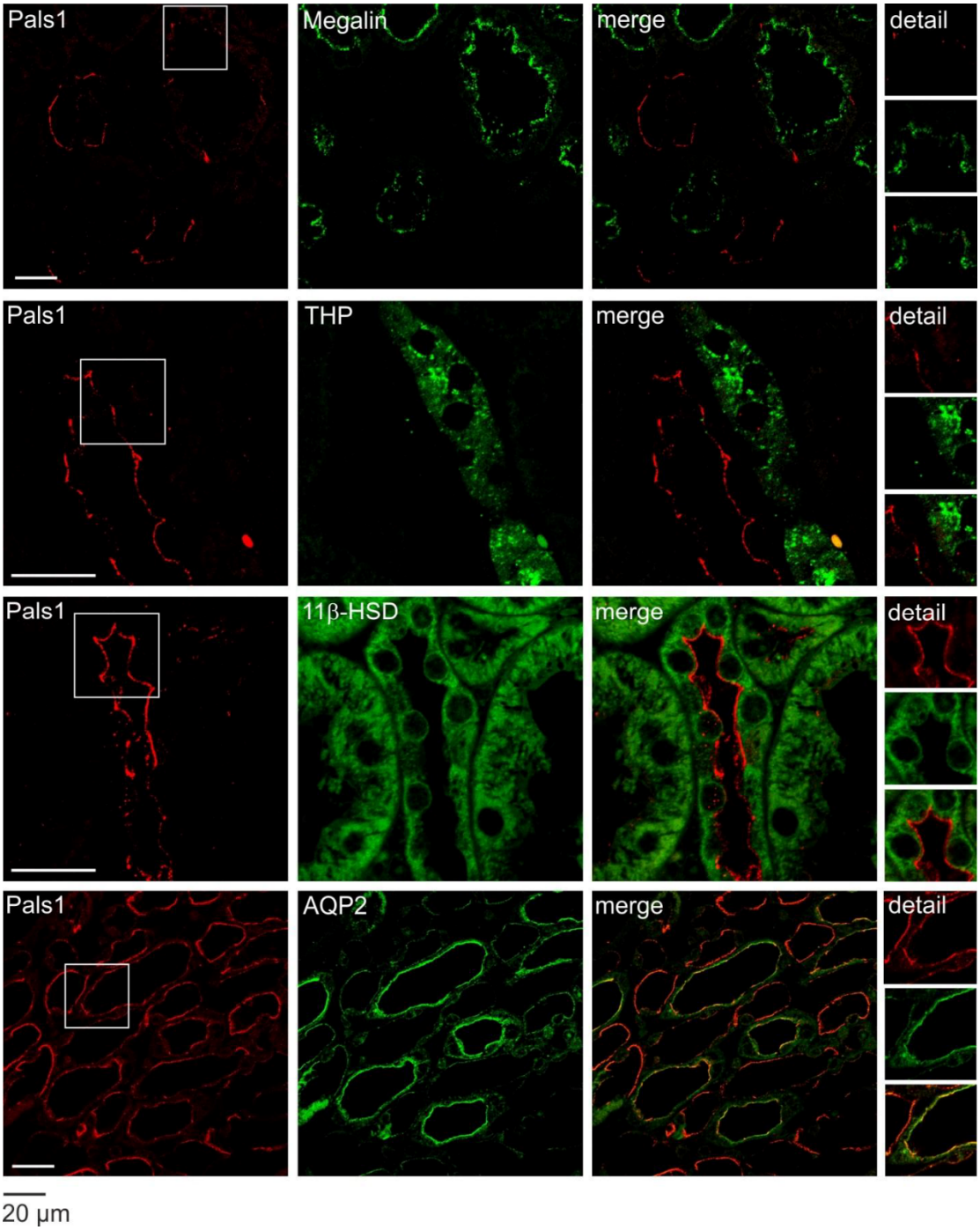

Figure 2.3-10 Immunofluorescence staining of Pals1 and co-staining with diverse tubulus markers in wildtype mice (6 months). Co-staining of Pals1 with Megalin (proximal tubule marker, A), Tamm-Horsfall Protein (thick ascending limb of the loop of Henle, B), 11β-HSD (distal tubules, C) and AQP2 (collecting duct, D). Scale bar: 50 µm.

2.3.9.3 In cyst-lining cells ADPKD biopsies, Pals1 polarization is only occasionally perturbed

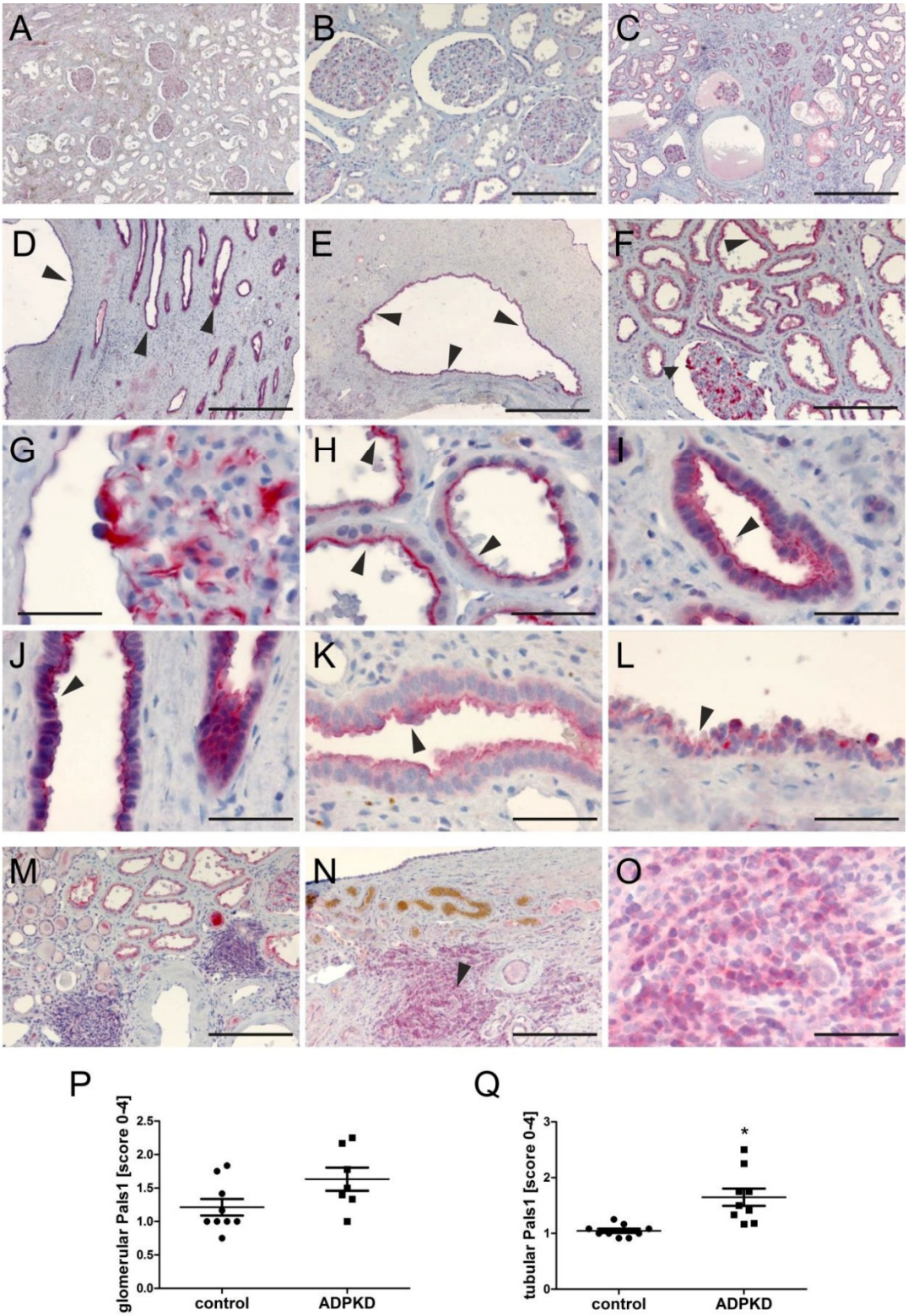

Figure 2.3-11 In cyst-lining cells of ADPKD biopsies, Pals1 polarization is only occasionally perturbed. A, B: Overview of Pals1 staining (red) in tumor-free kidney controls shows Pals1-positive staining in glomeruli and tubular cells. Scale bars: 500 µm (A) and 200 µm (B). C-E: Overview of Pals1 staining (red) in biopsies from ADPKD patients showed Pals1-positive staining in glomeruli (g) and tubular cells and cyst-lining cells (arrowheads, D-E). Scale bar: 500 µm (C-E). F-J: In ADPKD patients Pals1 is expressed in glomerular podocytes (F, scale bar: 200 µm, detail in G, scale bar: 30 µm), and predominantly in the apical membrane of dilated cystic tubuli (H, J, arrowheads, Scale bars: 50 µm). In addition, low levels of Pals1 are detectable in the cytoplasm of dilated cystic tubular cells (I, J). K-L: The overall impression is that Pals1 is strongly found in the apical membrane of cyst lining cells. However, in some cyst lining-cells, Pals1 staining is diffuse and not strongly polarized apically (scale bar: 50 µm). Thus, in ADPKD it seems that the hyperproliferative cysts show more diffuse staining. M-O: Diffuse Pals1 staining is detectable in infiltrating cells of ADPKD biopsies. The region marked by the arrowhead in N is shown at higher magnification in O. Scale bars: 200 µm (M, N) and 50 µm (O). P: Semi-quantitative evaluation of glomerular Pals1 staining in ADPKD compared to tumor-free controls. Q: Semi-quantitative evaluation of tubular Pals1 staining in ADPKD compared to tumor-free controls; *$p<0.002$.

2.3.9.3.1 Source of human renal tissue

Archival tissues from core needle biopsies performed between 2003 and 2012 at the Department of Nephropathology (Erlangen, Germany) were used for this study (n = 28). The morphological diagnosis of focal segmental glomerulosclerosis (FSGS; n=10) was made by the local pathologist. In addition, Pals1 expression was evaluated in 9 biopsies from patients with autosomal dominant polycystic renal disease (ADPKD). Control tissues without evidence of renal disease (n = 9) were obtained from distant portions of kidneys that were surgically excised because of the presence of a localized neoplasm. The use of tissue specimens was approved by the Ethics Committee of the Medical Faculty of the University of Erlangen.

2.3.9.3.2 Evaluation of Pals1/MPP5 expression in human renal biopsies

To determine the localization and expression level of MPP5 in the healthy and diseased kidney immunostaining of paraformaldehyde-fixed, paraffin-embedded biopsies was performed. A rabbit anti-Pals1/Mpp5 purchased from Sigma-Aldrich (HPA000993) was used as the primary antibody. After deparaffination, rehydration and blocking of endogenous peroxidase, antigens were retrieved in target retrieval solution (DAKO diagnostics, Hamburg, Germany) by heating for 1 minute in a pressure cooker. Bound anti-MPP5 antibody was detected by incubation with biotinylated donkey anti-rabbit antibody and horseradish-conjugated avidin (ZytoChem-Plus AP Polymer kit, Zytomed Systems GmbH, Berlin, Germany) following the manufacturer's instructions and using Fast red as substrate. Negative controls for immunostaining included either omission of the primary antibody or its substitution with equivalent concentrations of an irrelevant pre-immune rabbit IgG.

2.3.9.4 Analysis of tubular cyst development

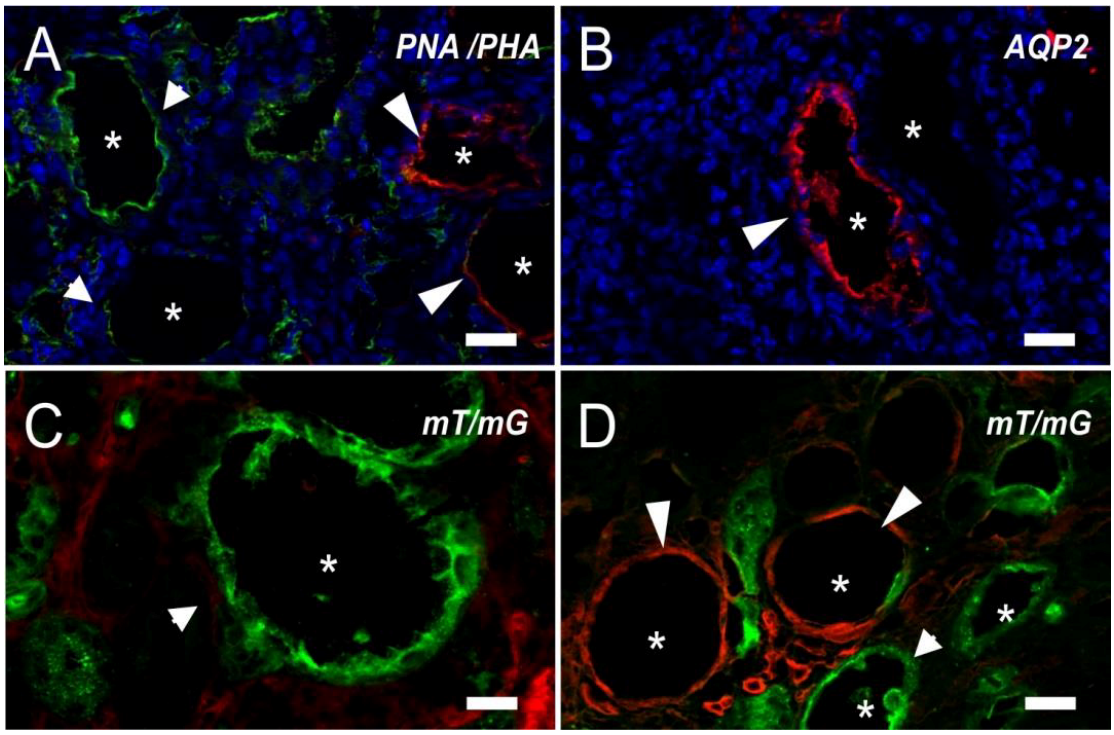

Figure 2.3-12 Analysis of tubular cyst development. A-D: Cysts in Pals1depleted kidneys (Six2-Cre+) were positive for proximal (PNA, red) and distal (PHA, green) tubular markers (A). Some cysts were positive for the collecting duct marker AQP2 (B). C, D: Crossing of Six2-Cre+ mice (Pals1wt/flox x Six2-Cre+) with the double fluorescence mTomato/mGFP reporter line allows one to visualize Cre-positive cells (green) in Pals1-deficient kidneys. Cysts showed a green (Cre+) (C), red (Cre-) or a mixed green-red (D) fluorescence, indicating secondary cyst formation in tubular regions that retain both Pals1 alleles. Asterisks mark cysts, arrowheads cyst-lining regions; Scale bars: 20 µm.

The different sizes and morphologies (Figure 2.3-12B, b1-b3) suggested that cysts developed from various sections of the nephron. We addressed this by staining with the lectins PHA (phytoheme agglutinin) and PNA (peanut agglutinin), which specifically mark regions of the proximal and distal tubular parts of the nephron, respectively. Most cysts could be labeled with PHA or PLA (Figure 2.3-12A). However, some cysts were positive for the collecting duct marker Aquaporin 2 (Figure 2.3-12B). Since Six2-positive cells are progenitors of proximal and distal tubules, but not of the collecting duct, this result argued for progressive cyst formation in nephron sections of non-cap-mesenchymal origin.

To further address this issue, we made use of a genetic approach. Crossing the Six2-Cre driver with mT/mG reporter mice results in a Cre-dependent fluorescence switch from red (mTomato) to green (mGFP) fluorescence in all Cre-expressing cells (Muzumdar et al., 2007; Kao et al., 2012). Therefore, we generated Six2-Cre; mT/mG mice and crossed them with homozygous conditional Pals1 knockout mice to obtain triple transgenic Six2-Cre; mT/mG x Pals1wt/fl progeny. These animals developed a strong kidney phenotype similar to that seen in Six2-Cre; Pals1wt/fl mice (not shown). As expected, most of the cyst-lining cells showed green fluorescence (Figure 2.3-12C). However, some cysts displayed a red or a mixed green-red fluorescence (Figure 2.3-12D), confirming the occurrence of secondary cyst formation in tubular regions that carry two wild-type Pals1 alleles.

2.3.9.5 Relative expression levels of target genes of the Hippo pathway and apical polarity genes

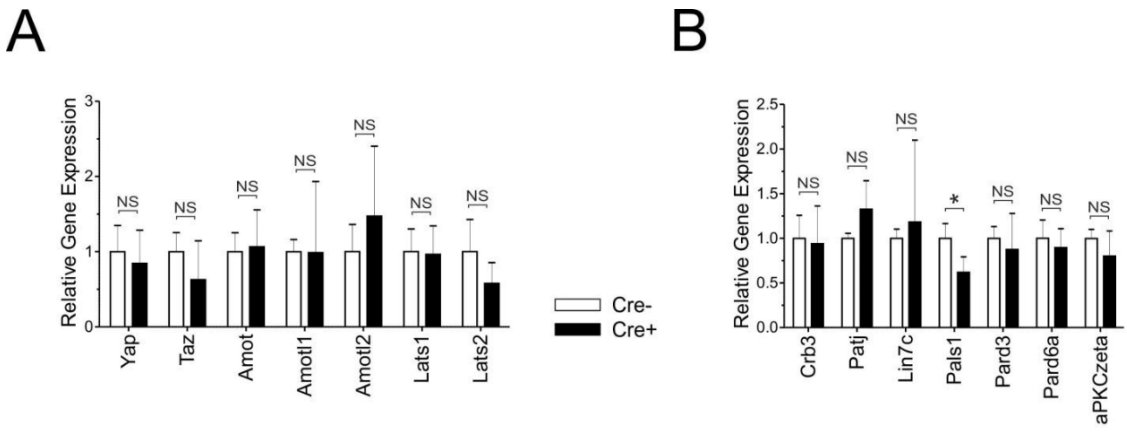

Figure 2.3-13 Relative expression levels of target genes of the Hippo pathway and apical polarity genes. A: Real-time PCR analysis revealed no significant differences in expression of targets of the Hippo pathway in Pals1-deficient kidneys (Six2-Cre+) relative to controls (Six2-Cre-). B: In Pals1-deficient kidneys (Six2-Cre+) decreased gene expression of Pals1 was confirmed. Expression of other polarity genes was not significantly altered. All data are shown as mean + SD of at least three independent experiments.

2.3.9.6 Immunohistology staining using Taz-/- tissue

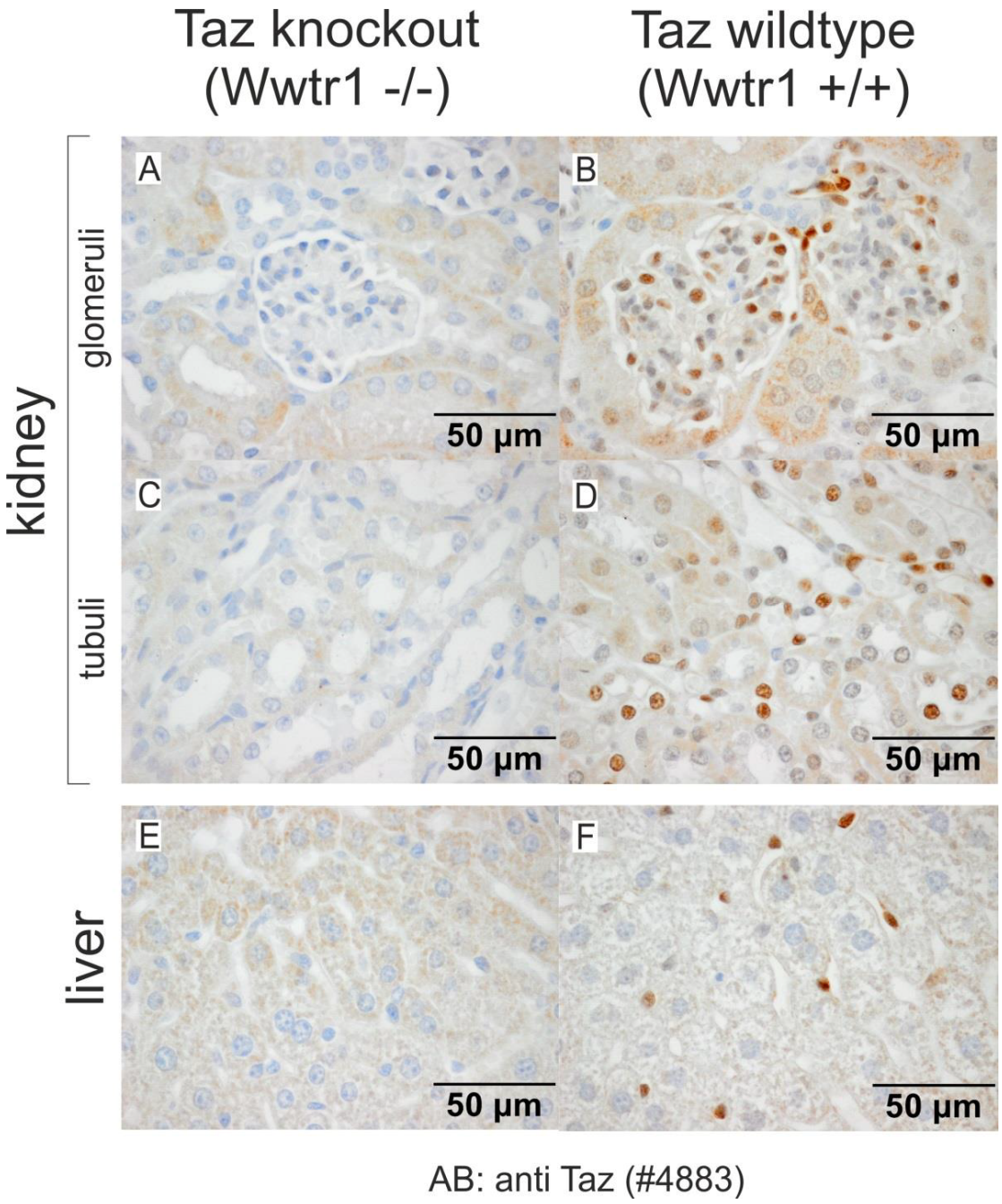

Figure 2.3-14 Immunohistology staining using Taz-/- tissue. The validation of the anti-Taz antibody from Cell Signaling (#4883) on Taz-/- tissues (kindly provided by T. Benzing and B. Schermer), indicates a high preference of this antibody for Taz. This antibody has also been used by Gandhirajan et al. (2016).

2.3.9.7 Nuclear export of Yap is delayed in Pals1 KD MDCK cells

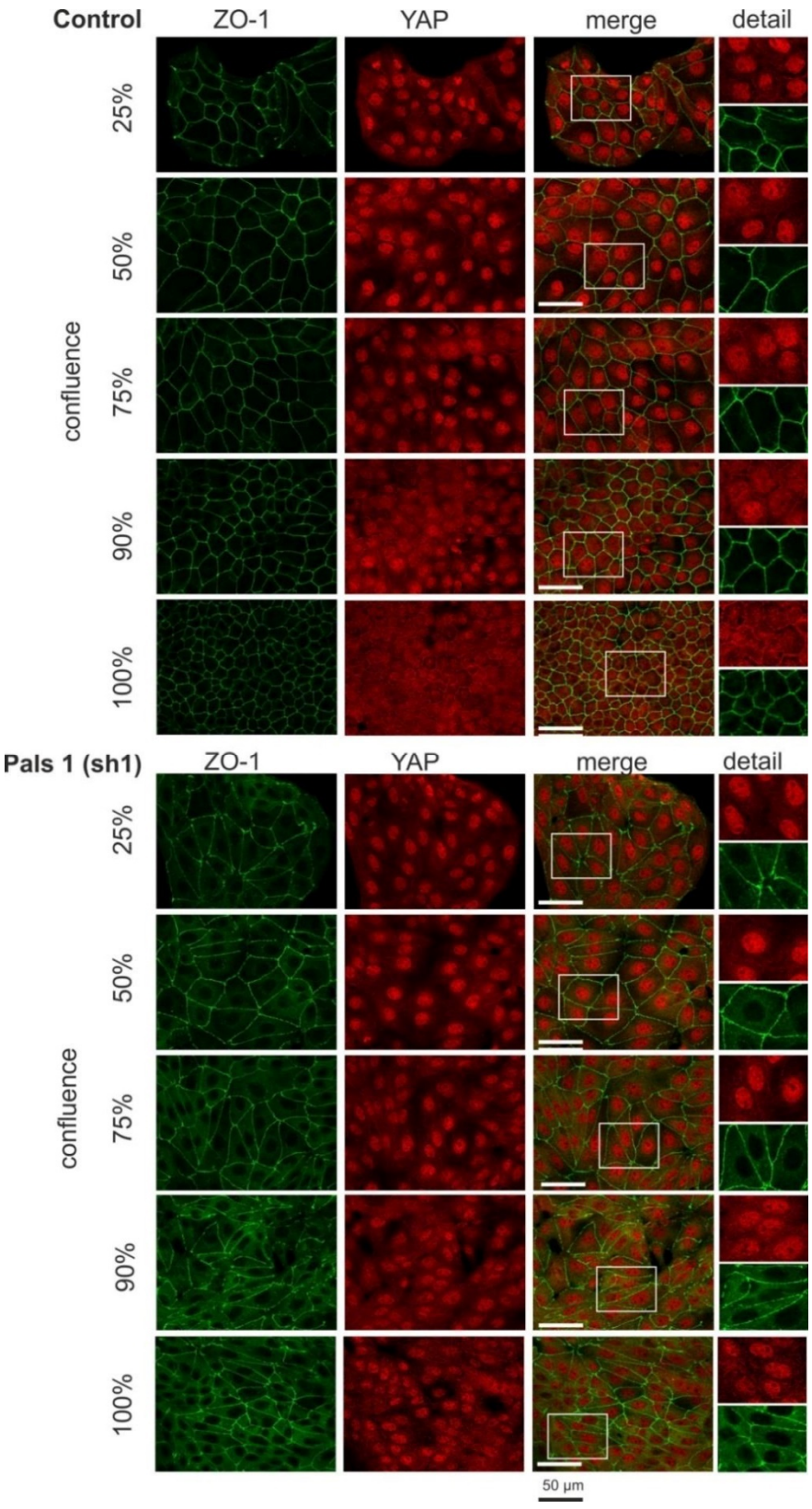

Figure 2.3-15 Nuclear export of Yap is delayed in Pals1 KD MDCK cells. Immunostaining analysis of Yap (red) and the junctional marker ZO-1 (green) in control and Pals1 KD cells. Increasing confluence is associated with increasing export of Yap from the nuclei to the cytoplasm in control cells. In Pals1 KD cells (sh1), export of YAP from the nucleus is delayed. Even in almost confluent cells (90-100% confluence) YAP remains predominantly localized in the nuclear compartment. In comparison with the control, ZO-1 shows a more diffuse distribution, and significant amounts of the protein remain in the cytoplasm. Scale bars: 50 µm.

2.3.9.8 Reduced Pals1 expression in HEK293T cells results in altered Hippo signaling.

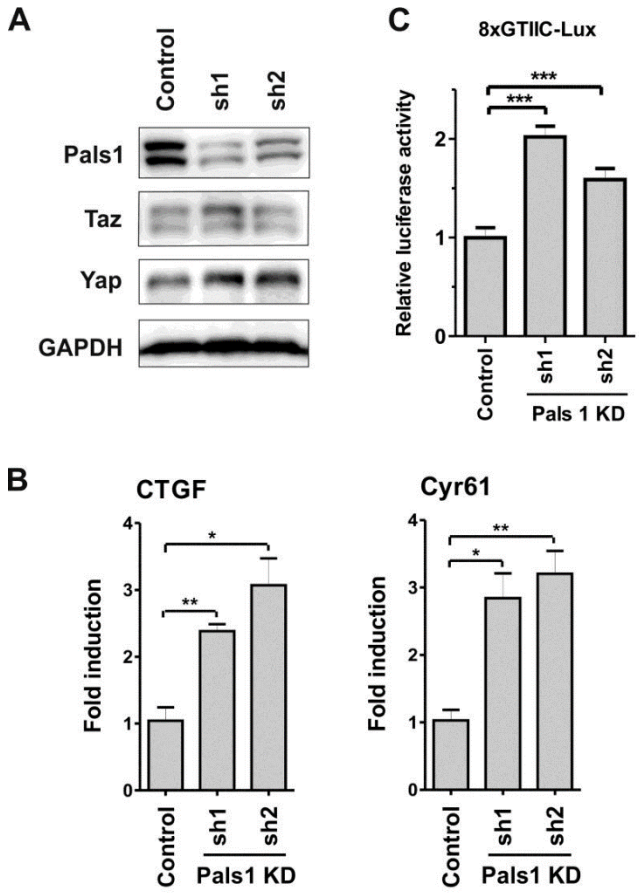

Figure 2.3-16 Reduced Pals1 expression in HEK293T cells results in altered Hippo signaling. A: Knockdown of Pals1 in HEK293T cells (sh1 and sh2) has no influence on Taz and Yap expression. Actin served as loading control. B: Expression of the Hippo target genes CTGF and CYR61 is increased in Pals1 KD cells (RT-PCR data are shown as mean + SD of at least three independent experiments). C: The results of the 8xGTIIC-Lux reporter gene assay showed that Pals1 knockdown significantly enhances Yap/Taz-dependent transcriptional activity (data are presented as mean + SD and normalized to lane 1).

2.3.9.9 Gene expression analysis in Pals1-depleted mice versus littermate controls.

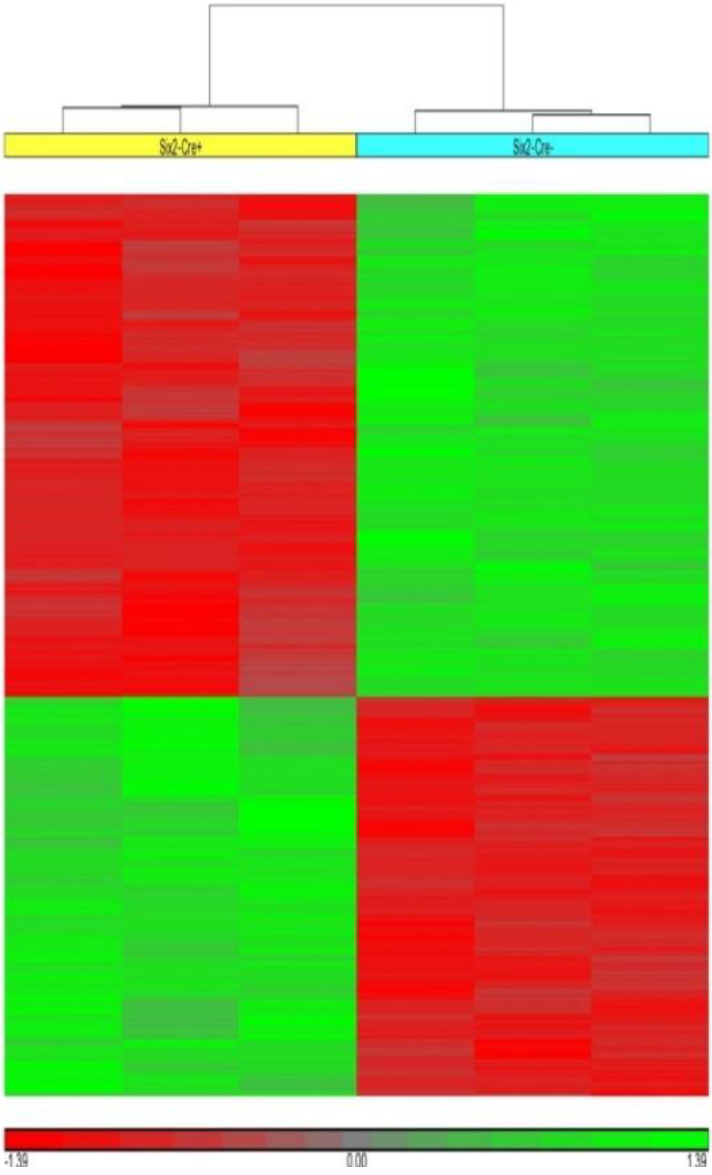

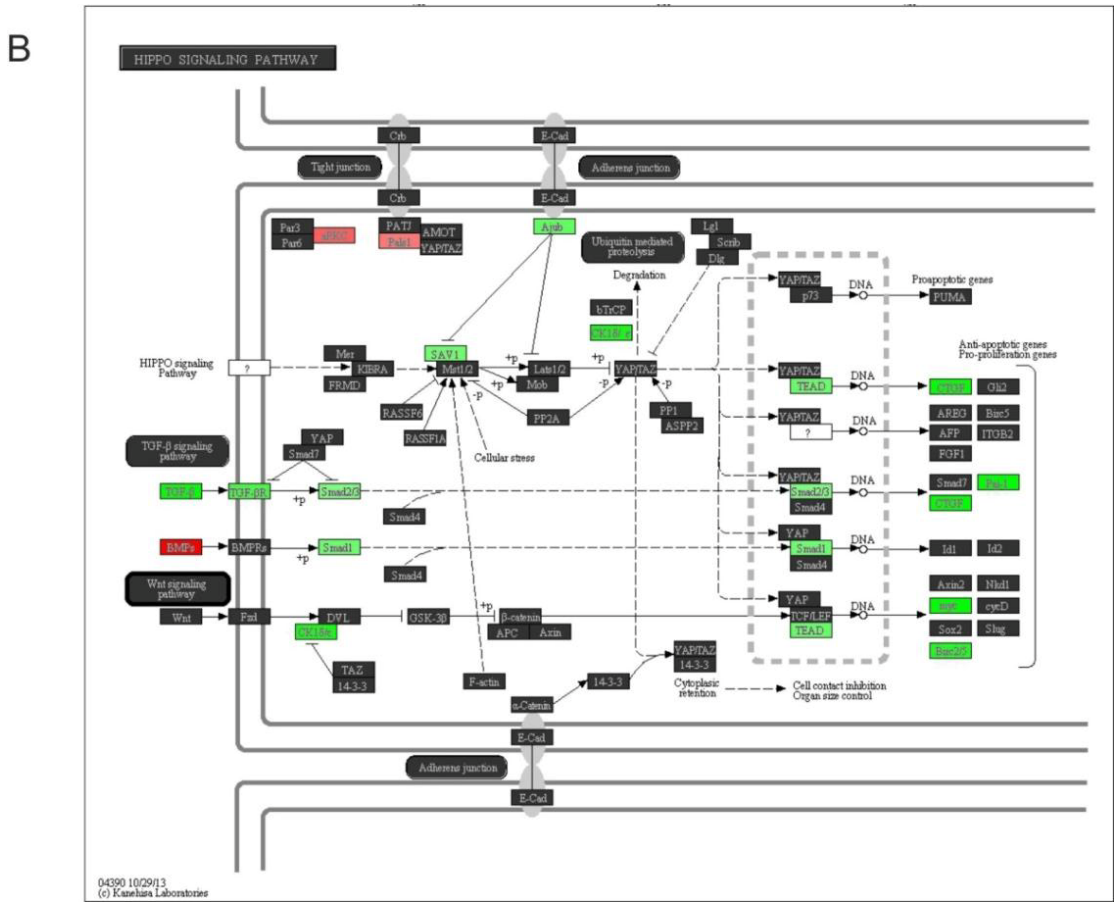

Figure 2.3-17 Gene expression analysis in Pals1-depleted mice versus littermate controls. Microarray experiments were performed to compare the gene expression profiles of Pals1-depleted Six2-Cre, Pals1wt/fl (Six2-Cre+) mice and their littermate controls Pals1wt/fl (Six2-Cre-). A: HEAT map showing the hierarchical clustering of differentially expressed genes. The data set (each N=3) was homogenous, allowing the different gene expression profiles to be compared. B: KEGG pathway diagram: Several target genes of the Hippo pathway, but also genes that respond to TGFβ signaling were up- (green) or downregulated (red) in Pals1-depleted kidneys.

2.3.9.10 Reduced Pals1 expression results in an increased expression of renal injury marker genes.

Table 2 Reduced Pals1 expression results in an increased expression of renal injury marker genes. In Pals1-deficient kidneys (Six2-Cre+) renal injury marker genes are highly upregulated (selection). The complete list of differentially expressed genes is given in the suppl. data files SD2 and SD3.

Gene	Alias / Protein	Fold change	p-Value	Reference*
Havcr1	Kidney injury molecule -1 (Kim-1)	29.37	1.03 E-03	Fassett et al., 2011
Lcn2	Lipocalin-2; Neutrophil gelatinase-associated lipocalin (Ngal)	12.98	1.16 E-05	Fassett et al., 2011
Edn1	Endothelin 1 (Et-1)	8.21	9.01 E-06	Kohan and Barton, 2014
C3	Complement component 3	7.46	5.76 E-04	Caliskan and Kiryluk, 2014
Serpine1	Serine/cysteine peptidase inhibitor, clade E, member 1 Plasminogen activator inhibitor type 1 (Pai-1)	8.60	3.56 E-04	Małgorzewicz et al., 2013
Ltbp2	Latent transforming growth factor beta binding protein 2	8.67	5.92 E-03	Haase et al., 2014
Gpnmb	Glycoprotein(transmembrane) Nmb (HGFIN, Osteoactivin)	8.74	5.33 E-04	Pahl et al., 2010; Patel-Chamberlin et al., 2011
Mmp7	Matrix metallopeptidase 7 (Matrilysin)	7.81	1.01 E-04	Surendran et al., 2004
Ccl2	CC-chemokine ligand 2; Monocyte chemoattractant protein-1 (Mcp-1)	8,93	2.56 E-04	Urbschat et al., 2011
Tagln	Transgelin 1 (SM22)	7.17	2.24 E-03	Ogawa et al., 2007; Marshall et al., 2011
Tagln2	Transgelin 2	8.93	2.56 E-04	Ogawa et al., 2007; Marshall et al., 2011

*) References or reviews (with reference therein) that previously linked these genes to renal injury.

2.3.9.11 Extended methods, details of antibodies and primer

Table 3 Antibodies used in the study.

Antigen	Species	Company	Cat #	Dilution Western Blot	Dilution IF, IHC
Pals1/Mpp5	rabbit	ProteinTech	17710-1-AP	1:1000	1:50
α-Actinin-4	rabbit	Alexis	ALX-210-356	1:1000	
GAPDH	mouse	Covance Inc.	MMS-580S	1:2000	
Nephrin	guinea pig	Acris	BP5030	1:500	1:100
Podocin	rabbit	Sigma-Aldrich	P0372	1:1200	
Actin	rabbit	Sigma-Aldrich	A2066	1:1000	
E-Cadherin	mouse	BD Transduction	610182	-	1:100
ZO-1	mouse	Invitrogen	61-7300	-	1:50
Yap	rabbit	Cell signaling technology (CST)	XP #14074	1:1000	1:100
pYap S-127	rabbit	CST	#4911	1:1000	
Taz	rabbit	CST	#4883	1:1000	1:100
Aquaporin2 (AQP2)	rabbit	Sigma Aldich	SAB5200110		1:50
11-beta-Hydroxysteroid Dehydrogenase Type II (11beta HSD2)	sheep	Millipore	AB1296		1:100
Tamm-Horsefall Protein	mouse	Santa Cruz laboratories	sc-71022		1:50
Megalin	mouse	Acris	DM3613P		1:100
Alexa Fluor 594 Phalloidin	-	Invitrogen	-		1:200
DAPI	-	Roche	-		1:1000
HRP-conjugated secondary antibodies		Dianova			1:2500
Alexa coupled 2nd Abs for IF	-	Life technologies			1:1000
Rabbit serum	rabbit	Dianova	011-000-120		10% in Tris
Anti-rabbit IgG Alexa647	donkey	Life technologies	A31573		1:200
Anti-rabbit IgG Alexa568	donkey	Life technologies	A10042		1:200
Anti-mouse IgG Alexa488	donkey	Life technologies	A21202		1:200
Anti-sheep IgG Alexa568	donkey	Life technologies	A21099	1:200	1:200
Anti-rabbit Fab fragment	donkey	Jackson Immuno research	711-007-003		1:50

Table 4 Primers used for SYBR Green RT-qPCR in mice.

Target	Species	Direction	Sequence (5'-3')
Amot	mouse	forward	CAGCCAGGGCAACACAGG
Amot	mouse	reverse	GACAGGTGAGCAGAGTGGTC
AmotL1	mouse	forward	GGGAAAAGCGTAGAGGACCC
AmotL1	mouse	reverse	TTGAGTGAGGGTTTCCGTGG
AmotL2	mouse	forward	GGACACCCTCTCTGGACTCT
AmotL2	mouse	reverse	CATGCACCAAGGCATCACTG
Birc2	mouse	forward	TGAGCAGCTGTTGTCCACTT
Birc2	mouse	reverse	GAACCGTCTGTCTCACCAGG
Birc5	mouse	forward	GAACCCGATGACAACCCGAT
Birc5	mouse	reverse	TGGTCTCCTTTGCAATTTTGTTCT
Ccl2	mouse	forward	AGCTGTAGTTTTTGTCACCAAGC
Ccl2	mouse	reverse	TGCTTGAGGTGGTTGTGGAA
Crb3	mouse	forward	GAGCCTAACAGCACCGGAC
Crb3	mouse	reverse	CCCGAAGTTTTCGCATGAGC
Ctgf	mouse	forward	GTGTGCACTGCCAAAGATGG
Ctgf	mouse	reverse	ATTTCCCAGGCAGCTTGACC
Cyr61	mouse	forward	CACTGAAGAGGCTTCCTGTCTT
Cyr61	mouse	reverse	GATCCGGGTCTCTTTCACCA
GAPDH	mouse	forward	TGGCCTTCCGTGTTCCTACC
GAPDH	mouse	reverse	GGTCCTCAGTGTAGCCCAAGATG
Havcr1	mouse	forward	GCATCTCTAAGCGTGGTTGC
Havcr1	mouse	reverse	TGCAGCTGGAAGAACCAACA
Lats1	mouse	forward	TGAGAAGAGTGCGGACAGTG
Lats1	mouse	reverse	TGAGATAATCCAACCCGCATCAT
Lats2	mouse	forward	GCAAGAGATTCGAGAGGGGC
Lats2	mouse	reverse	CCATCTCCTGGTCACATCCC
Lcn2	mouse	forward	ACGGACTACAACCAGTTCGC
Lcn2	mouse	reverse	AATGCATTGGTCGGTGGGG
Lin7c	mouse	forward	AATGGAGTGAGTGTTGAAGGGG
Lin7c	mouse	reverse	TACAATCACTGGCGTGGAGG
Pals1/Mpp5	mouse	forward	TCAGGCACTTTTACTGGCCC

Target	Species	Direction	Sequence (5'-3')
Pals1/Mpp5	mouse	reverse	AACTGTGGCACCCAATGGAA
Pard3	mouse	forward	GATGTAACGAGCTGCGGTCT
Pard3	mouse	reverse	ACCCATTATCCTGCTCAGTGC
Pard6a	mouse	forward	CAGAAACGGGCAGAAGGTGA
Pard6a	mouse	reverse	TGAACCATGTTTGTGCAGCC
Patj	mouse	forward	TATCCTGCAGGTTGTGGCAG
Patj	mouse	reverse	TTCCAGGGTCTCGCCATTTC
Prkcz	mouse	forward	TCCGTCTGAAGGCGCAC
Prkcz	mouse	reverse	ACAAGGGTCACCTTCACTGTC
Tagln	mouse	forward	TTATGAAGAAAGCCCAGGAGCA
Tagln	mouse	reverse	TTTGTGAGGCAGGCTAAGCA
Taz/Wwtr1	mouse	forward	CTGAGTCCACAGAACCACCC
Taz/Wwtr1	mouse	reverse	GGGCCCTCCATTGAGGAAAG
Yap1	mouse	forward	CCCTCGTTTTGCCATGAACC
Yap1	mouse	reverse	TGCTCCAGTGTAGGCAACTG

Table 5 Primers used for SYBR Green RT-qPCR in MDCK cell lines.

Target	Species	Direction	Sequence (5'-3')
Birc2	dog/MDCK	forward	GGCCGCGATTAACAGAGGG
Birc2	dog/MDCK	reverse	CCTTGCCTGTTTTGGCATGT
Cyr61	dog/MDCK	forward	CTGGTCAAAGTTACCGGCCA
Cyr61	dog/MDCK	reverse	CCGTTCCAAAAACTGGGAGG
Pai-1 /Serpine 1	dog/MDCK	forward	AACCTGGCGGACTTCTCAAG
Pai-1 /Serpine 1	dog/MDCK	reverse	ACTGTTCCTGTGGGGTTGTG

2.4 Distinct function of Crumbs regulating slit diaphragm assembly and endocytosis in *Drosophila* nephrocytes

Authors
Florian Hochapfel[1,2], Lucia Denk[1], Gudrun Mendl[1], Ulf Schulze[2], Christine Maaßen[1], Yulia Zaytseva[1], Hermann Pavenstädt[2], Thomas Weide[2], Reinhard Rachel[1], Ralph Witzgall[1], Michael P. Krahn[1,2]

Journal
Cellular and Molecular Life Sciences, December 2017, Volume 74, Issue 24, pp 4573–4586

Author Affiliations
1. Molecular and Cellular Anatomy, University of Regensburg, 93053 Regensburg, Germany
2. Internal Medicine D, University Hospital of Münster, 48149 Münster, Germany

Accepted for Publication
July 17, 2017

Contribution
The author of this thesis contributed everything for the manuscript except data on human and mouse kidney tissue, parts of the electron microscopy data on *Drosophila* nephrocytes and parts of the written text.

2.4.1 Abstract

Mammalian podocytes, the key determinants of the kidney's filtration barrier, differentiate from columnar epithelial cells and several key determinants of apical–basal polarity in the conventional epithelia have been shown to regulate podocyte morphogenesis and function. However, little is known about the role of Crumbs, a conserved polarity regulator in many epithelia, for slit-diaphragm formation and podocyte function.

In this study, we used *Drosophila* nephrocytes as model system for mammalian podocytes and identified a conserved function of Crumbs proteins for cellular morphogenesis, nephrocyte diaphragm assembly/maintenance, and endocytosis. Nephrocyte-specific knock-down of Crumbs results in disturbed nephrocyte diaphragm assembly/maintenance and decreased endocytosis, which can be rescued by *Drosophila* Crumbs as well as human Crumbs2 and Crumbs3, which were both expressed in human podocytes. In contrast to the extracellular domain, which facilitates nephrocyte diaphragm assembly/maintenance, the intracellular FERM-interaction motif of Crumbs is essential for regulating endocytosis. Moreover, Moesin, which binds to the FERM-binding domain of Crumbs, is essential for efficient endocytosis. Thus, we describe here a new mechanism of nephrocyte development and function, which is likely to be conserved in mammalian podocytes.

2.4.2 Introduction

In vertebrates, podocytes play a crucial role in the establishment of the filtration barrier. A dysfunction of these cells consequently leads to renal failure. During kidney development, podocytes acquire a highly specialized morphology, changing their shapes from columnar epithelial cells to an elaborated outstretched form with primary-, secondary-, and foot processes, which encompass the glomerular arterioles. Subsequently, the slit diaphragm, a highly organized structure composed of glycosylated transmembrane proteins and their intracellular adaptors, is established to regulate the filtration slit between the foot processes.

Beside its core components of podocyte-specific proteins (most importantly, the immunoglobulin-domain proteins Nephrin and Neph1 and the adaptor protein Podocin (Patrakka and Tryggvason, 2007)), assembly of the slit diaphragm has been reported to depend on several proteins which localize to the Tight junctions (TJ) in conventional epithelia (Fukasawa et al., 2009), e.g., *Zonula Occludens* protein 1 (Huber et al., 2003; Itoh et al., 2014), PARtitioning defective 3 (Hartleben et al., 2008), and atypical Protein Kinase C (Hartleben et al., 2008; Hirose et al., 2009; Huber et al., 2009; Hartleben et al., 2013; Satoh et al., 2014). Thus, podocytes maintain their intrinsic apical–basal polarity while extending the apical domain [cell body and (foot) processes, facing the urinary space] and shrinking the basolateral plasma membrane (anchored on the glomerular basal membrane).

One key determinant of apical–basal polarity in many if not all epithelia is the transmembrane protein Crumbs (Crb). *Drosophila* Crb (DmCrb) functions together with PAR-3 (Bazooka in *Drosophila*) to determine the apical plasma membrane domain. Both complexes counterbalance the activity of the basolateral determinants lethal giant larvae

(Lgl), discs large (Dlg), and scribble (Scrib) (Tepass, 2012). Apart from one described exception in boundary cells of the hindgut (Kumichel and Knust, 2014), DmCrb has to be stabilized at the TJ (or the TJ-homologous region in *Drosophila* epithelia) by binding its adaptor protein Stardust (Sdt, Protein associated with Lin-7 one, Pals-1, in mammals) (Bachmann et al., 2001; Hong et al., 2001; Makarova et al., 2003; Roh et al., 2003; Straight et al., 2004). The third member of the canonical Crb complex, PATJ (Pals1-associated TJ protein), is not essential for stabilization of Crb–Sdt in epithelial cells of the embryonic epidermis but in photoreceptor cells and in cultured mammalian cells (Michel et al., 2005; Shin et al., 2005; Pénalva and Mirouse, 2012; Zhou and Hong, 2012; Sen et al., 2012; Sen et al., 2015). Loss of DmCrb results in disturbed apical–basal polarity and defects in adherens junction (AJ) formation (Tepass, 1996).

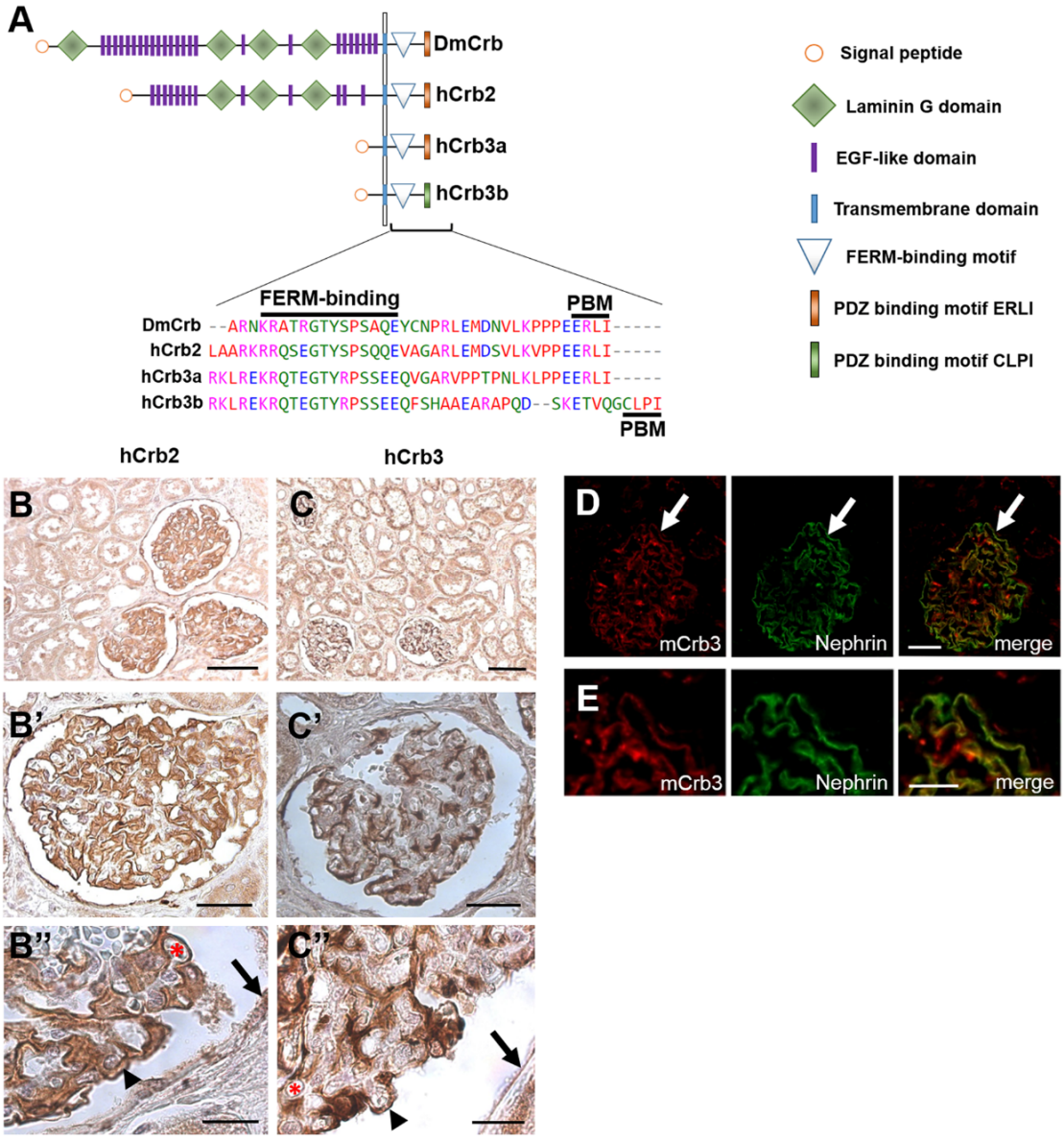

Figure 2.4-1 Crb2 and Crb3 are expressed in human podocytes. a Scheme of *Drosophila* Crb and hCrb2 and hCrb3 proteins including a sequence alignment of the intracellular domain. PBM PDZ-

binding motif, FERM 4.1-protein–Ezrin–Radixin–Moesin. **b, c** Immunostainings of human kidney sections (cortex). Note that hCrb2 expression is prominent in glomeruli [podocytes (arrow head), endothelial cells (asterisk), and parietal cells (arrow) in b″ and c″] but only faint in tubules, whereas hCrb3 is strongly expressed in both glomeruli and tubules (c). d Mouse Crb3 colocalizes with mouse Nephrin in glomeruli of kidney sections of an adult mouse (3 months). e Magnification of the arrow-marked area is shown in the right panels. Scale bars 100 µm in b and c, 50 µm in b′ and c′, 20 µm in b″, c″, and d, and 10 µm in e

In contrast to *Drosophila*, three genes encode Crb proteins in mammals: Expression of Crb1 is restricted to the nervous system (and testis), whereas Crb2 is present in kidney, testis, placenta, and cerebral cortex. Finally, Crb3 can be detected in many if not all epithelia (the human protein atlas (Uhlén et al., 2015)) (Lemmers et al., 2004). Loss of Crb3 in mice has been recently described to be postnatal lethal, but the described defects in apical–basal polarity in epithelia are not as strong as seen for its *Drosophila* counterpart: For instance, the formation of TJ/AJ in the tubular system of the kidney is largely unaffected (Whiteman et al., 2014). Apart from its function in the retina (Alves et al., 2013), there is little information about the molecular function of Crb2, although it resembles DmCrb regarding its protein domain structure and is thus likely the direct homologue in certain tissues. In contrast, Crb3 virtually lacks the extracellular domain (Figure 2.4-1). Crb2-deficient mice die in embryonic stages, displaying gastrulation defects (Xiao et al., 2011). Interestingly, mutations in Crb2 are found in patients suffering from nephrotic syndrome (Ebarasi et al., 2015) or congenital nephrosis (Slavotinek et al., 2015). Moreover, loss of Crb2 in zebrafish results in defects in foot-process development and slit-diaphragm assembly (Ebarasi et al., 2009; Ebarasi et al., 2015).

To further explore the function of Crb in podocytes, we used *Drosophila* nephrocytes as model system. Nephrocytes have been recently identified as podocyte-homologous cells exhibiting a striking similarity in morphology, protein expression, and function (Weavers et al., 2009; Zhuang et al., 2009; Tutor et al., 2014; Na et al., 2015): nephrocytes are more or less round, mono- (pericardial) or di- (garland) nucleated cells. They are floating in the larval and adult stage hemolymph in two populations: Garland nephrocytes surrounding the foregut and pericardial nephrocytes lining up on both sides of the heart tube. One hallmark of these cells is the formation of elongated infoldings of their plasma membrane. These structures resemble podocyte foot processes and are connected by a nephrocyte diaphragm at the most exterior part (Figure 2.4-2g). Narrow lacunae are formed between the foot processes and the nephrocyte diaphragms seal this microcompartment towards the extracellular space. The nephrocyte diaphragm has been shown to be composed of similar proteins as the slit diaphragm in mammals (e.g., Nephrin, NEPH1, Podocin), exhibiting a size-selective barrier (Zhuang et al., 2009; Weavers et al., 2009). Upon filtration of certain substances, presumably toxins and metabolic wastes, from the hemolymph, these components are endocytosed and intracellularly stored.

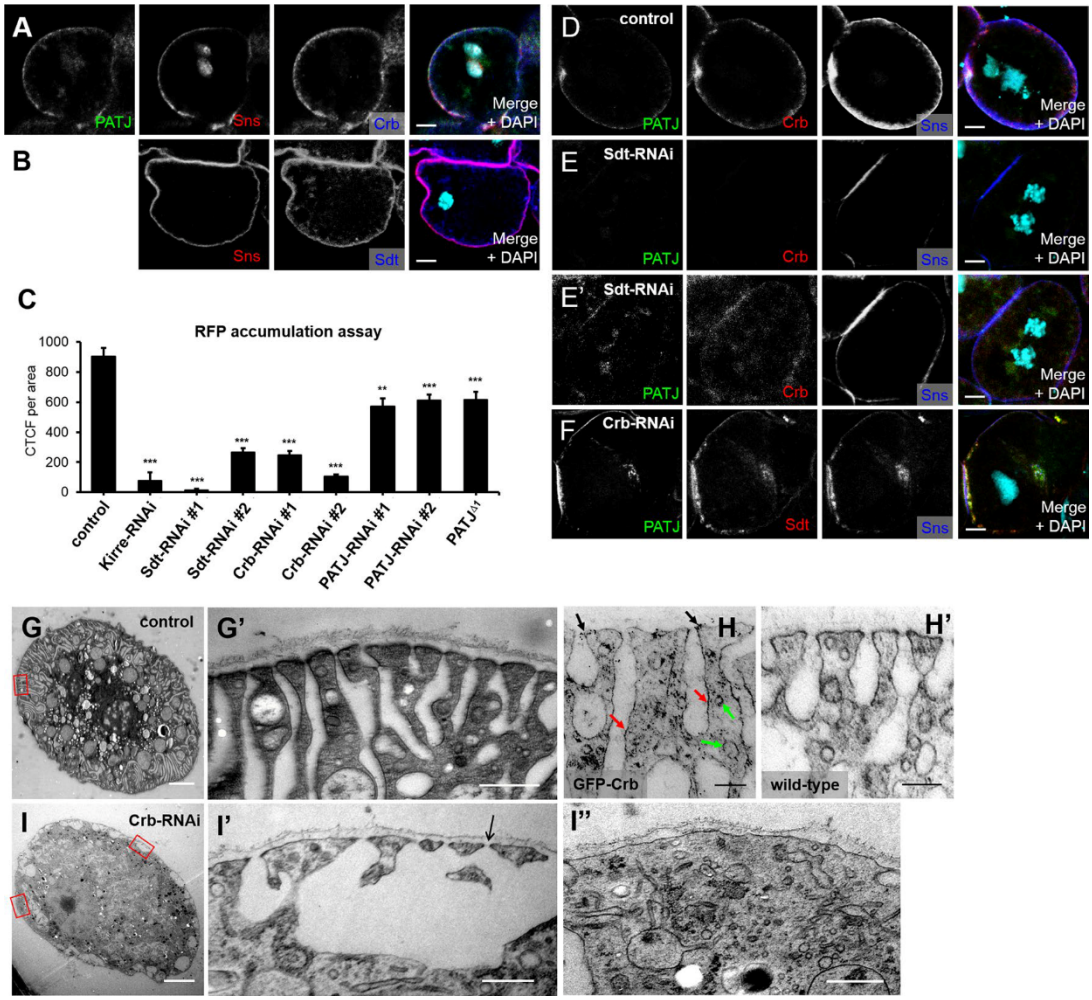

Figure 2.4-2 DmCrb is essential for the function of nephrocytes. a, b DmCrb, Sdt, and PATJ are expressed in garland nephrocytes and colocalize at the cortex with the Nephrin homologue sticks and stones (Sns). **c** Accumulation of secreted RFP in garland nephrocytes was quantified. All RNAi lines were specifically expressed in nephrocytes using sns::GAL4. An RNAi line against mCherry was used as control. As PATJ null flies survive until pupal stages, filtration efficiency was scored in larvae homozygous for *PATJ*$^{\Delta 1}$, which resulted in approximately the same filtration efficiency as the two RNAi lines used. **d, e** Nephrocytes with impaired Sdt expression (Sdt–RNAi#1) show loss of Crb, PATJ, and (to some extent) Sns from the cortical region (same settings in d and e). Note that increased imaging settings give a cortical signal for Sns, but a rather cytosolic or vesicular signal for Crb and Sdt (e′). **f** Downregulation of DmCrb by DmCrb–RNAi#1 does not impair localization of PATJ or Sdt, but results in weaker cortical Sns staining. **g–i** Transmission electron micrographs of garland nephrocytes. In wild-type (not shown) or control nephrocytes (g), long, regularly aligned foot processes compose a broad peripheral area of the cells, outlining parallel lacunae in between the foot processes, which are sealed with a slit diaphragm. **h** GFP–Crb expressed from its endogenous promoter [74] localizes at the nephrocyte diaphragms (*black arrow*) as well as along the peripheral outline of the lacunae (*red arrows*) and in vesicles close to the cell cortex (*green arrows*). Garland cells of wild-type flies incubated with GFP antibody were used as negative control (h′). In nephrocytes with impaired DmCrb expression (i), this peripheral area is severely disturbed and surface area with nephrocyte diaphragms is drastically reduced (quantified in Figure 2.4-3j). i′, i″ are higher magnifications from i taken from an area with irregular nephrocyte diaphragms (i′) or a nephrocyte diaphragm free area (i″). *Scale bar* 5 µm in a, b, and d–f, 2 µm in g and i, 500 nm in g′, i′, and i″, and 200 nm in h

In this study, we investigated the function of Crb in morphogenesis and function of nephrocytes. DmCrb localizes to the cell periphery and colocalizes with nephrocyte diaphragm markers. Knock-down of DmCrb results in a drastic decrease in filtration rate, disturbed morphology of foot processes, and reduced nephrocyte diaphragms. These defects can be rescued by introduction of RNAi-resistant DmCrb as well as by expression of each of its human homologues, which are expressed in mouse podocytes, hCrb2 or hCrb3. Notably, knock-down of Crb disturbs the accumulation of early and late endosomes, which can partly be rescued by simultaneous overexpression of Moesin, which binds to the FERM-binding domain of Crb. In contrast, the assembly or maintenance of nephrocyte diaphragms does not depend on the interaction with Moesin but on the extracellular domain.

2.4.3 Materials and methods

2.4.3.1 *Drosophila* stocks and genetics

Fly stocks were cultured on the standard cornmeal agar food and maintained at 25 C. For evaluation of filtration efficiency, the nephrocyte-specific driver line *sns::GAL4* (Zhuang et al., 2009) was recombined with *mhc::*ANP–RFP (Zhang et al., 2013b) and subsequently crossed to the responder lines UAS::mCherry–RNAi (#35778), UAS::Sdt–RNAi#1 (#37510), UAS::Crb–RNAi#1 (#38373), UAS::PATJ–RNAi (#35747), UAS::Yrt–RNAi (#36118), UAS::Ex–RNAi (#34968) (Bloomington Stock Center, Bloomington, IL, USA), UAS::Sdt–RNAi#2 (#15342R-2), UAS::PATJ–RNAi#2 (#12021R-4) (National Institute of Genetics, Shizuoka, Japan), UAS::Moesin–RNAi (#110654), and UAS::Crb–RNAi#2 (#22076) (Vienna *Drosophila* Resource Center, Austria). For rescue experiments, *sns::GAL4, mhc::*ANP–RFP was recombined with *UAS::Crb–RNAi#1.* The 21-nucleotide targeting sequence of Crb–RNAi#1 is located in the 3′ UTR of Crb mRNA, and thus, expression of this shRNA downregulates endogenous Crb but not Crb expressed from UASt as all constructs used in this study lack the 3′ UTR.

The following stocks were established in this study using Phi-C31-integrase system (Groth et al., 2004) with attP40 (25C) and attPVK00002 (28E): UASt::DmCrb, UASt::DmCrb$_{\Delta FERM}$ (Y10A, E16A, Klebes and Knust, 2000), UASt::DmCrb$_{\Delta ERLI}$, UASt::DmCrb$_{\Delta intra}$, UASt::DmCrb$_{intra}$, UASt::DmCrb$_{intra\Delta ERLI}$, UASt::GFP–hCrb2, UASt::GFP–hCrb2$_{\Delta ERLI}$, UASt::GFP–hCrb2$_{\Delta FERM}$, UASt::GFP–hCrb2$_{C620S}$, UASt::GFP–hCrb2$_{C633W}$, UASt::GFP–hCrb2$_{R1249Q}$, UASt::GFP–hCrb3a, UASt::GFP–hCrb3a$_{\Delta ERLI}$, UASt::GFP–hCrb3b, and UASt::GFP–hCrb3b$_{\Delta CLPI}$. For GFP–hCrb2, the ORF of GFP was cloned into an endogenous SalI restriction site in hCrb2 pDONOR201 (Mitsuishi et al., 2010), placing the GFP 130aa upstream of the transmembrane domain. Cloning of GFP into the extracellular fragment of hCrb3a and hCrb3b was described elsewhere (Djuric et al., 2016).

2.4.3.2 Generation of sticks-and-stones antibody

The Sns antibody was generated by injecting chicken with recombinant GST–Sns$_{intra}$ protein purified from *E. coli* (Davids Biotechnology, Regensburg, Germany).

2.4.3.3 ANP-RFP accumulation assay

Garland cell nephrocytes from wandering third instar larvae were microdissected in HL3.1 saline (Feng et al., 2004), fixed in 4% PFA in PBS for 1 h, stained with DAPI for 20 min, washed with PBS, and mounted in mowiol. Samples were imaged using an LSM-510 confocal microscope (ZEISS, Jena, Germany) and ANP–RFP accumulation per nephrocyte area (CTCF = corrected total cell fluorescence) was subsequently analyzed and quantified with ImageJ after subtracting the autofluorescent background of dissected larvae. For each genotype, at least 40 nephrocytes of five independent larvae were quantified. Error bars indicate the standard error of the mean. Significance was determined by unequal two sample t test with unequal variances: ns > 0.05, $^{*}p < 0.05$, $^{**}p < 0.01$, $^{***}p < 0.001$.

2.4.3.4 Immunohistochemistry

Garland nephrocytes were dissected as described above and heat-fixed for 20 s in boiling heat fix saline (0.03% Triton-X100). Subsequently, nephrocytes were washed three times in PBS + 0.1% Tween 20 and blocked with 1% BSA for 1 h, incubated over night with primary antibodies in PBS + 0.1% Tween 20 + 1% BSA, washed three times, and incubated for 2 h with secondary antibodies. After three washing steps and DAPI staining, nephrocytes were mounted with Mowiol. For staining of F-actin, garland nephrocytes were fixed in 4% PFA in PBS and stained with Phalloidin-Alexa-568 (Molecular Probes).

Primary antibodies used were as follows: mouse anti-Crb (Cq4, 1:50, Development Study Hybridoma Bank, DSHB), rabbit anti-GFP (1:500, sc-8334, Santa Cruz), guinea pig anti-PATJ (1:500, Sen et al., 2012), rabbit anti-Sdt (1:1000, Koch et al., in revision), mouse anti-Sdt (1:20, Berger et al., 2007), and chicken anti-Sns (1:1000, this study). Guinea pig anti-Rab5 (1:2000), rabbit anti-Rab7 (1:2000), and rabbit anti-Rab11 (1:2000) were kindly provided by A. Nakamura (Tanaka and Nakamura, 2008). Rabbit anti-Moesin (1:2000) was kindly provided by D. Kiehart (Edwards et al., 1997). Secondary antibodies conjugated with Alexa 488, Alexa 568, and Alexa 647 (Life technologies) were used at 1:400. Images were taken on a Zeiss LSM 710 Meta confocal microscope and processed using Adobe Photoshop.

Sections of paraffin-embedded human kidney specimen were stained using rabbit anti-Crb2 (1:50, HPA043674, SIGMA) and rabbit anti-Crb3 (1:50, HPA013835, SIGMA). For co-staining of Crb3 with Nephrin, Cryo-sections of mouse kidneys were stained using the following antibodies: rabbit anti-Crb3 (1:50, HPA13835, Sigma) and guinea pig anti-Nephrin (1:50, Acris, #BP5030).

2.4.3.5 Transmission electron microscopy

Garland nephrocytes of the third instar larvae were microdissected in HL3.1 saline, high-pressure frozen (EM-PACT2, Leica, Wetzlar, Germany), freeze-substituted in acetone/2% OsO4/5% H_2O/0.25% uranyl acetate (AFS2, Leica, Wetzlar, Germany), and embedded in Epon. For transmission electron microscopy, 70-nm-thick sections were cut using an ultramicrotome (Leica UC6 or UC7, Wetzlar, Germany). For immunostainings of ultrathin sections, freeze-substitution was performed in acetone/0.2% OsO_4/5% H_2O/0.25% uranyl acetate and also embedded in Epon. The GFP-fusion protein was

stained on 70-nm sections using goat anti-GFP (1:20, 600-101-215, Rockland) and a secondary 6-nm gold-coupled rabbit-α-goat IgG (dilution 1:20). All samples were imaged with a TEM-902 transmission electron microscope (ZEISS, Jena, Germany).

2.4.4 Results

2.4.4.1 Crb2 and Crb3 are expressed in mammalian podocytes

To study the function of Crb in podocytes development and slit-diaphragm assembly, we aimed to identify the expression pattern of Crb proteins in this cell type. In contrast to *Drosophila*, mammalian genomes contain three genes encoding Crb proteins: CRB1, CRB2, and CRB3 (Figure 2.4-1a). As expression of Crb1 is restricted to neuronal tissues (and testis), we focused on immunostainings of Crb2 and Crb3 on sections of human kidney tissue. As depicted in Figure 2.4-1b, Crb2 is highly expressed in human podocytes (the visceral layer of Bowman's capsule, arrow head in Figure 2.4-1b″ as well as in endothelial cells surrounding the capillaries (asterisk in Figure 2.4-1b″) and in the squamous epithelial cells of the parietal layer (arrow in Figure 2.4-1b″), whereas epithelial cells of the tubular system are only slightly stained (Figure 2.4-1b), as reported before (Ebarasi et al., 2015).

In contrast, Crb3 is present in the glomeruli (endothelial cells, podocytes and parietal cells, Figure 2.4-1c″) as well as in tubular epithelial cells (Figure 2.4-1c) and colocalizes with the slit-diaphragm component Nephrin (murine kidney sections, Figure 2.4-1d, e). Loss of Crb3 in mice results in kidney cysts, which emerge from tubular segments of the nephron, whereas most glomeruli seem to be intact (Whiteman et al., 2014). On the other hand, dysfunction of Crb2 has recently been reported to impair slit-diaphragm/foot-process maintenance in zebrafish and mutations in human CRB2 are associated with congenital nephrosis or nephrotic syndrome in patients (Ebarasi et al., 2009; Ebarasi et al., 2015; Slavotinek et al., 2015). However, the strong expression of two Crb variants with high similarity of its intracellular domain in podocytes suggests the possibility that these two proteins function (partly) in redundancy. Therefore, we chose *Drosophila* nephrocytes as model system to study the function of Crb *in vivo*.

2.4.4.2 DmCrb and Sdt are essential for nephrocyte function and morphology

DmCrb, Sdt, and PATJ are expressed in nephrocytes, partly overlapping with the staining of Sticks-and-stones (Sns), one of the *Drosophila* Nephrin homologues, in the peripheral area, where the nephrocyte diaphragms are assembled (Tepass and Knust, 1990) (Figure 2.4-2a, b).

To investigate the function of DmCrb in nephrocyte development and filtration efficiency, we performed filtration assays as described previously (Zhang et al., 2013b). In this system, soluble red fluorescence protein (RFP) is secreted into the larval hemolymph, which is subsequently filtrated, endocytosed, and stored by nephrocytes (an example for

the RFP-accumulation assay is described in Figure 2.4-7). Thus, intracellular accumulation of RFP in garland nephrocytes of wandering L3 larvae reflects filtration efficiency and endocytosis. Indeed, downregulation of Kirre, one of the *Drosophila* NEPH1 homologues, results in almost abolished filtration efficiency (Figure 2.4-2c).

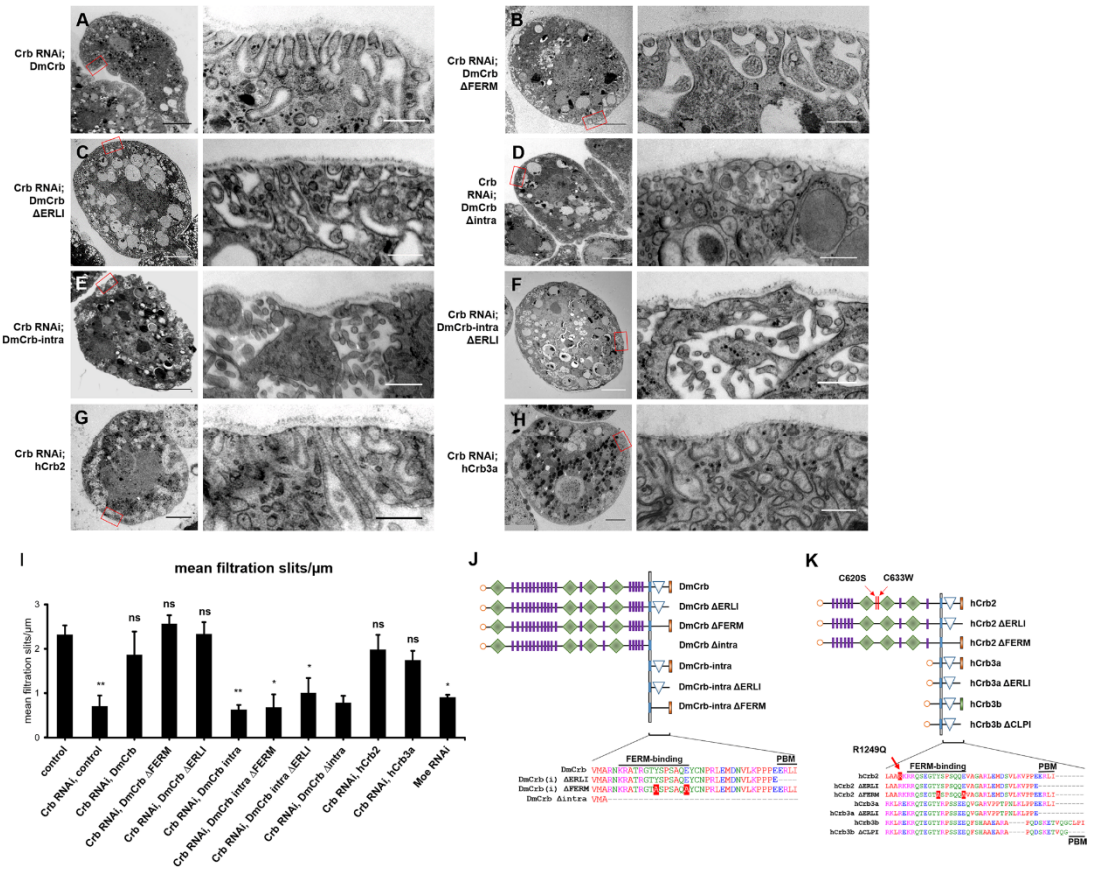

Figure 2.4-3 Transmission electron microscopy analysis of rescue nephrocytes. a–h Garland nephrocytes expressing Crb–RNAi and the indicated rescue transgene were analyzed by electron microscopy. **i** Amount of nephrocyte diaphragms (NDs) per µm surface area (basal membrane) was quantified. At least three nephrocytes from different individuals were scored. **j, k** Schematic representation of Crb-deletion constructs and mutations used in this study. Graphic symbols used are explained in Figure 2.4-1a

Downregulation of DmCrb as well as Sdt significantly decreased filtration efficiency (Figure 2.4-2c). This effect is specific for DmCrb and Sdt, because it can be rescued by expression of an RNAi-resistant variant (Figure 2.4-3d). Interestingly, downregulation or knock-out of PATJ in nephrocytes does not reduce RFP filtration to the same extent as downregulation of DmCrb or Sdt (Figure 2.4-2c), suggesting that PATJ is not necessary to stabilize the DmCrb/Sdt complex in nephrocytes, which corresponds to the situation in the embryonic epidermis and to some extent in cells of the follicular epithelium (Sen et al., 2012; Pénalva and Mirouse, 2012; Zhou and Hong, 2012).

Loss of Sdt in epithelia leads to destabilization and endocytosis of DmCrb (Hong et al., 2001; Lin et al., 2015). Similarly, we observed a strong decrease in DmCrb (and

PATJ) staining in nephrocytes with decreased Sdt expression (Figure 2.4-2e, same settings as in d). Importantly, accumulation of the Nephrin homologue sticks-and-stones at the peripheral area appears weaker compared to the control. Enhanced exposure reveals a cytosolic/vesicular staining of DmCrb and PATJ, whereas residual Sns is still cortically localized (Figure 2.4-2e'). In contrast, downregulation of DmCrb does not affect localization of Sdt or PATJ (Figure 2.4-2f, same setting as d), which is in line with previous observations in epithelial cells of the embryonic epidermis, where Sdt and PATJ can be recruited to the apical junction by Bazooka in the absence of Crb (Krahn et al., 2010; Sen et al., 2015).

Finally, we investigated whether downregulation of DmCrb affects development and morphology of nephrocytes using electron microscopy. Indeed, formation of foot processes is significantly disturbed in nephrocytes with downregulated DmCrb. In control nephrocytes, the peripheral area is composed of a regularly aligned system of parallel foot processes outlining narrow lacunae, which are sealed to the hemolymph compartment by nephrocyte diaphragms (Figure 2.4-2g).

Notably, Crb localizes to the dense structures of nephrocyte diaphragms (Figure 2.4-2h, black arrow), as well to subcortical vesicles (Figure 2.4-2h, green arrow) and around the outline of lacunae (Figure 2.4-2h, red arrow), which is in line with immunostainings (Figure 2.4-2a, d), showing a cortical staining of Crb, which is significantly broader than that of sns (Figure 2.4-2d). In contrast to their control counterparts, nephrocytes with strongly reduced DmCrb protein expression exhibit a dramatically disturbed morphology (Figure 2.4-2i). The peripheral area is irregularly shaped, with a complete loss of correctly aligned foot processes and strongly reduced amount of nephrocyte diaphragms (Figure 2.4-3i). Instead, some big lacunae can be observed, whereas other parts of the cell periphery lack any lacunae. However, some intact nephrocyte diaphragms remain at the border of enlarged lacunae (arrow in Figure 2.4-2i′), which correlates with (reduced but detectable) cortical staining of Sns (Figure 2.4-2f). Morphological defects and amount of nephrocyte diaphragms in Crb–RNAi expressing nephrocytes can be rescued by expression of an RNAi-resistant DmCrb transgene (Figure 2.4-3a, i).

2.4.4.3 The function of DmCrb regulating nephrocyte diaphragms and RFP accumulation is conserved in its mammalian homologues 2 and 3

Next, we aimed to investigate whether the function of DmCrb in nephrocytes is conserved in mammalian Crb2 and Crb3, which are both expressed in mammalian podocytes (Figure 2.4-1b–e). Human Crb2 (hCrb2) and human Crb3a (hCrb3a) exhibit a high sequence similarity in the cytoplasmic domain, both containing the FERM (4.1-protein–Ezrin–Radixin–Moesin)-binding motif and the C-terminal ERLI motif (Figure 2.4-1a), which is capable of binding the PDZ domain containing proteins Sdt/Pals1 or PAR-6 (Bachmann et al., 2001; Hong et al., 2001; Roh et al., 2002; Roh et al., 2003; Lemmers et al., 2004; Wang et al., 2004; Kempkens et al., 2006; Whitney et al., 2016). In contrast to hCrb3a, a second Crb3 isoform, hCrb3b, does not contain the ERLI motif due to alternative splicing (Fan et al., 2007) (Figure 2.4-1a), and thus, this protein is likely not

able to bind Pals1/Sdt. Instead, hCrb3b exhibits a CLPI motif, which has been described to be implicated in ciliogenesis and cell division control (Fan et al., 2007).

hCrb2 and hCrb3a differ in the extracellular domain, which is quite similar to DmCrb (EGF-like and Laminin A/G-like domains) in case of hCrb2, whereas Crb3a exhibits only a very short extracellular portion (Figure 2.4-1a) which, however, seems to be sufficient for localization of the protein to cell–cell contacts (Djuric et al., 2016).

To test, which of the human homologues can complement the DmCrb–RNAi phenotypes, we confirmed that overexpressed GFP-tagged hCrb2, GFP–hCrb3a, and GFP–hCrb3b are to some extent colocalizing with DmCrb in the peripheral area of nephrocytes, overlapping with Sns expression (Figure 2.4-4a–c). Notably, overexpression of its mammalian counterparts resulted in a slight expansion of cortical DmCrb localization (Figure 2.4-4a–c, compared to Figure 2.4-2a). Next, we expressed these proteins in nephrocytes together with DmCrb–RNAi. As depicted in Figure 2.4-4d, e, not only RNAi-resistant DmCrb but also hCrb2 and all hCrb3 variants can rescue downregulation of DmCrb regarding the RFP accumulation. Neither deletion of the ERLI motif in hCrb3a ($hCrb3a_{\Delta ERLI}$), nor deletion of the CLPI motif in hCrb3b ($hCrb3b_{\Delta CLPI}$) decreases the rescue capacity of the mutated proteins, but rather results in enhanced filtration (Figure 2.4-4e). Notably, two recently described mutations of hCrb2 (C620S, located within the extracellular domain of hCrb2 between Laminin G domains 1 and 2 and R1249Q, adjacent to the transmembrane domain within the cytoplasmic tail), which are associated with nephrosis (Ebarasi et al., 2015; Slavotinek et al., 2015) rescue downregulation of DmCrb as efficiently as wild-type hCrb2 (Figure 2.4-4d), producing even an increased accumulation of RFP in comparison to control nephrocytes. In contrast, a third mutation (C633W, located in the extracellular domain between Laminin G domains 1 and 2) exhibits only a rescue comparable to control RFP values (Figure 2.4-4d). Considering that these proteins are overexpressed in the rescue experiments, these results might indicate a crucial role of the latter mutation in nephrocyte/podocyte function. However, further experiments using a mammalian system have to be used to elucidate the detailed pathomechanism.

Ultrastructural analysis of hCrb2- and hCrb3a-rescued nephrocytes reveals a complete rescue of morphology and nephrocyte diaphragms (Figure 2.4-3g–i). Thus, both human homologues of DmCrb, which are expressed in human podocytes, are capable of fully accomplishing DmCrb function in nephrocytes regarding filtration efficiency.

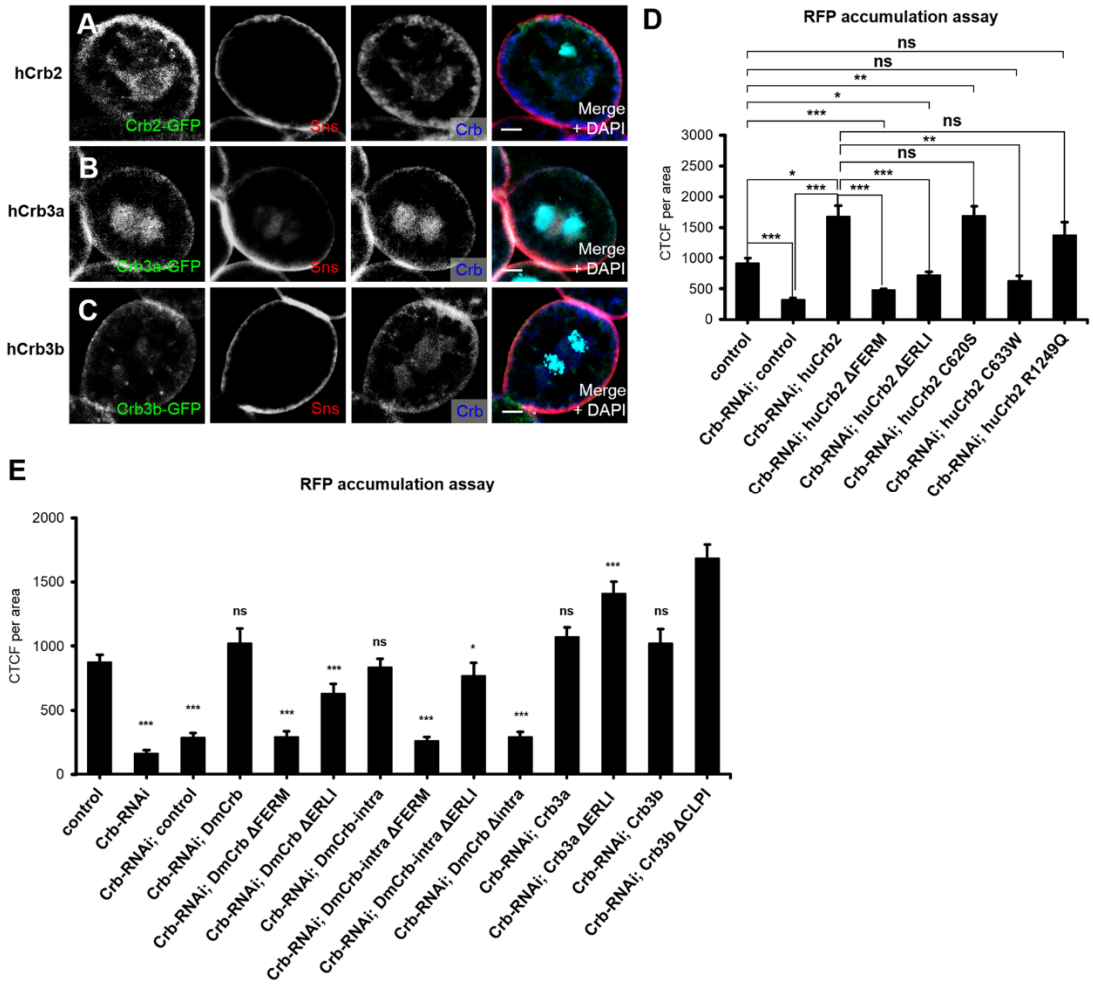

Figure 2.4-4 Crb function for nephrocyte filtration is conserved throughout evolution. a–c hCrb2 and hCrb3 isoforms (hCrb3a and hCrb3b, differing at the very C-terminus, as depicted in Figure 2.4-1a) tagged with a GFP (fused into the extracellular domain, next to the transmembrane domain) were expressed in garland nephrocytes and detected by immunostaining. All three hCrb variants colocalize with Sns at the cellular cortex, but show - similar to endogenous DmCrb - an additional subcortical localization. **d**, **e** Rescue experiments in nephrocytes with downregulated endogenous DmCrb and simultaneous expression of indicated transgenes: accumulation of secreted RFP in garland nephrocytes was quantified as described above. *Scale bars* 5µm

2.4.4.4 The extracellular domain is essential for assembly or maintenance of nephrocyte diaphragms but not for endocytosis

The extracellular domain of DmCrb has been reported to facilitate transcellular homophilic interaction, thereby stabilizing the protein and contributing to DmCrb function in regulating apical–basal polarity in epithelia (Letizia et al., 2013). Similarly, dimerization of the extracellular domain of two Crb2 isoforms regulates cell adhesion in zebrafish photoreceptor cells (Zou et al., 2012). However, expression of a DmCrb variant, which consists of the transmembrane domain and the intracellular domain, can at least to some extent restore apical–basal polarity in crb-deficient epithelia (Wodarz et al., 1995; Klebes and Knust, 2000). This prompted us to test whether homophilic dimerization or other interactions of the extracellular domain of DmCrb are essential for its function in nephrocytes. Indeed, a truncated version of DmCrb ($DmCrb_{intra}$), consisting only of the signal

peptide, the transmembrane domain and the intracellular tail, is able to restore RFP accumulation in nephrocytes with downregulated DmCrb (Figure 2.4-4e).

Remarkably, deletion of the Sdt-interaction motif (ERLI) in this construct does not impair the rescue capacity (Figure 2.4-4e), indicating that Sdt interaction of this motif is not essential for its function in nephrocyte filtration. However, electron microscopy analysis and quantification of nephrocyte diaphragms indicate a failure in restoring ultrastructure and nephrocyte diaphragms in $DmCrb_{intra}$ and $DmCrb_{intra\Delta ERLI}$ (Figure 2.4-3e, f, i). Thus, rescue potential of the intracellular fragment is likely due to restored/enhanced endocytosis rather than due to nephrocyte diaphragm assembly or maintenance.

In contrast, deletion of the entire cytoplasmic tail in DmCrb ($DmCrb_{\Delta intra}$) abolishes the rescue capacity regarding slit-diaphragm assembly (Figure 2.4-3d, i) as well as endocytosis (Figure 2.4-4e), suggesting that the cytoplasmic domain of Crb is essential for these processes, presumably due to targeting of the protein to the cortex/slit diaphragms via interaction with either Sdt (by the ERLI motif) or Moesin (via the FERM-binding motif).

In contrast, hCrb3a exhibits a robust rescue capacity in RFP accumulation as well as in the amount of nephrocyte diaphragms (Figure 2.4-3h, i, 4f), which is in line with a recent study describing a role of the short extracellular domain of Crb3 isoforms in localizing the protein to sites of cell–cell contacts, likely by homophilic interactions (Djuric et al., 2016).

2.4.4.5 The FERM-binding motif but not the ERLI motif is essential for RFP accumulation

Finally, we elucidated the contribution of the two known intracellular motifs, which are conserved from fly to men: the FERM-binding motif facilitates binding of DmCrb to Yurt, Expanded, and Moesin, thereby modulating the actin cytoskeleton and suppressing cell proliferation and organ growth by controlling the Hippo pathway (Médina et al., 2002; Laprise et al., 2006; Grzeschik et al., 2010; Chen et al., 2010; Robinson et al., 2010; Sherrard and Fehon, 2015).

The C-terminal ERLI motif binds to the adaptor protein Sdt, which is essential for stabilization of Crb at the subapical region in most epithelial cells (Bachmann et al., 2001; Hong et al., 2001; Makarova et al., 2003; Roh et al., 2003; Straight et al., 2004), except of boundary cells in the *Drosophila* hindgut (Kumichel and Knust, 2014). Furthermore, the adaptor protein PAR-6 has been described to compete with Sdt for binding to the ERLI motif of DmCrb and mammalian Crb *in vitro* and in cell culture (Lemmers et al., 2004; Kempkens et al., 2006; Whitney et al., 2016).

However, the robust rescue capacity of hCrb3b and $hCrb3a_{\Delta ERLI}$ suggests that binding to Pals1/Sdt might not be essential for the filtration efficiency of nephrocytes. Surprisingly, deletion of the ERLI motif in DmCrb ($DmCrb_{\Delta ERLI}$) and hCrb2 ($hCrb2_{\Delta ERLI}$) results in a slightly decreased rescue capacity in comparison to DmCrb, hCrb3b, and $hCrb3a_{\Delta ERLI}$, whereas deletion of the ERLI motif in $DmCrb_{intra}$ does not affect its rescue capacity (Figure 2.4-4d, e). One reason might be that the turnover (by endocytosis) of $DmCrb_{\Delta ERLI}$ could be higher compared to DmCrb, thus disturbing the proteins function

at the cell surface. In contrast to the ERLI motif, mutation of the FERM motif ($DmCrb_{\Delta FERM}$ and $hCrb2_{\Delta FERM)}$ entirely abolishes the ability to restore DmCrb function regarding nephrocytes filtration efficiency (Figure 2.4-4d, e). Ultrastructural analyses and nephrocyte diaphragm quantifications revealed a close to normal morphology and regular amount of nephrocyte diaphragms in $DmCrb_{\Delta FERM}$ and $DmCrb_{\Delta ERLI}$ (Figure 2.4-3b, c, i). These surprising findings—together with the vice versa effects of $DmCrb_{intra}$—suggest that Crb functions in two pathways to regulate nephrocyte function: The extracellular domain facilitates (presumably by homophilic interaction) nephrocyte diaphragm assembly and/or maintenance and (foot-process) morphology, whereas the intracellular tail (in particular the FERM-binding domain) controls endocytosis (of secreted RFP). Notably, overexpression of DmCrb or its mammalian homologues hCrb2, hCrb3a, and hCrb3b in nephrocytes results in an increased accumulation of RFP (Figure 2.4-9), indicating an enhancement of endocytosis, which is in line with previous results, demonstrating a gain of apical membrane compartment upon overexpression of Crb in epithelial cells (Wodarz et al., 1995).

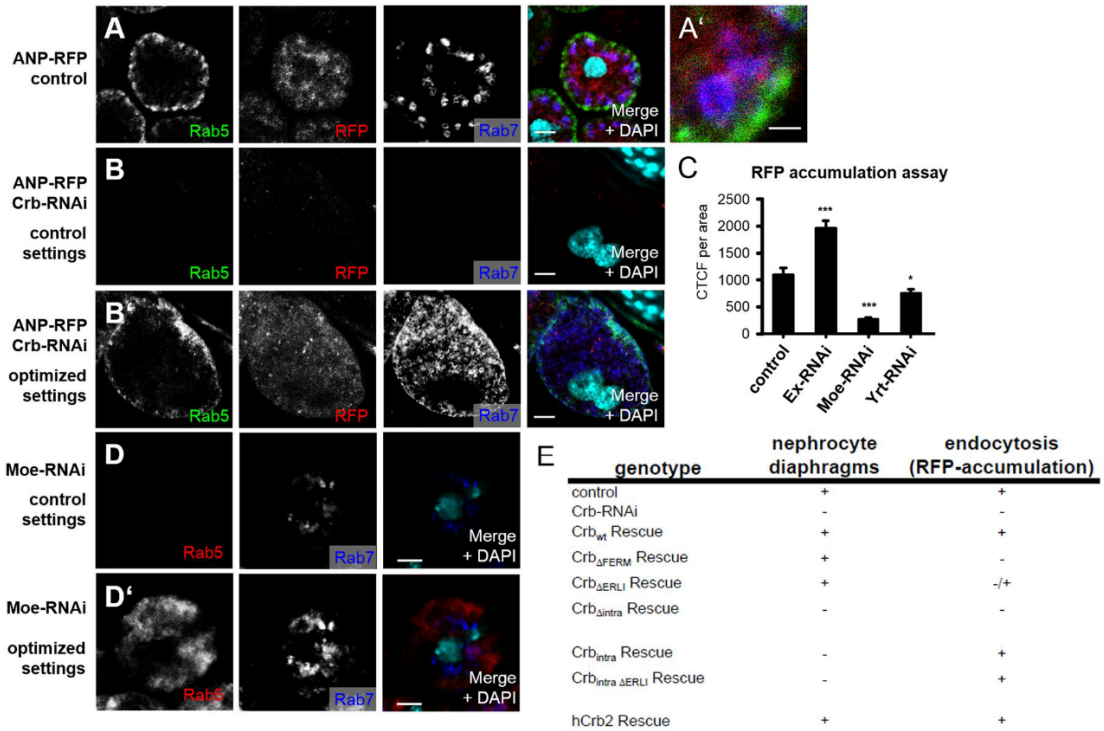

E

genotype	nephrocyte diaphragms	endocytosis (RFP-accumulation)
control	+	+
Crb-RNAi	-	-
Crb_{wt} Rescue	+	+
$Crb_{\Delta FERM}$ Rescue	+	-
$Crb_{\Delta ERLI}$ Rescue	+	-/+
$Crb_{\Delta intra}$ Rescue	-	-
Crb_{intra} Rescue	-	+
$Crb_{intra\ \Delta ERLI}$ Rescue	-	+
hCrb2 Rescue	+	+
$hCrb2_{\Delta ERLI}$ Rescue	n.d.	+
$hCrb2_{\Delta FERM}$ Rescue	n.d.	-
hCrb3a Rescue	+	+
$hCrb3a_{\Delta ERLI}$ Rescue	n.d.	+
hCrb3b Rescue	+	+
$hCrb3b_{\Delta CLPI}$ Rescue	n.d.	+
Moe-RNAi	-	-

Figure 2.4-5 Crb controls nephrocyte function by regulating endocytosis. a Endocytosed RFP accumulates in Rab7-positive vesicles, but does not show overlap with Rab5 (higher magnification in **a′**). **b** Rab7-labeled late endosomes and Rab5-positive early endosomes are decreased in nephrocytes with downregulated DmCrb (**b**, same exposure settings as in **a**, **b′** shows optimized settings) in contrast to control nephrocytes (**a**). **c** RFP-accumulation assay of garland nephrocytes with downregulated expression of Expanded (Ex), Moesin (Moe), or Yurt (Yrt). **d** Nephrocytes expressing Moesin–RNAi show

decreased Rab5 and to some extent lower Rab7 staining (same exposure settings as in **a**, **d′** shows optimized settings). **e** Table summarizing the phenotypes observed in nephrocytes with Crb-knock-down and expression of indicated rescue constructs. *Scale bars* 1.5 µm in **a′** and 5 µm in all other

2.4.4.6 Loss of the FERM-binding domain interaction partner Moesin phenocopy Crb-knock-down in nephrocytes

Drosophila nephrocytes accumulate and store filtrated substances upon endocytosis. Interestingly, mammalian podocytes exhibit a similar high endocytosis capacity to regulate slit-diaphragm assembly and maintenance (recently reviewed in Inoue and Ishibe, 2015). *Drosophila* nephrocytes endocytose secreted RFP and accumulate it in vesicular structures, which are surrounded by Rab7 staining (but do not costain with Rab5 for early endosomes or Rab11 for recycling endosomes), characterizing them as late endosomes or lysosomes (Figure 2.4-5a and data not shown and Soukup et al., 2009). In contrast to the nephrocyte diaphragm marker Sns (Figure 2.4-2a), DmCrb shows a staining pattern, which is not precisely restricted to the absolute outline of the cell, but exhibits a broader localization (Figure 2.4-2a, d). Furthermore, DmCrb localizes not only to nephrocyte diaphragms, but also to subcortical vesicles and along the outline of lacunae (Figure 2.4-2h). To investigate whether Crb is implicated in the regulation of endocytosis, we stained control and DmCrb-downregulated nephrocytes with markers for early (Rab5) and late endosomes (Rab7). Strikingly, Rab5 and Rab7 staining is dramatically decreased in nephrocytes with downregulated DmCrb (Figure 2.4-4b, same exposure settings as in A, B' shows enhanced settings), reflecting a decrease of early endosomes and late endosomes/lysosomes.

To further explore the mechanism how Crb regulates endocytosis, we analyzed the knock-down phenotypes of the three described interaction partners of the FERM-binding motif: Whereas knock-down of Yurt and Expanded had only a slight decreasing (Yurt) or even enhancing (Expanded) effect on RFP accumulation, reduction of Moesin expression results in a strong reduction of fluorochrome accumulation (Figure 2.4-5c).

Interestingly, knock-down of Moesin in nephrocytes results in a strong decrease in Rab5-positive early endosomes and a substantial decrease in Rab7-positive late endosomes/lysosomes (Figure 2.4-5d), which could be a secondary effect because of the defects in earlier steps of endocytosis. Besides, downregulation of Moesin also affects the actin cytoskeleton, ultrastructure, and the amount of nephrocyte diaphragms (Figure 2.4-8a-c; Figure 2.4-2i). Downregulation of DmCrb in nephrocytes results in a loss of cortical Moesin (Figure 2.4-6b), which can be rescued by wild-type DmCrb but not by $DmCrb_{\Delta FERM}$ (Figure 2.4-6c, d). Interestingly, downregulation of Moesin in nephrocytes leads to abolished cortical staining of Crb (Figure 2.4-8D), indicating that Moesin stabilizes Crb at the cortex, which might explain the morphological defects and reduced nephrocyte diaphragms in Moesin–RNAi expressing nephrocytes.

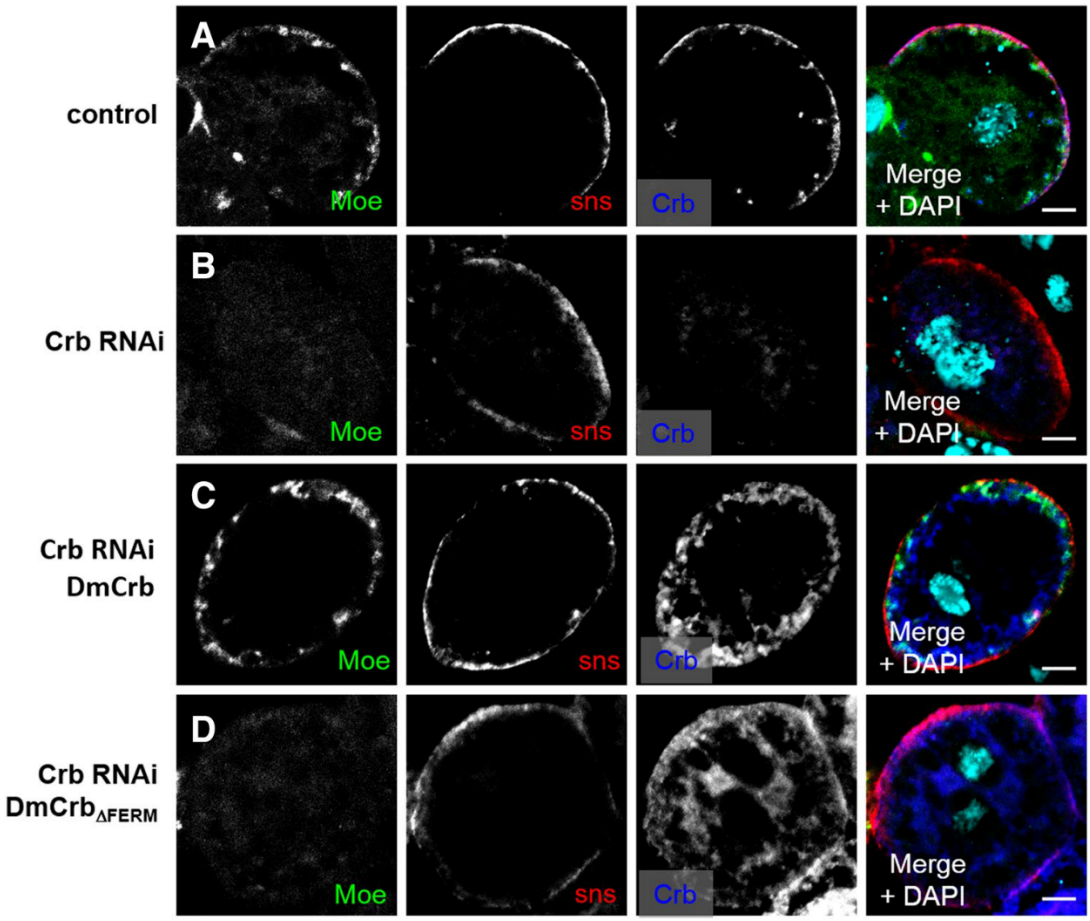

Figure 2.4-6 Cortical Moesin localization depends on the FERM domain of Crb. a In control garland nephrocytes, Moesin localizes in a *dotted* pattern at the cell cortex. **b** Nephrocytes with decreased Crb expression show a decreased cortical Moesin accumulation (**b**), which is diffusely distributed within the cell. **c**, **d** Wild-type DmCrb but not $DmCrb_{\Delta FERM}$ rescues cortical Moesin localization. *Scale bars* 5 µm

2.4.5 Discussion

Taken together, we have demonstrated that in *Drosophila* nephrocytes, DmCrb regulates early endocytosis by interacting with Moesin via its FERM-binding domain. In contrast, its function in nephrocyte diaphragm assembly/maintenance depends on (presumably homophilic interaction of) the extracellular domain. These two distinct functions are conserved throughout evolution as both mammalian homologues, hCrb2, and both hCrb3 isoforms can rescue the defects observed in nephrocytes with downregulation of DmCrb. Control of endocytosis by Moesin might occur either directly (Barroso-González et al., 2009; Nomachi et al., 2013) or indirectly by affecting the actin cytoskeleton (Speck et al., 2003; Karagiosis and Ready, 2004): Moesin links the Crb apical polarity complex to the actin cytoskeleton in *Drosophila* (Médina et al., 2002; Sherrard and Fehon, 2015; Wei et al., 2015) and mouse Crb3a interacts with a related FERM-domain containing protein, Ezrin, suggesting a similar mechanism (Whiteman et al., 2014). Moreover, Moesin regulates the subcortical actin cytoskeleton and loss of Moesin results in polarity defects (Speck et al., 2003; Karagiosis and Ready, 2004). Consequently, downregulation of Moesin disturbs cortical accumulation of DmCrb (Figure 2.4-9d), which explains the morphological defects and decreased amount of nephrocyte diaphragms in these cells. On the other hand, Moesin has been described to facilitate the pinching-off of clathrin-coated pits as endocytic vesicles in T cells (Nomachi et al., 2013) and in cervix carcinoma cells (HeLa) (Barroso-González et al., 2009), and thus, it seems to be involved in early steps of endocytosis. Although we provide compelling evidence that Crb regulates endocytosis in nephrocytes by recruiting Moesin via its FERM-binding domain, we cannot exclude that other proteins, which bind directly or indirectly to the FERM-binding motif, are involved in this process, too. Downregulation of Moesin results in severe morphological defects and a strong reduction of nephrocyte diaphragms. In contrast, $DmCrb_{\Delta FERM}$ rescues nephrocyte morphology and diaphragms but not endocytosis. Thus, we conclude that the Crb–Moesin interaction is essential for regulation of endocytosis, but Moesin accomplishes independently of its recruitment by Crb another function in regulating cell morphology and nephrocyte diaphragm assembly, presumably by modulating the actin cytoskeleton.

Notably, hCrb3a without the ERLI motif and hCrb3b without the CLPI motif as well as hCrb2 are capable of rescuing DmCrb–RNAi nephrocytes more efficiently compared to DmCrb or $DmCrb_{intra}$ (Figure 2.4-4d, e). This is in line with the fact that expression of hCrb2 and hCrb3b but not of hCrb3a in wild-type nephrocytes increased the endocytosis rate more efficiently than DmCrb (Figure 2.4-9). Although being highly conserved, the cytoplasmic tails of DmCrb, hCrb2, and hCrb3 isoforms differ in a few amino acids. Thus, fine-tuned differences in the interaction of these proteins with Moesin (or other proteins regulating endocytosis) might produce these differences. Apart from that, it might also be just a matter of either protein stability or protein mobility, which might be increased in proteins without Sdt binding (ΔERLI variants). However, the latter is obviously not the case for the "bigger" Crb proteins DmCrb and hCrb2, because in these cases, the RFP accumulation is weaker upon deletion of the Sdt-interaction motif. In contrast, the rescue capacities of Crb3 variants without the Sdt-interaction motif are

similar or even increased. One explanation would be that in the absence of Sdt binding, hCrb3 is not as fast removed from the membrane as DmCrb or hCrb2.

Importantly, endocytosis of core components of the slit diaphragm in mammalian podocytes plays a crucial role in maintaining the filtration barrier (reviewed in Soda and Ishibe, 2013): Nephrin is endocytosed by clathrin-dependent (Soda et al., 2012) and independent (Qin et al., 2009) endocytosis. Damaged podocytes in patients, which suffer from nephrotic syndrome, exhibit an increase in the amount of endocytic vesicles and decreased Nephrin surface localization. On the other hand, defects in maturation of endocytic vesicles result in disturbed morphology of podocytes with vacuoles and loss of foot processes and slit diaphragms (Klose et al., 2013; Chen et al., 2013). These results reflect an important role of the endocytic machinery in development and function of podocytes, which are in line with our findings of a conserved role of Crb-regulating nephrocyte development and function by modulating endocytosis.

2.4.6 Notes

2.4.6.1 Acknowledgements

We thank D. Kiehart, E. Knust, A. Nakamura, R. Roepman, the Bloomington stock center at the University of Indiana (USA), the National Institute of Genetics, (Shizuoka, Japan), the Vienna *Drosophila* Resource Center (Austria), and the Developmental Studies Hybridoma Bank at the University of Iowa (USA) for sending reagents. Thanks to Karin Wacker for excellent technical assistance. This work was supported by grants of the German research foundation (DFG) to M. P. K. (DFG3901/2-1, DFG3901/1-2, SFB699-A13) and to T.W. (SCHL1845/2-1, WE2550/2-2).

2.4.6.2 Compliance with ethical standards

2.4.6.3 Conflict of interest

The authors declare no competing interests.

2.4.7 Supplementary material

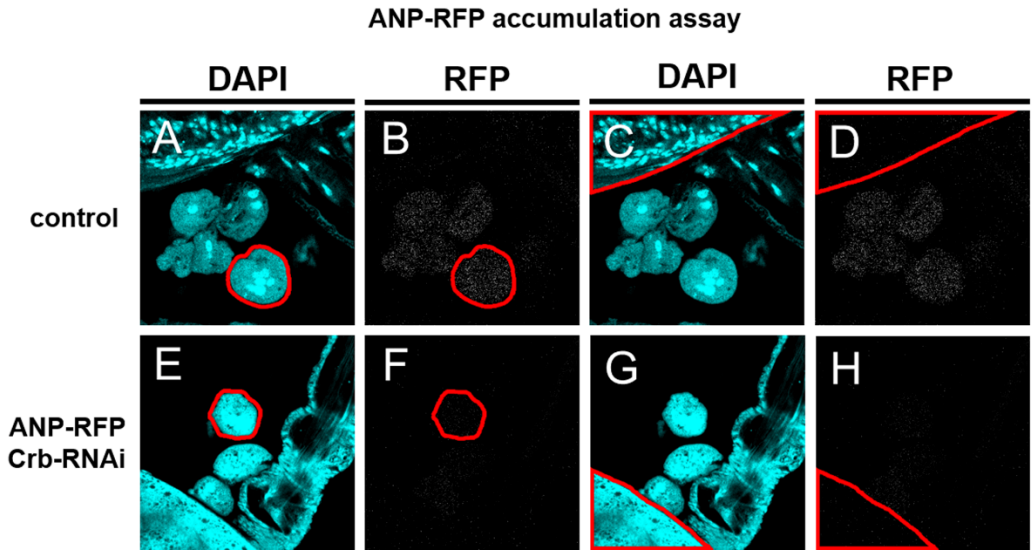

Figure 2.4-7 ANP–RFP-accumulation assay. Example of garland nephrocytes with accumulated RFP (RFP channel is depicted in B, D, F, and H). RFP expressed from the Myosin heavy chain promoter was secreted into the hemolymph and taken up by cell garland nephrocytes. The tissue was counter-stained with DAPI (without permeabilizing reagents) to visualize cellular structures (A, C, E, and G). A garland nephrocyte was outlined in red in A, B, E, and F. The RFP signal within the encircled area was measured and the signal from unspecific staining ("background", taken from the tissue of the stomach) was subtracted (encircled in red in C and D and G and H) to obtain a quantification of RFP accumulation within a single nephrocyte. To quantify the overall accumulation efficiency (as described in the methods section), we scored at least 40 nephrocytes from 5 independent larvae

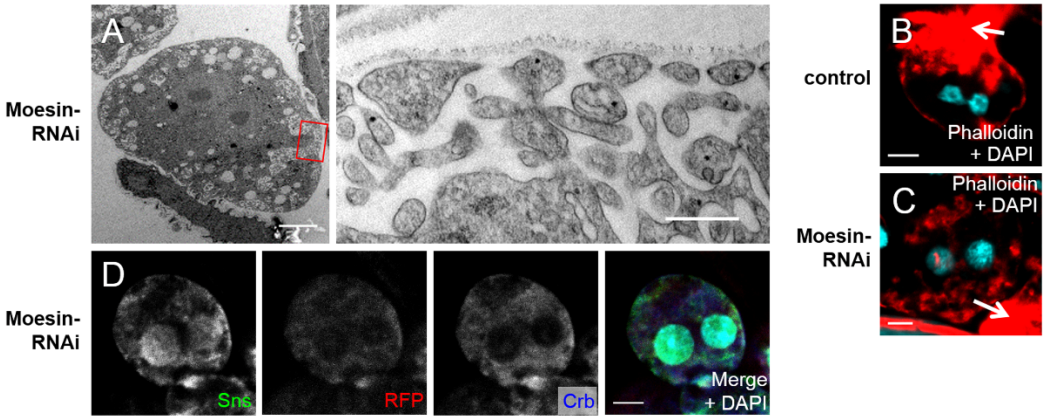

Figure 2.4-8 Downregulation of Moesin affects the ultrastructure and filamentous actin accumulation of nephrocytes. (A) Transmission electron micrographs of nephrocytes expressing Moesin–RNAi show a disturbed ultrastructure similar to Crb–RNAi nephrocytes. (B and C) Phalloidin staining of control (B) and Crb–RNAi (C) garland nephrocytes demonstrates a disturbance of cortical actin in Moesin–RNAi expressing cells. Note that even in control nephrocytes, actin staining is rather weak in comparison with surrounding tissues (e.g., proventriculus, arrows). (D) Immunostaining of garland nephrocytes with Moesin–RNAi visualizes a loss of cortical Crb and Sns

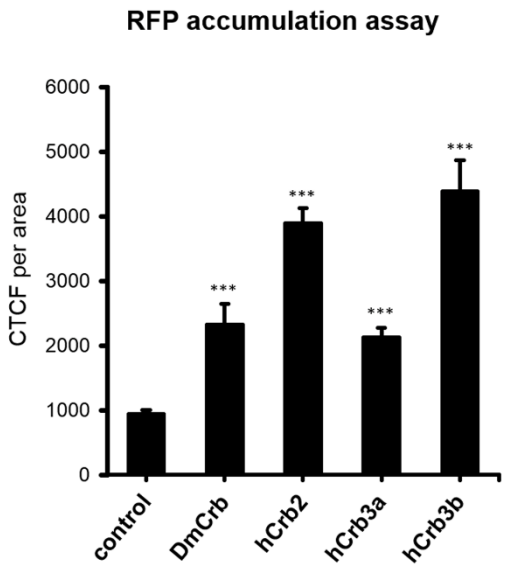

Figure 2.4-9 Cortical Moesin localization depends on the FERM domain of Crb. a In control garland nephrocytes, Moesin localizes in a *dotted* pattern at the cell cortex. **b** Nephrocytes with decreased Crb expression show a decreased cortical Moesin accumulation (**b**), which is diffusely distributed within the cell. **c**, **d** Wild-type DmCrb but not DmCrb$_{\Delta FERM}$ rescues cortical Moesin localization. *Scale bars* 5 µm

3 Discussion

3.1 The *Drosophila* nephrocyte: an innovative approach to research genetic kidney disease

In modern industrialized nations, chronic non-communicable diseases (NCDs) have become the main cause of mortality (Mascie-Taylor and Karim, 2003), including chronic kidney diseases (CKD), which contribute to the global health burden at an increasing rate (Mathers and Loncar, 2006). To keep pace with the challenges of modern kidney medicine, the established methods of research need to be diversified. Scientific progress in genome analysis led to the identification of numerous genes, which contribute to nephrotic syndrome (NS), when mutated. In many of these cases, the mutations have a negative effect on podocyte morphology and function (Hildebrandt, 2010; Vivante et al., 2014; Sadowski et al., 2015), which is detrimental to normal kidney function and a key factor to precipitate CKD (Smoyer and Mundel, 1998; Greka and Mundel, 2012; Greka, 2016).

During the last decade, *Drosophila* nephrocytes were shown to be very similar to mammalian podocytes, both in morphology and molecular features (Weavers et al., 2009; Zhuang et al., 2009). Most of the orthologs of genes causing nephrosis in human were found to cause an impairment of nephrocyte function in the fly as well (Hermle et al., 2017) and the resulting disrupted morphological phenotypes of filtration barrier components resembles those found in the mammalian system (Weavers et al., 2009).

In the course of this work, four projects covered different aspects of modelling nephrotic syndrome via the fly nephrocyte system to gain novel or supportive insights in addition to other model systems. The first manuscript dealt with the characterization of sample preparation methods, namely the importance of the preparation medium and the chances and limitations of different fixation methods regarding sample preservation. It further offered a means of indirect immunodetection of epitopes and described a reconstructed 3D model of the periphery of a wildtype nephrocyte using STEM tomography. In the second project, the question was addressed, whether the foot processes of the same podocyte can interact with one another. To this end, a whole podocyte was reconstructed from a FIB-SEM dataset. Additionally, the nature of the cell-cell contacts between the foot processes were characterized in three dimensions by using dual-axis electron tomography, combining data obtained from human, mouse and fly. The third project took a closer look at the role of the cell polarity protein Pals1 in epithelial morphogenesis, suggesting an essential, specific and dose-dependent function during nephrogenesis and the fly system was used to substantiate the data generated in the mouse model. Pals1 was found to be a negative regulator of Hippo and TGF-β signaling and was hence shown to be directly involved in nephrogenesis. The last project focused on the role of *Drosophila*

Crumbs (DmCrb) in the regulation of early endocytosis due to its interaction with Moesin through its C-terminal FERM-binding domain and its contribution to nephrocyte diaphragm assembly/maintenance via its extracellular domain. In a series of rescue experiments with its human homologs and different deletion constructs, the functions of the different protein domains and the evolutionary conservation within the Crumbs family were examined.

3.2 The optimal sample preparation method is key to high quality morphological data

Transmission electron microscopy (TEM) has turned out to be key in the development of modern cell biology. Compared to classical light microscopy (LM), TEM offers a greatly higher resolution, thereby paving the way to the initial discovery of several organelles and other subcellular structures (PALADE and PORTER, 1954). Unfortunately, electron microscopy does not allow for imaging of water containing samples at room temperature and under normal pressure, since accelerated electrons only move unhindered under vacuum conditions, in which water would evaporate.

Published data on nephrocyte morphology exclusively rely on standard procedures, including chemical immersion fixation of the sample via (combinations of) aldehydes and osmium tetroxide in different buffered salines, dehydration at room temperature and embedding into a resin. In a comparative study, we demonstrated that the choice of saline is paramount to ensure optimal preservation of prepared nephrocytes. Due to the open accessibility to the surrounding medium, their intricate peripheral channel system is extremely vulnerable to inadequate conditions, e.g. the pH value or the amount of solvents, like sugars or salts. Phosphate buffered saline (PBS), which is often adjusted to a pH of 7.4 to mimic the pH of blood, which is often said to represent a physiological condition in biology and medicine, is not universally suitable for investigation of biological samples in an *in vitro* setting, since pH and osmolarity can differ significantly between body compartments (Gad, 2008). Especially during preparation for electron microscopy, residual phosphate in the sample can lead to high-contrast precipitates with heavy metals like uranyl acetate, lead, or other ions used for negative staining, and obscure important details of the sample ultrastructure (Dykstra and Reuss, 2003). Conducting the preparation and fixation in HL3.1 saline (Feng et al., 2004), a medium imitating the larval hemolymph regarding constituents and pH, lead to strongly improved ultra-structural preservation, offering highly detailed electron micrographs for morphological analysis.

Further improvement in preservation was achieved by applying a combination of high-pressure freezing (HPF) and freeze-substitution (FS). Instead of exposing it to a slowly diffusing chemical crosslinking agent and subsequent dehydration at room temperature, risking delayed and incomplete immobilization as well as introduction of unnecessary artifacts, the sample is exposed to high-pressure at a very low temperature, immobilizing the subcellular features, while inhibiting the growth of disruptive ice crystals.

During the following FS, the sample is gently dehydrated and resin infused, leading to minimal artifact formation, including shrinkage or varying degrees of fixation. Due to the limitations imposed by the physics of high-pressure freezing, vitrification of a whole fly is not possible (Studer et al., 2008). So micro-dissection in hemolymph-like saline, together with cryo-processing of the samples, produced optimal results and was used to generate TEM data for all other projects of this work.

We subsequently modified this protocol, to embed nephrocytes for immunostaining, by reducing the contrasting and post-fixation agent OsO_4 in the freeze-substitution mixture to 0.2%, thereby creating a trade-off between contrast and loss of antigenicity. After initial difficulties of direct immunodetection of Crumbs, we chose the indirect approach via a transgenic fly line containing a GFP-tagged version of the *Crb* gene and detecting the tag via an anti-GFP antibody. Considering the abundance of commercially available animal lines carrying GFP-tagged genes (Morin et al., 2001; Kelso et al., 2004; Buszczak et al., 2007; Nagarkar-Jaiswal et al., 2015a; Nagarkar-Jaiswal et al., 2015b; Sarov et al., 2016), this is a universal approach to detect proteins of interest with a single commercial antibody, which is known to work reliably on Epon sections.

Important for antigenicity is the choice of resin. Compared to acrylic resins like Lowicryl or LR-White, epoxy resins provide superior ultrastructural preservation and epoxide ultrathin sections of embedded samples are characterized by a smooth surface, resulting in comparably few epitopes reaching out of the resin, thereby reducing their accessibility to the primary antibody. By contrast, sections from a Lowicryl block, are more difficult to section, but offer a rougher surface, leading to a comparably high immunostaining success. Hence, specific antibody detection on Epon sections indicates a robust and well-suited method of preparation.

However, in order to approximate the living state of a sample, it is imperative to avoid unnecessary destructive chemical treatment during the preparation procedure. It is crucial to preserve the structure of the sample to allow antibody detection of epitopes. No or little osmium tetroxide should be used and aldehyde fixation / room temperature dehydration should be avoided in favor of HPF / FS. Contrast should mainly be generated by *en bloc* negative staining with uranyl acetate and post-staining of the sections should be avoided in order not to obscure antibody signal.

In further studies, additional improvements could be gained, by via using the cryo-sectioning method described by Tokuyasu (1973 and 1978), developing a gentler alternative via solidification by freezing and cutting cryo-sections. He discovered that by immersing aldehyde-fixed samples in high concentrations of sucrose, it could be frozen with liquid nitrogen and sectioned at very low temperatures (-100°C) in a cryo-ultramicrotome, avoiding hardening the sample by resin embedding altogether. Further development and research of the technique lead to one of the best and most efficient approaches to localization studies (Slot and Geuze, 2007).

The aforementioned fluorescent fusion proteins also offer the opportunity to conduct correlated light and electron microscopy (CLEM): The fluorescent tag can be used to locate rare events of interest in space and time inside a sample / cell population via LM and subsequently to take a closer look at the region at a higher resolution via EM or tomography, revealing its precise ultrastructure and putting the LM data into its cellular

context (Boer et al., 2015; Karreman et al., 2016). Recently, this approach has been realized in a semi-automated manner (Schorb et al., 2017).

3.3 The third dimension is essential to understand complex subcellular structures

Being three-dimensional objects, cells offer a lot of depth information, which can only be approximated by 2D imaging techniques. Both in the first and second manuscript, electron tomography is utilized both to enrich the current opinion on the morphology of nephrocyte cell periphery and to closely characterize the cell-cell contacts between foot processes. Benefiting from the optimized sample preparation techniques mentioned in the last chapter, wildtype nephrocytes were micro-dissected, high-pressure frozen and freeze-substituted, then an 800 µm section was subjected to a STEM tomography and subsequently reconstructed and sectioned to create a three-dimensional model of the lacunar system as well as the prominent subcellular features. Compared to classical TEM tomography, a STEM tomography can be applied to relatively thick sections at relatively low infliction of unnecessary damage (Aoyama et al., 2008), while STEM with a parallel beam produces tomograms with fewer distortions and artifacts compared to STEM with a converging beam (Biskupek et al., 2010). Passing through the model along the Z-axis of the model, a shape on one of the Z-layers indicating a straight tube may emerge as a curved tunnel or even a corridor further extending in Z-direction. A vesicle seemingly budding off a lacuna turns out to be a long tube or corridor, connecting it to another lacuna seemingly separated from the first in another layer, and so forth. In sum, we demonstrated that most of the channel system is interconnected and offered deeper insights into the overall organization of the cell periphery. Future studies, however, should include the reconstruction of a whole nephrocyte to fully understand its complex ultrastructure.

The second project addressed the question, whether foot processes of the same murine podocyte can interact with each other or just exclusively with those of other podocytes. Although light microscopical data on murine podocytes indicated that adjacent foot processes originate from different podocytes only (Höhne et al., 2013), the limited resolution of light microscopy makes an interpretation of the results difficult at best. With the ultrastructural reconstruction of a complete murine podocyte created in this project, unambiguous evidence is offered that podocytes exclusively form slit diaphragms between foot processes of other podocytes. These strictly heterophilic interactions may be harnessed for long range information transfer, i.e. regarding capillary pressure, along the podocyte network spanning the whole glomerulus.

How are podocytes prevented to form contacts between their own foot processes? It is conceivable that there are different variants or “flavors” of podocytes instead of a uniform podocyte population. These flavors would be equipped with different cell adhesion proteins, only able to conduct heterophilic interactions, which is the preferred interaction mode of nephrin and Neph1 in the slit diaphragm (Dworak et al., 2001). In rat, however, one single podocyte is able to interact with more than one other podocyte, according to Ichimura et al. (2015), implying the necessity of at least three different

flavors. A more likely reason for the exclusively heterophilic interaction between mature podocytes can be found in their development. The complexly branched cells develop from columnar cells resembling classical epithelium, connected by tight junctions (Schell et al., 2014), which can only be formed between adjacent cells. During further differentiation, the junctional belt transitions to the basal aspect and apparently, the contacts are not severed during this process, thereby remaining unaffected until the podocyte is totally differentiated.

Within this project, it was moreover discovered that foot processes are connected to each other by two different types of cell-cell contact. In the past, slit diaphragms in different species were described as being two-layered, probably a misinterpretation based on conventional two-dimensional TEM data (Wartiovaara et al., 2004; Kramer-Zucker et al., 2005). Our three-dimensional datasets indicate, that in human, mouse and fly only one layer of cell-cell contact continuously connects foot processes to each other, i.e. the slit diaphragm, and that it is only supplemented by various locally limited filamentous contacts. The characterizations of these newly discovered contacts remain speculative. They could be transitional stages of the slit diaphragm, which are either still in development or already in degradation. Data from Ruotsalainen et al. (2000) shows, that the foot processes of podocytes in kidneys of patients lacking NPHS1, which is necessary for proper development and maintenance of a slit diaphragm, are nevertheless normally spaced. One could conclude, that this novel kind of contact structure is used to establish and keep up regular spacing of the interstice between foot processes and that the slit diaphragm is particularly responsible for the its sieving function. Also, the novel connection might be a contributing factor to the exclusively heterophilic binding arrangement mentioned earlier.

3.4 Pals1 is a key regulator of epithelial morphogenesis in the kidney

In the third project, the role of Pals1 during renal morphogenesis is examined by utilizing the mouse model and then substantiating the findings with data acquired from *Drosophila*. Heterozygous mice lacking one Pals1 allele in the nephron showed strong renal phenotypes like heavy proteinuria, glomerular and tubular cysts, as well as premature death. This degree of impairment is especially striking, since in comparable mouse models a total depletion of apical polarity proteins, e.g. Lin7c (Olsen et al., 2007) or Crb3 (Whiteman et al., 2014; Szymaniak et al., 2015; Charrier et al., 2015), led to milder phenotypes, despite the complete lack of the respective protein, leading to the conclusion that Pals1 is an essential regulator of renal epithelial morphogenesis.

Pals1 apparently is necessary for the development of complexly structured tissues, since partial depletion in mouse embryos caused strong malformations in retinal precursor cells and the cerebral cortex (Kim et al., 2010; Cho et al., 2012). Depletion of Pals1 takes a strong toll on the renal filtration barrier, indicating that podocyte injury is the main reason for the proteinuria and that the detrimental influence is mainly present during glomerulogenesis. Data from the fly model confirms the effect on the filtration barrier

and points out a link between cell polarity and Hippo signaling, since knockdown of the Yap/Taz-homolog Yki rescued a simultaneous Sdt knockdown of the Pals1-homolog Sdt, reinforcing previous publications (Chen et al., 2010; Varelas et al., 2010; Robinson et al., 2010; Grzeschik et al., 2010).

The two Yki-homologs Yap and Taz seem to carry out tissue-specific functions in mammals. Yap-knockout mice die at early age (Morin-Kensicki et al., 2006), while Taz-knockout leads to both tubular and glomerular cysts (Hossain et al., 2007; Tian et al., 2007; Makita et al., 2008), which was also shown by Reginensi et al. (2013). In line with established knowledge, Pals1 depletion causes an increase of Yap/Taz target gene expression, with a simultaneous shift of Yap/Taz into the nucleus, which in parts was also confirmed in renal tissue of patients with ADPKD and autosomal recessive polycystic kidney disease (Happé et al., 2011).

Apparently Pals1-depletion is also delaying the development of the epithelial diffusion barrier, and thus weakening it, since the transepithelial electrical resistance is reduced (Straight et al., 2004; Wang et al., 2007). Our data indicate that dysregulation of cell-cell contacts leads to a weakened junctional tightness between cells, but for validation, additional experiments must be performed.

Localization of basolateral TGF-β receptors is abolished, when mature cell-cell contacts are belatedly established, causing a mislocalization to the apical aspect and higher expression levels of TGF-β target genes, leading to a higher susceptibility of TGF-β linked signaling (Varelas et al., 2010; Narimatsu et al., 2015). Both in cell culture experiments and the Pals1-deficient kidney tests, an upregulation of the TGF-β pathway could be observed. Hence, Pals1 was confirmed to play a role as upstream regulator of Hippo and TGF-β signaling in podocytes. The exact mechanism of the link between TGF-β signaling and Crb complex epithelial cell-density sensing is not fully understood yet. In previous studies, TGF-β signaling has been linked to fibrogenesis and cyst progression (Norman, 2011; Małgorzewicz et al., 2013), and compromised TGF-β signaling has been connected to glomerular diseases (Tossidou and Schiffer, 2012; Herman-Edelstein et al., 2013; Edeling et al., 2016). Hence, it is logical to assume that both activation of TGF-β signaling and inactivation of Hippo signaling contribute to cyst progression as well as impairment of tubular and glomerular epithelia. All in all, Pals1 was shown to be a negative regulator of the TGF-β and Hippo signaling pathways and hence directly connected to nephrogenesis.

3.5 Crumbs regulates early endocytosis in nephrocytes and is involved in diaphragm assembly and maintenance

The fourth project dealt with the role of Crumbs (DmCrb) in *Drosophila* nephrocytes and its involvement in early endocytosis as well as in assembly and maintenance of the nephrocyte diaphragm. Through its intracellular FERM-binding domain, DmCrb regulates endocytosis via interaction with Moesin, which links the Crb protein complex to the actin cytoskeleton in *Drosophila* (Médina et al., 2002; Sherrard and Fehon, 2015; Wei

et al., 2015). DmCrb also influences diaphragm assembly, likely by homophilic interaction to its counterparts in other foot processes between the long extracellular domains. According to our rescue experiments, these two functions are evolutionarily conserved, since hCrb2 as well as both hCrb3 variants can compensate for the defects caused by the knockdown of endogenous DmCrb expression. It was previously shown that Moesin is able to regulate endocytosis directly (Barroso-González et al., 2009; Nomachi et al., 2013) or indirectly via interaction with the cytoskeleton (Speck et al., 2003; Karagiosis and Ready, 2004). In *Drosophila*, the Crb complex is linked to the cytoskeleton by Moesin (Médina et al., 2002; Sherrard and Fehon, 2015; Wei et al., 2015) and in the murine system, the homolog Crb3a has been demonstrated to interact with Ezrin, a similar protein containing a FERM-binding domain, suggesting an analogous mechanism (Whiteman et al., 2014). Depletion of Moesin results in perturbed cell polarity in photoreceptor cells (Karagiosis and Ready, 2004).

Moesin was suggested to be involved in early endocytosis (Barroso-González et al., 2009; Nomachi et al., 2013), its knockdown disrupts the peripheral localization pattern of DmCrb in nephrocytes and, likely as a result, the number of nephrocyte diaphragms is reduced and ultrastructural defects are observable. Hence, we deduce that the interaction between DmCrb and Moesin is essential for the regulation of endocytosis. In addition, however, Moesin seems to be able to regulate cell morphology and assembly of the nephrocyte diaphragm independently of being recruited by DmCrb.

In the rescue experiments, hCrb2 as well as hCrb3a without ERLI motif and hCrb3b without CLPI motif counteracted the endocytic defect caused by the DmCrb knockdown more substantially than DmCrb or $DmCrb_{intra}$ (Figure 2.4-4d, e). In wildtype nephrocytes, overexpression of hCrb2, hCrb3b, but not of hCrb3a, increased the endocytosis rate more than DmCrb (Figure 2.4-9). These differences could be caused by protein mobility or stability positively influenced by loss of Sdt binding abilities (ΔERLI variants), or by the differences in the cytoplasmic protein between the Crumbs isoforms, causing variations in the fine regulation of Moesin interaction. Due to the reduction of endocytosis performance upon deletion of the ERLI-motif, protein mobility or stability cannot be considered as a reason for the increase of endocytosis performance regarding the longer Crb variants DmCrb and hCrb2. The rescue capacities of the Crb3 variants without functional ERLI-motif restore the endocytosis performance to normal or increased values, which can be explained by the aspect, that DmCrb or hCrb2 is faster removed from the membrane than hCrb3.

For the development and function of podocytes, the endocytic machinery plays a decisive role. In order to maintain the glomerular filtration barrier, endocytosis of core components of the SD in mammalian podocytes is very important (see Soda and Ishibe, 2013 for review). Nephrin is both endocytosed via clathrin-independent (Qin et al., 2009) and clathrin-dependent (Soda et al., 2012) uptake. Furthermore, it has been found that in patients suffering from nephrotic syndrome, injured podocytes show higher rates of endocytosis and a reduction of Nephrin at the cell surface. Also, endocytic defects led to podocytes with vacuoles, lost foot processes and SDs (Klose et al., 2013; Chen et al., 2013). Taken together, endocytosis can be considered an important factor in development

and maintenance of normal podocyte function and is affirmed by our data on the conserved role of Crumbs as a regulator of nephrocyte development and maintenance via modulation of the endocytosis machinery.

4 References

Adams, M. D. 2000. The Genome Sequence of Drosophila melanogaster. *Science* 287(5461):2185–2195. doi:10.1126/science.287.5461.2185.

Aggarwal, S. K., and R. C. King. 1967. The ultrastructure of the wreath cells of Drosophila melanogaster larvae. *Protoplasma* 63(4):343–352. doi:10.1007/BF01252944.

Akchurin, O., and K. J. Reidy. 2015. Genetic causes of proteinuria and nephrotic syndrome: Impact on podocyte pathobiology. *Pediatric nephrology (Berlin, Germany)* 30(2):221–233. doi:10.1007/s00467-014-2753-3.

Alves, C. H., A. S. Sanz, B. Park, L. P. Pellissier, N. Tanimoto, S. C. Beck, G. Huber, M. Murtaza, F. Richard, I. Sridevi Gurubaran, M. Garcia Garrido, C. N. Levelt, P. Rashbass, A. Le Bivic, M. W. Seeliger, and J. Wijnholds. 2013. Loss of CRB2 in the mouse retina mimics human retinitis pigmentosa due to mutations in the CRB1 gene. *Hum Mol Genet* 22(1):35–50. doi:10.1093/hmg/dds398.

Aoyama, K., T. Takagi, A. Hirase, and A. Miyazawa. 2008. STEM tomography for thick biological specimens. *Ultramicroscopy* 109(1):70–80. doi:10.1016/j.ultramic.2008.08.005.

Argüelles, J.-C. 2014. Why Can't Vertebrates Synthesize Trehalose? *Journal of Molecular Evolution* 79(3):111–116. doi:10.1007/s00239-014-9645-9.

Ashraf, S., H. Y. Gee, S. Woerner, L. X. Xie, V. Vega-Warner, S. Lovric, H. Fang, X. Song, D. C. Cattran, C. Avila-Casado, A. D. Paterson, P. Nitschké, C. Bole-Feysot, P. Cochat, J. Esteve-Rudd, B. Haberberger, S. J. Allen, W. Zhou, R. Airik, E. A. Otto, M. Barua, M. H. Al-Hamed, J. A. Kari, J. Evans, A. Bierzynska, M. A. Saleem, D. Böckenhauer, R. Kleta, S. El Desoky, D. O. Hacihamdioglu, F. Gok, J. Washburn, R. C. Wiggins, M. Choi, R. P. Lifton, S. Levy, Z. Han, L. Salviati, H. Prokisch, D. S. Williams, M. Pollak, C. F. Clarke, Y. Pei, C. Antignac, and F. Hildebrandt. 2013. ADCK4 mutations promote steroid-resistant nephrotic syndrome through CoQ10 biosynthesis disruption. *The Journal of clinical investigation* 123(12):5179–5189. doi:10.1172/JCI69000.

Bachmann, A., M. Schneider, E. Theilenberg, F. Grawe, and E. Knust. 2001. Drosophila Stardust is a partner of Crumbs in the control of epithelial cell polarity. *Nature* 414(6864):638–643. doi:10.1038/414638a.

Baines, A. D., and C. de Rouffignac. 1969. Functional heterogeneity of nephrons. II. Filtration rates, intraluminal flow velocities and fractional water reabsorption. *Pflugers Archiv European journal of physiology* 308(3):260–276.

Barroso-González, J., J.-D. Machado, L. García-Expósito, and A. Valenzuela-Fernández. 2009. Moesin regulates the trafficking of nascent clathrin-coated vesicles. *J. Biol. Chem.* 284(4):2419–2434. doi:10.1074/jbc.M805311200.

Bassett, A. R., C. Tibbit, C. P. Ponting, and J.-L. Liu. 2013. Highly efficient targeted mutagenesis of Drosophila with the CRISPR/Cas9 system. *Cell reports* 4(1):220–228. doi:10.1016/j.celrep.2013.06.020.

Bechtel, W., M. Helmstädter, J. Balica, B. Hartleben, B. Kiefer, F. Hrnjic, C. Schell, O. Kretz, S. Liu, F. Geist, D. Kerjaschki, G. Walz, and T. B. Huber. 2013. Vps34 deficiency reveals the importance of endocytosis for podocyte homeostasis. *JASN* 24(5):727–743. doi:10.1681/ASN.2012070700.

Beckerman, P., J. Bi-Karchin, A. S. D. Park, C. Qiu, P. D. Dummer, I. Soomro, C. M. Boustany-Kari, S. S. Pullen, J. H. Miner, C.-A. A. Hu, T. Rohacs, K. Inoue, S. Ishibe, M. A. Saleem, M. B. Palmer, A. M. Cuervo, J. B. Kopp, and K. Susztak. 2017. Transgenic expression of human APOL1 risk variants in podocytes induces kidney disease in mice. *Nature medicine* 23(4):429–438. doi:10.1038/nm.4287.

Berger, S., N. A. Bulgakova, F. Grawe, K. Johnson, and E. Knust. 2007. Unraveling the genetic complexity of Drosophila stardust during photoreceptor morphogenesis and prevention of light-induced degeneration. *Genetics* 176(4):2189–2200. doi:10.1534/genetics.107.071449.

Bernascone, I., and F. Martin-Belmonte. 2013. Crossroads of Wnt and Hippo in epithelial tissues. *Trends in cell biology* 23(8):380–389.

Bierzynska, A., K. Soderquest, P. Dean, E. Colby, R. Rollason, C. Jones, C. D. Inward, H. J. McCarthy, M. A. Simpson, G. M. Lord, M. Williams, G. I. Welsh, A. B. Koziell, and M. A. Saleem. 2017. MAGI2 Mutations Cause Congenital Nephrotic Syndrome. *JASN* 28(5):1614–1621. doi:10.1681/ASN.2016040387.

Bierzynska, A., K. Soderquest, and A. Koziell. 2014. Genes and podocytes - new insights into mechanisms of podocytopathy. *Frontiers in endocrinology* 5:226. doi:10.3389/fendo.2014.00226.

Biskupek, J., J. Leschner, P. Walther, and U. Kaiser. 2010. Optimization of STEM tomography acquisition — A comparison of convergent beam and parallel beam STEM tomography. *Ultramicroscopy* 110(9):1231–1237. doi:10.1016/j.ultramic.2010.05.008.

Boer, P. de, J. P. Hoogenboom, and B. N. G. Giepmans. 2015. Correlated light and electron microscopy: Ultrastructure lights up! *Nat Methods* 12(6):503–513. doi:10.1038/nmeth.3400.

Brand, A. H., and N. Perrimon. 1993. Targeted gene expression as a means of altering cell fates and generating dominant phenotypes. *Development (Cambridge, England)* 118(2):401–415.

Brinkkoetter, P. T., C. Ising, and T. Benzing. 2013. The role of the podocyte in albumin filtration. *Nature reviews. Nephrology* 9(6):328–336. doi:10.1038/nrneph.2013.78.

Bryant, D. M., and K. E. Mostov. 2008. From cells to organs: Building polarized tissue. *Nature reviews. Molecular cell biology* 9(11):887–901. doi:10.1038/nrm2523.

Bulgakova, N. A., O. Kempkens, and E. Knust. 2008. Multiple domains of Stardust differentially mediate localisation of the Crumbs-Stardust complex during photoreceptor development in Drosophila. *Journal of Cell Science* 121(Pt 12):2018–2026. doi:10.1242/jcs.031088.

Bulgakova, N. A., and E. Knust. 2009. The Crumbs complex: From epithelial-cell polarity to retinal degeneration. *Journal of Cell Science* 122(Pt 15):2587–2596. doi:10.1242/jcs.023648.

Burghardt, T., F. Hochapfel, B. Salecker, C. Meese, H.-J. J. Gröne, R. Rachel, G. Wanner, M. P. Krahn, and R. Witzgall. 2015. Advanced electron microscopic techniques provide a deeper insight into the peculiar features of podocytes. *American journal of physiology. Renal physiology* 309(12):9. doi:10.1152/ajprenal.00338.2015.

Buszczak, M., S. Paterno, D. Lighthouse, J. Bachman, J. Planck, S. Owen, A. D. Skora, T. G. Nystul, B. Ohlstein, A. Allen, J. E. Wilhelm, T. D. Murphy, R. W. Levis, E. Matunis, N. Srivali, R. A. Hoskins, and A. C. Spradling. 2007. The carnegie protein trap library: A versatile tool for Drosophila developmental studies. *Genetics* 175(3):1505–1531. doi:10.1534/genetics.106.065961.

Caliskan, Y., and K. Kiryluk. 2014. Novel biomarkers in glomerular disease. *Advances in chronic kidney disease* 21(2):205–216. doi:10.1053/j.ackd.2013.12.002.

Callus, B. A., A. M. Verhagen, and D. L. Vaux. 2006. Association of mammalian sterile twenty kinases, Mst1 and Mst2, with hSalvador via C-terminal coiled-coil domains, leads to its stabilization and phosphorylation. *The FEBS journal* 273(18):4264–4276. doi:10.1111/j.1742-4658.2006.05427.x.

Campbell, K., E. Knust, and H. Skaer. 2009. Crumbs stabilises epithelial polarity during tissue remodelling. *Journal of Cell Science* 122(Pt 15):2604–2612. doi:10.1242/jcs.047183.

Campbell, N. A., J. B. Reece, and J. Markl, editors. 2003. Biologie. Spektrum Akad. Verl., Heidelberg. 1606 pp.

Chan, E. H. Y., M. Nousiainen, R. B. Chalamalasetty, A. Schäfer, E. A. Nigg, and H. H. W. Silljé. 2005. The Ste20-like kinase Mst2 activates the human large tumor suppressor kinase Lats1. *Oncogene* 24(12):2076–2086. doi:10.1038/sj.onc.1208445.

Charrier, L. E., E. Loie, and P. Laprise. 2015. Mouse Crumbs3 sustains epithelial tissue morphogenesis in vivo. *Scientific reports* 5.

Chen, C.-L., K. M. Gajewski, F. Hamaratoglu, W. Bossuyt, L. Sansores-Garcia, C. Tao, and G. Halder. 2010. The apical-basal cell polarity determinant Crumbs regulates Hippo signaling in Drosophila. *PNAS* 107(36):15810–15815. doi:10.1073/pnas.1004060107.

Chen, J., M. X. Chen, A. B. Fogo, R. C. Harris, and J.-K. Chen. 2013. mVps34 deletion in podocytes causes glomerulosclerosis by disrupting intracellular vesicle trafficking. *JASN* 24(2):198–207. doi:10.1681/ASN.2012010101.

Chen, Y. M., and H. Liapis. 2015. Focal segmental glomerulosclerosis: Molecular genetics and targeted therapies. *BMC nephrology* 16:101. doi:10.1186/s12882-015-0090-9.

Cho, S.-H., J. Y. Kim, D. L. Simons, J. Y. Song, J. H. Le, E. C. Swindell, M. Jamrich, S. M. Wu, and S. Kim. 2012. Genetic ablation of Pals1 in retinal progenitor cells models the retinal pathology of Leber congenital amaurosis. *Hum Mol Genet* 21(12):2663–2676. doi:10.1093/hmg/dds091.

Costantini, F., and R. Kopan. 2010. Patterning a complex organ: Branching morphogenesis and nephron segmentation in kidney development. *Developmental cell* 18(5):698–712.

D'Agati, V. D., F. J. Kaskel, and R. J. Falk. 2011. Focal segmental glomerulosclerosis. *The New England journal of medicine* 365(25):2398–2411. doi:10.1056/NEJMra1106556.

Das, D., R. Aradhya, D. Ashoka, and M. Inamdar. 2008. Macromolecular uptake in Drosophila pericardial cells requires rudhira function. *Experimental cell research* 314(8):1804–1810. doi:10.1016/j.yexcr.2008.02.009.

Delous, M., N. E. Hellman, H.-M. Gaudé, F. Silbermann, A. Le Bivic, R. Salomon, C. Antignac, and S. Saunier. 2009. Nephrocystin-1 and nephrocystin-4 are required for epithelial morphogenesis and associate with PALS1/PATJ and Par6. *Hum Mol Genet* 18(24):4711–4723. doi:10.1093/hmg/ddp434.

den Hollander, A. I., J. B. ten Brink, Y. J. de Kok, S. van Soest, L. I. van den Born, M. A. van Driel, D. J. van de Pol, A. M. Payne, S. S. Bhattacharya, U. Kellner, C. B. Hoyng, A. Westerveld, H. G. Brunner, E. M. Bleeker-Wagemakers, A. F. Deutman, J. R. Heckenlively, F. P. Cremers, and A. A. Bergen. 1999. Mutations in a human homologue of Drosophila crumbs cause retinitis pigmentosa (RP12). *Nature genetics* 23(2):217–221. doi:10.1038/13848.

den Hollander, A. I., J. R. Heckenlively, L. I. van den Born, Y. J. de Kok, S. D. van der Velde-Visser, U. Kellner, B. Jurklies, M. J. van Schooneveld, A. Blankenagel, K. Rohrschneider, B. Wissinger, J. R. Cruysberg, A. F. Deutman, H. G. Brunner, E. Apfelstedt-Sylla, C. B. Hoyng, and F. P. Cremers. 2001. Leber congenital amaurosis and retinitis pigmentosa with Coats-like exudative vasculopathy are associated with mutations in the crumbs homologue 1 (CRB1) gene. *American journal of human genetics* 69(1):198–203.

Denholm, B., and H. Skaer. 2009. Bringing together components of the fly renal system. *Current opinion in genetics & development* 19(5):526–532. doi:10.1016/j.gde.2009.08.006.

Dietzl, G., D. Chen, F. Schnorrer, K.-C. Su, Y. Barinova, M. Fellner, B. Gasser, K. Kinsey, S. Oppel, S. Scheiblauer, A. Couto, V. Marra, K. Keleman, and B. J. Dickson. 2007. A genome-wide transgenic RNAi library for conditional gene inactivation in Drosophila. *Nature* 448(7150):151–156. doi:10.1038/nature05954.

Djuric, I., J. P. Siebrasse, U. Schulze, D. Granado, M. A. Schlüter, U. Kubitscheck, H. Pavenstädt, and T. Weide. 2016. The C-terminal domain controls the mobility of Crumbs 3 isoforms. *Biochimica et biophysica acta* 1863(6 Pt A):1208–1217. doi:10.1016/j.bbamcr.2016.03.008.

Dong, J., G. Feldmann, J. Huang, S. Wu, N. Zhang, S. A. Comerford, M. F. Gayyed, R. A. Anders, A. Maitra, and D. Pan. 2007. Elucidation of a universal size-control mechanism in Drosophila and mammals. *Cell* 130(6):1120–1133. doi:10.1016/j.cell.2007.07.019.

Dow, J. A. T., and M. F. Romero. 2010. Drosophila provides rapid modeling of renal development, function, and disease. *American journal of physiology. Renal physiology* 299(6):F1237-44. doi:10.1152/ajprenal.00521.2010.

Dubochet, J. 2007. The Physics of Rapid Cooling and Its Implications for Cryoimmobilization of Cells. In Cellular Electron Microscopy. J. R. McIntosh, editor. Elsevier textbooks, s.l. 7–21.

Dupont, S., L. Morsut, M. Aragona, E. Enzo, S. Giulitti, M. Cordenonsi, F. Zanconato, J. Le Digabel, M. Forcato, and S. Bicciato. 2011. Role of YAP/TAZ in mechanotransduction. *Nature* 474(7350):179–183.

Dworak, H. A., M. A. Charles, L. B. Pellerano, and H. Sink. 2001. Characterization of Drosophila hibris, a gene related to human nephrin. *Development* 128(21):4265–4276.

Dykstra, M. J., and L. E. Reuss. 2003. Biological Electron Microscopy: Theory, Techniques, and Troubleshooting. Springer US.

Ebarasi, L., S. Ashraf, A. Bierzynska, H. Y. Gee, H. J. McCarthy, S. Lovric, C. E. Sadowski, W. Pabst, V. Vega-Warner, H. Fang, A. Koziell, M. A. Simpson, I. Dursun, E. Serdaroglu, S. Levy, M. A. Saleem, F. Hildebrandt, and A. Majumdar. 2015. Defects of CRB2 cause steroid-resistant nephrotic syndrome. *American journal of human genetics* 96(1):153–161. doi:10.1016/j.ajhg.2014.11.014.

Ebarasi, L., L. He, K. Hultenby, M. Takemoto, C. Betsholtz, K. Tryggvason, and A. Majumdar. 2009. A reverse genetic screen in the zebrafish identifies crb2b as a regulator of the glomerular filtration barrier. *Developmental biology* 334(1):1–9. doi:10.1016/j.ydbio.2009.04.017.

Edeling, M., G. Ragi, S. Huang, H. Pavenstädt, and K. Susztak. 2016. Developmental signalling pathways in renal fibrosis: The roles of Notch, Wnt and Hedgehog. *Nature reviews. Nephrology* 12(7):426–439.

Edwards, K. A., M. Demsky, R. A. Montague, N. Weymouth, and D. P. Kiehart. 1997. GFP-moesin illuminates actin cytoskeleton dynamics in living tissue and demonstrates cell shape changes during morphogenesis in Drosophila. *Developmental biology* 191(1):103–117. doi:10.1006/dbio.1997.8707.

Eisenhart, C. 1947. The Assumptions Underlying the Analysis of Variance. *Biometrics* 3(1):1. doi:10.2307/3001534.

Eknoyan, G., N. Lameire, R. Barsoum, K.-U. Eckardt, A. Levin, N. Levin, F. Locatelli, A. MacLeod, R. Vanholder, R. Walker, and H. Wang. 2004. The burden of kidney disease: Improving global outcomes. *Kidney international* 66(4):1310–1314. doi:10.1111/j.1523-1755.2004.00894.x.

Ernkvist, M., N. Luna Persson, S. Audebert, P. Lecine, I. Sinha, M. Liu, M. Schlueter, A. Horowitz, K. Aase, T. Weide, J.-P. Borg, A. Majumdar, and L. Holmgren. 2009. The Amot/Patj/Syx signaling complex spatially controls RhoA GTPase activity in migrating endothelial cells. *Blood* 113(1):244–253. doi:10.1182/blood-2008-04-153874.

Fan, S., V. Fogg, Q. Wang, X.-W. Chen, C.-J. Liu, and B. Margolis. 2007. A novel Crumbs3 isoform regulates cell division and ciliogenesis via importin beta interactions. *The Journal of cell biology* 178(3):387–398. doi:10.1083/jcb.200609096.

Fassett, R. G., S. K. Venuthurupalli, G. C. Gobe, J. S. Coombes, M. A. Cooper, and W. E. Hoy. 2011. Biomarkers in chronic kidney disease: A review. *Kidney international* 80(8):806–821. doi:10.1038/ki.2011.198.

Feng, Y., A. Ueda, and C.-F. Wu. 2004. A modified minimal hemolymph-like solution, HL3.1, for physiological recordings at the neuromuscular junctions of normal and mutant Drosophila larvae. *Journal of neurogenetics* 18(2):377–402. doi:10.1080/01677060490894522.

Fischbach, K.-F., G. A. Linneweber, T. F. M. Andlauer, A. Hertenstein, B. Bonengel, and K. Chaudhary. 2009. The irre cell recognition module (IRM) proteins. *Journal of neurogenetics* 23(1-2):48–67. doi:10.1080/01677060802471668.

Fogg, V. C., C.-J. Liu, and B. Margolis. 2005. Multiple regions of Crumbs3 are required for tight junction formation in MCF10A cells. *Journal of Cell Science* 118(Pt 13):2859–2869. doi:10.1242/jcs.02412.

Frank, J., T. Wagenknecht, B. F. McEwen, M. Marko, C.-E. Hsieh, and C. A. Mannella. 2002. Three-dimensional imaging of biological complexity. *Journal of structural biology* 138(1-2):85–91.

Fu, Y., J.-Y. Zhu, A. Richman, Y. Zhang, X. Xie, J. R. Das, J. Li, P. E. Ray, and Z. Han. 2017a. APOL1-G1 in Nephrocytes Induces Hypertrophy and Accelerates Cell Death. *JASN* 28(4):1106–1116. doi:10.1681/ASN.2016050550.

Fu, Y., J.-Y. Zhu, A. Richman, Z. Zhao, F. Zhang, P. E. Ray, and Z. Han. 2017b. A Drosophila model system to assess the function of human monogenic podocyte mutations that cause nephrotic syndrome. *Human molecular genetics* 26(4):768–780. doi:10.1093/hmg/ddw428.

Fu, Y., J.-Y. Zhu, F. Zhang, A. Richman, Z. Zhao, and Z. Han. 2017c. Comprehensive functional analysis of Rab GTPases in Drosophila nephrocytes. *Cell and tissue research*. doi:10.1007/s00441-017-2575-2.

Fukasawa, H., S. Bornheimer, K. Kudlicka, and M. G. Farquhar. 2009. Slit diaphragms contain tight junction proteins. *Journal of the American Society of Nephrology JASN* 20(7):1491–1503. doi:10.1681/ASN.2008101117.

Gad, S. C. 2008. Preclinical Development Handbook: ADME and Biopharmaceutical Properties. John Wiley & Sons.

Gandhirajan, R. K., M. Jain, B. Walla, M. Johnsen, M. P. Bartram, M. Huynh Anh, M. M. Rinschen, T. Benzing, and B. Schermer. 2016. Cysteine S-Glutathionylation Promotes Stability and Activation of the Hippo Downstream Effector Transcriptional Co-activator with PDZ-binding Motif (TAZ). *The Journal of biological chemistry* 291(22):11596–11607. doi:10.1074/jbc.M115.712539.

Gee, H. Y., P. Saisawat, S. Ashraf, T. W. Hurd, V. Vega-Warner, H. Fang, B. B. Beck, O. Gribouval, W. Zhou, K. A. Diaz, S. Natarajan, R. C. Wiggins, S. Lovric, G. Chernin, D. S. Schoeb, B. Ovunc, Y. Frishberg, N. A. Soliman, H. M. Fathy, H. Goebel, J. Hoefele, L. T. Weber, J. W. Innis, C. Faul, Z. Han, J. Washburn, C. Antignac, S. Levy, E. A. Otto, and F. Hildebrandt. 2013. ARHGDIA mutations cause nephrotic syndrome via defective RHO GTPase signaling. *The Journal of clinical investigation* 123(8):3243–3253. doi:10.1172/JCI69134.

Gee, H. Y., F. Zhang, S. Ashraf, S. Kohl, C. E. Sadowski, V. Vega-Warner, W. Zhou, S. Lovric, H. Fang, M. Nettleton, J.-Y. Zhu, J. Hoefele, L. T. Weber, L. Podracka, A. Boor, H. Fehrenbach, J. W. Innis, J. Washburn, S. Levy, R. P. Lifton, E. A. Otto, Z. Han, and F. Hildebrandt. 2015. KANK deficiency leads to podocyte dysfunction and nephrotic syndrome. *The Journal of clinical investigation* 125(6):2375–2384. doi:10.1172/JCI79504.

Gleixner, E. M., G. Canaud, T. Hermle, M. C. Guida, O. Kretz, M. Helmstädter, T. B. Huber, S. Eimer, F. Terzi, and M. Simons. 2014. V-ATPase/mTOR signaling regulates megalin-mediated apical endocytosis. *Cell reports* 8(1):10–19.

Grahammer, F., C. Schell, and T. B. Huber. 2013. The podocyte slit diaphragm--from a thin grey line to a complex signalling hub. *Nature reviews. Nephrology* 9(10):587–598. doi:10.1038/nrneph.2013.169.

Greka, A. 2016. Human genetics of nephrotic syndrome and the quest for precision medicine. *Current opinion in nephrology and hypertension* 25(2):138–143. doi:10.1097/MNH.0000000000000204.

Greka, A., and P. Mundel. 2012. Cell biology and pathology of podocytes. *Annual review of physiology* 74:299–323. doi:10.1146/annurev-physiol-020911-153238.

Groth, A. C., M. Fish, R. Nusse, and M. P. Calos. 2004. Construction of transgenic Drosophila by using the site-specific integrase from phage phiC31. *Genetics* 166(4):1775–1782.

Grzeschik, N. A., L. M. Parsons, M. L. Allott, K. F. Harvey, and H. E. Richardson. 2010. Lgl, aPKC, and Crumbs regulate the Salvador/Warts/Hippo pathway through two distinct mechanisms. *Current biology CB* 20(7):573–581. doi:10.1016/j.cub.2010.01.055.

Gupta, I. R., C. Baldwin, D. Auguste, K. C. H. Ha, J. E. Andalousi, S. Fahiminiya, M. Bitzan, C. Bernard, M. R. Akbari, S. A. Narod, D. S. Rosenblatt, J. Majewski, and T. Takano. 2013. ARHGDIA: A novel gene implicated in nephrotic syndrome. *Journal of Medical Genetics* 50(5):330–338. doi:10.1136/jmedgenet-2012-101442.

Haase, M., R. Bellomo, C. Albert, G. Vanpoucke, G. Thomas, W. Laroy, K. Verleysen, S. Kropf, H. Kuppe, R. Hetzer, and A. Haase-Fielitz. 2014. The identification of three novel biomarkers of major adverse kidney events. *Biomarkers in medicine* 8(10):1207–1217. doi:10.2217/bmm.14.90.

Hackl, M. J., J. L. Burford, K. Villanueva, L. Lam, K. Suszták, B. Schermer, T. Benzing, and J. Peti-Peterdi. 2013. Tracking the fate of glomerular epithelial cells in vivo using serial multiphoton imaging in new mouse models with fluorescent lineage tags. *Nature medicine* 19(12):1661–1666.

Hamano, Y., J. A. Grunkemeyer, A. Sudhakar, M. Zeisberg, D. Cosgrove, R. Morello, B. Lee, H. Sugimoto, and R. Kalluri. 2002. Determinants of Vascular Permeability in the Kidney Glomerulus. *J. Biol. Chem.* 277(34):31154–31162. doi:10.1074/jbc.M204806200.

Hansen, C. G., T. Moroishi, and K.-L. Guan. 2015. YAP and TAZ: A nexus for Hippo signaling and beyond. *Trends in cell biology* 25(9):499–513.

Hao, Y., A. Chun, K. Cheung, B. Rashidi, and X. Yang. 2008. Tumor suppressor LATS1 is a negative regulator of oncogene YAP. *J. Biol. Chem.* 283(9):5496–5509. doi:10.1074/jbc.M709037200.

Happé, H., A. M. van der Wal, W. N. Leonhard, S. J. Kunnen, M. H. Breuning, E. de Heer, and D. J. M. Peters. 2011. Altered Hippo signalling in polycystic kidney disease. *The Journal of pathology* 224(1):133–142.

Hartleben, B., H. Schweizer, P. Lubben, M. P. Bartram, C. C. Moller, R. Herr, C. Wei, E. Neumann-Haefelin, B. Schermer, H. Zentgraf, D. Kerjaschki, J. Reiser, G. Walz, T. Benzing, and T. B. Huber. 2008. Neph-Nephrin proteins bind the Par3-Par6-atypical protein kinase C (aPKC) complex to regulate podocyte cell polarity. *The Journal of biological chemistry* 283(34):23033–23038. doi:10.1074/jbc.M803143200.

Hartleben, B., E. Widmeier, M. Suhm, K. Worthmann, C. Schell, M. Helmstadter, T. Wiech, G. Walz, M. Leitges, M. Schiffer, and T. B. Huber. 2013. aPKClambda/iota and aPKCzeta contribute to podocyte differentiation and glomerular maturation. *Journal of the American Society of Nephrology JASN* 24(2):253–267. doi:10.1681/ASN.2012060582.

Hartleben, B., E. Widmeier, N. Wanner, M. Schmidts, S. T. Kim, L. Schneider, B. Mayer, D. Kerjaschki, J. H. Miner, G. Walz, and T. B. Huber. 2012. Role of the Polarity Protein Scribble for Podocyte Differentiation and Maintenance. *PLOS ONE* 7(5):e36705. doi:10.1371/journal.pone.0036705.

Hartley, P. S., K. Motamedchaboki, R. Bodmer, and K. Ocorr. 2016. SPARC-Dependent Cardiomyopathy in Drosophila. *Circulation. Cardiovascular genetics* 9(2):119–129. doi:10.1161/CIRCGENETICS.115.001254.

Helmstädter, M., K. Luthy, M. Godel, M. Simons, Ashish, D. Nihalani, S. A. Rensing, K.-F. Fischbach, and T. B. Huber. 2012. Functional study of mammalian Neph proteins in Drosophila melanogaster. *PloS one* 7(7):e40300. doi:10.1371/journal.pone.0040300.

Helmstädter, M., and M. Simons. 2017. Using Drosophila nephrocytes in genetic kidney disease. *Cell and tissue research* 369(1):119–126. doi:10.1007/s00441-017-2606-z.

Herman-Edelstein, M., T. Weinstein, and U. Gafter. 2013. TGF β 1-dependent podocyte dysfunction. *Current opinion in nephrology and hypertension* 22(1):93–99.

Hermle, T., D. A. Braun, M. Helmstädter, T. B. Huber, and F. Hildebrandt. 2017. Modeling Monogenic Human Nephrotic Syndrome in the Drosophila Garland Cell Nephrocyte. *Journal of the American Society of Nephrology JASN* 28(5):1521–1533. doi:10.1681/ASN.2016050517.

Hildebrandt, F. 2010. Genetic kidney diseases. *The Lancet* 375(9722):1287–1295. doi:10.1016/S0140-6736(10)60236-X.

Hirose, T., D. Satoh, H. Kurihara, C. Kusaka, H. Hirose, K. Akimoto, T. Matsusaka, I. Ichikawa, T. Noda, and S. Ohno. 2009. An essential role of the universal polarity protein, aPKClambda, on the maintenance of podocyte slit diaphragms. *PloS one* 4(1):e4194. doi:10.1371/journal.pone.0004194.

Hochapfel, F., L. Denk, G. Mendl, U. Schulze, C. Maaßen, Y. Zaytseva, H. Pavenstädt, T. Weide, R. Rachel, R. Witzgall, and M. P. Krahn. 2017. Distinct functions of Crumbs regulating slit diaphragms and endocytosis in Drosophila nephrocytes. *Cellular and molecular life sciences CMLS*. doi:10.1007/s00018-017-2593-y.

Höhne, M., C. Ising, H. Hagmann, L. A. Völker, S. Brähler, B. Schermer, P. T. Brinkkoetter, and T. Benzing. 2013. Light microscopic visualization of podocyte ultrastructure demonstrates oscillating glomerular contractions. *The American journal of pathology* 182(2):332–338.

Hong, Y., B. Stronach, N. Perrimon, L. Y. Jan, and Y. N. Jan. 2001. Drosophila Stardust interacts with Crumbs to control polarity of epithelia but not neuroblasts. *Nature* 414(6864):634–638. doi:10.1038/414634a.

Hossain, Z., S. M. Ali, H. L. Ko, J. Xu, C. P. Ng, K. Guo, Z. Qi, S. Ponniah, W. Hong, and W. Hunziker. 2007. Glomerulocystic kidney disease in mice with a targeted inactivation of Wwtr1. *PNAS* 104(5):1631–1636. doi:10.1073/pnas.0605266104.

Huang, J., S. Wu, J. Barrera, K. Matthews, and D. Pan. 2005. The Hippo signaling pathway coordinately regulates cell proliferation and apoptosis by inactivating Yorkie, the Drosophila Homolog of YAP. *Cell* 122(3):421–434. doi:10.1016/j.cell.2005.06.007.

Huber, T. B., B. Hartleben, K. Winkelmann, L. Schneider, J. U. Becker, M. Leitges, G. Walz, H. Haller, and M. Schiffer. 2009. Loss of Podocyte aPKCλ /ι Causes Polarity Defects and Nephrotic Syndrome. *JASN* 20(4):798–806. doi:10.1681/ASN.2008080871.

Huber, T. B., M. Schmidts, P. Gerke, B. Schermer, A. Zahn, B. Hartleben, L. Sellin, G. Walz, and T. Benzing. 2003. The carboxyl terminus of Neph family members binds to the PDZ domain protein zonula occludens-1. *The Journal of biological chemistry* 278(15):13417–13421. doi:10.1074/jbc.C200678200.

Hurd, T. W., L. Gao, M. H. Roh, I. G. Macara, and B. Margolis. 2003. Direct interaction of two polarity complexes implicated in epithelial tight junction assembly. *Nature cell biology* 5(2):137–142.

Ichimura, K., N. Miyazaki, S. Sadayama, K. Murata, M. Koike, K.-i. Nakamura, K. Ohta, and T. Sakai. 2015. Three-dimensional architecture of podocytes revealed by block-face scanning electron microscopy. *Scientific reports* 5:8993.

Inoue, K., and S. Ishibe. 2015. Podocyte endocytosis in the regulation of the glomerular filtration barrier. *American Journal of Physiology - Renal Physiology* 309(5):F398-405. doi:10.1152/ajprenal.00136.2015.

Itoh, M., K. Nakadate, Y. Horibata, T. Matsusaka, J. Xu, W. Hunziker, and H. Sugimoto. 2014. The structural and functional organization of the podocyte filtration slits is regulated by Tjp1/ZO-1. *PloS one* 9(9):e106621. doi:10.1371/journal.pone.0106621.

Ivy, J. R., M. Drechsler, J. H. Catterson, R. Bodmer, K. Ocorr, A. Paululat, P. S. Hartley, and R. Artero. 2015. Klf15 Is Critical for the Development and Differentiation of Drosophila Nephrocytes. *PloS one* 10(8):e0134620. doi:10.1371/journal.pone.0134620.

Kamberov, E. 2000. Molecular Cloning and Characterization of Pals, Proteins Associated with mLin-7. *Journal of Biological Chemistry* 275(15):11425–11431. doi:10.1074/jbc.275.15.11425.

Kao, R. M., A. Vasilyev, A. Miyawaki, I. A. Drummond, and A. P. McMahon. 2012. Invasion of distal nephron precursors associates with tubular interconnection during nephrogenesis. *JASN* 23(10):1682–1690. doi:10.1681/ASN.2012030283.

Karagiosis, S. A., and D. F. Ready. 2004. Moesin contributes an essential structural role in Drosophila photoreceptor morphogenesis. *Development* 131(4):725–732. doi:10.1242/dev.00976.

Karreman, M. A., L. Mercier, N. L. Schieber, G. Solecki, G. Allio, F. Winkler, B. Ruthensteiner, J. G. Goetz, and Y. Schwab. 2016. Fast and precise targeting of single tumor cells in vivo by multimodal correlative microscopy. *Journal of Cell Science* 129(2):444–456. doi:10.1242/jcs.181842.

Kellenberger, E., R. Johansen, M. Maeder, B. Bohrmann, E. Stauffer, and W. Villiger. 1992. Artefacts and morphological changes during chemical fixation. *Journal of microscopy* 168(2):181–201.

Kelso, R. J., M. Buszczak, A. T. Quinones, C. Castiblanco, S. Mazzalupo, and L. Cooley. 2004. Flytrap, a database documenting a GFP protein-trap insertion screen in Drosophila melanogaster. *Nucleic acids research* 32(Database issue):D418-20. doi:10.1093/nar/gkh014.

Kempkens, O., E. Médina, G. Fernandez-Ballester, S. Ozüyaman, A. Le Bivic, L. Serrano, and E. Knust. 2006. Computer modelling in combination with in vitro studies reveals similar binding affinities of Drosophila Crumbs for the PDZ domains of Stardust and DmPar-6. *European journal of cell biology* 85(8):753–767. doi:10.1016/j.ejcb.2006.03.003.

Kestila, M., U. Lenkkeri, M. Mannikko, J. Lamerdin, P. McCready, H. Putaala, V. Ruotsalainen, T. Morita, M. Nissinen, R. Herva, C. E. Kashtan, L. Peltonen, C. Holmberg, A. Olsen, and K. Tryggvason. 1998. Positionally cloned gene for a novel glomerular protein--nephrin--is mutated in congenital nephrotic syndrome. *Molecular cell* 1(4):575–582.

Kim, J. M., H. Wu, G. Green, C. A. Winkler, J. B. Kopp, J. H. Miner, E. R. Unanue, and A. S. Shaw. 2003. CD2-Associated Protein Haploinsufficiency Is Linked to Glomerular Disease Susceptibility. *Science* 300(5623):1298–1300. doi:10.1126/science.1081068.

Kim, S., M. K. Lehtinen, A. Sessa, M. W. Zappaterra, S.-H. Cho, D. Gonzalez, B. Boggan, C. A. Austin, J. Wijnholds, and M. J. Gambello. 2010. The apical complex couples cell fate and cell survival to cerebral cortical development. *Neuron* 66(1):69–84.

Klebes, A., and E. Knust. 2000. A conserved motif in Crumbs is required for E-cadherin localisation and zonula adherens formation in Drosophila. *Current Biology* 10(2):76–85.

Klipper-Aurbach, Y., M. Wasserman, N. Braunspiegel-Weintrob, D. Borstein, S. Peleg, S. Assa, M. Karp, Y. Benjamini, Y. Hochberg, and Z. Laron. 1995. Mathematical formulae for the prediction of the residual beta cell function during the first two years of disease in children and adolescents with insulin-dependent diabetes mellitus. *Medical hypotheses* 45(5):486–490.

Klose, S., D. Flores-Benitez, F. Riedel, and E. Knust. 2013. Fosmid-based structure-function analysis reveals functionally distinct domains in the cytoplasmic domain of Drosophila crumbs. *G3 (Bethesda, Md.)* 3(2):153–165. doi:10.1534/g3.112.005074.

Knust, E., U. Tepaß, and A. Wodarz. 1993. crumbs and stardust, two genes of Drosophila required for the development of epithelial cell polarity. *Development* 119(Supplement):261–268.

Kobayashi, A., M. T. Valerius, J. W. Mugford, T. J. Carroll, M. Self, G. Oliver, and A. P. McMahon. 2008. Six2 defines and regulates a multipotent self-renewing nephron progenitor population throughout mammalian kidney development. *Cell stem cell* 3(2):169–181.

Kohan, D. E., and M. Barton. 2014. Endothelin and endothelin antagonists in chronic kidney disease. *Kidney international* 86(5):896–904. doi:10.1038/ki.2014.143.

Kokkinopoulou, M., M. A. Güler, B. Lieb, M. Barbeck, S. Ghanaati, and J. Markl. 2014. 3D-ultrastructure, functions and stress responses of gastropod (Biomphalaria glabrata) rhogocytes. *PloS one* 9(6):e101078.

Krahn, M. P., J. Bückers, L. Kastrup, and A. Wodarz. 2010. Formation of a Bazooka-Stardust complex is essential for plasma membrane polarity in epithelia. *J Cell Biol* 190(5):751–760. doi:10.1083/jcb.201006029.

Kramer-Zucker, A. G., S. Wiessner, A. M. Jensen, and I. A. Drummond. 2005. Organization of the pronephric filtration apparatus in zebrafish requires Nephrin, Podocin and the FERM domain protein Mosaic eyes. *Developmental biology* 285(2):316–329.

Krause, M., A. Rak-Raszewska, I. Pietilä, S. E. Quaggin, and S. Vainio. 2015. Signaling during kidney development. *Cells* 4(2):112–132.

Kreidberg, J. A. 1996. Gene targeting in kidney development. *Pediatric Blood & Cancer* 27(5):445–452.

Kremer, J. R., D. N. Mastronarde, and J. R. McIntosh. 1996. Computer visualization of three-dimensional image data using IMOD. *Journal of structural biology* 116(1):71–76. doi:10.1006/jsbi.1996.0013.

Krendel, M., S. V. Kim, T. Willinger, T. Wang, M. Kashgarian, R. A. Flavell, and M. S. Mooseker. 2009. Disruption of Myosin 1e Promotes Podocyte Injury. *JASN* 20(1):86–94. doi:10.1681/ASN.2007111172.

Kriz, W., B. Hähnel, H. Hosser, S. Rösener, and R. Waldherr. 2014. Structural analysis of how podocytes detach from the glomerular basement membrane under hypertrophic stress. *Frontiers in endocrinology* 5:207. doi:10.3389/fendo.2014.00207.

Kriz, W., I. Shirato, M. Nagata, M. LeHir, and K. V. Lemley. 2013. The podocyte's response to stress: The enigma of foot process effacement. *American Journal of Physiology-Renal Physiology* 304(4):F333-F347.

Kruzel-Davila, E., R. Shemer, A. Ofir, I. Bavli-Kertselli, I. Darlyuk-Saadon, P. Oren-Giladi, W. G. Wasser, D. Magen, E. Zaknoun, M. Schuldiner, A. Salzberg, D. Kornitzer, Z. Marelja, M. Simons, and K. Skorecki. 2017. APOL1-Mediated Cell Injury Involves Disruption of Conserved Trafficking Processes. *JASN* 28(4):1117–1130. doi:10.1681/ASN.2016050546.

Kumichel, A., and E. Knust. 2014. Apical localisation of crumbs in the boundary cells of the Drosophila hindgut is independent of its canonical interaction partner stardust. *PloS one* 9(4):e94038. doi:10.1371/journal.pone.0094038.

Lai, Z.-C., X. Wei, T. Shimizu, E. Ramos, M. Rohrbaugh, N. Nikolaidis, L.-L. Ho, and Y. Li. 2005. Control of cell proliferation and apoptosis by mob as tumor suppressor, mats. *Cell* 120(5):675–685. doi:10.1016/j.cell.2004.12.036.

Laprise, P., S. Beronja, N. F. Silva-Gagliardi, M. Pellikka, A. M. Jensen, C. J. McGlade, and U. Tepass. 2006. The FERM protein Yurt is a negative regulatory component of the Crumbs complex that controls epithelial polarity and apical membrane size. *Developmental cell* 11(3):363–374. doi:10.1016/j.devcel.2006.06.001.

Lei, Q.-Y., H. Zhang, B. Zhao, Z.-Y. Zha, F. Bai, X.-H. Pei, S. Zhao, Y. Xiong, and K.-L. Guan. 2008. TAZ promotes cell proliferation and epithelial-mesenchymal transition and is inhibited by the hippo pathway. *Mol. Cell. Biol.* 28(7):2426–2436. doi:10.1128/MCB.01874-07.

Lemmers, C., D. Michel, L. Lane-Guermonprez, M.-H. Delgrossi, E. Médina, J.-P. Arsanto, and A. Le Bivic. 2004. CRB3 binds directly to Par6 and regulates the morphogenesis of the tight junctions in mammalian epithelial cells. *Mol. Biol. Cell* 15(3):1324–1333. doi:10.1091/mbc.E03-04-0235.

Letizia, A., S. Ricardo, B. Moussian, N. Martín, and M. Llimargas. 2013. A functional role of the extracellular domain of Crumbs in cell architecture and apicobasal polarity. *Journal of Cell Science* 126(Pt 10):2157–2163. doi:10.1242/jcs.122382.

Levey, A. S., K.-U. Eckardt, Y. Tsukamoto, A. Levin, J. Coresh, J. Rossert, D. de Zeeuw, T. H. Hostetter, N. Lameire, and G. Eknoyan. 2005. Definition and classification of chronic kidney disease: A position statement from Kidney Disease: Improving Global Outcomes (KDIGO). *Kidney international* 67(6):2089–2100. doi:10.1111/j.1523-1755.2005.00365.x.

Li, P. K.-T., and T. K.-W. Ma. 2017. Global impact of nephropathies. *Nephrology (Carlton, Vic.)* 22 Suppl 4:9–13. doi:10.1111/nep.13146.

Lin, Y.-H., H. Currinn, S. M. Pocha, A. Rothnie, T. Wassmer, and E. Knust. 2015. AP-2-complex-mediated endocytosis of Drosophila Crumbs regulates polarity by antagonizing Stardust. *Journal of Cell Science* 128(24):4538–4549. doi:10.1242/jcs.174573.

Ling, C., Y. Zheng, F. Yin, J. Yu, J. Huang, Y. Hong, S. Wu, and D. Pan. 2010. The apical transmembrane protein Crumbs functions as a tumor suppressor that regulates Hippo signaling by binding to Expanded. *PNAS* 107(23):10532–10537. doi:10.1073/pnas.1004279107.

Lőrincz, P., Z. Lakatos, Á. Varga, T. Maruzs, Z. Simon-Vecsei, Z. Darula, P. Benkő, G. Csordás, M. Lippai, I. Andó, K. Hegedűs, K. F. Medzihradszky, S. Takáts, and G. Juhász. 2016. MiniCORVET is a Vps8-containing early endosomal tether in Drosophila. *eLife* 5. doi:10.7554/eLife.14226.

Lotery, A. J., S. G. Jacobson, G. A. Fishman, R. G. Weleber, A. B. Fulton, P. Namperumalsamy, E. Héon, A. V. Levin, S. Grover, J. R. Rosenow, K. K. Kopp, V. C. Sheffield, and E. M. Stone. 2001. Mutations in the CRB1 gene cause Leber congenital amaurosis. *Archives of ophthalmology (Chicago, Ill. 1960)* 119(3):415–420.

Lovric, S., S. Ashraf, W. Tan, and F. Hildebrandt. 2016. Genetic testing in steroid-resistant nephrotic syndrome: when and how? *Nephrology, dialysis, transplantation official publication of the European Dialysis and Transplant Association - European Renal Association* 31(11):1802–1813. doi:10.1093/ndt/gfv355.

Lovric, S., S. Goncalves, H. Y. Gee, B. Oskouian, H. Srinivas, W.-I. Choi, S. Shril, S. Ashraf, W. Tan, J. Rao, M. Airik, D. Schapiro, D. A. Braun, C. E. Sadowski, E. Widmeier, T. Jobst-Schwan, J. M. Schmidt, V. Girik, G. Capitani, J. H. Suh, N. Lachaussée, C. Arrondel, J. Patat, O. Gribouval, M. Furlano, O. Boyer, A. Schmitt, V. Vuiblet, S. Hashmi, R. Wilcken, F. P. Bernier, A. M. Innes, J. S. Parboosingh, R. E. Lamont, J. P. Midgley, N. Wright, J. Majewski, M. Zenker, F. Schaefer, N. Kuss, J. Greil, T. Giese, K. Schwarz, V. Catheline, D. Schanze, I. Franke, Y. Sznajer, A. S. Truant, B. Adams, J. Désir, R. Biemann, Y. Pei, E. Ars, N. Lloberas, A. Madrid, V. R. Dharnidharka, A. M. Connolly, M. C. Willing, M. A. Cooper, R. P. Lifton, M. Simons, H. Riezman, C. Antignac, J. D. Saba, and F. Hildebrandt. 2017. Mutations in sphingosine-1-phosphate lyase cause nephrosis with ichthyosis and adrenal insufficiency. *The Journal of clinical investigation* 127(3):912–928. doi:10.1172/JCI89626.

Machuca, E., G. Benoit, and C. Antignac. 2009. Genetics of nephrotic syndrome: Connecting molecular genetics to podocyte physiology. *Hum Mol Genet* 18(R2):R185-R194. doi:10.1093/hmg/ddp328.

Makarova, O., M. H. Roh, C.-J. Liu, S. Laurinec, and B. Margolis. 2003. Mammalian Crumbs3 is a small transmembrane protein linked to protein associated with Lin-7 (Pals1). *Gene* 302(1-2):21–29.

Makita, R., Y. Uchijima, K. Nishiyama, T. Amano, Q. Chen, T. Takeuchi, A. Mitani, T. Nagase, Y. Yatomi, H. Aburatani, O. Nakagawa, E. V. Small, P. Cobo-Stark, P. Igarashi, M. Murakami, J. Tominaga, T. Sato, T. Asano, Y. Kurihara, and H. Kurihara. 2008. Multiple renal cysts, urinary concentration defects, and pulmonary emphysematous changes in mice lacking TAZ. *American Journal of Physiology - Renal Physiology* 294(3):F542-F553. doi:10.1152/ajprenal.00201.2007.

Małgorzewicz, S., E. Skrzypczak-Jankun, and J. Jankun. 2013. Plasminogen activator inhibitor-1 in kidney pathology (Review). *International journal of molecular medicine* 31(3):503–510.

Mallipattu, S. K., R. Liu, F. Zheng, G. Narla, A. Ma'ayan, S. Dikman, M. K. Jain, M. Saleem, V. D'Agati, P. Klotman, P. Y. Chuang, and J. C. He. 2012. Kruppel-like factor 15 (KLF15) is a key regulator of podocyte differentiation. *The Journal of biological chemistry* 287(23):19122–19135. doi:10.1074/jbc.M112.345983.

Marshall, C. B., R. D. Krofft, M. J. Blonski, J. Kowalewska, C. M. Logar, J. W. Pippin, F. Kim, R. Feil, C. E. Alpers, and S. J. Shankland. 2011. Role of smooth muscle protein SM22α in glomerular epithelial cell injury. *American Journal of Physiology - Renal Physiology* 300(4):F1026-42. doi:10.1152/ajprenal.00187.2010.

Mascie-Taylor, C. G. N., and E. Karim. 2003. The burden of chronic disease. *Science (New York, N.Y.)* 302(5652):1921–1922. doi:10.1126/science.1092488.

Mathers, C. D., and D. Loncar. 2006. Projections of global mortality and burden of disease from 2002 to 2030. *PLoS medicine* 3(11):e442. doi:10.1371/journal.pmed.0030442.

McCarthy, H. J., and M. A. Saleem. 2011. Genetics in clinical practice: Nephrotic and proteinuric syndromes. *Nephron. Experimental nephrology* 118(1):e1-8. doi:10.1159/000320878.

McDonald, K. 1999. High-pressure freezing for preservation of high resolution fine structure and antigenicity for immunolabeling. *Methods in molecular biology (Clifton, N.J.)* 117:77–97. doi:10.1385/1-59259-201-5:77.

McGee, A. W., S. R. Dakoji, O. Olsen, D. S. Bredt, W. A. Lim, and K. E. Prehoda. 2001. Structure of the SH3-guanylate kinase module from PSD-95 suggests a mechanism for regulated assembly of MAGUK scaffolding proteins. *Molecular cell* 8(6):1291–1301.

McNeill, H., and A. Reginensi. 2017. Lats1/2 Regulate Yap/Taz to Control Nephron Progenitor Epithelialization and Inhibit Myofibroblast Formation. *JASN* 28(3):852–861. doi:10.1681/ASN.2016060611.

Médina, E., J. Williams, E. Klipfell, D. Zarnescu, G. Thomas, and A. Le Bivic. 2002. Crumbs interacts with moesin and beta(Heavy)-spectrin in the apical membrane skeleton of Drosophila. *The Journal of cell biology* 158(5):941–951. doi:10.1083/jcb.200203080.

Mele, C., P. Iatropoulos, R. Donadelli, A. Calabria, R. Maranta, P. Cassis, S. Buelli, S. Tomasoni, R. Piras, M. Krendel, S. Bettoni, M. Morigi, M. Delledonne, C. Pecoraro, I. Abbate, M. R. Capobianchi, F. Hildebrandt, E. Otto, F. Schaefer, F. Macciardi, F. Ozaltin, S. Emre, T. Ibsirlioglu, A. Benigni, G. Remuzzi, and M. Noris. 2011. MYO1E Mutations and Childhood Familial Focal Segmental Glomerulosclerosis. *New England Journal of Medicine* 365(4):295–306. doi:10.1056/NEJMoa1101273.

Michaud, J.-L., L. I. Lemieux, M. Dubé, B. C. Vanderhyden, S. J. Robertson, and C. R.J. Kennedy. 2003. Focal and Segmental Glomerulosclerosis in Mice with Podocyte-Specific Expression of Mutant α -Actinin-4. *JASN* 14(5):1200–1211. doi:10.1097/01.ASN.0000059864.88610.5E.

Michel, D., J.-P. Arsanto, D. Massey-Harroche, C. Béclin, J. Wijnholds, and A. Le Bivic. 2005. PATJ connects and stabilizes apical and lateral components of tight junctions in human intestinal cells. *Journal of Cell Science* 118(Pt 17):4049–4057. doi:10.1242/jcs.02528.

Michgehl, U., H. Pavenstädt, and B. Vollenbröker. 2017. Cross talk between the Crumbs complex and Hippo signaling in renal epithelial cells. *Pflügers Archiv - European Journal of Physiology* 469(7):917–926. doi:10.1007/s00424-017-2004-0.

Mitsuishi, Y., H. Hasegawa, A. Matsuo, W. Araki, T. Suzuki, S. Tagami, M. Okochi, M. Takeda, R. Roepman, and M. Nishimura. 2010. Human CRB2 inhibits gamma-secretase cleavage of amyloid precursor protein by binding to the presenilin complex. *The Journal of biological chemistry* 285(20):14920–14931. doi:10.1074/jbc.M109.038760.

Morin, X., R. Daneman, M. Zavortink, and W. Chia. 2001. A protein trap strategy to detect GFP-tagged proteins expressed from their endogenous loci in Drosophila. *Proceedings of the National Academy of Sciences of the United States of America* 98(26):15050–15055. doi:10.1073/pnas.261408198.

Morin-Kensicki, E. M., B. N. Boone, M. Howell, J. R. Stonebraker, J. Teed, J. G. Alb, T. R. Magnuson, W. O'Neal, and S. L. Milgram. 2006. Defects in Yolk Sac Vasculogenesis, Chorioallantoic Fusion, and Embryonic Axis Elongation in Mice with Targeted Disruption of Yap65. *Mol. Cell. Biol.* 26(1):77–87. doi:10.1128/MCB.26.1.77-87.2006.

Muzumdar, M. D., B. Tasic, K. Miyamichi, L. Li, and L. Luo. 2007. A global double-fluorescent Cre reporter mouse. *genesis* 45(9):593–605. doi:10.1002/dvg.20335.

Na, J., M. T. Sweetwyne, A. S. D. Park, K. Susztak, and R. L. Cagan. 2015. Diet-Induced Podocyte Dysfunction in Drosophila and Mammals. *Cell reports* 12(4):636–647. doi:10.1016/j.celrep.2015.06.056.

Nagarkar-Jaiswal, S., S. Z. DeLuca, P.-T. Lee, W.-W. Lin, H. Pan, Z. Zuo, J. Lv, A. C. Spradling, and H. J. Bellen. 2015a. A genetic toolkit for tagging intronic MiMIC containing genes. *eLife* 4. doi:10.7554/eLife.08469.

Nagarkar-Jaiswal, S., P.-T. Lee, M. E. Campbell, K. Chen, S. Anguiano-Zarate, M. C. Gutierrez, T. Busby, W.-W. Lin, Y. He, K. L. Schulze, B. W. Booth, M. Evans-Holm, K. J. T. Venken, R. W. Levis, A. C. Spradling, R. A. Hoskins, and H. J. Bellen. 2015b. A library of MiMICs allows tagging of genes and reversible, spatial and temporal knockdown of proteins in Drosophila. *eLife* 4. doi:10.7554/eLife.05338.

Nagata, M., Y. Yamaguchi, and K. Ito. 1993. Loss of mitotic activity and the expression of vimentin in glomerular epithelial cells of developing human kidneys. *Anatomy and embryology* 187(3):275–279.

Nallet-Staub, F., X. Yin, C. Gilbert, V. Marsaud, S. B. Mimoun, D. Javelaud, E. B. Leof, and A. Mauviel. 2015. Cell density sensing alters TGF-β signaling in a cell-type-specific manner, independent from Hippo pathway activation. *Developmental cell* 32(5):640–651.

Narimatsu, M., P. Samavarchi-Tehrani, X. Varelas, and J. L. Wrana. 2015. Distinct polarity cues direct Taz/Yap and TGF β receptor localization to differentially control TGF β-induced Smad signaling. *Developmental cell* 32(5):652–656.

Nation, J. L. 2016. Insect physiology and biochemistry. CRC Press, Boca Raton. 644 pp.

Neal, C. R., H. Crook, E. Bell, S. J. Harper, and D. O. Bates. 2005. Three-dimensional reconstruction of glomeruli by electron microscopy reveals a distinct restrictive urinary subpodocyte space. *Journal of the American Society of Nephrology* 16(5):1223–1235.

Neal, C. R., P. R. Muston, D. Njegovan, R. Verrill, S. J. Harper, W. M. Deen, and D. O. Bates. 2007. Glomerular filtration into the subpodocyte space is highly restricted under physiological perfusion conditions. *American Journal of Physiology-Renal Physiology* 293(6):F1787-F1798.

Nomachi, A., M. Yoshinaga, J. Liu, P. Kanchanawong, K. Tohyama, D. Thumkeo, T. Watanabe, S. Narumiya, and T. Hirata. 2013. Moesin controls clathrin-mediated S1PR1 internalization in T cells. *PloS one* 8(12):e82590. doi:10.1371/journal.pone.0082590.

Norman, J. 2011. Fibrosis and progression of Autosomal Dominant Polycystic Kidney Disease (ADPKD). *Biochimica et Biophysica Acta (BBA) - Molecular Basis of Disease* 1812(10):1327–1336. doi:10.1016/j.bbadis.2011.06.012.

Ogawa, A., M. Sakatsume, X. Wang, Y. Sakamaki, Y. Tsubata, B. Alchi, T. Kuroda, H. Kawachi, I. Narita, F. Shimizu, and F. Gejyo. 2007. SM22alpha: The novel phenotype marker of injured glomerular epithelial cells in anti-glomerular basement membrane nephritis. *Nephron. Experimental nephrology* 106(3):e77-87. doi:10.1159/000103020.

Oh, H., and K. D. Irvine. 2009. In vivo analysis of Yorkie phosphorylation sites. *Oncogene* 28(17):1916–1927. doi:10.1038/onc.2009.43.

Oka, T., V. Mazack, and M. Sudol. 2008. Mst2 and Lats kinases regulate apoptotic function of Yes kinase-associated protein (YAP). *J. Biol. Chem.* 283(41):27534–27546. doi:10.1074/jbc.M804380200.

Olsen, O., L. Funke, J.-f. Long, M. Fukata, T. Kazuta, J. C. Trinidad, K. A. Moore, H. Misawa, P. A. Welling, A. L. Burlingame, M. Zhang, and D. S. Bredt. 2007. Renal defects associated with improper polarization of the CRB and DLG polarity complexes in MALS-3 knockout mice. *J Cell Biol* 179(1):151–164. doi:10.1083/jcb.200702054.

Omran, A. R. 2005. The Epidemiologic Transition: A Theory of the Epidemiology of Population Change. *The Milbank Quarterly* 83(4):731–757. doi:10.1111/j.1468-0009.2005.00398.x.

Pahl, M. V., N. D. Vaziri, J. Yuan, and S. G. Adler. 2010. Upregulation of monocyte/macrophage HGFIN (Gpnmb/Osteoactivin) expression in end-stage renal disease. *Clinical journal of the American Society of Nephrology CJASN* 5(1):56–61. doi:10.2215/CJN.03390509.

PALADE, G. E., and K. R. PORTER. 1954. Studies on the endoplasmic reticulum. I. Its identification in cells in situ. *The Journal of experimental medicine* 100(6):641–656.

Patel-Chamberlin, M., Y. Wang, B. Satirapoj, L. M. Phillips, C. C. Nast, T. Dai, R. A. Watkins, X. Wu, R. Natarajan, A. Leng, K. Ulanday, R. R. Hirschberg, J. Lapage, E. J. Nam, T. Haq, and S. G. Adler. 2011. Hematopoietic growth factor inducible neurokinin-1 (Gpnmb/Osteoactivin) is a biomarker of progressive renal injury across species. *Kidney international* 79(10):1138–1148. doi:10.1038/ki.2011.28.

Patrakka, J., M. Kestila, J. Wartiovaara, V. Ruotsalainen, P. Tissari, U. Lenkkeri, M. Mannikko, I. Visapaa, C. Holmberg, J. Rapola, K. Tryggvason, and H. Jalanko. 2000. Congenital nephrotic syndrome (NPHS1): features resulting from different mutations in Finnish patients. *Kidney international* 58(3):972–980. doi:10.1046/j.1523-1755.2000.00254.x.

Patrakka, J., and K. Tryggvason. 2007. Nephrin--a unique structural and signaling protein of the kidney filter. *Trends in molecular medicine* 13(9):396–403. doi:10.1016/j.molmed.2007.06.006.

Patrakka, J., and K. Tryggvason. 2009. New insights into the role of podocytes in proteinuria. *Nature Reviews Nephrology* 5(8):463. doi:10.1038/nrneph.2009.108.

Pellikka, M., G. Tanentzapf, M. Pinto, C. Smith, C. J. McGlade, D. F. Ready, and U. Tepass. 2002. Crumbs, the Drosophila homologue of human CRB1/RP12, is essential for photoreceptor morphogenesis. *Nature* 416(6877):143–149. doi:10.1038/nature721.

Pellissier, L. P., C. H. Alves, P. M. Quinn, R. M. Vos, N. Tanimoto, D. M. S. Lundvig, J. J. Dudok, B. Hooibrink, F. Richard, S. C. Beck, G. Huber, V. Sothilingam, M.

Garcia Garrido, A. Le Bivic, M. W. Seeliger, and J. Wijnholds. 2013. Targeted ablation of CRB1 and CRB2 in retinal progenitor cells mimics Leber congenital amaurosis. *PLoS Genet* 9(12):e1003976. doi:10.1371/journal.pgen.1003976.

Pénalva, C., and V. Mirouse. 2012. Tissue-specific function of Patj in regulating the Crumbs complex and epithelial polarity. *Development (Cambridge, England)* 139(24):4549–4554. doi:10.1242/dev.085449.

Peschke, M., D. Moog, A. Klingl, U. G. Maier, and F. Hempel. 2013. Evidence for glycoprotein transport into complex plastids. *Proceedings of the National Academy of Sciences of the United States of America* 110(26):10860–10865. doi:10.1073/pnas.1301945110.

Piccolo, S., S. Dupont, and M. Cordenonsi. 2014. The Biology of YAP/TAZ: Hippo Signaling and Beyond. *Physiological reviews* 94(4):1287–1312. doi:10.1152/physrev.00005.2014.

Pieczynski, J., and B. Margolis. 2011. Protein complexes that control renal epithelial polarity. *American journal of physiology. Renal physiology* 300(3):F589-601. doi:10.1152/ajprenal.00615.2010.

Pielage, J., T. Stork, I. Bunse, and C. Klambt. 2003. The Drosophila cell survival gene discs lost encodes a cytoplasmic Codanin-1-like protein, not a homolog of tight junction PDZ protein Patj. *Developmental cell* 5(6):841–851.

Pocha, S. M., and E. Knust. 2013. Complexities of Crumbs function and regulation in tissue morphogenesis. *Current biology CB* 23(7):R289-93. doi:10.1016/j.cub.2013.03.001.

Praskova, M., F. Xia, and J. Avruch. 2008. MOBKL1A/MOBKL1B phosphorylation by MST1 and MST2 inhibits cell proliferation. *Current Biology* 18(5):311–321. doi:10.1016/j.cub.2008.02.006.

Qin, X.-S., H. Tsukaguchi, A. Shono, A. Yamamoto, H. Kurihara, and T. Doi. 2009. Phosphorylation of nephrin triggers its internalization by raft-mediated endocytosis. *JASN* 20(12):2534–2545. doi:10.1681/ASN.2009010011.

Quaggin, S. E., and J. A. Kreidberg. 2008. Development of the renal glomerulus: Good neighbors and good fences. *Development* 135(4):609–620. doi:10.1242/dev.001081.

Rachel, R., C. Meyer, A. Klingl, S. Gurster, T. Heimerl, N. Wasserburger, T. Burghardt, U. Kuper, A. Bellack, S. Schopf, R. Wirth, H. Huber, and G. Wanner. 2010. Analysis of the ultrastructure of archaea by electron microscopy. *Methods in cell biology* 96:47–69. doi:10.1016/S0091-679X(10)96003-2.

Reeve, E.C.R., and I. Black. 2001. Encyclopedia of Genetics. Fitzroy Dearborn.

Reeves, W., J. P. Caulfield, and M. G. Farquhar. 1978. Differentiation of epithelial foot processes and filtration slits: Sequential appearance of occluding junctions, epithelial polyanion, and slit membranes in developing glomeruli. *Laboratory investigation; a journal of technical methods and pathology* 39(2):90–100.

Reginensi, A., R. P. Scott, A. Gregorieff, M. Bagherie-Lachidan, C. Chung, D.-S. Lim, T. Pawson, J. Wrana, and H. McNeill. 2013. Yap-and Cdc42-dependent nephrogenesis and morphogenesis during mouse kidney development. *PLoS Genet* 9(3):e1003380.

Reiter, L. T., L. Potocki, S. Chien, M. Gribskov, and E. Bier. 2001. A systematic analysis of human disease-associated gene sequences in Drosophila melanogaster. *Genome research* 11(6):1114–1125. doi:10.1101/gr.169101.

Robinson, B. S., J. Huang, Y. Hong, and K. H. Moberg. 2010. Crumbs regulates Salvador/Warts/Hippo signaling in Drosophila via the FERM-domain protein Expanded. *Current biology CB* 20(7):582–590. doi:10.1016/j.cub.2010.03.019.

Rodewald, R., and M. J. Karnovsky. 1974. Porous substructure of the glomerular slit diaphragm in the rat and mouse. *The Journal of cell biology* 60(2):423.

Rodriguez-Boulan, E., and I. G. Macara. 2014. Organization and execution of the epithelial polarity programme. *Nature reviews Molecular cell biology* 15(4):nrm3775. doi:10.1038/nrm3775.

Roh, M. H., S. Fan, C.-J. Liu, and B. Margolis. 2003. The Crumbs3-Pals1 complex participates in the establishment of polarity in mammalian epithelial cells. *Journal of Cell Science* 116(14):2895–2906. doi:10.1242/jcs.00500.

Roh, M. H., O. Makarova, C.-J. Liu, Shin, S. Lee, S. Laurinec, M. Goyal, R. Wiggins, and B. Margolis. 2002. The Maguk protein, Pals1, functions as an adapter, linking mammalian homologues of Crumbs and Discs Lost. *The Journal of cell biology* 157(1):161–172. doi:10.1083/jcb.200109010.

Roignot, J., X. Peng, and K. Mostov. 2013. Polarity in mammalian epithelial morphogenesis. *Cold Spring Harbor perspectives in biology* 5(2). doi:10.1101/cshperspect.a013789.

Ruotsalainen, V., J. Patrakka, P. Tissari, P. Reponen, M. Hess, M. Kestilä, C. Holmberg, R. Salonen, M. Heikinheimo, and J. Wartiovaara. 2000. Role of nephrin in cell junction formation in human nephrogenesis. *The American journal of pathology* 157(6):1905–1916.

Sadowski, C. E., S. Lovric, S. Ashraf, W. L. Pabst, H. Y. Gee, S. Kohl, S. Engelmann, V. Vega-Warner, H. Fang, J. Halbritter, M. J. Somers, W. Tan, S. Shril, I. Fessi, R. P. Lifton, D. Bockenhauer, S. El-Desoky, J. A. Kari, M. Zenker, M. J. Kemper, D. Mueller, H. M. Fathy, N. A. Soliman, and F. Hildebrandt. 2015. A single-gene cause in 29.5% of cases of steroid-resistant nephrotic syndrome. *JASN* 26(6):1279–1289. doi:10.1681/ASN.2014050489.

Salmon, A. H. J., I. Toma, A. Sipos, P. R. Muston, S. J. Harper, D. O. Bates, C. R. Neal, and J. Peti-Peterdi. 2007. Evidence for restriction of fluid and solute movement across the glomerular capillary wall by the subpodocyte space. *American Journal of Physiology-Renal Physiology* 293(6):F1777-F1786.

Sarov, M., C. Barz, H. Jambor, M. Y. Hein, C. Schmied, D. Suchold, B. Stender, S. Janosch, V. V. K J, R. T. Krishnan, A. Krishnamoorthy, I. R. S. Ferreira, R. K. Ejsmont, K. Finkl, S. Hasse, P. Kampfer, N. Plewka, E. Vinis, S. Schloissnig, E. Knust, V. Hartenstein, M. Mann, M. Ramaswami, K. VijayRaghavan, P. Tomancak, and F. Schnorrer. 2016. A genome-wide resource for the analysis of protein localisation in Drosophila. *eLife* 5:e12068. doi:10.7554/eLife.12068.

Satoh, D., T. Hirose, Y. Harita, C. Daimon, T. Harada, H. Kurihara, A. Yamashita, and S. Ohno. 2014. aPKClambda maintains the integrity of the glomerular slit diaphragm through trafficking of nephrin to the cell surface. *Journal of biochemistry* 156(2):115–128. doi:10.1093/jb/mvu022.

Saxén, L., and H. Sariola. 1987. Early organogenesis of the kidney. *Pediatric Nephrology* 1(3):385–392. doi:10.1007/BF00849241.

Schell, C., N. Wanner, and T. B. Huber. 2014. Glomerular development--shaping the multi-cellular filtration unit. *Seminars in Cell & Developmental Biology* 36:39–49. doi:10.1016/j.semcdb.2014.07.016.

Schneider, C. A., W. S. Rasband, and K. W. Eliceiri. 2012. NIH Image to ImageJ: 25 years of image analysis. *Nature methods* 9(7):671.

Schorb, M., L. Gaechter, O. Avinoam, F. Sieckmann, M. Clarke, C. Bebeacua, Y. S. Bykov, A. F.-P. Sonnen, R. Lihl, and J. A.G. Briggs. 2017. New hardware and workflows for semi-automated correlative cryo-fluorescence and cryo-electron microscopy/tomography. *Journal of structural biology* 197(2):83–93. doi:10.1016/j.jsb.2016.06.020.

Schulze, U., B. Vollenbroker, D. A. Braun, van T, D. Granado, J. Kremerskothen, B. Franzel, R. Klosowski, J. Barth, C. Fufezan, D. A. Wolters, H. Pavenstadt, and T. Weide. 2014. The Vac14-interaction network is linked to regulators of the endolysosomal and autophagic pathway. *Molecular & cellular proteomics MCP* 13(6):1397–1411. doi:10.1074/mcp.M113.034108.

Scott, R. P., S. P. Hawley, J. Ruston, J. Du, C. Brakebusch, N. Jones, and T. Pawson. 2012. Podocyte-Specific Loss of Cdc42 Leads to Congenital Nephropathy. *JASN* 23(7):1149–1154. doi:10.1681/ASN.2011121206.

Sen, A., Z. Nagy-Zsvér-Vadas, and M. P. Krahn. 2012. Drosophila PATJ supports adherens junction stability by modulating Myosin light chain activity. *The Journal of cell biology* 199(4):685–698. doi:10.1083/jcb.201206064.

Sen, A., R. Sun, and M. P. Krahn. 2015. Localization and Function of Pals1-associated Tight Junction Protein in Drosophila Is Regulated by Two Distinct Apical Complexes. *The Journal of biological chemistry* 290(21):13224–13233. doi:10.1074/jbc.M114.629014.

Shankland, S. J. 2006. The podocyte's response to injury: Role in proteinuria and glomerulosclerosis. *Kidney international* 69(12):2131–2147.

Sherrard, K. M., and R. G. Fehon. 2015. The transmembrane protein Crumbs displays complex dynamics during follicular morphogenesis and is regulated competitively by Moesin and aPKC. *Development (Cambridge, England)* 142(10):1869–1878. doi:10.1242/dev.115329.

Shin, K., S. Straight, and B. Margolis. 2005. PATJ regulates tight junction formation and polarity in mammalian epithelial cells. *The Journal of cell biology* 168(5):705–711. doi:10.1083/jcb.200408064.

Simons, M., B. Hartleben, and T. B. Huber. 2009. Podocyte polarity signalling. *Current opinion in nephrology and hypertension* 18(4):324–330.

Slavotinek, A., J. Kaylor, H. Pierce, M. Cahr, S. J. DeWard, D. Schneidman-Duhovny, A. Alsadah, F. Salem, G. Schmajuk, and L. Mehta. 2015. CRB2 mutations produce a phenotype resembling congenital nephrosis, Finnish type, with cerebral ventriculomegaly and raised alpha-fetoprotein. *American journal of human genetics* 96(1):162–169. doi:10.1016/j.ajhg.2014.11.013.

Slot, J. W., and H. J. Geuze. 2007. Cryosectioning and immunolabeling. *Nature protocols* 2(10):2480–2491. doi:10.1038/nprot.2007.365.

Smith, H. W. 1951. The Kidney: Structure and Function in Health and Disease. Oxford University Press.

Smoyer, W. E., and P. Mundel. 1998. Regulation of podocyte structure during the development of nephrotic syndrome. *Journal of Molecular Medicine* 76(3-4):172–183. doi:10.1007/s001090050206.

Soda, K., D. M. Balkin, S. M. Ferguson, S. Paradise, I. Milosevic, S. Giovedi, L. Volpicelli-Daley, X. Tian, Y. Wu, H. Ma, S. H. Son, R. Zheng, G. Moeckel, O. Cremona, L. B. Holzman, P. de Camilli, and S. Ishibe. 2012. Role of dynamin, synaptojanin, and endophilin in podocyte foot processes. *The Journal of clinical investigation* 122(12):4401–4411. doi:10.1172/JCI65289.

Soda, K., and S. Ishibe. 2013. The function of endocytosis in podocytes. *Current opinion in nephrology and hypertension* 22(4):432–438. doi:10.1097/MNH.0b013e3283624820.

Soukup, S. F., J. Culi, and D. Gubb. 2009. Uptake of the necrotic serpin in Drosophila melanogaster via the lipophorin receptor-1. *PLoS Genet* 5(6):e1000532. doi:10.1371/journal.pgen.1000532.

Speck, O., S. C. Hughes, N. K. Noren, R. M. Kulikauskas, and R. G. Fehon. 2003. Moesin functions antagonistically to the Rho pathway to maintain epithelial integrity. *Nature* 421(6918):83–87. doi:10.1038/nature01295.

Straight, S. W., K. Shin, V. C. Fogg, S. Fan, C.-J. Liu, M. Roh, and B. Margolis. 2004. Loss of PALS1 Expression Leads to Tight Junction and Polarity Defects. *Mol. Biol. Cell* 15(4):1981–1990. doi:10.1091/mbc.E03-08-0620.

Studer, D., B. M. Humbel, and M. Chiquet. 2008. Electron microscopy of high pressure frozen samples: Bridging the gap between cellular ultrastructure and atomic resolution. *Histochemistry and Cell Biology* 130(5):877–889. doi:10.1007/s00418-008-0500-1.

Surendran, K., T. C. Simon, H. Liapis, and J. K. McGuire. 2004. Matrilysin (MMP-7) expression in renal tubular damage: Association with Wnt4. *Kidney international* 65(6):2212–2222. doi:10.1111/j.1523-1755.2004.00641.x.

Szymaniak, A. D., J. E. Mahoney, W. V. Cardoso, and X. Varelas. 2015. Crumbs3-mediated polarity directs airway epithelial cell fate through the Hippo pathway effector Yap. *Developmental cell* 34(3):283–296.

Tanaka, K., A. Mitsushima, Y. Kashima, T. Nakadera, and H. Osatake. 1989. Application of an ultrahigh-resolution scanning electron microscope (UHS-T1) to biological specimens. *Journal of electron microscopy technique* 12(2):146–154.

Tanaka, T., and A. Nakamura. 2008. The endocytic pathway acts downstream of Oskar in Drosophila germ plasm assembly. *Development* 135(6):1107–1117. doi:10.1242/dev.017293.

Tanentzapf, G., and U. Tepass. 2003. Interactions between the crumbs, lethal giant larvae and bazooka pathways in epithelial polarization. *Nature cell biology* 5(1):46–52. doi:10.1038/ncb896.

Tao, W., S. Zhang, G. S. Turenchalk, R. A. Stewart, M. A. St John, W. Chen, and T. Xu. 1999. Human homologue of the Drosophila melanogaster lats tumour suppressor modulates CDC2 activity. *Nature genetics* 21(2):177–181. doi:10.1038/5960.

Tavares, G. A., E. H. Panepucci, and A. T. Brunger. 2001. Structural characterization of the intramolecular interaction between the SH3 and guanylate kinase domains of PSD-95. *Molecular cell* 8(6):1313–1325.

Tepass, U. 1996. Crumbs, a component of the apical membrane, is required for zonula adherens formation in primary epithelia of Drosophila. *Developmental biology* 177(1):217–225. doi:10.1006/dbio.1996.0157.

Tepass, U. 2012. The apical polarity protein network in Drosophila epithelial cells: regulation of polarity, junctions, morphogenesis, cell growth, and survival. *Annual review of cell and developmental biology* 28:655–685. doi:10.1146/annurev-cellbio-092910-154033.

Tepass, U., and E. Knust. 1990. Phenotypic and developmental analysis of mutations at thecrumbs locus, a gene required for the development of epithelia inDrosophila melanogaster. *Roux's archives of developmental biology the official organ of the EDBO* 199(4):189–206. doi:10.1007/BF01682078.

Tepass, U., C. Theres, and E. Knust. 1990. crumbs encodes an EGF-like protein expressed on apical membranes of Drosophila epithelial cells and required for organization of epithelia. *Cell* 61(5):787–799.

Thomson, R., G. Genovese, C. Canon, D. Kovacsics, M. K. Higgins, M. Carrington, C. A. Winkler, J. Kopp, C. Rotimi, A. Adeyemo, A. Doumatey, G. Ayodo, S. L. Alper, M. R. Pollak, D. J. Friedman, and J. Raper. 2014. Evolution of the primate trypanolytic factor APOL1. *PNAS* 111(20):E2130-E2139. doi:10.1073/pnas.1400699111.

Tian, Y., R. Kolb, J.-H. Hong, J. Carroll, D. Li, J. You, R. Bronson, M. B. Yaffe, J. Zhou, and T. Benjamin. 2007. TAZ Promotes PC2 Degradation through a SCF β-Trcp E3 Ligase Complex. *Mol. Cell. Biol.* 27(18):6383–6395. doi:10.1128/MCB.00254-07.

Tokuyasu, K. T. 1973. A technique for ultracryotomy of cell suspensions and tissues. *The Journal of cell biology* 57(2):551–565.

Tokuyasu, K. T. 1978. A study of positive staining of ultrathin frozen sections. *Journal of ultrastructure research* 63(3):287–307.

Tossidou, I., and M. Schiffer. 2012. TGF-β/BMP Pathways and the Podocyte. *Seminars in nephrology* 32(4):368–376. doi:10.1016/j.semnephrol.2012.06.008.

Tryggvason, K., J. Patrakka, and J. Wartiovaara. 2006. Hereditary proteinuria syndromes and mechanisms of proteinuria. *The New England journal of medicine* 354(13):1387–1401.

Tutor, A. S., S. Prieto-Sánchez, and M. Ruiz-Gómez. 2014. Src64B phosphorylates Dumbfounded and regulates slit diaphragm dynamics: Drosophila as a model to study nephropathies. *Development (Cambridge, England)* 141(2):367–376. doi:10.1242/dev.099408.

Uhlén, M., L. Fagerberg, B. M. Hallström, C. Lindskog, P. Oksvold, A. Mardinoglu, Å. Sivertsson, C. Kampf, E. Sjöstedt, A. Asplund, I. Olsson, K. Edlund, E. Lundberg, S. Navani, C. A.-K. Szigyarto, J. Odeberg, D. Djureinovic, J. O. Takanen, S. Hober, T. Alm, P.-H. Edqvist, H. Berling, H. Tegel, J. Mulder, J. Rockberg, P. Nilsson, J. M. Schwenk, M. Hamsten, K. von Feilitzen, M. Forsberg, L. Persson, F. Johansson, M. Zwahlen, G. von Heijne, J. Nielsen, and F. Pontén. 2015. Proteomics. Tissue-based map of the human proteome. *Science (New York, N.Y.)* 347(6220):1260419. doi:10.1126/science.1260419.

Urbschat, A., N. Obermüller, and A. Haferkamp. 2011. Biomarkers of kidney injury. *Biomarkers biochemical indicators of exposure, response, and susceptibility to chemicals* 16 Suppl 1:S22-30. doi:10.3109/1354750X.2011.587129.

van den Hurk, J. A. J. M., P. Rashbass, R. Roepman, J. Davis, K. E. J. Voesenek, M. L. Arends, M. N. Zonneveld, M. H. G. van Roekel, K. Cameron, K. Rohrschneider, J. R. Heckenlively, R. K. Koenekoop, C. B. Hoyng, F. P. M. Cremers, and A. I. den Hollander. 2005. Characterization of the Crumbs homolog 2 (CRB2) gene and analysis of its role in retinitis pigmentosa and Leber congenital amaurosis. *Molecular vision* 11:263–273.

Varelas, X., P. Samavarchi-Tehrani, M. Narimatsu, A. Weiss, K. Cockburn, B. G. Larsen, J. Rossant, and J. L. Wrana. 2010. The Crumbs complex couples cell density sensing to Hippo-dependent control of the TGF- β -SMAD pathway. *Developmental cell* 19(6):831–844.

Vivante, A., S. Kohl, D.-Y. Hwang, G. C. Dworschak, and F. Hildebrandt. 2014. Single-gene causes of congenital anomalies of the kidney and urinary tract (CAKUT) in humans. *Pediatric nephrology (Berlin, Germany)* 29(4):695–704. doi:10.1007/s00467-013-2684-4.

Wang, Q., X.-W. Chen, and B. Margolis. 2007. PALS1 Regulates E-Cadherin Trafficking in Mammalian Epithelial Cells. *Mol. Biol. Cell* 18(3):874–885. doi:10.1091/mbc.E06-07-0651.

Wang, Q., T. W. Hurd, and B. Margolis. 2004. Tight junction protein Par6 interacts with an evolutionarily conserved region in the amino terminus of PALS1/stardust. *J. Biol. Chem.* 279(29):30715–30721. doi:10.1074/jbc.M401930200.

Wartiovaara, J., L.-G. Öfverstedt, J. Khoshnoodi, J. Zhang, E. Mäkelä, S. Sandin, V. Ruotsalainen, R. H. Cheng, H. Jalanko, U. Skoglund, and K. Tryggvason. 2004. Nephrin strands contribute to a porous slit diaphragm scaffold as revealed by electron tomography. *J Clin Invest* 114(10):1475–1483. doi:10.1172/JCI22562.

Weavers, H., S. Prieto-Sanchez, F. Grawe, A. Garcia-Lopez, R. Artero, M. Wilsch-Brauninger, M. Ruiz-Gomez, H. Skaer, and B. Denholm. 2009. The insect nephrocyte is a podocyte-like cell with a filtration slit diaphragm. *Nature* 457(7227):322–326. doi:10.1038/nature07526.

Wei, X., and J. Malicki. 2002. nagie oko, encoding a MAGUK-family protein, is essential for cellular patterning of the retina. *Nature genetics* 31(2):150–157.

Wei, Z., Y. Li, F. Ye, and M. Zhang. 2015. Structural basis for the phosphorylation-regulated interaction between the cytoplasmic tail of cell polarity protein crumbs and the actin-binding protein moesin. *The Journal of biological chemistry* 290(18):11384–11392. doi:10.1074/jbc.M115.643791.

Weide, T., B. Vollenbröker, U. Schulze, I. Djuric, M. Edeling, J. Bonse, F. Hochapfel, O. Panichkina, D.-O. Wennmann, B. George, S. Kim, C. Daniel, J. Seggewiß, K. Amann, W. Kriz, M. P. Krahn, and H. Pavenstädt. 2017. Pals1 Haploinsufficiency Results in Proteinuria and Cyst Formation. *JASN*:ASN.2016040474. doi:10.1681/ASN.2016040474.

Wells, C. D., J. P. Fawcett, A. Traweger, Y. Yamanaka, M. Goudreault, K. Elder, S. Kulkarni, G. Gish, C. Virag, C. Lim, K. Colwill, A. Starostine, P. Metalnikov, and T. Pawson. 2006. A Rich1/Amot complex regulates the Cdc42 GTPase and apical-polarity proteins in epithelial cells. *Cell* 125(3):535–548. doi:10.1016/j.cell.2006.02.045.

Wennmann, D. O., B. Vollenbröker, A. K. Eckart, J. Bonse, F. Erdmann, D. A. Wolters, L. K. Schenk, U. Schulze, J. Kremerskothen, T. Weide, and H. Pavenstädt. 2014. The Hippo pathway is controlled by Angiotensin II signaling and its reactivation induces apoptosis in podocytes. *Cell Death & Disease* 5(11):e1519. doi:10.1038/cddis.2014.476.

Whiteman, E. L., S. Fan, J. L. Harder, K. D. Walton, C.-J. Liu, A. Soofi, V. C. Fogg, M. B. Hershenson, G. R. Dressler, G. H. Deutsch, D. L. Gumucio, and B. Margolis. 2014. Crumbs3 Is Essential for Proper Epithelial Development and Viability. *Mol. Cell. Biol.* 34(1):43–56. doi:10.1128/MCB.00999-13.

Whitney, D. S., F. C. Peterson, A. W. Kittell, J. M. Egner, K. E. Prehoda, and B. F. Volkman. 2016. Binding of Crumbs to the Par-6 CRIB-PDZ Module Is Regulated by Cdc42. *Biochemistry* 55(10):1455–1461. doi:10.1021/acs.biochem.5b01342.

Wodarz, A., U. Hinz, M. Engelbert, and E. Knust. 1995. Expression of crumbs confers apical character on plasma membrane domains of ectodermal epithelia of Drosophila. *Cell* 82(1):67–76.

World Health Organization. 2008. 2008–2013 action plan for the global strategy for the prevention and control of noncommunicable diseases: prevent and control cardiovascular diseases, cancers, chronic respiratory diseases and diabetes.

Wrana, J. L., L. Attisano, J. Cárcamo, A. Zentella, J. Doody, M. Laiho, X.-F. Wang, and J. Massague. 1992. TGF β signals through a heteromeric protein kinase receptor complex. *Cell* 71(6):1003–1014.

Wu, S., J. Huang, J. Dong, and D. Pan. 2003. hippo encodes a Ste-20 family protein kinase that restricts cell proliferation and promotes apoptosis in conjunction with salvador and warts. *Cell* 114(4):445–456.

Wyatt, G. R. 1957. THE CHEMISTRY OF INSECT HEMOLYMPH: II. TREHALOSE AND OTHER CARBOHYDRATES. *The Journal of General Physiology* 40(6):833–847. doi:10.1085/jgp.40.6.833.

Xiao, Z., J. Patrakka, M. Nukui, L. Chi, D. Niu, C. Betsholtz, T. Pikkarainen, T. Pikkarainan, S. Vainio, and K. Tryggvason. 2011. Deficiency in Crumbs homolog 2 (Crb2) affects gastrulation and results in embryonic lethality in mice. *Developmental dynamics an official publication of the American Association of Anatomists* 240(12):2646–2656. doi:10.1002/dvdy.22778.

Yaoita, E., Y. Yoshida, M. Nameta, H. Takimoto, and H. Fujinaka. 2017. Induction of interdigitating cell processes in podocyte culture. *Kidney international*. doi:10.1016/j.kint.2017.06.031.

Zhang, F., Y. Zhao, Y. Chao, K. Muir, and Z. Han. 2013a. Cubilin and Amnionless Mediate Protein Reabsorption in Drosophila Nephrocytes. *JASN* 24(2):209–216. doi:10.1681/ASN.2012080795.

Zhang, F., Y. Zhao, and Z. Han. 2013b. An in vivo functional analysis system for renal gene discovery in Drosophila pericardial nephrocytes. *Journal of the American Society of Nephrology JASN* 24(2):191–197. doi:10.1681/ASN.2012080769.

Zhao, B., X. Wei, W. Li, R. S. Udan, Q. Yang, J. Kim, J. Xie, T. Ikenoue, J. Yu, L. Li, P. Zheng, K. Ye, A. Chinnaiyan, G. Halder, Z.-C. Lai, and K.-L. Guan. 2007. Inactivation of YAP oncoprotein by the Hippo pathway is involved in cell contact inhibition and tissue growth control. *Genes & development* 21(21):2747–2761. doi:10.1101/gad.1602907.

Zhou, W., and Y. Hong. 2012. Drosophila Patj plays a supporting role in apical-basal polarity but is essential for viability. *Development (Cambridge, England)* 139(16):2891–2896. doi:10.1242/dev.083162.

Zhuang, S., H. Shao, F. Guo, R. Trimble, E. Pearce, and S. M. Abmayr. 2009. Sns and Kirre, the Drosophila orthologs of Nephrin and Neph1, direct adhesion, fusion and formation of a slit diaphragm-like structure in insect nephrocytes. *Development (Cambridge, England)* 136(14):2335–2344. doi:10.1242/dev.031609.

Zou, J., X. Wang, and X. Wei. 2012. Crb apical polarity proteins maintain zebrafish retinal cone mosaics via intercellular binding of their extracellular domains. *Developmental cell* 22(6):1261–1274. doi:10.1016/j.devcel.2012.03.007.

5 Appendix

5.1 Abbreviations

A

aa – Amino acid
AB – Antibody
ABP – Apicobasal polarity
ADPKD – Autosomal dominant polycystic kidney disease
AJ – Adherens junction
AMOT – Angiomotin
ANP – Atrial natriuretic peptide
aPKC – Atypical protein kinase C
APOL1 – Apolipoprotein L1
AQP2 – Aquaporin 2

B

BIRC2 – Baculoviral IAP repeat containing 2
bp – Base pairs
BSA – Bovine serum albumine

C

Ca - Calcium
$CaCl_2$ – Calcium chloride
cAMP – Cyclic adenosine monophosphate
CD2 – Cluster of differentiation 2
Cdc42 – Cell division control protein 42 homolog
CKD – Chronic kidney disease
cKO – Conditional knockout
CLEM – Correlated light and electron microscopy
CMOS – Complementary metal-oxide-semiconductor
CO_2 – carbon dioxide
Crb – Crumbs
CTEM – Conventional transmission electron microscopy
CTGF – Connective tissue growth factor
CVD – Cardiovascular disease
CYR61 – Cysteine rich angiogenic inducer 61

D

DAPI – 4′,6-Diamidin-2-phenylindol
Dlg – Disc-large
DM – Diabetes mellitus
DMEM – Dulbecco's Modified Eagle's medium

E

EBF2 – Early B-Cell Factor 2
ECM – Extracellular matrix
EGFP – Enhanced green fluorescent protein
EMT – Epithelial-mesenchymal transition
ESRD – End stage renal disease
ET – Electron tomography

F

FBM – FERM binding motif
FERM – 4.1, Ezrin, Radixin and Moesin
FIB-SEM – Focused ion beam scanning electron microscopy
fl – floxed (gene deletion by Cre-lox recombination)
FP – Foot process
FSGS – Focal segmental glumerosclerosis
FS – Freeze-substitution

G

GAD – Glutardialdehyde
GAPDH – Glyceraldehyde 3-phosphate dehydrogenase
GAL4 – Galactose-responsive transcription factor 4
GBM – Glomerular basement membrane
GCN – Garland cell nephrocyte
GFP – Green fluorescent protein
GFR – Glomerular filtration rate

H

HEPES – 2-[4-(2-hydroxyethyl)piperazin-1-yl]ethanesulfonic acid
HEK – Human embryonic kidney
HL3.1 – Hemolymph-like saline 3.1
HPF – High-pressure freezing
HSD – Hydroxysteroid dehydrogenase

I

IF – Immunofluorescence
IgG – Immunoglobulin G

K

KCl – Potassium chloride
KD – Knockdown
KEGG – Kyoto Encyclopedia of Genes and Genomes
KO – Knockout
kV – Kilovolt

L

LATS – Large tumor suppressor
Lins7c – Lin-7 homolog C
Lgl – Lethal giant larvae

M

MAGUK – Membrane-associated guanylate kinase
MDCK – Madin-Darby canine kidney
$MgCl_2$ – Magnesium chloride
Mpp5 – Membrane protein, palmitoylated 5

N

NaCl – Sodium chloride
$NaHCO_3$ – Sodium bicarbonate
NCD – Non-communicable disease
ND – Nephrocyte diaphragm
NP-40 – Nonyl phenoxypolyethoxylethanol

O

OsO_4 – Osmium tetroxide

P

Pai-1 – Plamsinogen activator inhibitor 1
PALS1 – Protein associated with Lin-7 protein
Par – Partition defective
PATJ – PALS1-associated TJ protein
PBM – PDZ binding motif or parietal basement membrane
PBS – Phosphate buffered saline
PCNA – Proliferating cell nuclear antigen
PCP – Planar cell polarity
PCR – Polymerase chain reaction
PDZ – Postsynaptic-density-95/Disc-large/Zona-occludens 1
PHA – Phytoheme agglutinin
PNA – Peanut agglutinin
PVDF – Polyvinylidene fluoride

R

REGf – Rabbit anti goat
RFP – Red fluorescent protein
RNA – Ribonucleic acid
RNAi – Ribonucleic acid interference
RT-PCR – Realtime polymerase chain reaction

S

SCRIB – Scribble

SD – Slit diaphragm
SDS-PAGE – Sodium dodecyl sulfate polyacrylamide gel electrophoresis
Sdt – Stardust
SEM – Scanning electron microscopy
sh – Short hairpin
SIRT – Semi iterative reconstruction technique
Six2 – Sine oculis homeobox homolog 2
SJ – Septate junction
Sns – Sticks-and-stones
SPARC – Secreted protein acidic and rich on cysteine
SRNS – Steroid-resistant nephrotic syndrome
STEM – Scanning transmission electron microscopy

T

Taz - Transcriptional co-activator with PDZ-binding motif (=Wwtr1)
TBS – Tris buffered saline
TEM –Transmission electron microscopy
TGF-β – Transforming growth factor beta 1
THP – Tamm-Horsfall protein
TJ – Tight junction
TM – Transmembrane region
Tris – Tris(hydroxymethyl)aminomethane

U
UAS – Upstream activating sequence

V
vol – Volume

W
wt – Wildtype
WT1 – Wilms tumor 1 protein
Wwtr1 – WW domain containing transcription regulator 1 (=Taz)

Y
Yap – Yes-associated protein
Yki – Yorkie (*Drosophila* ortholog of Yap and Taz

Z
ZA – Zonula adherens
ZO-1 – Zonula occludens-1

5.2 Figures

5.3 Acknowledgements

Am Schluss dieser Arbeit möchte ich allen Leuten danken, die durch ihr Mitwirken zum Gelingen dieser Arbeit beitrugen.

Zuallererst gilt mein aufrichtiger Dank meinem Doktorvater **Prof. Dr. Michael Krahn**, der mir die Möglichkeit eröffnete, diese spannenden Projekte zu bearbeiten, und mir stets mit viel Unterstützung und Fachkompetenz zur Seite stand.

Neben meinem Betreuer möchte ich mich auch bei meinen Mentoren **Prof. Dr. Ralph Witzgall** und **Prof. Dr. Bernhard Banas** bedanken, die meine Forschungsarbeit beständig mit guten Ideen und Ratschlägen zu unterstützen wussten, sowie **Prof. Dr. Reinhard Rachel**, der sich oft ausgiebig Zeit nahm, um mit mir an den Präparationsstrategien für die Nephrozyten zu tüfteln.

Beim Thema Elektronenmikroskopie, möchte ich **Christine Maaßen** für die amüsanten HPF/FS-Vormittage und die daraus resultierenden, unzähligen eingebetteten Nephrozyten, **Lucia Denk, Yulia Zaytseva, Helga Othmen und Karin Schadendorf** für die vielen geschnittenen und betrachteten Proben, **Anita Zügner** für die Bayern2-Nachmittage im Schneideraum und **Cornelia Niemann** für die anfängliche Einweisung und Unterstützung an der AMW danken.

Für die gute Laune im Labor danke ich (der guten) **Gudrun Mendl, Giada Dogliotti, Laura Schebelle, Markus Dietz, Veronika Menath** und auch **Arnab Sen**, selbst wenn er diese Zeilen leider nicht mehr lesen kann. Außerdem danke ich **Ann-Kristin Frerking** für Kreativität am Arbeitsplatz (Balletttänzer in Epoxid) und **Diana Gallus** (Freunde der Weisheit, guten Abend).

Weiterhin gilt mein Dank **Edeltraud Lautenschlager** für ihr sonniges Gemüt, **Antje Zenker, Anita Hecht** und **Ton Maurer** für die Hilfe bei den Tomografien und bei allen grafischen Dingen. Außerdem danke ich allen Mitarbeitern und Studenten der AGs Witzgall und Krahn für ein paar schöne Jahre am Lehrstuhl.

Auch möchte ich **Bernhard Zilker** danken, der mich mit voller Kraft unterstützte und mir während der Zeit mit Geduld, Rückhalt und guter Laune zur Seite stand.

Ganz besonders danke ich meiner Familie **Helga** und **Erwin Bachmaier**, **Kathrin Hochapfel** und meinem bereits verstorbenen Vater **Kurt Hochapfel**, die mich den ganzen Weg entlang tatkräftig unterstützte und mir das alles erst ermöglichte.